MITOCHONDRIAL OXIDATIVE METABOLISM REGULATES MATERNAL-FETAL METABOLIC COMMUNICATION

by

Caitlyn E. Bowman

A dissertation submitted to Johns Hopkins University in conformity with the requirements for the degree of Doctor of Philosophy

Baltimore, Maryland

April 2018

Abstract

Macronutrient metabolism includes the suite of chemical transformations that sustain cells and allow for organismal growth and development. Mammalian pregnancy is perhaps the most nutritionally sensitive stage in life as all nutrients for fetal growth are provided by the mother. Glucose and oxygen are two of the most important molecules transferred to the fetus, and their metabolic fates converge at the metabolism of pyruvate in mitochondria. Pyruvate enters the mitochondrial matrix through the mitochondrial pyruvate carrier (MPC), a complex that consists of two essential components, MPC1 and MPC2. Here we define the requirement for mitochondrial pyruvate metabolism during development with a progressive allelic series of Mpc1 deficiency in mouse. While Mpc1 deletion was lethal during mid-gestation, a hypomorphic knock-in (KI) allele of Mpc1 resulted in perinatal lethality. Late-gestation Mpc1 KI fetuses were smaller than littermates with tissue-specific compensatory changes in lipid and amino acid metabolism. These data show that impaired mitochondrial pyruvate transport results in biosynthetic deficiencies that can be partially mitigated by alternative anaplerotic substrates *in utero*.

To further probe the capacity for metabolic plasticity in this model, late-gestation dams were fasted for 24 hours. Maternal fasting increased serum lipid metabolites, promoted fetal liver triglyceride accumulation, and stunted fetal growth. To determine the contribution of maternally-derived lipids to the fetal fasting response, we used two genetic models of impaired fatty acid oxidation: (1) liver-specific loss of mitochondrial β-oxidation of long-chain fatty acids via carnitine palmitoyltransferase 2 (Cpt2) and (2) genetic loss of a transcriptional regulator of lipid oxidative metabolism, PPARα. Upon fasting, these mice exhibit differing degrees of hepatic lipid accumulation and impaired ketogenesis. The fetal response to maternal fasting was determined by

liver transcriptional program and steady-state metabolite measurements. The maternal fasting response is a better indicator of fetal outcome than is fetal genotype, suggesting that maternally-derived factors dominate this communication. Furthermore, maternal effects persist into the early postnatal period, highlighting the importance of maternal lipid metabolism during gestation and lactation. The use of genetic models and biochemical approaches to obtain a greater mechanistic understanding of maternal-fetal metabolic communication may inform interventions for conditions such as gestational diabetes.

Thesis Advisor: Michael J. Wolfgang, Ph.D. Department of Biological Chemistry

Reader: Steven M. Claypool, Ph.D. Department of Physiology

Acknowledgments

Many thanks to my advisor, Michael Wolfgang, Ph.D., for supporting my curiosity and enthusiasm; for encouraging me to ask big questions, to think independently, and to read widely; and for granting me the independence to go after what has become an entirely new line of investigation in the lab. I'd also like to thank the current (Cory White, Ebru Selen Alpergin, Ph.D., Joe Choi, and Kyle Cavagnini) and former (Jessica Ellis, Ph.D., Susana Rodriguez, Ph.D., Jieun Lee, Ph.D., and Elsie Gonzalez-Hurtado) members of the Wolfgang Lab.

Thank you to Susanna Scafidi, M.D. for always reminding us of the clinical implications of our work and for a constant willingness to talk about brain metabolism/neurodevelopment.

I'd like to thank Liang Zhao, Ph.D. and Thomas Hartung, M.D., Ph.D. for assistance with steady-state metabolite measurements and metabolic flux analyses. I'm also grateful to Paul Watkins, M.D., Ph.D. for introducing us to an enigmatic acyl-CoA synthetase called ACSF3, and to Michelle Acoba from the Mitochondrial Phospholipid Research Center (aka Claypool Lab) for teaching me several assays of mitochondrial function.

Thank you to my thesis committee: Gerald W. Hart, Ph.D., Steven M. Claypool, Ph.D., and Hiromi Sesaki, Ph.D. I'm also grateful to Mike Delannoy, M.S. for help with electron microscopy studies, to Ann Moser for assistance with fatty acid analysis, to the Research Animal Resources staff for keeping tabs on my mice and greeting me with a smile every morning, to Susan Aja, Ph.D. for assistance with metabolic cage studies, and to Nadine Forbes-McBean, M.S for assistance with MRI and body composition analysis.

Thank you to the Department of Biological Chemistry administrative staff and the Biochemistry, Cellular, and Molecular Biology Graduate Program administrators and staff.

And thank you to my family and friends who put up with my poor ability to estimate time when it comes to planning experiments…

Contents

List of Tables

List of Figures

1. Introduction

Pregnancy may be the most nutritionally sensitive stage in the life cycle, which also means that nutritional interventions during pregnancy may have the greatest capacity to benefit maternal, fetal, and infant health. Furthermore, improved nutrition during gestation and early postnatal life may improve overall health and reduce the likelihood of chronic disease in adulthood (1). In this section, the basis of maternal-fetal metabolic communication will be introduced, including a discussion of the modes of communication and whether this maternal-fetal dialogue is one of harmony, conflict, neither, or both. Additionally, the basic metabolic needs of the developing fetus will be addressed in terms of the physiological adaptations in place to ensure their proper allocation. Maternal energy expenditure and changing metabolic demands over the course of gestation will also be discussed.

The placenta is a key regulator of fetal metabolism and it is the site where conflicts over maternal-fetal resource allocation and communication take place. The placenta is also unique in that it transiently provides this vital lifeline through which the developing fetus obtains all nutrients. Interestingly, placentation has independently evolved in multiple distinct lineages. Even within the same taxonomic order, different strategies of placentation exist (2, 3). The role of the placenta in nutrient transport will be discussed with particular attention to comparative placentation among different species and different model organisms.

The discussion of nutrient transport at the organ level via the placenta will lead into a molecular survey of particular substrates and how they are transported across this barrier that is anything but passive. This will set the stage for a discussion of the particular metabolites that are key players in fetal metabolism and how genetic loss-of-function models can define the developmental requirements for the metabolic pathways to be discussed in Part 2.

1.1 Maternal-Fetal Metabolic Communication: Harmony vs. Conflict

Successful mammalian pregnancy and parturition requires metabolic, hormonal, and immunological communication between mother and fetus (4). The types and intensities of signals conveyed vary considerably across gestation, as do the responses elicited by these messages. Metabolic communication throughout pregnancy is essential as a growing fetus obtains all nutrients from (and excretes all wastes to) the mother. While hormonal cues from both mother and conceptus can affect nutrient mobilization, the metabolic demands of the growing fetus may also directly modify maternal metabolism and behavior (5, 6). Fetal metabolic demand is highest during late gestation, which is coincident with the highest basal metabolic rate and energy expenditure in pregnant women and mice (7-9).

Alterations to macronutrient metabolism during pregnancy balance the competing interests of fetal growth and maternal fecundity (10, 11). However, the extent to which maternal-fetal communication reflects coordinated adaptations versus conflicting interests is not well understood and is likely context-dependent. For example, the competing interests of the maternally-inherited and the paternally-inherited genomes have resulted in some genomic regions being imprinted—that is, transcriptionally silenced or expressed from only one allele in particular tissues or at particular times in development. Importantly, of the more than 100 imprinted genes that have been identified in mice, the majority are expressed and imprinted in the placenta, the hub of hormonal communication and resource allocation during pregnancy (12). In this way, genomic imprinting has been likened to a tug-of-war over resource allocation that would support fetal growth or maternal fecundity (13). However, the distinction between these two seemingly opposed goals is rarely so clear-cut: Consider, for example, if additional maternal investment now will result in a more vigorous offspring that will require less maternal investment later, such that the mother can begin preparing for future offspring. While a great deal of metabolic

communication is necessary between mother and fetus, particularly when nutrients are limiting as to be discussed in Part 3, fetal demands and maternal countermeasures are always at work to compromise for a balance that will suit both mother and fetus. There is both harmony and conflict under nearly all maternal-fetal interactions.

1.2 Physiological Adaptations of Eutherian Pregnancy

Pregnancy demands a multitude of physiological adaptations that affect every organ system of the mother (4). Many changes are communicated by hormonal signals from both mother and conceptus (5), and the metabolic demands of the growing fetus may also directly modify maternal metabolism and behavior (6). Canonically, glucose is the principal substrate driving fetal growth (14). Many maternal metabolic adaptations ensure sufficient glucose delivery to the fetus by rendering the mother's tissues transiently insulin resistant and by enhancing maternal glucose production by 30% from early to late pregnancy (15). Concomitant with this, blood flow to the uterus increases to 25% of cardiac output to ensure substrate and oxygen availability for mitochondrial oxidative metabolism (16). The rate of fetal blood delivery to the placenta via umbilical flow is approximately proportional to fetal weight and gestational age.

The villous organization of the placenta increases the surface area such that the total surface area available for exchange during late pregnancy in humans is 10-15 m^2 (the approximate surface area of a tennis court) (17).

Interestingly, in multiparous species such as rats, there is a 2-fold difference in uteroplacental blood flow rates from middle positions to ovary/cervix positions (18). Studies from a crowded uterine horn mouse model demonstrate the effect of uteroplacental bloodflow on fetal outcomes (19). Mice were subjected to a unilateral ovariectomy and mated such that a normal-sized litter was born from a crowded uterine horn, in which there is a 4-fold difference in blood

flow to offspring from the same pregnancy (19). Fetuses in the middle positions between the ovary and the cervix experienced the lowest perfusion pressure (18), and the smallest 5% of offspring were half the weight of the largest 5% of offspring from this crowded uterine horn model (19). The smallest pups exhibited dramatic catch-up growth over the first three weeks of postnatal life, and by adulthood, both intrauterine growth-restricted male mice and macrosomic male mice weighed significantly more than littermates born at median birth weights (19). These data suggest that both fetal undernutrition and overnutrition can result in similar adverse metabolic outcomes in adulthood, although the mechanisms behind these outcomes are likely different. Multiparous species have the additional challenge of meeting the metabolic demands of several fetuses that may be competing against one another for maternal resources.

Another remarkable physiological adaptation of pregnancy is a greater metabolic flexibility than in the non-pregnant state in order to protect fetal growth from maternal nutrient deprivation (1). One way in which the pregnant woman is poised to provide this metabolic plasticity is through increased adipose tissue lipolysis and re-esterification, even in the fed state (20, 21). Maternal circulating lipids (triglyceride, free fatty acids, and phospholipids) increase throughout gestation (17, 22) and are mobilized from adipose depots established during early pregnancy (21, 23). Circulating lipids are further elevated by fasting and are available for placental transport (17, 22). Fetal uptake of lipids (and catabolic products such as ketones) may be particularly important during prolonged maternal nutrient deprivation (14). The extent to which fetal tissues rely upon lipids for energy metabolism is not well understood, but the early postnatal switch in nutrition from glucose *in utero* to lipid-rich milk suggests that late-gestation fetal tissues may have the capacity to utilize maternally-derived lipids (24). In this way, the metabolic plasticity of the mother may affect the fetal response to maternal nutrient deprivation.

1.3 Metabolic Demands of Pregnancy

Human weight increases 6 billion times over the course of prenatal life (25). As such, it is understandable how dramatically fetal metabolic demands must change over the course of gestation. Similarly, maternal energy expenditure also increases during gestation, but it is unclear if this increase is simply proportional to increased tissue mass and food intake (26). Longitudinal studies of energy expenditure and body composition have attempted to address this to better understand the metabolic costs of pregnancy.

Primate reproduction is characterized by a slow rate of growth over a long gestation which results in a lower nutritional stress per unit time than what is observed in species with faster generation times (1). Interestingly, there is greater variation among mammals in birth weight than there is in terms of length of gestation; therefore, there are vast differences in rates of fetal growth across species (25). Fetal growth rates are not linear but growth accelerates as gestation advances. In humans, birth occurs on the steepest part of the growth curve, while in rodents, for example, the greatest rates of growth occur in the first two weeks of postnatal life (25), even though fetal rats exhibit a 25-30% increase in weight in the last day of gestation (27). Because of the slow rate of growth of humans, the daily energy stress of human pregnancy relative to maternal body size is lower than for most other mammals (1). Species with higher metabolic demands during pregnancy must meet that need through substantial increases in food intake, whereas humans, with a lower nutritional stress per unit time, may instate metabolic adaptations to protect fetal growth from adverse circumstances such as food shortages.

In healthy human pregnancies, the average maternal weight gain was 12.5 kg (28 lbs) over the course of gestation (23). Fetal weight may account for 25% of the weight gained in a well-nourished human pregnancy, but up to 60% in suboptimal nutritional conditions (1). Calculations of the human energy budget during pregnancy suggests there are three ways in

which energy is used: (i) energy deposited as new tissue (~20 MJ); (ii) energy deposited as fat (~150 MJ); and (iii) energy required to maintain the new tissue (~150 MJ) (1). There are vast differences in energy budgets during pregnancy in the developed vs. developing world, depending on maternal (and pre-pregnancy) nutrition. When maternal resources are limited, energy deposition as fat is the metabolic fate that gets re-routed. Pair-feeding of pregnant mice based on non-pregnant controls revealed no reduction in fetal body weights from pregnancies fed *ad libitum*; however, there was a significant reduction in maternal body weight, suggesting that maternal hyperphagia in later rodent gestation fuels adipose deposition that is particularly important during lactation (28). In humans, maternal adipose deposition occurs in the first trimester, and it is these adipose stores that will be mobilized during late gestation to promote fetal fat accretion (17, 23). Fat accounts for 16% of birth weight in humans, but only 1 to 2% in mice and rats (25). Furthermore, this late-gestation increase in adiposity is unique to humans as most other mammals, including primates, are born lean (14, 24). Some species, such as rabbits and guinea pigs, accumulate fat in their livers just prior to birth, and it is these hepatic stores rather than adipose depots that are of principal importance for early postnatal metabolic adaptation in these species (24, 29).

In small mammals such as rodents, fetal mass may account for 30% of maternal body weight, hence certain metabolic adaptations may, out of necessity, increase energetic efficiency over what is observed in human pregnancy (30). In sheep, fetal body weights are 8% of maternal body weight, which may make them a better model for human pregnancy (30), although there are fundamental differences in placental morphology between humans and sheep that will be addressed in the next section. The gold standard for assessing changes in bioenergetic demand during pregnancy is to collect longitudinal data on metabolic rates, however, it can be challenging to collect this data from a sufficient sample size since there is often considerable variation among

women (31). Several longitudinal studies of pregnant women have demonstrated increasing energy expenditure across gestation by indirect calorimetry measurements (7, 8, 32, 33). Women with a normal BMI displayed a 28% increase in basal metabolic rate and a 13% increase in total energy expenditure from pre-pregnancy to 36 weeks gestation (7). There is considerable variability in total energy expenditure (TEE)—some women have a net negative difference in TEE across the course of pregnancy—and this suggests that pregnant women use a diverse array of strategies to meet the metabolic demands of pregnancy (8). Therefore, a single recommendation for increased energy intake during pregnancy is likely not applicable to all women. Importantly, little or no increase in energy intake was observed during human pregnancy (8). Additionally, a study of early- and late-gestation pregnant women found no difference in postprandial energy expenditure compared to non-pregnant controls, suggesting that there are no significant alterations in efficiency of energy extraction from dietary sources (30). This is consistent with the studies of pair-fed mice in which reducing maternal food intake was still sufficient to meet the biosynthetic and bioenergetic needs of the developing fetus (28). While human nutrition varies greatly between and within populations around the world, remarkably, a healthy human newborn is the same in any population, in large part due to the adaptive measures that protect against nutritional deficiency *in utero*.

Another obstacle in studies of the energetic requirements of pregnancy, in laboratory model organisms in particular, is the challenge of accounting for fetal metabolic rate in a system where fetal mass may account for up to 30% of maternal weight. Measurements by indirect calorimetry in newborn mice suggest that metabolic rate relative to fetal body weight is likely 30% lower than the metabolic rate of maternal body, such that maternal changes in energy expenditure account for the bulk of the increase in metabolic rate during pregnancy (9). Additionally, in a mouse model in which placentae persist after fetuses are rendered inviable

during late gestation (15 dpc), increased metabolic rate was still observed (9). This suggests that hormonal contributions from placenta, rather than fetal demand *per se*, may contribute significantly to the increase in metabolic rate across gestation. In rats, as in humans, energy expenditure was 10% higher than non-pregnant values at the peak of energy expenditure just prior to parturition (26). Altogether, the increased basal metabolic rate during pregnancy can be attributed to the combined effects of increased tissue mass, accelerated tissue synthesis, and increased cardiovascular, respiratory, and renal work (31).

1.4 Placental Development and Comparative Placentation

The placenta is a key regulator of fetal and maternal metabolism and it is the site where conflicts over maternal-fetal resource allocation and communication take place (10). The placenta is also unique in that it is a transient organ that provides the vital lifeline through which the developing fetus obtains all nutrients. The placenta develops from interactions between the trophectoderm of the implanting blastocyst and the endometrium. In humans, the placenta is functionally mature by 10-12 weeks' gestation, and placental growth precedes fetal growth such that the placenta is larger than the fetus until 15-16 weeks (full term at 38 weeks) (4). In mice, placentation begins just before mid-gestation, the definitive placenta is established at e11, and the maximum placental volume is reached by e16.5, as determined by stereology (parturition at day 19-20) (34, 35). The size and transport capacity of the placenta is often indicative of fetal health and growth. Placental insufficiency is linked to miscarriage, intrauterine growth restriction (IUGR), and preeclampsia.

Humans and rodents both have hemochorial placentae where maternal blood comes into direct contact with the syncytiotrophoblast, which is the first barrier to maternal-fetal exchange (36, 37). The specialized syncytiotrophoblast has a microvillous membrane in contact with the

maternal blood and a basal membrane facing the fetal blood. Humans also have a villous placental organization where each chorionic villus is composed of (i) an epithelial layer derived from syncytiotrophoblast and cytotrophoblasts and (ii) an inner vascular network (including fetal vessels) and connective tissue stroma derived from embryonic mesoderm (4, 34). Invasive endovascular trophoblasts remodel the uterine spiral arteries and replace maternal endothelium such that maternal blood flows directly around the terminal villi (34, 37). This villous organization maximizes the surface area available for exchange. Although the discoid, hemochorial placentae of humans and rodents have similar forms, rodent placenta lacks the well-defined villous structures of human placenta. Instead, in rodents, maternal blood bathes branching structures in a region called the placental labyrinth where most nutrient and gas exchange occurs (37, 38). The rodent structures analogous to human chorionic villi have a trichorial arrangement with two layers of syncytiotrophoblast in contact with fetal endothelium and a cytotrophoblast cell layer in contact with maternal blood (34, 36). The rodent placenta also has a junctional zone, comprised of spongiotrophoblasts, which serves an endocrine function (37). The multinucleated giant cells of the outer layer of the rodent placenta promote implantation and are somewhat analogous to the extravillous trophoblasts that invade the maternal spiral arteries in humans (36). Despite subtle differences in cell types and organization, the structures of rodent and human placentae are more similar than certain other modes of placentation among eutherian mammals. A comparison of several model organisms for the study of placental development and function highlights the advantages and limitations of using these models as they relate to human placentation and parturition (39).

Placentation has independently evolved in multiple distinct lineages. Even within the same taxonomic order, different strategies of placentation exist (2, 3). Humans and rodents, with hemochorial placentae, are among the species with the most invasive form of placentation, as

fetal tissues are in direct contact with maternal blood (3). In the endotheliochorial placenta, maternal blood vessels are adjacent to fetal tissues but separated by maternal endothelium. In the least invasive type of placenta, the epitheliochorial placenta, maternal blood and fetal tissues are separated by maternal endothelium, connective tissue, and epithelia, which provides considerably more membranes across which nutrients must be transported to reach the fetal compartment (3). Species with the least invasive mode of placentation include sheep, which is an important consideration when comparing studies of fetal sheep metabolism to other species. For instance, that sheep have the least invasive form of placentation while rodents and lagomorphs have the most invasive form may help explain some of the discrepancies in placental fatty acid transport capacity observed across species (29, 40). In sheep, fetal blood concentrations of both free fatty acids and ketones remain low relative to maternal concentrations, even upon maternal nutrient deprivation (14). Consistent with this, radiolabeled palmitate was found to be transported poorly across the sheep placenta; however, circulating free fatty acid levels in newborn sheep were rapidly increased from 10% to 80% of maternal levels within an hour after birth (40). In rabbits, on the other hand, maternal fasting nearly doubled fetal fat storage in both adipose and liver (29). In this regard, the most invasive (hemochorial) placenta may allow for greatest lipid transport from mother to fetus, and species with this mode of placentation exhibit higher rates of prenatal brain growth and higher ratios of brain mass to body mass in both neonates and adult animals (2). In humans, for example, the brain of a newborn weighs 25% the weight of an adult brain, but the body weighs only 5% of the adult body weight (25). A study of brain-body allometry across eutherian mammals demonstrated patterns of faster prenatal brain growth and slower prenatal body growth among species with more invasive forms of placentation (2). This suggests that, in these species, nutrients essential for brain growth and development (such as essential fatty acids) are made more readily available to the fetus earlier in life. Modes of placentation across taxa

reflect life history traits that reveal how and when offspring obtain these essential nutrients during their development. The brain is an energetically expensive tissue, both in terms of development and maintenance (41-43), and the brain is characterized by a unique lipid composition (44). It is of no surprise that placentation strategies may affect nutrient availability for important developmental processes that vary among species. A more mechanistic understanding of how species-specific differences in nutrient transport affect these life history traits remains to be determined.

A final point of interest about comparative placentation is the reproductive strategy employed by marsupials—the other lineage of mammals that gives birth to live young. Marsupials have more anatomically simple placentae and give birth to young at a much earlier stage of development than eutherian mammals. Lactation, therefore, plays a greater role in marsupial development, emulating later stages of eutherian *in utero* development (45). Marsupials have a more complex milk repertoire than eutherians, and some classes of genes expressed by marsupial mammary gland are shared with eutherian placenta and eutherian mammary gland while others are only shared with eutherian placenta (46). Among these genes are nutrient transporters and transcriptional regulators known to be important in eutherian placenta which are conserved by their expression in marsupial mammary gland (46). Altogether, mammals have a diverse array of strategies related to placental invasiveness, degree of maturity at parturition, and early postnatal nutritional approaches to ensure offspring health and manage the energetic costs of pregnancy and lactation.

1.5 Placental Nutrient Transport: A Molecular Survey of Substrates

Placental structure maximizes the surface area available for exchange of membrane-permeable molecules as well as ions and polar molecules which require transporter-mediated

movement across cellular membranes. The developing fetus is in a constant anabolic state, increasing biomass with substrates delivered from the mother. Canonically, glucose is the principal substrate driving fetal growth (14). In addition to carbohydrates, amino acids, and lipids are also required for fetal growth. While some of these molecules can be synthesized by the fetus, others are essential and must be supplied from the mother. Here, some of the key classes of nutrients provided by the placenta for fetal growth will be surveyed: carbohydrates, amino acids, and lipids. Their transport and metabolic fates will be reviewed, with special emphasis on the oxidative metabolism of these molecules within mitochondria. The requirement for mitochondrial oxidative metabolism of glucose-derived pyruvate during mammalian development will be defined in Part 2.

1.5.1 Carbohydrates

Glucose and oxygen are arguably the two most important molecules transferred from mother to fetus during pregnancy. Pyruvate is the end-product of glycolysis, and pyruvate can be converted to lactate to regenerate NAD^+, a necessary cofactor for glycolysis (**Fig. 1**). Oxygen, glucose, and lactate all coalesce at the transport and metabolism of pyruvate in mitochondria. While oxygen tension *in utero* is low relative to atmospheric levels, measurement of oxygen consumption and lactate uptake in fetal lamb provided evidence that the fetus is a net consumer rather than producer of lactate (14). Consistent with this, fetal myocardium consumes a large amount of lactate in addition to glucose, indicating that oxidative metabolism of carbohydrate is an important energy source in developing heart (47, 48). Additionally, lactate utilization is high in neonatal brain, and the capacity for lactate import is higher in neonatal brain than in adult (43, 49). Furthermore, recent studies revealed significant lactate utilization in adult tissues, suggesting that circulating lactate is an important oxidizable substrate in mammals (50, 51). Together, these

observations provide evidence for the importance of mitochondrial oxidative metabolism early in mammalian development.

The predominant glucose transporter expressed in placenta is GLUT1, and it is found on both the microvillous and basal membranes of the syncytiotrophoblast (52). GLUT3 can be found in the vascular endothelium where it likely enhances placental uptake of glucose (52). In rodents and sheep, GLUT3 is expressed by the placenta and increases as gestation progresses. The expression of this high affinity glucose transporter may help scavenge glucose uptake in species with a faster rate of *in utero* growth and a higher daily energy stress of pregnancy than humans (52). Interestingly, placental GLUT1 expression has been found to be increased in gestational diabetes mellitus (GDM). Normally, there is more GLUT1 expression on the microvillous membrane than on the basal membrane, but in GDM pregnancies there is increased expression of GLUT1 on the basal membrane which could promote elevated glucose transport to the fetus (52, 53). It is unclear whether maternal or fetal factors mediate this increase in GLUT1 expression in GDM, but it has been suggested that fetal hyperglycemia and increased IGF-1 expression could result in elevated glucose transporter expression (54).

It is unclear exactly how glucose is made available for transport across the basal membrane of the syncytiotrophoblast since hexokinase will readily phosphorylate glucose transported across the maternal microvillous membrane. There are a few reports of glucose-6-phosphatase expression in the endoplasmic reticulum of the syncytiotrophoblast, and that may represent one path by which glucose can be transferred to the fetal side (55, 56). Some reports even provide evidence for glucose production by the placenta, but the capacity for and regulation of this potential source of increased glucose production during late gestation is not well understood (56, 57). In one study, women undergoing elective cesarean delivery at term (after a 10 hour fast) were administered deuterated glucose, and the label was found to be diluted in the

umbilical vein with no further dilution in the umbilical artery, suggesting a uteroplacental source of this glucose rather than a fetal contribution (57). Glycogen stores are another potential source of glucose available for placental use or transport to the fetus. While glycogen stores have been observed in multiple cell types in human and rodent placentae, the functions of these stores and their role in normal physiology and pathogenesis are poorly understood and may vary across gestation (58).

The placenta not only transports glucose to the fetus but it also catabolizes glucose. Umbilical uptake of oxygen and glucose were found to be 45% and 75% lower, respectively, than the total uterine uptake in sheep, suggesting significant glucose oxidation by the placenta (59). In an ovine model of impaired placental growth, oxidative metabolism of glucose by placenta was impaired, but lactate efflux to the umbilical vein was increased and fetal lactate consumption increased as a result (60). In late gestation, maternal gluconeogenesis is elevated to ensure adequate glucose supply to the fetal compartment, and lactate is an important gluconeogenic substrate. However, only 40-50% of lactate was used for gluconeogenesis in late-gestation pregnant rats, as compared to 70-80% in non-pregnant rats, suggesting that fetal utilization of lactate may account for the difference (27). Studies in fetal lamb confirm that lactate concentrations are higher in fetal umbilical vein than in fetal artery, again consistent with the fetus being a net consumer of lactate (61). Recent magnetic resonance imaging studies using hyperpolarized [1-^{13}C]pyruvate administered to late-gestation pregnant rats resulted in clear placental localization of signal as well as evidence of conversion to [1-^{13}C]lactate and [1-^{13}C]alanine in maternal organs and in placenta. Importantly, the intensity of the [1-^{13}C]lactate signal from placenta was lower in a rat model of preeclampsia, and this reduction in signal is not due to changes in placental perfusion but rather likely represents impaired placental metabolism of pyruvate (62). Together, these observations challenge the dogma that *in utero* development is

characterized by low oxygen tension and is not conducive to mitochondrial oxidative metabolism. While this may be true during early development, once placental exchange function is developed and fetal mitochondrial biogenesis begins (63), the fetus is poised to utilize oxidative metabolism for energy production and anabolism.

1.5.2 Amino Acids

Amino acids can be utilized for protein synthesis and biomass accumulation as well as for energy production. In contrast to glucose utilization by placenta, similar rates of uterine and umbilical uptake of amino acids were measured in sheep, suggesting that amino acids are preferentially transferred to the late-gestation fetus (59). In humans, fetal umbilical vein concentrations of amino acid were higher than maternal circulating levels (64). A thorough catalog of placental amino acid transporters is beyond the scope of this survey, but the reader is directed to these excellent reviews (38, 65-68) and a comprehensive model of integrated placental amino acid transport (since some amino acids are accumulated against a concentration gradient and others are used in concert with exchangers/antiporters that will swap one amino acid for another across a membrane) (69). Impaired placental amino acid transport has been observed in intrauterine growth restriction (IUGR), and there was decreased mTOR activation in IUGR placentae, indicative of impaired nutrient sensing relative to healthy placentae (70). Hyperpolarized ^{13}C magnetic resonance imaging was able to observe [1-^{13}C]alanine and urea *in vivo* in rat placenta. Urea was demonstrated to cross the placenta and reach fetal liver, although the physiologically relevant direction of urea transport is from fetus to placenta as a waste product (62). A similar imaging approach in pregnant women could possibly be used to test for the placental dysfunction that is characteristic of complications such as IUGR and preeclampsia.

1.5.3 Lipids

Lipids are an important class of molecules for cellular biosynthesis, biomass accretion, energy production, and signaling purposes during fetal development. The fetus is capable of *de novo* lipogenesis from precursors derived from the tricarboxylic acid (TCA) cycle (**Fig. 1**). Because of the predominance of glucose as a metabolic substrate *in utero*, much of the carbon available for lipogenesis likely derives from glucose. In mouse, whole-body deletion of acetyl-CoA carboxylase 1 is embryonic lethal by day 8.5, and whole-body deletion of fatty acid synthase results in pre-implantation embryonic lethality (71, 72). Remarkably, adult mice with liver-specific deletion of these essential enzymes in lipogenesis are not phenotypic when dietary fat is available, suggesting that, even *in utero*, liver fatty acid synthesis is not essential under normal dietary conditions (73, 74). *De novo* lipogenesis has been measured in fetal rat by the incorporation of $^{3}H_2O$ into the lipid fraction. From e17 to e20 in rats, there was a 3-fold increase in fatty acid synthesis; however this study failed to provide fetal tissue-specific resolution as to where these lipids were accumulating, although it was reported that fetal liver triglyceride content accounted for 20% of total fetal triglyceride content (75). The same study also compared exogenous uptake of [^{14}C]oleate, but the relative contributions of lipogenesis vs lipid uptake to total tissue lipid accretion cannot be determined from these labeling experiments. Glucose-derived lipogenesis is likely of greater significance in species with limited fatty acid transport across the placenta, such as species with epitheliochorial placentae like sheep and cows. Although the relative contribution of *de novo* synthesized lipid vs placental uptake of lipid is not well established, the importance of lipid accretion during late gestation cannot be contested. Human fetal liver accumulated 51mg fatty acid per week from 22 weeks of gestation to term (76). Much of this lipid is maternally-derived from maternal adipose depots that are mobilized in late

gestation (21, 23). How these lipids are made available for fetal uptake via the placenta is discussed next.

1.5.3.1 Sources of lipids for placental transfer

While some studies have suggested that rates of placental transfer of lipids (particularly in species with epitheliochorial placentae) are quite low, it is important to consider that cumulative lipid transfer and accumulation in fetal tissues may be highly significant even if rates of transfer are slow. During late gestation, maternal non-esterified fatty acid (NEFA) concentrations are elevated, but circulating triglyceride (TG) levels are increased even more dramatically, such that levels are 250% higher than levels in non-pregnant women (17). These concentrations are more than two-fold higher than the postprandial peak in TG after a high-fat meal. It is largely accepted that maternal circulating triglycerides do not cross the placenta intact, yet the acyl content of TG is available for fetal accumulation (6). In humans, for example, a TG emulsion administered to pregnant women near term was able to cross the placenta as evidenced by increased fetal arterio-venous lipid concentrations and by the observation that fetal circulating NEFA and TG fatty acid composition resembled the composition of the TG emulsion that was administered to the mother (77). NEFA availability at the placenta can be from mobilization of maternal adipose depots or from local TG hydrolysis by maternal or placental lipases. The human placental microvillous membrane is capable of binding lipoproteins that transport triglyceride and other esterified lipids (78, 79) and the placenta has lipase activity to liberate NEFA from triglyceride (80, 81). Indeed, studies from guinea pig indicate that more of the NEFA available to placenta is derived from maternal TG than from circulating NEFA (82). Increased lipase activity has been measured from placenta from diabetic pregnancies and the higher availability of maternal lipids may be associated with the increased fetal weight gain that is characteristic of gestational diabetes (80). Placental lipases may have increased selectivity to release long-chain

poly-unsaturated fatty acids from triglyceride because lipoprotein lipases preferentially hydrolyze the sn-2 position which is more likely to be unsaturated (17). Different placental cell types may also contribute to making fatty acids available for uptake. For example, placental macrophages express high levels of lipoprotein lipase, and endothelial cell expression of endothelial lipase may contribute significantly to hydrolysis of maternal lipoproteins throughout gestation (83).

After fatty acids have been liberated from maternal TG at the microvillous membrane, they are available for placental transport and metabolism. Placental fatty acid binding proteins (FABPs) and fatty acid transport protein (FAT/CD36) may facilitate fatty acid transport down a concentration gradient (83). In humans, the concentration of NEFA in maternal blood is about three-fold higher than in fetal blood at term, but fetal blood has a higher concentration of albumin and a higher concentration of bound NEFA than maternal blood (17, 84). In this way, the fetus can exert a steeper effective concentration gradient to increase fetal fatty acid uptake which is particularly important during late gestation when fetal fat accretion is greatest in humans. The fatty acid transport proteins Fatp1 (Slc27a1) and Fatp4 (Slc27a4), two members of the very long-chain acyl-CoA synthetase family, are also expressed in placenta (83) and may help shuttle acyl groups to particular metabolic fates within the placenta (85-88). Acyl-CoA thioesterases, which hydrolyze acyl-CoAs to free fatty acids and free coenzyme A in several cellular compartments, could conceivably play a role in making fatty acids available for transport as a free acid. One report has detected long-chain acyl-CoA thioesterase activity in BeWo human placental choriocarcinoma cells, and treatment of cells with particular fatty acids resulted in increased thioesterase activity and enhanced expression of PPARγ target genes (89). Another way acyl groups could be transported across the placenta is as acylcarnitine species. Transacylation of long-chain acyl-CoAs to acylcarnitines is essential for long-chain fatty acid transport into the mitochondrial matrix for β-oxidation (**Fig. 1**). The organic cation/carnitine transporter Octn2 is

expressed in placenta (90), and carnitine levels in cord blood are higher than in maternal blood (91). Moreover, in Part 4, evidence for acyl transfer from mother to fetus as acylcarnitines is presented.

1.5.3.2 Metabolic fates of lipids within the placenta

It has been speculated that NEFA transported into placenta are likely esterified to placental TG, and fetal TG levels may be better correlated with placental TG content than with maternal circulating lipid concentrations (75). Placental TG is comprised of that which has been taken up from maternal lipoproteins (VLDL) and also from placental TG synthesis. Studies of rat placenta demonstrated that NEFA could be esterified in a concentration-dependent manner (92). Placental TG content increased with progressing gestation, and a severe 48h fast also dramatically increased placental TG levels. Radiolabeled oleate was readily incorporated into TG, diacylglycerol, and cholesterol esters. There was no difference in the capacity for oleate esterification in fed vs fasted placentae, suggesting that the capacity for esterification cannot account for the difference in TG content and that the availability of maternal circulating lipids may be a more important regulator of placental TG content (92). A recent computational-experimental approach used human placental *ex vivo* perfusions to model fatty acid uptake and transfer to the fetus (93). Placental uptake of fatty acids was largely dependent on placental metabolism of fatty acids rather than on microvillous membrane transport. The idea here is that when membrane transport capacity is high, the transmembrane gradient becomes small and the rate-determining factor becomes metabolism of the molecules of interest. Rates of fatty acid delivery to the fetal compartment were determined by placental metabolic pools and basal membrane transport (93). Further studies are needed to characterize the metabolic fates of placental fatty acids to better understand how these pools of lipids affect transport and whether fatty acid β-oxidation provides energy for placental nutrient transport. The observation that the

placenta may serve as metabolic pool for fatty acid delivery to the fetus is in agreement with the observation that glucose transport is also best understood in terms of a three-pool model where maternal, placental, and fetal metabolism are all taken into consideration (94).

The capacity for and role of fatty acid oxidation in the placenta is not well understood. Human placenta was found to express the necessary enzymatic machinery for mitochondrial β-oxidation (95, 96). Oleate oxidation by placental explants has been observed—although at lower rates than oleate esterification into neutral lipids—and was moderately increased with gestational age (92). This study, however, cannot account for differences in fatty acid utilization among placental cell types, which may account for some of the differences in fatty acid oxidation vs esterification. To this end, isolated trophoblasts can oxidize fatty acids as a significant metabolic fuel, but the contribution of other cell types is less well understood (95). Broadly, placental metabolism can affect nutrient availability by sequestering nutrients from the dam, by storing nutrients for subsequent delivery to the fetus, or by providing new or bio-transformed substrates for fetal nutrition that were produced as a result of placental metabolism (in the case of fatty acids, the production and transport of acylcarnitines or ketone bodies as possible metabolites for transport).

1.5.3.3 Transport and availability of polyunsaturated fatty acids

Now the transport and availability of a class of fatty acids that are particularly important for mammalian brain development—the long-chain polyunsaturated fatty acids (PUFAs)—will be discussed. Long-chain polyunsaturated fatty acids (LCPUFAs) can be derived from the essential fatty acids linoleic acid (18:2 n-6) and α-linolenic acid (18:3 n-3), but during pregnancy, LCPUFAs may become conditionally essential if dietary intake and biotransformation cannot keep pace with fetal demand (17). Arachidonic acid (20:4 n-6), eicosapentaenoic acid (20:5 n-3), and docosahexaenoic acid (DHA) (22:6 n-3) are the metabolically most important LCPUFAs, and

the very presence of these essential fatty acids in fetal tissues stands as evidence for fetal uptake and accumulation (17). In the human fetus, lipid deposition increases exponentially with gestational age until it reaches the maximal rate of accretion of 7g/day just before term (25), and DHA requirements triple from 100 mg/day to 300 mg/day from mid to late gestation (17). The measurement of elevated concentrations of LCPUFAs in fetal blood and tissues has been called biomagnification (17). One method of bioaccumulation of these lipids is the conversion of NEFA into phospholipids within the fetal liver to trap select fatty acids and accumulate them from the circulation (97). Similarly, other tissues, most notably adipose, may serve as a pool for these lipids. Remarkably, 16-fold more DHA is stored in fetal adipose tissue than is deposited in fetal brain, and this accumulation of DHA in adipose is specific to fetal adipose tissue and is not reflective of maternal adipose tissue DHA content (17).

The placenta also likely plays a major role in the selective uptake of PUFAs. Administration of ^{13}C-labeled fatty acids to pregnant women just prior to cesarean delivery revealed that placenta preferentially accumulated DHA relative to other labeled fatty acids (palmitate, oleate, and linoleate) at the concentrations tested at this time just prior to parturition (84). Furthermore, [^{13}C]DHA was esterified in similar proportions in cord blood NEFA, phospholipids, and triglyceride, while other tracers were primarily retained as NEFA or incorporated into TG (84). These studies provide evidence for selective channeling of individual fatty acids into different placental pools and eventually into the fetal circulation. One way that DHA has been shown to cross membranes is via MFSD2a, the recently characterized lysophospholipid transporter that facilitates DHA accumulation in the developing brain (98, 99). Without this transporter, mice exhibit microcephaly, impaired blood-brain barrier function, neuronal cell loss, and cognitive deficits (98, 99). Placental expression of MFSD2a, the lysophosphatidylcholine-DHA transporter, was found to be decreased in women with gestational

diabetes, and low levels of the DHA transporter were found to correlate with low levels of DHA in cord serum total lipids, although these levels still exceeded maternal circulating levels (100).

Placental elongation/desaturation is one way that fetal levels of LCPUFAs could be accumulated over maternal levels; however, there is little evidence of this activity in placenta (101). Fetal and neonatal liver microsomes have the capacity to elongate and desaturate fatty acids (101, 102). Additionally, isotopic labeling studies in human infants administered labeled linoleic (18:2 n-6) and linolenic (18:3 n-3) acid resulted in labeled PUFAs in plasma fatty acids and phospholipids (97, 103). Mice lacking *Elovl2*, a PUFA elongase, were used to characterize the maternal provision of and neonatal requirements for DHA (104). These mice exhibit a systemic deficiency in DHA, including a 90% suppression in serum DHA concentrations that can be rescued by dietary DHA supplementation. Importantly, neonatal heterozygous mice reared by DHA-deficient null dams were able to compensate via neonatal synthesis of DHA, although the exact timing of when this capacity is established is not fully known (104). Altogether, these examples demonstrate that there are multiple mechanisms in place to ensure adequate fetal uptake or neonatal synthesis of essential fatty acids required for mammalian brain development. Maternal, placental, and fetal adaptations work in concert to ensure adequate nutrient supply.

1.6 Genetic Models of Impaired Mitochondrial Nutrient Transport

To determine the requirements of mitochondrial pyruvate metabolism and mitochondrial β-oxidation of long-chain fatty acids in oxidative metabolism in cultured cells and *in vivo* during mouse development, loss-of-function alleles were generated for two essential components of the transport processes by which pyruvate and long-chain acylcarnitines enter the mitochondrial matrix: the mitochondrial pyruvate carrier (MPC) component, Mpc1, and carnitine

palmitoyltransferase 2, Cpt2 (**Fig. 1**). Carnitine palmitoyltransferase 2 is an obligate component of the long-chain fatty acid carnitine shuttle in mitochondria that converts acylcarnitines back to acyl-CoAs that can enter the β-oxidation pathway, and Cpt2 will be discussed in further detail in Part 3 and Part 4. Here the history of the discovery of the mitochondrial pyruvate carrier is discussed as the molecular identity of this non-canonical mitochondrial carrier was only identified in 2012. In Part 2, the genetic requirement for mitochondrial pyruvate metabolism via the MPC during fetal mouse development is described.

1.6.1 Sources and Fates of Mitochondrial Pyruvate

Pyruvate is an important metabolite that lies at the intersection of carbohydrate, lipid, and amino acid catabolic and anabolic pathways (**Fig. 1**). Dysregulation of carbon metabolism between these fates is a hallmark of many metabolic disorders including diabetes, obesity, and cancer (105, 106). Most notably, pyruvate is the end product of glycolysis, and the transport of pyruvate from the cytoplasm into mitochondria allows for its oxidative decarboxylation to acetyl-coenzyme A (CoA) via the pyruvate dehydrogenase complex. Mitochondrial acetyl-CoA is oxidized to carbon dioxide through the tricarboxylic acid (TCA) cycle which generates reducing equivalents for ATP production and provides the biosynthetic precursors of lipids, amino acids, and glucose (**Fig. 1**).

The sources and fates of pyruvate depend upon cell-type-specific processes and physiological state. For example, pyruvate may be converted to oxaloacetate via pyruvate carboxylase in the first step of gluconeogenesis in fasting liver. Pyruvate that enters the TCA cycle may be siphoned off as citrate to support *de novo* lipogenesis in the cytoplasm of hepatocytes and adipocytes. In the central nervous system, neurons may convert astrocyte-derived lactate to pyruvate for oxidative phosphorylation. Although the fate of mitochondrial pyruvate

depends upon cell type and physiological state, the transport of pyruvate across the inner mitochondrial membrane (IMM) and into the mitochondrial matrix in all cells is mediated by the mitochondrial pyruvate carrier (MPC). Substrate partitioning is a fundamental way to regulate metabolic pathways. For a transport process to be a metabolic control point, it may be the rate-limiting step (as in the case of the carnitine shuttle for mitochondrial β-oxidation of fatty acids) or there may be physiological mechanisms for activation and inhibition of the transporter (107). The MPC was first characterized in 1971, but its molecular identity remained a mystery for 40 years (reviewed in (108, 109)). Now that the identity of the genes encoding the MPC have been determined, it is possible to directly investigate mechanisms of regulation of the MPC.

1.6.2 Identification of the Mitochondrial Pyruvate Carrier (MPC)

While pyruvate, a weak acid, can freely diffuse across the IMM, the concentration of undissociated acid is very low at physiological pH (107, 110). Evidence for the presence of a specific transporter for pyruvate was first demonstrated in 1971 when pyruvate uptake into isolated rat liver mitochondria was shown to follow saturation kinetics and to be pH-dependent, with higher pyruvate import at acidic pH (111). The finding that pyruvate transport was coupled to a proton gradient was rationalized as a way to provide actively respiring mitochondria with additional fuel in a positive feedback loop (111). Despite this evidence, some researchers remained skeptical of the presence of a pyruvate transporter until a specific chemical inhibitor (α-cyano-4-hydroxycinnamate) was identified in 1974 (112). The identification of a specific MPC inhibitor allowed for better characterization of pyruvate transport kinetics, including the ability to distinguish MPC transport activity from free diffusion of pyruvate or the activity of other transporters (113). However, the molecular identity of the MPC remained a mystery. Several

different groups worked to isolate the MPC (114, 115), including attempts to use immobilized inhibitor to purify MPC (116, 117), but none successfully identified the components of the mitochondrial pyruvate carrier.

Many researchers expected that the mitochondrial pyruvate carrier would have sequence homology to other characterized mitochondrial carriers, such as the mitochondrial carrier family (MCF), of which there are 53 members in humans that have six transmembrane domains and are 30-35 kDa in size (108, 118). Studies in yeast strains lacking the uncharacterized MCF members failed to identify the MPC, although one study identified a deletion strain lacking inhibitor-sensitive pyruvate transport (119), but this carrier was later identified as the mitochondrial NAD+ transporter in yeast (120).

Two groups, who were not actively trying to isolate the MPC, ultimately revealed the molecular identity of the MPC in 2012 (121, 122). Herzig *et al.* described that yeast strains lacking the MPC paralogs—Mpc1, Mpc2, (and Mpc3 in yeast)—had defects in lipoic acid biosynthesis and impaired pyruvate uptake into isolated mitochondria. Additionally, expression of mouse MPC1 and MPC2 in the bacteria *Lactococcus lactis* was sufficient for pyruvate uptake in a manner that was sensitive to membrane potential and to the known MPC inhibitor UK5099, an α-cyanocinnamate compound (121). Bricker *et al.* show that Mpc1 and Mpc2 are approximately 15 kDa by SDS-PAGE and that they are part of a ~150 kDa complex when separated by blue native-PAGE that does not form in the absence of Mpc2. Mpc1 and Mpc2 have two to three predicted transmembrane domains and do not have sequence homology with members of the mitochondrial carrier family. Chromatographic purification and immunoprecipitation of tagged Mpc variants demonstrated that Mpc2 and Mpc3 are the major interacting proteins of Mpc1, and Mpc1 and Mpc3 are the major interacting proteins of Mpc2 (122). Another group has found that Mpc3, a

yeast paralog that does not seem to be conserved in higher eukaryotes, is expressed under different conditions from yeast Mpc2 such that Mpc3 replaces Mpc2 under stress conditions or when high respiration rates are required (123). That tissue-specific differential regulation of MPC subunits could be a mechanism of regulating mitochondrial pyruvate uptake and mitochondrial respiratory capacity in mammals is a tantalizing possibility. There is much to be learned about the structure and function of this non-canonical mitochondrial transporter (124, 125).

1.6.3 Regulation of and Requirement for the MPC

Both Herzig *et al*. and Bricker *et al*. demonstrated that yeast lacking Mpc1or Mpc2 display growth defects on glucose media, non-fermentable carbon sources like glycerol, and a strong growth defect in the absence of leucine. Bricker *et al.* also show that loss of the MPC1 ortholog in *Drosophila* is lethal when flies are switched to a sucrose-only diet. Characterization of metabolite changes in MPC1-deficient flies revealed decreased ATP, increased glucose and pyruvate, and decreased TCA intermediates. Bricker *et al.* identified two disease-causing point mutations in human *MPC1*, and re-expression of wild-type *MPC1* was sufficient to rescue the defect in pyruvate oxidation in patient fibroblasts. Mutations in *MPC1* cause devastating multisystem metabolic deficits characterized by hyperpyruvatemia and hyperlactacidemia even on low-carbohydrate diets, resulting in neurological defects and death early in childhood (126). Previously, defects in the MPC resembled deficiencies in the pyruvate dehydrogenase (PDH) complex, but no mutations in PDH components could be identified in these patients. The determination of the molecular identity of the MPC will allow better characterization of the regulation of the MPC and may lead to therapies to enhance mitochondrial pyruvate transport and oxidation in these patients. Additionally, knowledge about the role and regulation of the MPC

may have broader implications for understanding and/or treating pathologies such as cancer, diabetes, and ischemia/reperfusion injury.

MPC1 had been previously named brain protein 44-like (Brp44L) from its abundance in brain and spinal cord cDNA libraries (127). Brp44L had also been detected at the protein level in a proteomics survey of the inner mitochondrial membrane from mouse liver (128). Brp44L (MPC1) and Brp44 (MPC2) were also detected in a proteomics study of the lysine acetylome in liver mitochondria, with one acetyl-lysine identified in MPC1 and 3 sites found in MPC2 (129). Brp44L mRNA expression has also been characterized in a model of tissue regeneration by studying expression in the spinal cord of geckos after tail amputation (127). In this study, MPC1 (Brp44L) expression was found to be highest in brain, spinal cord, and liver, and *in situ* hybridization signal was confined to gray matter of the spinal cord. Expression of Brp44L increased 3 days after amputation, was highest after one week, and began to return to lower levels two weeks after injury (127). The authors had speculated that Brp44L might be involved in promoting the apoptotic events necessary for tissue remodeling in this system. Upregulation of the mitochondrial pyruvate carrier in regenerating tissue may be essential to promote rapid proliferation and may be coordinated with mitochondrial biogenesis. It is likely that the mitochondrial pyruvate carrier plays a similar role in fetal tissues during mouse development.

2. Requirement for the MPC in Mammalian Development

Adapted from (130): Bowman CE, Zhao L, Hartung T, Wolfgang MJ. 2016. Requirement for the Mitochondrial Pyruvate Carrier in Mammalian Development Revealed by a Hypomorphic Allelic Series. *Mol Cell Biol* **36:**2089-2104.

2.1 Summary

Glucose and oxygen are two of the most important molecules transferred from mother to fetus during eutherian pregnancy, and the metabolic fates of these nutrients converge at the transport and metabolism of pyruvate in mitochondria. Pyruvate enters the mitochondrial matrix through the mitochondrial pyruvate carrier (MPC), a complex in the inner mitochondrial membrane that consists of two essential components, MPC1 and MPC2. Here we define the requirement for mitochondrial pyruvate metabolism during development with a progressive allelic series of Mpc1 deficiency in mouse. Mpc1 deletion was homozygous lethal in mid-gestation, but Mpc1 hypomorphs and tissue-specific deletion of Mpc1 presented as early perinatal lethality. The allelic series demonstrated that graded suppression of MPC resulted in dose-dependent metabolic and transcriptional changes. Steady-state metabolomics analysis of brain and liver from Mpc1 hypomorph embryos identified compensatory changes in amino acid and lipid metabolism. Flux assays in Mpc1-deficient embryonic fibroblasts also reflected these changes, including a dramatic increase in mitochondrial alanine utilization. The mitochondrial alanine transaminase, GPT2, was found to be necessary and sufficient for increased alanine flux upon MPC inhibition. These data show that impaired mitochondrial pyruvate transport results in biosynthetic deficiencies that can be mitigated in part by alternative anaplerotic substrates *in utero*.

2.2 Introduction

Embryonic development in eutherian mammals is defined by ongoing metabolic interactions between mother and fetus. Placentas evolved a sophisticated suite of adaptations to ensure adequate nutrient, gas, and waste exchange between fetus and mother, as well as hormonal and immunological communication (38, 66). To meet the fetal requirements for nutrient and oxygen consumption during pregnancy, maternal cardiac output increases such that uteroplacental blood flow accounts for ~25% of total cardiac output (16). Glucose and oxygen are arguably the two most important molecules transferred from mother to fetus, both in terms of concentration and the multitude of physiological adaptations in place to ensure their adequate transport; however, the requirement for mitochondrial oxidative metabolism during embryonic development remains poorly defined.

While oxygen tension *in utero* is low relative to atmospheric levels, measurement of oxygen consumption and lactate uptake in fetal lamb provided evidence that the fetus is a net consumer rather than producer of lactate (14). Consistent with this, fetal myocardium consumes a large amount of lactate in addition to glucose, indicating that oxidative metabolism of carbohydrate is an important energy source in developing heart (47, 48). Additionally, lactate utilization is high in neonatal brain, and the capacity for lactate import is higher in neonatal brain than in adult (43). Together, these observations provide evidence for the importance of mitochondrial oxidative metabolism early in mammalian development. Supporting these metabolic preferences, a robust period of mitochondrial biogenesis has been characterized in mid-gestation mouse embryos (63). Indeed, many mouse models deficient in genes involved in mitochondrial DNA metabolism, electron transport chain components, and mitochondrial biogenesis, fission, and fusion die during this time (embryonic day 8-13), (reviewed in (63)). These genetic models provide further evidence that mitochondrial oxidative metabolism plays an

essential role before parturition in meeting the bioenergetic and biosynthetic needs of the developing fetus. In fact, many inborn errors of metabolism in humans manifest early in postnatal life, suggesting that these metabolic insufficiencies can be somewhat mitigated *in utero* but are exacerbated after parturition in the absence of maternal exchange.

Oxygen, glucose, and lactate all coalesce at the transport and metabolism of pyruvate in mitochondria. Although the mitochondrial pyruvate carrier (MPC) has been characterized biochemically since the 1970s (111, 112), the molecular identity was only recently determined when two essential components, MPC1 and MPC2, were shown to be necessary and sufficient to promote pyruvate transport across a membrane (121, 122). Unlike any other mitochondrial transporter studied to date, yeast Mpc1 and Mpc2 are small 15 kDa proteins that are part of a 150 kDa complex in the inner mitochondrial membrane as determined by blue native-polyacrylamide gel electrophoresis (BN-PAGE) (122, 124). While pyruvate is most notable as the end product of glycolysis in the cytosol, pyruvate lies at the intersection of carbohydrate, lipid, and amino acid catabolic and anabolic pathways. The transport of pyruvate into the mitochondrial matrix permits two main biochemical pathways: 1) its oxidative decarboxylation to acetyl-coenzyme A (CoA) via the pyruvate dehydrogenase complex or 2) its carboxylation to oxaloacetate via the biotin-dependent pyruvate carboxylase. These two fates enable catabolic and anabolic pathways through the tricarboxylic acid (TCA) cycle to generate ATP and provide biosynthetic precursors of lipids and amino acids. Additionally, glucose can be derived from mitochondrial pyruvate and the cytosolic enzymes of gluconeogenesis in liver and kidney. Although the sources and fates of pyruvate depend upon cell-type-specific processes and physiological state, the transport of pyruvate across the inner mitochondrial membrane in all cells is mediated by the mitochondrial pyruvate carrier (MPC).

Here we define the requirement for mitochondrial pyruvate metabolism during eutherian development with an allelic series for Mpc1 deficiency in mouse. Using a combination of steady-state metabolomics and metabolic flux assays, we describe both tissue-specific and highly conserved compensatory adaptations to impaired mitochondrial pyruvate metabolism. Furthermore, substrate flux studies in cells derived from these genetic models define the metabolic requirement for mitochondrial pyruvate metabolism. These data provide evidence for significant crosstalk and counter-regulation between mitochondrial pyruvate utilization and other pathways of central carbon metabolism, highlighting the metabolic fate of pyruvate as a key regulatory node in carbohydrate, amino acid, and lipid metabolism.

2.3 Materials and Methods

Generation of Mpc1 conditional knock-in and deletion alleles in mice

Mpc1 knock-in mice were generated by targeting loxP sequences to introns flanking exons 3 to 5 of the mouse *Mpc1* gene and targeting a transcriptional reporter construct to the 3' untranslated region of *Mpc1* (**Fig. 2.S1A**) by homologous recombination in C57Bl/6 embryonic stem cells by standard methods. To generate mice with a germline deletion of *Mpc1*, $Mpc1^{lox/+}$ mice were bred to CMV-Cre transgenic mice, and deletion in Cre-negative F2 progeny was verified by PCR genotyping (Mpc1 D/+). Additionally, $Mpc1^{lox/+}$ mice were bred to Nestin-Cre transgenic mice to delete Mpc1 specifically in the nervous system. Mpc1 knock-in (Mpc1 KI/+), Mpc1 deletion (Mpc1 D/+) and littermate controls were housed in a facility with ventilated racks on a 14h light/10h dark cycle with *ad libitum* access to a standard rodent chow (2018SX Teklad Global, 18% protein). For timed matings, the presence of a copulatory plug in the morning was designated as 0.5 days, and pregnant females were housed separately.

Ethical Statement

All procedures were performed in accordance with the NIH's *Guide for the Care and Use of Laboratory Animals* and under the approval of the Johns Hopkins Medical School Animal Care and Use Committee.

Cell culture

Mouse embryonic fibroblasts (MEFs) were obtained from timed pregnant dams by standard methods. Primary MEFs were maintained in DMEM (25mM glucose) supplemented with 10% fetal bovine serum and 1% pen/strep antibiotic (Invitrogen) at 37°C in a humidity-controlled incubator at 10% CO_2. For cell proliferation assays, MEFs were seeded in 35mm dishes at 100,000 cells per well and cell number was counted every other day with regular media changes.

Generation of GPT KO 293s

HEK293T cells were grown in DMEM (25mM glucose) supplemented with 10% bovine calf serum and 1% pen/strep antibiotic and maintained as described above. Cells were transfected with plasmid expressing both hCas9 and hGPT1, hGPT2, or panGPT gRNA or hCas9 alone using FuGENE HD (Promega) transfection reagent according to manufacturer's instructions. Selection with 7.5 μg/mL blasticidin was started 48 post-transfection and continued for two weeks. Individual clones were selected by limited dilution plating and screened for loss of GPT1, GPT2, or both by qRT-PCR, by genomic PCR and Sanger sequencing, and by functional assay. For rescue experiments, human GPT1 and GPT2 were cloned from HEK293T cell oligo(dT)-primed cDNA, were cloned into pEF6 expression vectors by InFusion Cloning (Clontech), and were sequence verified. Alanine transaminase activity was determined by colorimetric assay (Sigma).

CRISPR/Cas9 cloning strategy

Human codon-optimized Cas9 expression vector was obtained from Addgene, plasmid #41815 (131), and hCas9 was cloned into a pEF6 expression vector, downstream and in-frame with a nuclear-localized YFP, linked by a viral 2A bicistronic peptide, such that nls-YFP and Cas9 are expressed in approximate equimolar quantities. A 3x nuclear localization signal and a FLAG tag were also appended to the C-terminus of hCas9 to allow screening for loss of Cas9 protein in mutant cell lines. Guide RNAs (gRNAs) targeting human *GPT1*, *GPT2*, and a highly conserved site in both *GPT1* and *GPT2* were designed according to the recommendations of Mali *et al.* (131) and were computed as candidate unique gRNA targets. The gRNAs, including the U6 promoter, were synthesized as 500bp gBlocks fragment (Integrated DNA Technologies) and were cloned into the pEF6-nls-YFP-2A-Cas9-3x-NLS-FLAG vector by InFusion Cloning (Clontech).

Metabolic flux assays

To measure glucose uptake, MEFs were plated in 24-well dishes and labeled with 0.5μCi [1,2-^{3}H]2-deoxy-glucose at a final concentration of 6.5mM 2-deoxy-glucose for 5, 10, and 20 minutes after 2h in KRH buffer (20mM HEPES, 136mM NaCl, 4.7mM KCl, 1.25mM $MgSO_4$, 1.25mM $CaCl_2$, 0.1% bovine serum albumin). After incubation, cells were washed 4x with KRH buffer and lysed with 0.3mL 1% TritonX-100 in PBS. Lysate was transferred to a vial containing 3mL of scintillation fluid, and counts were normalized to total protein as determined by bicinchoninic acid (BCA) assay (Thermo Scientific).

To determine substrate incorporation into the total lipid fraction, MEFs were plated in 24-well dishes and labeled with radiolabeled substrates ([2-^{14}C]pyruvate, [U-^{14}C]L-glutamine, [U-^{14}C]L-alanine, or [^{3}H]acetate) for 4h. Total lipids were extracted with 2:1 chloroform:methanol via the Folch method (132), and radioactivity was counted by liquid scintillation. For pyruvate,

glutamine, and alanine incorporation, 0.2μCi/mL of radioactivity was used, and 0.3μCi/mL for [^{3}H]acetate, in serum-free DMEM containing 2.5 mM glucose, 2 mM glutamine (or 0.5 mM cold glutamine for glutamine-labeling experiments), 0.25 mM pyruvate, and 0.1 mM L-alanine. All counts were normalized to total protein as determined by BCA assay. For pharmacological inhibition of the MPC, cells were pre-incubated with 1μM UK-5099 (Santa Cruz Biotechnology) or 0.2% (v/v) DMSO vehicle for 4 hours, and 1μM UK-5099 or DMSO was included in the labeling media.

Stable isotope labeling and LC-MS/MS Analysis

Control and Mpc1 D/D primary MEFs were labeled with 2.5mM [2-^{13}C]pyruvate (Cambridge Isotope Laboratories) in DMEM containing 2.5mM glucose, 2mM glutamine, and 0.1mM alanine for 30 minutes. Cell extracts were collected in ice-cold HPLC-grade 80:20 methanol: water with rapid quenching in liquid nitrogen. Cellular debris was pelleted by centrifugation, and the supernatant was dried by vacuum centrifugation prior to resuspension in 50% acetonitrile and analysis by LC-MS/MS. Targeted metabolic analysis were performed on an Agilent 6490 triple quadropole LC-MS/MS system with iFunnel and Jet-Stream technology (AgilentTechnologies, Santa Clara, CA) equipped with an Agilent 1260 infinity pump and autosampler. Chromatographic separation was performed on a Diamond Hydride column (150mm x 2.1 mm i.d., 4μm particle size, Microsolv, Eatontown, NJ). The LC parameters were as follows: autosampler temperature, 4°C; injection volume, 4 μl; column temperature, 35°C; and flow rate, 0.4 ml/min. The solvents and optimized gradient conditions for LC were: Solvent A, 50% methanol with 0.05% acetic acid; Solvent B, 90% acetonitrile with 10mM ammonium acetate, pH=7.0; elution gradient: 0 min 99.5% B; 12–14 min 50% B; 15–19 min 0% B; post-run time for equilibration, 5 min in 99.5% B. MS/MS experiment was performed in positive/negative

switching electrospray mode as described previously (133). The optimized operating ESI conditions were: gas temperature 230°C (nitrogen); gas flow 15 L/min; nebulizer pressure 40 psi; sheath gas temperature 350°C and sheath gas flow 12 L/min. Capillary voltages were optimized to 4000V in both modes with nozzle voltages of 2000 V. All data processing was performed with Mass Hunter Quantitative Analysis software package.

Steady-state metabolite analysis

To reliably determine the concentration of short-lived metabolites *in vivo*, e17.5 embryos were rapidly frozen in liquid nitrogen *in utero*, and tissues were collected from frozen embryos for determination of tissue-specific metabolite concentrations by enzymatic methods or by unbiased metabolomics analysis as we have done previously (134, 135). For metabolomics analysis on e17.5 brain and liver from Mpc1 KI/KI embryos and WT littermate controls (n=8 for each tissue), metabolite concentrations are expressed as fold-change over WT, and Welch's two-sample t-test was used to determine statistically significant differences between genotypes ($p<0.05$) To quantify total fatty acid content and the abundance of individual acyl species, fatty acids were measured by GC-MS as pentafluorobenzyl bromide esters with abundance normalized to protein content at the Kennedy Krieger Diagnostic Laboratory.

Steady-state lactate, ATP, glycogen, triglyceride, and cholesterol concentrations were determined from rapid frozen embryonic tissue by enzymatic assay and were normalized to protein concentration as measured by BCA assay. Lactate (Sigma), cholesterol (Wako), and triglyceride (Sigma) assays were performed according to manufacturer's instructions. Steady-state ATP was determined by a luciferase-based assay (Promega Enliten ATP assay). For glycogen measurements (136, 137), approximately 10mg of rapid frozen liver was homogenized on ice in 300 µL 2M HCl and another piece of tissue from the same liver homogenized in 300 µL 2M

NaOH. Homogenates were boiled on a 100° heat block for 5 minutes and cooled to room temperature before neutralization with an equal amount of NaOH or HCl. Samples were spun at 16,000g for 10 minutes at 4°, and supernatant was transferred to a new tube and used for glucose determination by hexokinase-coupled enzymatic assay (Sigma Glucose (HK) kit) per manufacturer's instructions. The glucose content of base-homogenized control samples was subtracted from the corresponding acid-hydrolyzed samples in order to determine glycogen content in terms of μg glucose per mg protein, as determined by BCA assay.

Immunoblotting

Tissue lysates for SDS-PAGE were prepared by homogenization of tissue in RIPA buffer (50mM Tris-HCl, pH 7.4, 150mM NaCl, 1mM EDTA, 1% Triton X-100, 0.25% deoxycholate) with protease inhibitor cocktail (Roche), followed by pelleting of insoluble debris at 13,000g for 15 min at 4°C. Protein concentrations of lysates were determined by BCA assay (Thermo Scientific), and 30μg of lysate was separated by Tris-Glycine SDS-PAGE (15% polyacrylamide), unless otherwise noted. Proteins were transferred to PVDF membranes (Immobilon), blocked in 5% nonfat-milk TBST, and incubated with primary antibodies overnight. Primary antibodies used include: We generated and validated affinity-purified rabbit polyclonal antibodies against mouse Mpc1 and Mpc2; Complex V alpha subunit (Atp5a) mouse monoclonal at 1:1000 (ab14748); aconitase 2 (Aco2) rabbit polyclonal at 1:1000 (Cell Signaling 6922); heat shock chaperone 70 (Hsc70) mouse monoclonal at 1:1000 (Santa Cruz sc-7298); MitoProfile total OXPHOS mouse monoclonal antibody cocktail at 1:500 (Abcam ab110413); phospho-mTOR (Ser2448) rabbit polyclonal at 1:1000 (Cell Signaling 5536); total mTOR rabbit polyclonal at 1:1000 (Cell Signaling 2983); phospho-AMPK (Thr172) rabbit polyclonal at 1:1000 (Cell Signaling 2535); total AMPK rabbit polyclonal at 1:1000 (Cell Signaling 5831). Cy3-conjugated anti-mouse

(Invitrogen) or Cy5-conjugated anti-rabbit (Invitrogen) secondary antibodies at 1:1500, or horseradish peroxidase (HRP)-conjugated anti-mouse (GE Healthcare NA931V) or anti-rabbit (GE Healthcare NA934V) secondary antibodies at 1:2000 were incubated with washed membranes, and proteins were visualized with Amersham Prime enhanced chemiluminescent substrate (GE Healthcare) or epifluorescence on an Alpha Innotech MultiImage III instrument. Protein abundance was quantified using Alpha Innotech FluorChem Q software (Santa Clara, CA) and was normalized to Hsc70 expression.

Quantitative real-time-PCR and mtDNA content determination

Total RNA was extracted using Trizol reagent, per manufacturer's recommendations (Life Technologies) and was further purified using the RNeasy Mini kit (Qiagen). RNA was quantified by NanoDrop, and cDNA was synthesized using random primers and MultiScribe High-Capacity cDNA reverse transcription kit (Applied Biosystems). RT-PCR was performed using 10 ng of template cDNA in a 20μL reaction using Bio-Rad SsoAdvanced SYBR Green master mix with primers specific to the genes of interest (**Table 2.1**). All PCR reactions were carried out in a Bio-Rad CFX Connect Thermocycler and were concluded with a melt-curve determination step. Expression data from mouse tissues was normalized to the average C_t values for 4 reference genes: 18S, Rpl22, β-actin, and Gapdh, and data are expressed as 2^{-dCt} and shown relative to e17.5 or relative to wild-type, as appropriate.

Genomic DNA (gDNA) was isolated from Trizol extracts as per manufacturer's recommendations, and 10 ng of template gDNA was used per 20μL reaction using Bio-Rad SsoAdvanced SYBR Green master mix with primers specific to the mitochondrially-encoded *Nd1* (NADH dehydrogenase subunit 1) and to two nuclear loci. *Nd1* abundance was calculated by the

2^{-dCt} method, relative to the average C_t value of the two nuclear reference genes, and data are expressed as fold-change relative to controls (mean ± SEM).

Mouse glucose metabolism qPCR arrays (Qiagen RT^2 Profiler PCR arrays) were prepared with 10ng template cDNA per 20µL reaction using Bio-Rad SsoAdvanced SYBR Green master mix, as per manufacturer's instructions. Gene expression was calculated relative to the provided reference genes using the 2^{-dCt} method.

Transmission electron microscopy

Liver was excised and fixed in 2% paraformaldehyde, 2% glutaraldehyde-PBS solution and was further processed with osmium tetroxide. Ultrathin sections were cut and imaged on a Hitachi 7600 TEM.

2.4 Results

Tissue-specific developmental regulation of the mitochondrial pyruvate carrier

The high dependence of the fetus on glucose metabolism and the tremendous increase in blood flow/oxygen delivery via the placenta converge at mitochondrial pyruvate metabolism. A period of robust mitochondrial biogenesis occurs during mid-gestation, coincident with the initiation of organogenesis, and persists through early postnatal life (63). Therefore, we characterized MPC expression across development by immunoblotting for mouse Mpc1 and Mpc2 in three metabolically distinct tissues (brain, heart, and liver) from late-gestation (embryonic day 17.5 (e17.5)) through the first week of postnatal life (through postnatal day 7 (P7)) and into adulthood (8 weeks) (**Fig. 2.1A**). Atp5a, a component of the ATP synthase (Complex V) and resident of the inner mitochondrial membrane, and aconitase 2 (Aco2), a

mitochondrial matrix enzyme, were used as additional markers. In all three tissues, dramatic upregulation of the mitochondrial pyruvate carrier components, Mpc1 and Mpc2, was observed across development at the level of both protein and transcript (**Fig. 2.1B**). We observed tissue-specific differences, however, in the timing of increased MPC abundance and subtle differences in the ratio of Mpc1 to Mpc2 protein across development (**Fig. 2.2A**). For example, in liver, approximately equal ratios of Mpc1: Mpc2 were seen across development. Mpc2 expression in brain was higher than Mpc1 early during development, and Mpc1 increased dramatically by P14. MPC expression in heart followed a different trend, where Mpc1 was expressed more constitutively across development while Mpc2 increased later, around P6-7. Interestingly, there were no differences detected in the ratio of Mpc1: Mpc2 in adult cerebral cortex, heart, or liver (**Fig. 2.2B**). These data show tissue-specific regulation of the mitochondrial pyruvate carrier across development.

Mpc1 is required for mammalian embryonic development and efficient pyruvate metabolism

To define the metabolic requirement for mitochondrial pyruvate metabolism *in vivo*, we generated mice with a deletion allele of Mpc1 (Mpc1 D). The last three exons (encoding 84/109 amino acids) of *Mpc1* were flanked by loxP sites that were deleted by Cre-mediated recombination in the germline to generate a line of mice carrying the Mpc1 deletion allele (**Fig. 2.S1A**). We observed expected Mendelian ratios of inheritance of the Mpc1 deletion allele in late-gestation e17.5 embryos; however, Mpc1 D/D e17.5 embryos were significantly developmentally delayed compared to wild-type (WT) and D/+ littermates and did not appear to be viable (**Fig. 2.3A and B**). These data are consistent with the deletion of other MPC components (138, 139).

Rapid cell division requires biosynthesis of nucleic acids, proteins, and lipids, and mitochondrial metabolism supports these anabolic processes (140-142). To determine the requirements for the mitochondrial pyruvate carrier in mitochondrial metabolism, we characterized the flux of radiolabeled substrates in mouse embryonic fibroblasts (MEFs) null for Mpc1. Despite the embryonic lethality, primary Mpc1 D/D MEFs were successfully isolated and cultured. Mpc1 D/D MEFs did not exhibit altered growth rates under standard culture conditions (**Fig. 2.3C**). As expected for a block in mitochondrial pyruvate metabolism and an increased glycolytic demand, Mpc1 D/D MEFs exhibited increased glucose uptake, analogous to the Pasteur effect (**Fig. 2.3D**). With few exceptions, in order for the carbons of glucose, pyruvate, or glutamine to effectively contribute to *de novo* fatty acid synthesis, these substrates must first be metabolized in mitochondria. To determine the mitochondrial flux of pyruvate and glutamine in Mpc1 D/D MEFs, we measured the rate of ^{14}C-labeled substrate incorporation into the total lipid fraction. Pyruvate contribution to the total lipid fraction was dramatically reduced in Mpc1 D/D MEFs, as expected (**Fig. 2.3E**). Glutamine incorporation was unchanged in Mpc1 D/D MEFs relative to controls (**Fig. 2.3E**), suggesting that glutamine anaplerosis was not compensating for the loss of mitochondrial pyruvate metabolism in these non-transformed cells. [^{3}H]acetate incorporation into lipid was included as a control (**Fig. 2.3E**) to demonstrate that these cells have equal capacity for *de novo* fatty acid synthesis from a substrate that does not require mitochondrial metabolism to provide cytosolic acetyl-CoA. These metabolic adaptations demonstrate the plasticity of cellular metabolism to maintain cellular proliferation in cultured cells where substrates are not limiting.

Mpc1 hypomorphic allelic series reveals requirements for mitochondrial pyruvate metabolism in embryonic development

The floxed *Mpc1* gene used to generate the deletion allele was designed to have higher utility by the introduction of a reporter in the 3' untranslated region of *Mpc1* (**Fig. 2.S1A**). Unexpectedly, inclusion of this reporter resulted in a hypomorphic allele, such that steady-state levels of Mpc1 transcript and protein were dramatically reduced in heterozygous knock-in animals (KI/+) and below the level of detection by immunoblotting in homozygous knock-in animals (KI/KI) (e.g. >30-fold suppression in heart) (**Fig. 2.4A and B**). We did not observe a loss of *Mpc2* mRNA (**Fig. 2.4B**) but Mpc2 protein was not present in the absence of Mpc1 protein (**Fig. 2.4A**). Inclusion of the reporter directly following the stop codon resulted in an allele-specific suppression of transcript abundance. To assess the degree to which Mpc1 KI/KI functionally suppresses pyruvate metabolism, we derived Mpc1 KI/KI primary MEFs and measured the contribution of radiolabeled pyruvate to *de novo* lipid synthesis. Mpc1 KI/KI MEFs had reduced incorporation of radiolabeled pyruvate into lipids but not to the same degree as Mpc1 D/D MEFs (**Fig. 2.4C**). Treatment of WT and Mpc1 KI/KI MEFs with 1μM UK-5099, a pharmacological inhibitor of the MPC, reduced pyruvate incorporation into the total lipid fraction to the same level of suppression observed in Mpc1 D/D MEFs (**Fig. 2.4C**). Consistent with an intermediate pyruvate transport capacity in Mpc1 KI/KI MEFs, these cells also exhibited an intermediary glucose uptake phenotype, more than WT but less than D/D (**Fig. 2.3D**). Although the mitochondrial pyruvate carrier could not be detected by immunoblotting, Mpc1 KI/KI mice survived through gestation and died in the early perinatal period (**Fig. 2.4D**). Consistent with the substantive anabolic role of glucose in mammalian development, late-gestation Mpc1 KI/KI homozygotes were 22% smaller than littermate controls (**Fig. 2.4E**). These data demonstrate that the Mpc1 knock-in allele is hypomorphic and significantly reduces, but does not ablate,

mitochondrial pyruvate flux. Additionally, a very small fraction of Mpc1 is sufficient for embryonic development but not perinatal survival.

Mutations in human *MPC1* cause devastating multisystem metabolic deficits characterized by hyperpyruvatemia and hyperlactacidemia, resulting in neurological defects and death early in childhood (126). Indeed, we observed an accumulation of lactate in brain of Mpc1 KI/KI e17.5 embryos with only slight elevations in liver (**Fig. 2.4F**). Fetal liver has a high degree of accessibility to the maternal circulation, and, as such, lactate levels may be more efficiently cleared from this tissue in Mpc1 KI/KI late-gestation embryos. Neither Mpc1 KI/KI brain nor liver demonstrated a suppression in ATP concentration (**Fig. 2.4G**). Consistent with these data, we did not find alterations in canonical energy sensing pathways in Mpc1 KI/KI embryos (**Fig. 2.5A**). The lactate accumulation and perinatal lethality observed in the Mpc1 hypomorph mouse model closely resemble human inborn errors in *MPC1*, and this model permits study of metabolic compensation and pathologies associated with MPC deficiency.

Next we wanted to understand if the loss of such a critical component of mitochondrial metabolism affected other mitochondrial components. We did not observe differences in mitochondrial DNA content in Mpc1 KI/KI cerebral cortex, heart, or liver compared to controls (**Fig. 2.5B**). Additionally, there were no differences in mitochondrial protein abundance in Mpc1-deficient tissues (**Fig. 2.5C**). These data suggest that canonical mitochondrial structural components remain largely intact upon MPC deficiency.

Interestingly, we observed that the severity in suppression of *Mpc1* transcript abundance in Mpc1 KI/KI mice varied in a tissue-specific manner, such that *Mpc1* transcript was most severely decreased in liver (11% remaining) while more *Mpc1* steady-state transcript remained in brain (25% remaining) (**Fig. 2.6A**). To gain perspective on the amount of *Mpc1* transcript remaining in KI brain, we crossed Mpc1 KI/+ mice to Nestin-Cre transgenic mice (134, 143) to

produce mice with tissue-specific deletion of Mpc1 in the developing nervous system. Overt phenotypes of Nestin; Mpc1 knockout (KO) late-gestation embryos, such as e17.5 body weight and perinatal survival, were not different from homozygous Mpc1 KI littermate embryos (**Fig. 2.6B**); however, *Mpc1* transcript abundance was further reduced in Nestin; Mpc1 KO cortex (<4% of WT) compared to Mpc1 KI/KI cortex (**Fig. 2.6A**). Surprisingly, given the putative dependence of the nervous system on carbohydrate oxidation, the tissue-specific deletion of Mpc1 in the nervous system was compatible with mammalian development.

In order to further define the role of Mpc1 in embryonic development we expanded the Mpc1 allelic series by crossing Mpc1 KI/+ and Mpc1 D/+ mice to generate Mpc1 D/KI mice (**Fig. 2.6C**). In liver and heart of Mpc1 KI/KI embryos, <12% of WT levels of *Mpc1* expression remained. Due to the codominant expression of the *Mpc1* gene, the deletion of Mpc1 in the context of the hypomorphic Mpc1 KI allele (D/KI) further sensitized *Mpc1* expression and suppressed *Mpc1* abundance by approximately half. This left only 7% expression of *Mpc1* in heart and liver and 15% in brain (**Fig. 2.6A**). Lowering Mpc1 expression to this degree did not further perturb embryonic development by e17.5 body weight or viability (**Fig. 2.4C and Fig. 2.S1B**). Additionally, further suppression of Mpc1 expression in D/KI embryos and tissue-specific deletion of Mpc1 in the nervous system did not affect mitochondrial DNA content (**Fig. 2.5B**) nor the abundance of mitochondrial proteins (**Fig. 2.6D**). These data further support the observation that a very small amount of pyruvate transport in mitochondria by the MPC is sufficient to enable embryonic development and does not grossly alter mitochondrial composition.

Mitochondrial pyruvate carrier deficiency alters central carbon metabolism in a tissue-specific manner *in vivo*

Pyruvate-mediated anaplerosis is particularly relevant to mammalian pregnancy that relies heavily on glucose as the main macronutrient. It is generally thought that circulating fatty acids are not readily oxidized by fetal tissue (144), although mice null for enzymes in the rate-setting step of mitochondrial β-oxidation of long-chain fatty acids (Cpt1a and Cpt1b) exhibit embryonic lethality before e10 (145, 146). The extent to which fatty acids and other lipids are able to cross the placenta and contribute to lipid accumulation in the fetus is also contended and varies from species to species (24, 147). Nevertheless, *de novo* fatty acid synthesis from glucose, due to its abundance and importance as a biosynthetic and bioenergetic substrate *in utero*, is a significant source of lipid synthesis in late-gestation embryos. Because we observed dramatic differences in *de novo* lipid synthesis from pyruvate in Mpc1 KI/KI and D/D MEFs (**Fig. 2.4C**), we hypothesized that Mpc1 KI/KI embryos may also exhibit defects in fatty acid synthesis. Indeed, we observed decreased total fatty acid content by GC-MS (**Fig. 2.S2**) and dramatically lower triglyceride levels in Mpc1 KI/KI livers, with a slight compensation via increased total cholesterol content (**Fig. 2.7A-C**). Glycogen content was not affected (**Fig. 2.7D**). Transmission electron microscopy of e17.5 Mpc1 KI livers revealed fewer and smaller lipid droplets than WT littermates (**Fig. 2.7E**). Consistent with mitochondrial protein and DNA content across tissues, there were no abnormalities in mitochondrial abundance, size, or morphology in fetal hepatocytes (**Fig. 2.7E**). Together, these results suggest that Mpc1 deficiency alters lipid metabolism *in vivo* and further underscore the notion that the MPC-dependent metabolic fate of pyruvate is an important regulatory node in central carbon metabolism.

Given the central role of mitochondrial pyruvate flux in carbohydrate metabolism, we profiled genes of glucose metabolism by qRT-PCR arrays in WT and Mpc1 KI/KI brain, heart

and liver (**Fig. 2.S3**). Although there were multiple small tissue-specific changes in several genes, the transcript for phosphoenolpyruvate carboxykinase (PEPCK), *Pck,* was consistently up-regulated across tissues. Therefore, we again took advantage of the Mpc1 allelic series to understand the role of a graded defect in Mpc1 on *Pck* expression. Interestingly, in liver, the greater suppression in *Mpc1* expression resulted in a concomitant increase in *Pck1* expression, which encodes cytosolic PEPCK (**Fig. 2.7F**). *Pck2*, which encodes mitochondrial PEPCK, also increased upon decreasing *Mpc1* expression, however not to the same extent as *Pck1* (**Fig. 2.7F**). These data are consistent with recent reports that glucose deprivation results in an increase in Pck expression (148, 149) which promotes metabolic flexibility when nutrients are limiting (150, 151). Also, these data show the utility of assessing a phenotype across a series of genetic perturbations.

To probe the global metabolic effects of loss of the mitochondrial pyruvate carrier in mammalian development, unbiased steady-state metabolomics analysis was conducted on brain and liver of late-gestation Mpc1 KI/KI and WT littermate embryos. To ensure stable steady-state measurements, the embryos were snap frozen in liquid nitrogen *in utero* and subsequently genotyped and dissected frozen. In brain and liver, 416 and 541 total metabolites were identified, respectively, and of these, 155 and 157 were found to be significantly altered between Mpc1 KI/KI embryos and WT controls ($p<0.05$ as determined by Welch's two-sample t-test). The entire list of differentially regulated metabolites is included in **Table 2.S1.** Of those metabolites differentially regulated in Mpc1 KI/KI brain, amino acid-related metabolites were over-represented as a class, while lipids were enriched among differentially regulated metabolites in liver (**Fig. 2.8A**). Furthermore, of the 86 metabolites differentially regulated in both liver and brain, 75 were changed in the same direction in Mpc1-deficient brain as in liver, highlighting that the consequences of impaired mitochondrial pyruvate metabolism are highly conserved in

embryonic brain and liver. For example, lactate and pyruvate were both dramatically up-regulated in Mpc1 KI brain and liver, with greater accumulation of these metabolites in brain than in liver (**Fig. 2.8B**), consistent with the enzymatic measurement of lactate in **Fig. 2.4F**. Steady-state concentrations of TCA cycle intermediates were down in both Mpc1 KI tissues, and glucose levels were down in Mpc1 KI liver. These observations, together with the metabolic flux data above, provide evidence for enhanced glycolysis upon impaired mitochondrial pyruvate metabolism.

Amino acids provide anaplerotic compensation upon impaired mitochondrial pyruvate transport

Several interesting changes were noted in amino acid metabolism in Mpc1 KI/KI tissues. Broadly, amino acids that are catabolized to or synthesized from TCA cycle intermediates were downregulated, while those that can be derived from glycolytic intermediates were up-regulated in both tissues (**Fig. 2.8B**). Hypotaurine, an amino acid derivative that may function as a neurotransmitter or antioxidant in addition to its role in osmolyte balance (152, 153), was the most dramatically up-regulated metabolite in Mpc1 KI/KI brain at more than 15-times the concentration in WT brain (**Fig. 2.8B**). The high levels of hypotaurine are likely a consequence of and response to the hyperosmotic stress that lactate accumulation may cause (152).

Alanine was the most dramatically downregulated metabolite in Mpc1 KI/KI brain and was also found to be significantly downregulated in liver (**Fig. 2.8B**). Glutamine was the second most-downregulated metabolite in Mpc1 KI/KI brain, and glutamate was also decreased, suggesting that Mpc1-deficiency in developing brain likely affects neurotransmitter synthesis along with macronutrient metabolism (**Fig. 2.8B**). In agreement with the changes in steady-state amino acid concentrations observed *in vivo*, alanine and glutamate were also downregulated in

primary Mpc1 D/D MEFs (**Fig. 2.8C**). Aspartate was slightly increased in Mpc1 D/D MEFs, which may be consistent with a role for cytosolic pyruvate in stimulating aspartate synthesis to enable proliferation in cells with mitochondrial deficiencies (154).

To better understand how impaired mitochondrial pyruvate transport contributed to alterations in amino acid concentrations, ^{13}C-tracer experiments were conducted on primary Mpc1 D/D MEFs. When labeled with [2-^{13}C]pyruvate, the abundance of m+1 labeled TCA cycle intermediates in Mpc1-deficient cells was decreased as expected (**Fig. 2.8D**). Additionally, labeling of amino acids that can be derived from the TCA cycle (glutamate and aspartate, for example) was reduced in Mpc1 D/D MEFs relative to WT controls. Interestingly, m+1 labeling of alanine from pyruvate was dramatically reduced along with the decrease in steady-state alanine (**Fig. 2.8D**). Alanine can be interconverted with pyruvate in either the cytosol or the mitochondrial matrix by the alanine transaminase activity of glutamic-pyruvate transaminase 1 (GPT1, cytosolic) or glutamic-pyruvate transaminase 2 (GPT2, mitochondrial), as shown in **Fig. 2.9A**. The dramatic decrease in alanine labeling from pyruvate and the low steady-state alanine levels in Mpc1-deficient cells and tissues provide evidence that mitochondrial pyruvate is a significant source of cellular alanine. Indeed, in WT MEFs, 60% of total alanine was m+1 labeled from [2-^{13}C]pyruvate, while this was decreased to just 6% in Mpc1 D/D MEFs. To further test whether low steady-state alanine concentrations were the result of increased alanine flux or decreased alanine synthesis, we measured mitochondrial flux of alanine by labeling Mpc1 KI/KI and D/D MEFs with [U-^{14}C]L-alanine and measuring incorporation into the total lipid fraction as we did previously for pyruvate and glutamine. Alanine incorporation was up-regulated in a graded manner in Mpc1 KI/KI and Mpc1 D/D MEFs greater than 7-fold (**Fig. 2.9B**), indicative of higher mitochondrial flux of alanine. We also observed that HEK293T cells treated with UK-5099 exhibited a dose-dependent suppression of [2-^{14}C]pyruvate incorporation into lipids (**Fig.**

2.S4) and recapitulated the increase in mitochondrial alanine flux that we observed in primary MEFs also in a dose-dependent manner (**Fig. 2.9C**). UK-5099 also stimulated an increase of mitochondrial glutamine flux in a dose-dependent manner in HEK293T cells (**Fig. 2.9D**) although glutamine did not contribute significantly to anaplerosis in non-transformed Mpc1 D/D MEFs (**Fig. 2.3E**). These data show that alanine represents a major compensatory substrate in mitochondrial pyruvate carrier deficiency.

We next sought to use the HEK293T system as a model to determine the relative contributions of the cytosolic (GPT1) and mitochondrial (GPT2) alanine transaminases to the observed increase in alanine flux upon impaired mitochondrial pyruvate transport. To this end, we used CRISPR/Cas9-mediated genome editing to induce loss-of-function mutations in *GPT1*, *GPT2*, and both *GPT1* and *GPT2* (pan GPT) in HEK293T cells (131). Mutant clonal cell lines were screened by genomic PCR and functional assays (**Fig. 2.S4**). Control cells (which were derived from expression of Cas9 with no gRNA), GPT1 KO, GPT2 KO, and pan GPT KO HEK293T cells were subjected to a [U-^{14}C]L-alanine to lipid incorporation assay in the presence or absence of UK-5099. In addition, pan KO cells were transiently transfected with hGPT1 or hGPT2 expression vectors and subjected to the same alanine flux assay in the presence or absence of UK-5099. Loss of GPT2 completely abrogated the UK-5099-stimulated increase in mitochondrial flux of alanine (**Fig. 2.9E**). GPT1 was found to be dispensable for this phenomenon, suggesting that GPT1 does not promote increased alanine flux by converting pyruvate into alanine upon MPC inhibition. Indeed, overexpression of GPT1 in the pan GPT null background significantly reduced alanine incorporation into lipid upon UK-5099 treatment, suggesting that the equilibrium for GPT1 lies in favor of converting alanine to pyruvate within these cells (**Fig. 2.9E**). In further support of this, overexpression of GPT1 in the pan GPT null background significantly increased glutamine incorporation into lipid upon UK-5099 treatment

(**Fig. 2.9F**). These data show that GPT2 is necessary and sufficient for increased mitochondrial flux of alanine in the absence of mitochondrial pyruvate transport. Additionally, these data suggest that the increased utilization of alanine is largely from exogenous alanine, not alanine which is derived from cytosolic pyruvate by GPT1. In this way, GPT2 might be acting to use exogenous alanine as a source for mitochondrial pyruvate rather than working in concert with GPT1 to bring carbon from pyruvate into the mitochondrion via alanine.

2.5 Discussion

The placenta segregates maternal and fetal circulation while enabling selective nutrient uptake and waste excretion between fetus and mother. The fetus is a substantial oxygen consumer and preferentially transports and utilizes glucose as its main macronutrient (reviewed in (14)). Fetal glucose and oxygen consumption converge at the transport of pyruvate into mitochondria; therefore, we targeted Mpc1, an essential component of the mitochondrial pyruvate carrier, to determine the requirements for mitochondrial pyruvate metabolism during fetal development. Due to the severe metabolic and developmental derangements observed in patients with mutations in enzymes that participate in mitochondrial pyruvate metabolism (126, 155-159) and the embryonic lethality of mouse models with null mutations in these enzymes (138, 160), we were surprised that such a small fraction of mitochondrial pyruvate metabolism was sufficient for *in utero* development. MPC deficiency was well tolerated in egg-laying *Drosophila* under standard laboratory conditions; however, these mutations were lethal when carbohydrate (sucrose) was provided as the main macronutrient (122). Mammalian pregnancy is also a carbohydrate-dominated environment; however, mammals seem to be capable of more metabolic plasticity than previously envisioned. Maternal glucose utilization is spared to provide the fetus with adequate

glucose to sustain its biosynthetic and bioenergetic needs. The inability to properly communicate and regulate glucose availability can result in adverse consequences for maternal health (e.g. gestational diabetes) and fetal wellbeing (e.g. fetal growth). It will be interesting to further delineate the contribution and convergence of maternal nutrition and fetal metabolism on pregnancy-specific pathologies and long-term health of the offspring.

To define the metabolic requirement for mitochondrial pyruvate metabolism during mammalian embryonic development, we generated mice with a null deletion of *Mpc1*. While knockout mice provide an excellent model for assigning the physiological requirement for genes involved in metabolism, we sought to determine the effect of a graded suppression of MPC *in vivo* by generating a hypomorphic allelic series. We devised a series of genetic perturbations including the null allele, a less-severe hypomorphic allele, and tissue-specific loss of Mpc1 in developing nervous system to enable a more detailed definition of gene-phenotype relationships. Indeed, we have shown that the transcriptional regulation of some genes (e.g. *Pck1*) is directly related to the degree of Mpc1 suppression in a tissue-specific manner *in vivo* (**Fig. 2.7F**). Further characterization of an allelic series may identify phenotypes that are regulated by particular metabolites in a graded fashion or by impaired metabolism in a particular tissue (161, 162). Our approach highlights the utility of genetic approaches to dissect metabolic requirements and compensatory mechanisms *in vivo*.

Human inborn errors in *MPC1* are compatible with development to term but in the absence of maternal metabolite exchange result in severe adverse consequences in the perinatal period including lactic acidosis (126). Organic acidosis can be acutely life-threatening by lowering the oxygen-carrying capacity of hemoglobin (163). In agreement with Mpc1 KI/KI embryos being in a state of metabolic acidosis, we observed a 15-fold higher hypotaurine concentration in Mpc1 KI/KI brains, a likely adaptation to the hyperosmotic stress that lactate

accumulation may cause (152). Additionally, we observed 3-fold higher heme levels in Mpc1 KI/KI liver, along with elevated biliverdin (**Fig. 2.8B**). Fetal liver is the principal site for erythropoiesis during mid- to late-gestation in mouse embryonic development (164), and the observed increase in heme likely represents a response to lactic acidosis and impaired oxygen-carrying capacity of fetal hemoglobin. While the late-gestation fetus has adaptive mechanisms to survive acute hypoxia/acidosis during parturition (165), less is known about the fetal response to chronic acidosis. Mild acidosis has been shown to reprogram mitochondrial metabolism by increasing respiratory efficiency to preserve ATP production during cellular stress (166), and it is likely that similar adaptations occur in Mpc1-deficient tissues. Our finding that 75 of 86 metabolites significantly regulated in both brain and liver of Mpc1 KI/KI embryos were regulated in the same direction suggests that the metabolic effects of MPC deficiency are largely conserved across tissues, but that some responses are tissue-specific. Among those metabolites oppositely regulated by Mpc1 deficiency in brain and liver were carnitine, an important molecule in fatty acid metabolism, and argininosuccinic acid, an intermediate in the urea cycle (**Fig. 2.8B**). The tissue-specific regulation of these molecules may reflect broader patterns of altered lipid and amino acid metabolism in Mpc1-deficient liver and brain, respectively.

High rates of metabolic flux are particularly important in rapidly dividing cells such as cancer cells and during development. Mitochondria are the principal sites of cellular energy production via the generation of ATP for all cellular compartments. Additionally, the TCA cycle provides substrates for anabolic processes in the cytosol, and, as such, substrate partitioning between mitochondria and other subcellular locations is a fundamental way to regulate mitochondrial metabolic flux. While high rates of flux are necessary to maintain rapid growth and division, the requirement for mitochondrial oxidative metabolism and anaplerosis within the mitochondria is poorly defined. For example, it has long been observed that cancer cells rely

heavily on glycolysis for ATP production (the Warburg effect); yet, even highly glycolytic cells require mitochondrial metabolic flux to provide carbon and energy equivalents for nucleotide, protein, and lipid biosynthesis (140, 141, 167-169). Indeed, in mammalian cell culture and tumor xenograft models, chemical or enzymatic depletion of mitochondrial DNA results in impaired respiratory capacity and reduced proliferation (170-173).

Deletion of Mpc1 in primary non-transformed MEFs did not affect cellular proliferation and resulted in enhanced glucose uptake (**Fig. 2.3**), consistent with the Pasteur effect, which describes the inhibitory effects of glucose oxidation on glycolysis. Interestingly, non-transformed MEFs did not exhibit enhanced anaplerosis via glutamine (**Fig. 2.3E**), although transformed cells robustly utilized glutamine and pharmacological inhibition of mitochondrial pyruvate transport further pushed this adaptation (**Fig. 2.9D**). Increased oxidative glutaminolysis and reductive carboxylation upon MPC inhibition was observed in transformed cell lines, although the relative contribution of these fates of glutamine was dependent on cell line and growth conditions (174, 175). Glutamine anaplerosis supports cellular proliferation in transformed cells, and inhibition of glutaminase or glutamate dehydrogenase sensitized cells to growth inhibition upon treatment with UK-5099 (175). Analogous to the differences in glutamine metabolism observed in primary and transformed cultured cells, glutamine seems to play a more significant anaplerotic role in the brain than in the fetal liver, as glutamine was the second most-downregulated metabolite in Mpc1 KI/KI brain. Not surprisingly, there are tissue-specific differences in anaplerosis during normal development as well. Liver-specific deletion of MPC components in mice led to defects in gluconeogenesis from pyruvate/lactate; however both glutamine and alanine were found to compensate and contribute to fasting gluconeogenesis in MPC-deficient adult liver (176, 177). We find that alanine provides a robust anaplerotic substrate in several cellular models of MPC deficiency as well as *in vivo* in embryonic brain and liver. It has been demonstrated that Mpc2-

deficient mitochondria exhibit no alterations in alanine uptake (177), and decreased steady-state alanine concentrations have been observed in several MPC-deficient cell models and *in vivo* (174, 175, 177). The decrease in steady-state alanine has been interpreted as a result of most cellular alanine being derived from mitochondrial pyruvate, but we sought to test the flux of alanine itself. In addition to demonstrating increased mitochondrial flux of alanine into lipid in MPC deficiency, we have shown by deleting the cytoplasmic and mitochondrial alanine transaminases (GPT1 and GPT2) that alanine provides a direct source of mitochondrial pyruvate dependent upon the mitochondrial GPT2 while the cytoplasmic GPT1 is dispensable for this compensation (**Fig. 2.9**). This finding is consistent with knockdown of Gpt2 in mice with liver-specific deletion of Mpc2, which further decreased blood glucose during a pyruvate tolerance test (177). Interestingly, the expression of GPT2 and several other transaminases that use glutamate as a co-substrate was found to be positively correlated with proliferative capacity in human tumors (178), and knockdown of GPT2 decreased glutamine-dependent growth in cancer cells with mutant Kras (179). Our data suggest that GPT1 may also support glutamine anaplerosis, especially upon impaired mitochondrial pyruvate transport (**Fig. 2.9F**). The GPT1-catalyzed transamination reaction in these cells seems to favor the production of pyruvate and glutamate, at the expense of alanine and α-ketoglutarate. Glutamate and α-ketoglutarate are well characterized negative regulators of glutaminase (180) and glutamate dehydrogenase (181), respectively, and the regulation of glutaminolysis by allosteric regulation and product inhibition may depend on compartment-specific concentrations of these metabolites. The GPT1 reaction could relieve inhibition of glutamate dehydrogenase or elevate glutamate levels to promote glutamine anaplerosis; however, the flux of glutamate-utilizing transaminases and glutamate dehydrogenase is likely regulated at levels beyond substrate concentrations, as recently demonstrated (178). The metabolic plasticity demonstrated by MPC-deficient and GPT-deficient cells is evidence that

mitochondria have multiple mechanisms to generate mitochondrial pyruvate and provide anaplerotic carbon from alternative substrates when glucose is limiting.

Here we have shown that, although the mammalian fetus consumes large quantities of glucose and oxygen, a surprisingly small quantity of the mitochondrial pyruvate carrier is sufficient for mammalian development. MPC-deficient cells utilize alternative anaplerotic metabolites to meet the high biosynthetic burden of highly replicative cells, and this compensation varies in a tissue-specific manner *in vivo*. Further defining the cellular and organismal requirements of macronutrient metabolism has important implications in broad areas of biology including cancer, neurochemistry, obesity and diabetes.

2.6 Acknowledgments

The authors would like to thank Ann Moser for assistance with fatty acid analysis and Mike Delannoy for help with electron microscopy studies.

3. Metabolic Response to Fasting during Pregnancy

Our mouse model of Mpc1 deficiency *in utero* revealed that a surprisingly small quantity of the mitochondrial pyruvate carrier is sufficient for mammalian development and that alternative anaplerotic substrates are able to compensate to meet biosynthetic demand. The lethality associated with severe Mpc1 deficiency is likely due to lactic acidosis, and the maternal-fetal lactate gradient steepens at parturition (61). The complete interruption of maternal-fetal metabolic exchange and communication at birth overwhelms the Mpc1-deficient neonate's ability to compensate. Among the alternative substrates that contributed to meeting metabolic demand during late gestation were amino acids and lipids. Mitochondria play a key role in regulating fuel switching and crosstalk between these major branches of macronutrient metabolism as naturally occurs during times of nutrient deprivation. In this way, mitochondria help regulate transitions between fed and fasted states to promote metabolic flexibility that capitalizes on current nutrient availability while anticipating future nutrient limitation (182). Consistent with our observations that lipids and amino acids can compensate for Mpc1-deficiency *in utero*, another group developed a model of Mpc1 deficiency and lethality during embryonic development that can be rescued by feeding the dam a ketogenic diet (183, 184). Given that the ketogenic diet is meant to imitate a low-carbohydrate time of fasting, we sought to understand the role of impaired pyruvate metabolism on the maternal and fetal response to a metabolic challenge during late gestation. We chose a 24h fast as a nutritional stress that would increase lipid availability and test the capacity of both maternal and fetal mitochondria to demonstrate metabolic plasticity in the context of impaired mitochondrial pyruvate metabolism.

3.1 Accelerated Response to Fasting in Late Gestation

Human pregnancy is characterized by greater metabolic flexibility than in the non-pregnant state in order to protect fetal growth from maternal nutrient deprivation (1). One way that this metabolic plasticity is maintained is by promoting increasing maternal serum concentrations of triglyceride, phospholipids, and non-esterified fatty acids (NEFA) throughout gestation (17). Circulating triglyceride levels, for example, increase more than 250% by the end of pregnancy, which is almost twice the post-prandial concentration in a non-pregnant individual (185). The elevated levels of circulating lipid metabolites in fasting pregnant women combined with an earlier than normal shift from glucose to fat utilization by maternal tissues has been termed "accelerated starvation" (6, 186). The acceleration is so dramatic that overnight fasting (14-18h) in normal late term pregnancy leads to serum metabolite concentrations that rival the effects of 2-3 days of starvation in non-pregnant individuals (186, 187). The features of the accelerated starvation response include increased fat mobilization from adipose, exaggerated ketone production, decreased blood glucose despite enhanced gluconeogenic capacity, and increased maternal muscle catabolism (reviewed in (6)). Increased maternal utilization of lipids as metabolic fuel spares glucose and amino acids for fetal uptake (187). Maternal hormones certainly play a role in these adaptations, but the accelerated fasting response is most apparent during late-gestation when the conceptus is large enough to challenge maternal energy reserves. Additionally, both lean and obese women exhibit the accelerated fasting response on the same timescale (187). When paired with the "facilitated anabolism" that is also characteristic of late term pregnancy, this results in a pattern of dynamic metabolic oscillations in maternal fuel utilization between fed and fasted states—all in an effort to meet immediate maternal and fetal metabolic needs and to anticipate future nutrient depletion (6).

3.2 Epidemiology of Famine Exposure in Human Populations

Impaired fetal growth may be indicative of fetal metabolic deficiency, placental aberrations, or maternal undernutrition (1). Nutrient deprivation during pregnancy has been studied in human populations experiencing famine (188, 189) or electing to fast during Ramadan (190-192). Findings from these populations suggest that nutrient limitation during early vs. late gestation may affect the nature and severity of maternal effects and postnatal outcomes. For instance, intermittent fasting during Ramadan reduced abdominal visceral fat thickness in pregnant women from 12-27 weeks gestation but was not associated with any discernable differences in fetal outcomes (191). In another study, women who observed the Ramadan fast during the second- or third-trimester had significantly less maternal weight gain than others who did not fast (192). Children born to mothers who fasted in the first trimester had lower birth weights than children born to mothers who fasted in the second or third trimesters (190). Moreover, elevated cortisol levels were measured in women who fasted, and this could contribute to the maternal and fetal differences in weight gain (193). Related to this, placental expression of 11β-hydroxysteroid dehydrogenase, which normally serves to protect the fetus from maternal glucocorticoids, is down-regulated by maternal undernutrition, especially low-protein diets (194).

The nature of nutrient deprivation experienced by populations faced with food shortages and famine is entirely different from elective fasting. From patients who endured the Dutch famine of 1944-1945, prenatal famine exposure during early gestation led to increased rates of obesity and elevated risk of cardiovascular disease while exposure during late gestation was correlated with impaired glucose tolerance in adulthood (188). Famine exposure during mid or late gestation was associated with lower birth weights, while early gestation exposure led to slightly heavier and larger babies than controls not exposed to famine (188). Low birth weight, especially when small for placental size, is strongly associated with the risk for cardiovascular

disease later in life (54). Early nutrient deprivation and the associated "catch-up" growth upon transitioning back to adequate nutrition may be particularly detrimental (195). The Great Chinese Famine of 1959-1961 affected a larger population for a longer length of time than other widely studied food shortages of the twentieth century; as a result, studies of this population have revealed more subtle effects of nutritional deficiency. For example, women who were exposed to famine as fetuses have a higher risk of metabolic syndrome than women who were exposed postnatally, and that risk is higher than for men regardless of whether they were exposed to famine prenatally or postnatally (196). Another famine cohort from the Nigerian civil war (1967-1970) also associated fetal-infant exposure to famine with increased risk of hypertension and impaired glucose tolerance as adults (197). The effects of fetal undernutrition among this sub-Saharan cohort were even more pronounced and emerged at earlier ages than European cohorts. The hypothesis of "early programming of disease" posits that many chronic adult diseases—including immune diseases, neuropsychiatric disorders, and other conditions that are not overtly "metabolic"—are in part determined by fetal and infant nutrition (1, 198). The timing and duration of undernutrition during early development greatly affect chronic disease risk and manifestation.

3.3 Fetal and Placental Responses to Fasting

Despite the multitude of adaptations in place to protect the fetus from experiencing nutrient depletion, what is the fetal response to maternal nutrient deprivation, especially that which is beyond her capacity to maintain substrates for fetal metabolism? How does the fetus sense this metabolic state? Which metabolites, endocrine molecules, and metabolic pathways contribute to the metabolic communication between mother and fetus? And what is the role of the placenta in both sensing and adapting to this affront to fetal metabolism? In this section, the

placental and fetal responses to fasting will be described in order to provide context for the genetic mouse models we have used to begin to address some of these outstanding questions in maternal-fetal metabolic communication.

As the key interface for regulation of nutrient availability during pregnancy, how the placenta responds to maternal nutrient deprivation has the potential to greatly alter fetal outcomes. The placental response could include changes to placental metabolism, changes in hormonal communication, or changes in transporter expression or activity. The timing of placental sensing and responding to maternal nutrient deprivation could occur before the fetus experiences nutrient limitation, at the same time as the fetus, or in response to fetal signals of metabolic demand not being met. One thing known about the placental response to fasting is that triglycerides accumulate, consistent with the elevation in maternal circulating lipid concentrations upon fasting (92). Studies in late-gestation pregnant rats demonstrated that placental incorporation of radiolabeled triglyceride preceded fetal incorporation of the radiolabeled lipid (75). In addition, placental glycogen stores were decreased 40% by prolonged maternal fasting (199). Select glycolytic, lipogenic, and gluconeogenic enzyme activities were measured in maternal liver, fetal liver, and placenta in fed or fasted rats. While maternal liver enzyme activities were dramatically altered by fasting, fetal liver enzyme activities were only modestly changed, and placental enzyme activities were unaffected (199). Gestational age was found to be a better predictor of placental enzymatic activity than regulation by nutritional or hormonal influences, at least in the context of these *in vitro* assays that test the enzymatic capacity of a tissue.

During maternal starvation, or during an insulin-suppressed state such as streptozotocin-induced diabetes, fetal tissues were found to accumulate lipid in concert with elevated maternal serum triglyceride concentrations, which rose two-fold in this rat model of diabetes during

pregnancy (75). A rabbit model of late-gestation maternal fasting demonstrated a similar dramatic increase in fetal lipid uptake and accumulation (29). Moreover, the fetal capacity for lipid accumulation in rats increased over the course of gestation, tripling from day 17 to day 20 of gestation (75). The accumulation of maternally-derived lipids by the fetus may represent an adaptive mechanism to protect against further nutrient deprivation *in utero* and to prepare the fetus for the possibility of nutrient deficiency after parturition. Fatty acid oxidation by the fetal liver may fuel gluconeogenesis as it does in the adult fasting liver. Although the contribution of fetal liver gluconeogenesis *in vivo* is unknown, fetal rat liver from severely fasted dams demonstrated increased activity of gluconeogenic enzymes and increased conversion of gluconeogenic substrates to glucose by tissue explants (200). A uteroplacental source of glucose during fasting in late term pregnant women has also been suggested based on umbilical vein and artery blood glucose measurements (57). The enhanced gluconeogenic potential prior to birth provides evidence for a strong demand for glucose to fuel energy production at the cost of promoting growth because fetal weight was decreased with prolonged maternal fasting in rats (200). Liver glycogen could also be an important source for endogenous glucose availability in the fetal liver during a time of nutritional challenge. Glycogen stores accumulate during the last weeks before birth in humans and are critical for the first hours of postnatal life when hormonal signals such as glucagon promote glucose mobilization from these glycogen stores before the neonate consumes any milk (24, 25). The fetus can respond to maternal fasting, and if the nutritional challenge occurs in late gestation, the method of response may greatly alter neonatal outcomes when maternal-fetal metabolic communication is interrupted at parturition.

3.4 Metabolic Derangements in Pregnancy

The previous examples demonstrate how maternal-fetal metabolic communication can be dynamic to respond to changing nutrient status, but it raises the question: What happens when metabolic communication is disrupted or metabolic/hormonal signals misinterpreted? Not only is pregnancy a nutritionally sensitive time during the life cycle, the extreme physiological demands of mammalian pregnancy may lead to gestational complications which could affect both mother and fetus. Here, some metabolic disorders of pregnancy are described with particular attention to the miscommunication driving or resulting from these conditions.

Some pathologies of pregnancy develop as a result of a mismatch between fetal demands, maternal response, and maternal capacity to meet these needs. Gestational diabetes mellitus (GDM) is the most common metabolic abnormality during pregnancy, affecting 5-9% of pregnant women in the U.S. (201). Complications of GDM include increased birth weight (macrosomia) and predisposition of the mother to develop type 2 diabetes in the future (202). Pregnancy has been described as a diabetogenic challenge where the increased glucose demand for fetal growth and development means changes in maternal metabolism to support and sustain this high glucose demand while maintaining maternal euglycemia (6). In addition, GDM has been described as a "disorder of total fuel metabolism" since all major classes of insulin-dependent substrates are affected: Overnight fasted plasma glucose, NEFA, and TG are higher in patients with gestational diabetes than in unaffected pregnant women (6). Several adaptive responses to pregnancy contribute to the development of gestational diabetes, and many of these responses are likely mediated by hormonal (mis)communication. First, pregnancy is characterized by elevated insulin secretion and decreased peripheral insulin sensitivity. There was a 50-60% decrease in insulin-mediated glucose disposal in lean women from pre-gravid to late gestation (15, 203). Pregnant women are tested for GDM with an oral glucose tolerance test at 24 to 28 weeks gestation, and a

patient is diagnosed with GDM if her blood glucose is elevated after fasting or glucose challenge (202). Elevated insulin concentrations are not part of the diagnostic criteria, but fasting plasma insulin of women with GDM during late gestation was 250% the levels of late-gestation weight-matched non-diabetic pregnant controls (204). Women with GDM also demonstrated a two-fold increase in fasting plasma insulin levels in late gestation relative to pre-gravid measurements (204). A second adaptation of pregnancy that is dysregulated in GDM is the increase in gluconeogenic capacity. Isotopic labeling studies in pregnant women have demonstrated a 30% increase in total gluconeogenesis from early to late pregnancy (11 to 34 weeks gestation) (15). Absolute rates of glucose infusion to maintain euglycemia were 22% lower in late-gestation GDM pregnancies relative to lean non-diabetic pregnant controls (203). One explanation of GDM is that gluconeogenic placental hormones outpace the ability of maternal insulin secretion (and sensitivity) to maintain euglycemia. Some studies have implicated placental growth hormone or placental lactogen as molecules which could contribute to the development and progression of GDM (5, 205). Placental lactogen increases pancreatic beta cell proliferation during pregnancy, but it remains to be determined if the increase in insulin secretion is what induces insulin resistance during gestation (5). Placental growth hormone may contribute to increased placental GLUT1 expression and fetal hyperglycemia. Diabetogenic contributions for prolactin, cortisol, and glucagon have also been described (206). Patients with GDM may manage their condition with diet and physical activity or with insulin treatment if deemed necessary. Monogenic diabetes or "mature onset diabetes of the young" (MODY), although rare and representing only 1 to 2% of diabetes cases worldwide, presents some additional challenges during pregnancy. The treatment plan for pregnant diabetics may depend on maternal response to treatment, fetal genotype, and the placental transfer of certain classes of drugs (sulfonylureas). The treatment plan may change during gestation depending on fetal growth rates and maternal glycemic control (207). Glycemic

control is an important metabolic adaptation during pregnancy that, when dysregulated, may result in gestational diabetes.

Maternal liver is one of the main tissues regulating the metabolic effects of fasting during late gestation, including gluconeogenic potential and maternal lipid availability. Several liver disorders may present during the second half of gestation including preeclampsia; hemolysis, elevated liver enzymes, and low platelet count (HELLP); intrahepatic cholestasis of pregnancy; and the rare but life-threatening acute fatty liver of pregnancy (AFLP) (208). AFLP is characterized by liver failure and microvesicular steatosis, and there is a strong genetic connection to fetal fatty acid oxidation defects, most notably long-chain 3-hydroxyacyl-CoA dehydrogenase (LCHAD) deficiency (208). *Lcad*$^{-/-}$ mice were born at lower than expected Mendelian ratios suggesting frequent gestational loss and an important role for fetal fatty acid oxidation (209). Impaired fetal fatty acid degradation generates metabolic signals that also impair lipid-handling by the mother. These complications of pregnancy demonstrate the intricate nature of maternal-fetal metabolic communication, particularly during late-gestation when fetal energy demands are highest and the maternal energy economy may be most vulnerable.

4. Mitochondrial Oxidative Metabolism Regulates Late-Gestation Maternal-Fetal Metabolic Communication

Manuscript in preparation (210): Bowman C, Selen Alpergin ES, Scafidi S, Wolfgang MJ. 2018. Mitochondrial oxidative metabolism regulates late-gestation maternal-fetal metabolic communication. *In Preparation*.

4.1 Summary

Mammalian pregnancy is perhaps the most nutritionally sensitive stage in life as all nutrients for fetal growth are provided by the mother. Glucose is the principal macronutrient available for fetal biomass accretion, and the mitochondrial metabolism of glucose-derived pyruvate supports the bioenergetic and biosynthetic needs of rapidly dividing cells. We developed a mouse model of impaired mitochondrial pyruvate metabolism by generating a hypomorphic knock-in (KI) allele of an essential component of the mitochondrial pyruvate carrier (MPC), Mpc1, which resulted in perinatal lethality (130). Late-gestation Mpc1 KI fetuses were smaller than littermates with tissue-specific compensatory changes in lipid and amino acid metabolism. To further probe the capacity for metabolic plasticity in this model, late-gestation dams were fasted for 24 hours. Maternal fasting increased serum lipid metabolites, promoted fetal liver triglyceride accumulation, and stunted fetal growth. Transcriptional changes in Mpc1 KI fetal livers resembled the wild-type response to maternal fasting, and select aspects of fetal metabolic dysfunction in this model were ameliorated by maternal fasting. To determine the contribution of maternally-derived lipids to the fetal fasting response, we used two genetic models of impaired fatty acid oxidation: (i) liver-specific loss of mitochondrial β-oxidation of long-chain fatty acids via carnitine palmitoyltransferase 2 (Cpt2) and (ii) genetic loss of a transcriptional regulator of

lipid oxidative metabolism, PPARα. Upon fasting, these mice exhibit differing degrees of hepatic lipid accumulation and impaired ketogenesis. The fetal response to maternal fasting was determined by liver transcriptional program and steady-state metabolite measurements. The maternal fasting response is a better indicator of fetal outcome than is fetal genotype, suggesting that maternally-derived factors dominate this communication. A better understanding of maternal-fetal metabolic communication may inform interventions for conditions such as gestational diabetes.

4.2 Introduction

Successful eutherian pregnancy and parturition requires metabolic, hormonal, and immunological communication between mother and fetus (4). The types and intensities of signals conveyed vary considerably across gestation, as do the responses elicited by these messages (10). Metabolic communication throughout pregnancy is essential as a growing fetus obtains all nutrients from (and excretes all wastes to) the mother. While hormonal cues from both mother and conceptus can affect nutrient mobilization, the metabolic demands of the growing fetus may also directly modify maternal metabolism and behavior (5, 6). Fetal metabolic demand is highest during late gestation, which also coincides with the highest rates of energy expenditure during pregnancy (7, 8, 26, 32, 33). Some pathologies of pregnancy develop as a result of a miscommunication over fetal metabolic demands, maternal response, and maternal capacity to meet these needs. Gestational diabetes mellitus (GDM), for example, is thought to arise from a mismatch in maternal-fetal hormonal and metabolic communication, and GDM is the most common metabolic abnormality during pregnancy, affecting 5-9% of pregnant women in the U.S. (201, 202).

There are a host of physiological adaptations in place to ensure the adequate transport of glucose and oxygen to the developing conceptus (4). While oxygen tension *in utero* is low relative to atmospheric levels, measurement of lactate uptake and utilization by fetal tissues (including fetal heart and brain) provided evidence that the fetus is a net consumer rather than producer of lactate (14, 43, 47-49). Furthermore, recent studies revealed significant lactate utilization in adult tissues, suggesting that circulating lactate is an important oxidizable substrate in mammals (50, 51). Together, these observations challenge the dogma that *in utero* development is characterized by low oxygen tension and is not conducive to mitochondrial oxidative metabolism. While this may be true during early development, once placental exchange function is developed and fetal mitochondrial biogenesis begins (63), the fetus is poised to utilize oxidative metabolism for energy production and anabolism.

The mitochondrial pyruvate carrier (MPC) facilitates pyruvate transport across the inner mitochondrial membrane and thereby represents a control point at which the metabolic fates of glucose, lactate, and oxygen coalesce. The MPC is unlike any mitochondrial carrier identified to date and is made of two essential components, MPC1 and MPC2 (121, 122). Previously, we developed a mouse model of MPC deficiency by generating a hypomorphic knock-in (KI) allele of Mpc1that results in early perinatal lethality (130). This mouse model of Mpc1 deficiency *in utero* revealed that a surprisingly small quantity of the mitochondrial pyruvate carrier is sufficient for mammalian development and that alternative anaplerotic substrates are able to compensate to meet biosynthetic demand. The lethality associated with severe Mpc1 deficiency is likely due to lactic acidosis, and the maternal-fetal lactate gradient steepens at parturition (61). The complete interruption of maternal-fetal metabolic exchange and communication at birth overwhelms the Mpc1-deficient neonate's ability to compensate. Among the alternative substrates that contributed to meeting metabolic demand during late gestation were amino acids and lipids. Mitochondria

play a key role in regulating fuel switching and crosstalk between these major branches of macronutrient metabolism as naturally occurs during transitions between fed and fasted states (182). Consistent with our observations that lipids and amino acids can compensate for Mpc1-deficiency *in utero*, another group developed a model of Mpc1 deficiency and lethality during embryonic development that can be rescued by feeding the dam a ketogenic diet (183, 184). Given that the ketogenic diet is meant to imitate a low-carbohydrate time of fasting, we sought to understand the role of impaired pyruvate metabolism on the maternal and fetal response to a metabolic challenge during late gestation. We chose a 24h fast as a nutritional stress that would increase lipid availability and test the capacity of both maternal and fetal mitochondria to demonstrate metabolic plasticity in the context of impaired mitochondrial pyruvate metabolism. Here we describe the effects of maternal and fetal mitochondrial pyruvate transport on the response to nutrient deprivation during late-gestation. A better understanding of maternal-fetal metabolic communication may inform interventions for metabolic disorders of pregnancy.

4.3 Materials and Methods

Generation of genetic mouse models

Mpc1 knock-in mice were generated by targeting loxP sequences to introns flanking exons 3 to 5 of the mouse *Mpc1* gene and targeting a transcriptional reporter construct to the 3' untranslated region of *Mpc1* by homologous recombination in C57Bl/6 embryonic stem cells by standard methods, as previously described (130). To generate mice with a germline deletion of *Mpc1*, Mpc1$^{lox/+}$ mice were bred to CMV-Cre transgenic mice, and deletion in Cre-negative F2 progeny was verified by PCR genotyping (Mpc1 D/+). A conditional knock-out (KO) allele of mouse *Cpt2*, carnitine palmitoyltransferase 2, was generated by the same approach (211-217). To generate mice with a liver-specific loss of mitochondrial fatty acid β-oxidation, *Cpt2* floxed mice

were crossed to Albumin-Cre (Alb-Cre) transgenic mice (218) to generate animals ($Cpt2^{L-/-}$) that cannot oxidize long-chain fatty acids in hepatocytes (213, 219). $PPAR\alpha^{-/-}$ mice (stock number 008154) were obtained on a C57Bl/6 background from The Jackson Laboratory and were crossed to wild-type (WT) mice for studies of heterozygotes (220). *Fgf21* floxed mice (stock number 022361) were obtained from The Jackson Laboratory and were crossed to Alb-Cre or $Cpt2^{L-/-}$ mice in order to obtain liver-specific KO of Fgf21 or liver-specific KO of both Cpt2 and Fgf21 (221).

All mutant mice and littermate controls were housed in a facility with ventilated racks on a 14h light/10h dark cycle with *ad libitum* access to a standard rodent chow (2018SX Teklad Global, 18% protein). For timed matings, the presence of a copulatory plug in the morning was designated as 0.5 days post coitus (dpc), and pregnant females were housed separately. For 24h fasting experiments, food was removed from pregnant dams at 16.5 dpc between 13:00-15:00, and tissues were collected 24h later at 17.5 dpc.

Glucose tolerance tests

Oral glucose tolerance tests were administered to pregnant dams at 17.5 dpc. Mice were fasted for 6h from 7:00-13:00, and a 2g/kg dose of glucose in 0.9% NaCl was administered orally by a straight gavage needle (bolus volume 110-120µL). Blood glucose and lactate were measured at 0, 15, 30, 60, and 120 minutes after glucose challenge, and serum was collected for insulin measurement by ELISA at 0 and 15 min (Millipore EZMRI-13K). Blood glucose and lactate were measured with a Nova Max Plus glucometer and Lactate Plus meter (Nova Biomedical, Waltham, MA).

Body composition, calorimetry, and diet studies

Body composition of 11-week old male Mpc1 D/+ mice and littermate controls was determined by magnetic resonance imaging (MiniSpec MQ10) and reported in terms of percent-body fat and lean mass. To measure whole-body calorimetry under chow-feeding, fasting, and re-feeding, 12-week old male Mpc1 D/+ mice and littermate controls were individually housed in Comprehensive Laboratory Animal Monitoring System cages (OxyMax Equal Flow, Columbus Instruments) on a 12 hour light/dark cycle. O_2 consumption and CO_2 production were measured every 24 minutes, and food intake, water intake and ambulation were measured continuously. After a 2-day acclimation period, data were collected for 48 hour *ad libitum* feeding followed by a 24-hour fast. After re-feeding and a short 6-hour fast, the mice were subjected to an intraperitoneal glucose tolerance test (2g/kg body weight) to determine energy expenditure and respiratory exchange ratio (RER) (VCO_2/VO_2) in response to the glucose challenge. Five days later, the glucose tolerance test was repeated and blood glucose and lactate measurements were recorded from tail vein samples at 0, 15, 30, 60, and 120 minutes upon glucose administration after a 4h fast.

For high-fat diet studies, male Mpc1 D/+ mice and littermate controls were placed on a 60% (kcal%) high-fat diet D12492 (Research Diets, Inc., New Brunswick, NJ) from ages 6 wks to 18 wks. At 10 wks on the diet, an intraperitoneal glucose tolerance test (0.75g/kg body weight) was administered after a 4h fast, and at 12 wks on the diet an intraperitoneal insulin tolerance test was administered after a 4h fast (0.6 U/kg body weight). Body composition was determined by MRI, as above, and tissues were collected at 14wks on the high-fat diet after a brief 4h fast.

Ethical Statement

All procedures were performed in accordance with the NIH's *Guide for the Care and Use of Laboratory Animals* and under the approval of the Johns Hopkins Medical School Animal Care and Use Committee.

Serum and tissue metabolite measurement

Serum metabolites were determined by enzymatic, colorimetric assays, according to the manufacturer's instructions: β-hydroxybutyrate (Stanbio B-HB LiquiColor Assay, EKF Diagnostics, Boerne, TX), NEFA (NEFA-HR(2), Wako Diagnostics, Richmond, VA), triglyceride (TR0100, Sigma-Aldrich, St. Louis, MO). Placental and liver triglyceride content was also determined by enzymatic measurement after chloroform: methanol (2:1 (v/v)) extraction, drying, and resuspension in 3:1:1 (v/v/v) t-butanol: methanol: Triton X-100. Triglyceride levels were normalized to protein content as determined by bicinchoninic acid (BCA) assay (Thermo Fisher Scientific). Tissue lactate concentrations were determined enzymatically after homogenizing frozen tissues in lactate assay buffer on ice and were normalized to protein content (MAK065, Sigma-Aldrich, St. Louis, MO).

For ^{1}H-NMR of tissue and serum metabolites, extraction was performed as previously reported (219). For ^{1}H-NMR of cell extracts, mouse embryonic fibroblasts (MEFs) were washed with ice-cold PBS and scraped into ice-cold methanol and snap frozen in liquid nitrogen before two additional freeze-thaw rounds with methanol extraction (222). Cell extracts were subjected to a final spin at 15,000g for 1 min at 4°C, then the supernatant was dried under vacuum and the extract resuspended in 20 mM phosphate buffer, pH 7.4 ± 0.1, with 0.1 mM TMSP as an internal reference and 0.1 mM sodium azide. ^{1}H spectra were recorded on a Bruker Avance III 500MHz (Bruker Instruments, Germany) NMR spectrometer, operating at 499.9MHz and equipped with

room temperature quadruple nuclei probe. Typical ^{1}H spectra were acquired using presaturation solvent suppression pulse sequence (noesyprld). Acquisition parameters were set as follows; spectral width of 8012.820 with a 64K data points, 512 scans, with a relaxation delay of 7s for a total collection time of 1.14h. Samples were automatically tuned and match, and shimmed to TMSP signal. Spectra were exported into Bruker format and were processed with Chenomx NMR Suit 8.2 Professional (Chenomx Inc, Edmonton, Alberta, Canada). TMSP signal (0.0 ppm) was used as a reference peak, spectra manually phase corrected and spline function was applied for the baseline correction. Metabolites were profiled and quantified using built-in Chenomx 500MHz library. Metabolite concentrations were normalized to protein content.

Cell culture

Mouse embryonic fibroblasts (MEFs) were obtained from timed pregnant dams by standard methods. Primary MEFs were maintained in DMEM (25mM glucose) supplemented with 10% fetal bovine serum and 1% pen/strep antibiotic (Invitrogen) at 37°C in a humidity-controlled incubator at 10% CO_2. For ^{1}H-NMR of cell extracts, cells were switched to serum-free DMEM containing 2.5mM glucose, 2.5mM pyruvate, and 2mM glutamine in the presence or absence of 1mM D,L-β-hydroxybutyrate (Sigma-Aldrich, H6501) for 24h before collection of cell extracts for steady-state metabolite measurements as described above.

Immunoblotting

Tissue lysates for SDS-PAGE were prepared by homogenization of tissue in RIPA buffer (50mM Tris-HCl, pH 7.4, 150mM NaCl, 1mM EDTA, 1% Triton X-100, 0.25% deoxycholate) with protease inhibitor cocktail (Roche) and PhosSTOP phosphatase inhibitor (Roche), followed by pelleting of insoluble debris at 13,000g for 15 min at 4°C. Protein concentrations of lysates

were determined by BCA assay (Thermo Scientific), and 30µg of lysate was separated by Tris-Glycine SDS-PAGE (15% polyacrylamide), unless otherwise noted. Proteins were transferred to PVDF membranes (Immobilon), blocked in 5% nonfat-milk TBST, and incubated with primary antibodies overnight. Primary antibodies used include: We generated and validated affinity-purified rabbit polyclonal antibodies against mouse Mpc1 and Mpc2 (130); heat shock chaperone 70 (Hsc70) mouse monoclonal at 1:1000 (Santa Cruz sc-7298); acyl-CoA thioesterase 1 (Acot1) rabbit polyclonal at 1:1000 (abcam ab133948); phospho-S6 (Ser240/244) ribosomal protein rabbit polyclonal at 1:1000 (Cell Signaling 2215); S6 ribosomal protein (total S6) rabbit polyclonal at 1:1000 (Cell Signaling 2217); phospho-ACC (Ser79) rabbit polyclonal at 1:1000 (Cell Signaling 11818), total ACC rabbit polyclonal at 1:1000 (Cell Signaling 3676); glutamic-pyruvate transferase 1 (Gpt1) rabbit polyclonal at 1:1000 (abcam ab154034); aspartate aminotransferase 1 (Got1) rabbit polyclonal at 1:1000 (Novus NBP1-54778); fibroblast growth factor 21 (Fgf21) goat polyclonal at 1:2000 (R&D Systems AF3057); acetyl-lysine rabbit polyclonal at 1:1000 (Cell Signaling 9441). Cy3-conjugated anti-mouse (Invitrogen) or Cy5-conjugated anti-rabbit (Invitrogen) secondary antibodies at 1:1500, or horseradish peroxidase (HRP)-conjugated anti- -rabbit (GE Healthcare NA934V) or anti-goat (Millipore AP180P) secondary antibodies at 1:2000 were incubated with washed membranes, and proteins were visualized with Amersham Prime enhanced chemiluminescent substrate (GE Healthcare) or epifluorescence on an Alpha Innotech MultiImage III instrument. Protein abundance was quantified using Alpha Innotech FluorChem Q software (Santa Clara, CA) and was normalized to Hsc70 expression.

Quantitative real-time PCR

Total RNA was extracted using Trizol reagent, per manufacturer's recommendations (Life Technologies) and was further purified using the RNeasy Mini kit (Qiagen). RNA was

quantified by NanoDrop, and cDNA was synthesized using random primers and MultiScribe High-Capacity cDNA reverse transcription kit (Applied Biosystems). RT-PCR was performed using 10 ng of template cDNA in a 20μL reaction using Bio-Rad SsoAdvanced SYBR Green master mix with primers specific to the genes of interest (**Table 4.1**). All PCR reactions were carried out in a Bio-Rad CFX Connect Thermocycler and were concluded with a melt-curve determination step. Expression data from mouse tissues was normalized to the average C_t values for 4 reference genes: 18S, Rpl22, β-actin, and Gapdh, and data are expressed as 2^{-dCt} and shown relative to wild-type or fed controls, as appropriate.

Histology

Livers were collected in formalin (10%, neutral buffered), paraffin-embedded, sectioned, and stained with hematoxylin and eosin (H&E) (AML Laboratories, Inc.).

Acylcarnitine analysis of blood and liver

Acylcarnitine abundances were determined from dried blood spot samples (223, 224) or from frozen liver, as previously described (213, 219). Tissues acylcarnitine concentrations were normalized to frozen tissue weight. Briefly, samples were methanol extracted and butylated in the presence of acid, further extracted, and analyzed on an API 3200 (AB SCIEX) operated in positive ion mode, with a precursor ion scan for m/z 85, which is a characteristic product ion of butyl ester acylcarnitine species.

4.4 Results

Maternal response to nutrient deprivation with impaired mitochondrial pyruvate transport.

The rapidly growing fetus requires a continuous delivery of glucose and oxygen that places an incredible demand on maternal metabolism. The metabolism of glucose and oxygen converge at the transport of pyruvate into mitochondria via the Mitochondrial Pyruvate Carrier (MPC). We previously showed that late-gestation (e17.5) fetuses with a hypomorphic knock-in (KI) allele of Mpc1 exhibited impaired growth and lactic acidosis (130). To understand the role of impaired pyruvate metabolism on the maternal and fetal response to a metabolic challenge during late gestation, we subjected both wild-type (WT) and Mpc1 KI heterozygous ($Mpc1^{KI/+}$) pregnant dams to a 24 hour period of food deprivation from 16.5 to 17.5 dpc. $Mpc1^{KI/+}$ dams have a 50% reduction in Mpc1 and Mpc2 protein expression in liver in both the fed and fasted state (**Fig. 4.1A**). The 24 hour starvation paradigm induced an 8% loss in maternal body weight in both genotypes (**Fig. 4.S1A**). We observed that 24 hour food deprivation was sufficient to stunt fetal growth of WT and KI/+ littermates while $Mpc1^{KI/KI}$ fetal body weights were not further perturbed by maternal fasting (**Fig. 4.1B**). Maternal nutrient deprivation also reduced the average body weight of WT fetuses from WT dams (**Fig. 4.S1B**). Maternal blood glucose was suppressed by fasting, independent of Mpc1 expression (**Fig. 4.1C**), and blood lactate levels were not altered (**Fig. 4.S1C**). Fasting induced a marked upregulation of circulating β-hydroxybutyrate in both WT and $Mpc1^{KI/+}$ dams (**Fig. 4.1C**), consistent with the accelerated fasting response observed during pregnancy (6, 187). Serum non-esterified free fatty acid (NEFA) levels were also up-regulated by fasting, and $Mpc1^{KI/+}$ dams exhibited a slight decrease in circulating NEFA concentrations relative to WT dams (**Fig. 4.1C**). Consistent with this, liver triglyceride content in $Mpc1^{KI/+}$ dams was lower than WT dams with no difference in serum triglycerides (**Fig. 4.S1C**). Additionally, the induction of several fasting-regulated gene products involved in nutrient sensing

was blunted in the livers of $Mpc1^{KI/+}$ dams (**Fig. 4.S1D,E**). Together, these data suggest that $Mpc1^{KI/+}$ dams rely more on the utilization of fatty acids as an alternative energy source upon impaired mitochondrial pyruvate metabolism, as others have implicated in non-pregnant rodent models of MPC deficiency (176, 177, 225, 226).

We reasoned that the high glucose demands of mammalian pregnancy may reveal differences in whole-body glucose homeostasis beyond what was observed in non-pregnant Mpc1-deficient mice in response to fasting or diet challenges. Non-pregnant mice heterozygous for Mpc1 deletion ($Mpc1^{D/+}$) did not exhibit differences in body weight, body composition, energy expenditure, or glucose tolerance (**Fig. 4.S2A-C**). Upon a 12-week high-fat diet challenge, $Mpc1^{D/+}$ mice responded similarly to littermate controls (**Fig. 4.S2D-E**). Others have demonstrated that a whole-body hypomorphic allele of Mpc2 leads to defects in glucose homeostasis (138), and liver-specific loss of Mpc1 or Mpc2 leads to defects in gluconeogenesis (176, 177). Heterozygosity for Mpc1 deletion is less severe than the Mpc2 hypomorph or tissue-specific loss-of-function, and no significant differences were observed in Mpc1 D/+ mice. Glucose production and disposal are dramatically different during mammalian pregnancy in order to ensure sufficient nutrient delivery to the developing conceptus without compromising maternal health and fecundity (10, 11, 15). The high glucose demands of pregnancy may provide an additional metabolic stressor in the context of impaired mitochondrial pyruvate metabolism. To test this, $Mpc1^{KI/+}$ and WT pregnant dams were subjected to an oral glucose tolerance test at 17.5 dpc. Healthy pregnancy has been characterized as a state of glucose intolerance, and $Mpc1^{KI/+}$ dams were found to be slightly less glucose intolerant than WT dams (**Fig. 4.1D**). $Mpc1^{KI/+}$ dams were more prone to have higher blood lactate concentrations during the duration of the glucose tolerance test, similar to non-pregnant $Mpc1^{D/+}$ mice subjected to an acute glucose challenge (**Fig.**

4.S2C,E). These data show that pregnancy potentiates metabolic dysfunction upon impaired Mpc1 function.

Mpc1 hypomorphic fetuses exhibit a fasting metabolic program.

In $Mpc1^{KI/KI}$ hypomorphic fetal liver, the expression of both components of the MPC, Mpc1 and Mpc2, was below the level of detection by immunoblotting (**Fig. 4.2A)**. Maternal fasting does not alter the expression of these components. Previously, we observed that the expression of several genes that are regulated by fasting in adult liver were up-regulated in an Mpc1 dose-dependent manner in fetal liver (130). Interestingly, this same set of genes, including *Pck1*, *Acot1*, and *Cpt1b*, were up-regulated to the same degree by fasting in WT fetal liver (**Fig. 4.2B**). Maternal fasting did not further increase the expression of these genes in $Mpc1^{KI/KI}$ hypomorphic fetuses. The expression of these same genes was also increased during the normal course of late-gestation (**Fig. 4.2C**), consistent with a PPARα-dependent transcriptional program initiated in late gestation (227). Together, these data suggest that when mitochondrial pyruvate metabolism is impaired, the fetal liver initiates an alternative metabolic program similar to the fetal response to maternal fasting and approaching a liver transcriptome that is poised for independent life after parturition.

Maternal fasting rescues metabolic dysfunction in Mpc1 hypomorphic fetuses.

To better characterize nutrient allocation between the maternal and fetal compartments, we compared steady-state maternal serum metabolites and maternal liver and fetal liver metabolites by ^{1}H-NMR metabolomics. Consistent with the decrease in blood glucose and increase in serum β-hydroxybutyrate upon fasting, concentrations of these metabolites in maternal liver were similarly regulated (**Fig. 4.S1F**). As expected, $Mpc1^{KI/KI}$ fetal livers exhibited

elevated lactate relative to WT littermates. Interestingly, maternal fasting rescued the lactic acidosis in $Mpc1^{KI/KI}$ fetal liver by reducing lactate concentrations to WT levels (**Fig. 4.2D**). $Mpc1^{KI/KI}$ fetal brain lactate concentrations were also ameliorated by maternal fasting, while lactate levels in heart tissue were not regulated by maternal nutritional status (**Fig. 4.2E**). Fetal liver aspartate was also high in $Mpc1^{KI/KI}$ fetuses and was suppressed by fasting similar to liver lactate concentrations (**Fig. 4.2D**). Fasting induced a greater than 5-fold increase in β-hydroxybutyrate (βHB) levels in fetal liver, and $Mpc1^{KI/KI}$ fetal livers had slightly higher concentrations than WT littermates (**Fig. 4.2D**). To test whether βHB contributed to the fasting-induced suppression of lactic acidosis, WT and Mpc1 deletion mouse embryonic fibroblasts (MEFs) were cultured in the presence or absence of 1mM βHB for 24h, and steady-state lactate concentrations were measured. Consistent with its role as a fasting-induced alternative oxidative substrate, βHB treatment was sufficient to rescue lactate accumulation in cells lacking the MPC (**Fig. 4.2E**). These data are consistent with the finding that a maternal ketogenic diet can rescue fetal lactic acidosis and developmental delay in another model of impaired MPC function (183). Together, these data show that maternal fasting can ameliorate fetal defects in mitochondrial pyruvate metabolism.

Fasting induces adipose triglyceride mobilization and subsequent hepatic ketone generation. To begin to understand the role of the enhanced lipid mobilization during pregnancy (20, 21), we measured several indicators of fetal lipid metabolism during maternal fasting. First, we observed that placental triglyceride content was increased upon fasting in placentae from both $Mpc1^{KI/+}$ and WT dams, but fetal genotype did not affect placental TG levels (**Fig. 4.2F**). Fetal liver triglyceride content, however, depended on fetal genotype (**Fig. 4.2F**). Previously, $Mpc1^{KI/KI}$ late-gestation fetal livers were shown to have significantly lower triglyceride content in the fed state (130). Maternal fasting increased fetal liver triglyceride levels in $Mpc1^{KI/KI}$ fetuses, but WT

littermates did not demonstrate increased lipid accumulation during a maternal fast. WT fetuses from WT dams, however, did acquire more liver triglyceride upon fasting (**Fig. 4.2F**), likely consistent with the higher circulating NEFA in WT fasted dams relative to $Mpc1^{KI/+}$ dams (**Fig. 4.1C**). Despite the observed changes in liver triglyceride content, there were no obvious structural differences in WT and $Mpc1^{KI/KI}$ fetal livers (**Fig. 4.2G**). These data show that maternal fasting can alter lipid metabolism within the fetal compartment.

Maternal lipid metabolism drives the fetal response to fasting.

To determine the contribution of maternal lipid metabolism to the fetal response to fasting, we used a genetic model of impaired fasting—liver-specific loss of mitochondrial β-oxidation of long-chain fatty acids via carnitine palmitoyltransferase 2 (Cpt2) (213, 219). Cpt2 catalyzes an obligate step in the mitochondrial import of long-chain fatty acids and is encoded by a single gene, which makes it a genetically tractable target to block mitochondrial β-oxidation. Mice with liver-specific loss of Cpt2 ($Cpt2^{L-/-}$) have massive hepatic lipid accumulation and impaired ketogenesis upon fasting with, surprisingly, no defects in gluconeogenic capacity (213). Female mice homozygous for the floxed Cpt2 allele (ff) were crossed to males with albumin-driven Cre recombinase expression (C;ff), and C;ff females were crossed to ff males, such that both ff and C;ff fetuses could be studied from control Cpt2 ff or mutant $Cpt2^{L-/-}$ (C;ff) dams (**Fig. 4.S3A**). Cpt2 ff and $Cpt2^{L-/-}$ dams were subjected to 24h food deprivation from 16.5 to 17.5 dpc, and, remarkably, $Cpt2^{L-/-}$ dams were able to maintain blood glucose concentrations to the same level as fasted ff dams (**Fig. 4.3A).** Consistent with a defect in liver fatty acid oxidation, however, $Cpt2^{L-/-}$ dams could not produce β-hydroxybutyrate (βHB) during a fast, and circulating βHB levels in fasted $Cpt2^{L-/-}$ dams were even lower than fed ff controls (**Fig. 4.3A**). Fasting also induced triglyceride accumulation in maternal liver (**Fig. 4.S3B**), and fasting $Cpt2^{L-/-}$ dams had

elevated circulating free fatty acid and triglyceride concentrations (**Fig. 4.3A**, **Fig. 4.S3B**). Altogether, the impaired ketogenesis, hepatic lipid accumulation, and elevated circulating lipid metabolite concentrations of $Cpt2^{L-/-}$ dams provide a useful model of impaired maternal fasting to better understand the fetal response to maternal nutrient deprivation.

In the model of impaired maternal fasting by liver-specific deletion of Cpt2, fasting reduced late-gestation fetal body weights to the same extent as had been observed in WT litters, with no effect of fetal or maternal genotype (**Fig. 4.3B**). Importantly, loss of mitochondrial β-oxidation of long-chain fatty acids in fetal liver did not alter βHB concentrations as determined by ^{1}H-NMR (**Fig. 4.3C**). Instead, fetal liver βHB levels reflected maternal circulating concentrations such that fetuses from fasted $Cpt2^{L-/-}$ (C;ff) dams had levels as low as fetuses from fed dams of either genotype (**Fig. 4.3C**). Fetal liver triglyceride content was also increased upon maternal fasting, but there was no significant effect of fetal or maternal genotype (**Fig. 4.3D**). Fetal liver and placental triglyceride content were tightly correlated, and triglyceride content was not increased in tissues from fetuses of fasted C;ff dams, despite their having higher circulating concentrations of free fatty acids and triglycerides (**Fig. 4.3D**). Although liver triglyceride content was unaffected by fetal or maternal genotype, the transcriptional response to maternal fasting was highly dependent on maternal genotype but not fetal genotype (**Fig. 4.3E**). The mRNA abundances of several fasting-regulated genes (*Acot1*, *Acot2*, and *Pdk4*) were increased in fetal liver in response to maternal nutrient deprivation. While fetuses from fasted ff dams responded similarly to WT fetuses from WT fasted dams, both ff and C;ff fetuses from fasted C;ff dams had significantly higher induction of these fasting-regulated genes than litters from ff dams (**Fig. 4.3E**). This suggests that there may be some molecular signal whose presence or absence in fasted $Cpt2^{L-/-}$ dams promotes the exacerbated fasting transcriptional program observed in fetuses exposed to this intrauterine environment.

To further determine the effects of altered maternal lipid metabolism on fetal response, we sought to characterize the abundance of a class of molecules that can serve as substrates for the enzymatic function of Cpt2: the long-chain acylcarnitines. Cpt2 catalyzes the transacylation of long-chain acylcarnitines to become long-chain acyl-CoAs in the mitochondrial matrix; therefore, loss of Cpt2 would be expected to increase long-chain acylcarnitine concentrations. Acylcarnitines can be transported out of cells and into the circulation, and the profiling of acylcarnitine species is useful for the diagnosis of certain metabolic disorders including impairments in fatty acid oxidation (228). We measured both maternal blood acylcarnitines and fetal liver acylcarnitines from ff and C;ff dams in both the fed and 24h fasted state (**Fig. 4.4A-B**). Similar to $Cpt2^{L-/-}$ mice on a ketogenic diet, pregnant $Cpt2^{L-/-}$ mice had elevated circulating long-chain acylcarnitine concentrations during fasting and suppressed short-chain acylcarnitines such as C2 (acetylcarnitine) (213). Additional short-chain acylcarnitines (C4, C5), which are derived from amino acid catabolism, were also down-regulated in $Cpt2^{L-/-}$ circulation. Free carnitine concentrations (C0) were also suppressed in $Cpt2^{L-/-}$ dams, both in the fed and fasted state (**Fig. 4.4A**), consistent with previous observations that the abundance of long-chain acylcarnitines may be driving a systemic carnitine deficiency (213).

We reasoned that comparing maternal blood acylcarnitines to fetal liver acylcarnitines may reveal patterns of similar regulation among classes of acylcarnitines while differences may highlight fetal liver-autonomous responses to maternal fasting. Indeed, we observed similar patterns of suppressed carnitine and acetylcarnitine (C2) in fetal livers from C;ff dams (**Fig. 4.4B**). Again, fetal genotype did not affect acylcarnitine concentrations, and all ff and C;ff fetuses from the same intrauterine environment had the same acylcarnitine profiles. Interestingly, C4 and C5 acylcarnitines were elevated in fetal livers from ff dams upon fasting, suggesting that the increase of these species is part of the WT response to maternal nutrient deprivation. C4 and C5

acylcarnitines were not induced to higher levels in fetuses from fasted C;ff dams. These short-chain acylcarnitines may be derived from amino acid catabolism, particularly of branched-chain amino acids. Interestingly, while the concentrations of isoleucine, leucine, and valine were slightly up-regulated in fetal liver upon fasting, steady-state concentrations of these amino acids were further increased in fetal livers from fasted C;ff dams, despite lower concentrations of the acylcarnitines that can be derived from these amino acids (**Fig. 4.4C**). Again, this response was independent of fetal genotype. The upregulation of these particular amino acids in fetal liver while maternal circulating concentrations of the corresponding acylcarnitines are unchanged may point to a fetal liver-autonomous response to maternal fasting.

Long-chain acylcarnitine abundances were up-regulated in fetal liver from fasted ff dams, consistent with the increases in maternal circulating concentrations in response to fasting (**Fig. 4.4B**). Interestingly, however, long-chain acylcarnitine abundances in fetal livers from C;ff dams were not increased to the extent that is seen in maternal blood (**Fig. 4.4A**). One reason for this may be increased maternal utilization of long-chain acylcarnitines by tissues other than liver in fasted $Cpt2^{L-/-}$ dams. Alternatively, the lower concentrations of long-chain acylcarnitines in fetal liver from fasted $Cpt2^{L-/-}$ dams could be indicative of impaired fatty acid catabolism in the fetal liver, perhaps related to the lower free carnitine levels observed in these livers. Acylcarnitines are an important class of metabolites regulated by maternal fasting that could participate in mediating metabolic communication between mother and fetus.

Loss of hepatic fatty acid oxidation improves maternal glucose tolerance.

Since glucose is one of the most important metabolites made available for fetal uptake and metabolism, we next characterized maternal glucose homeostasis via an oral glucose tolerance test in late-gestation pregnant liver-specific Cpt2 KO mice. We had previously shown

that chow-fed Cpt2L$^{-/-}$ mice exhibit a modest improvement in glucose tolerance which becomes more apparent upon high-fat feeding (219). Much of this effect can be attributed to impaired hepatic gluconeogenic capacity in liver-specific Cpt2 KO mice, despite their ability to maintain euglycemia during a fast. Pregnancy is also a state of enhanced hepatic gluconeogenic capacity and transient maternal insulin resistance to promote glucose availability for fetal uptake. Late-gestation Cpt2L$^{-/-}$ dams at 17.5 dpc exhibited improved glucose clearance relative to ff controls (**Fig. 4.5A**). Glucose-stimulated insulin secretion was lower in Cpt2L$^{-/-}$ dams, suggestive of enhanced insulin sensitivity in combination with the improved glucose tolerance (**Fig. 4.5B**).

The secreted hepatokine Fgf21 is known to modulate glucose homeostasis (229), and, previously, *Fgf21* mRNA in liver and circulating Fgf21 were found to be dramatically up-regulated in Cpt2L$^{-/-}$ mice, particularly in response to fasting (213, 219). Fgf21 is known to be regulated by PPARα and to play an important role in pro-catabolic states such as fasting (230, 231). Interestingly, we observed no difference in circulating Fgf21 between ff and C;ff dams in the fed state, but upon fasting, serum Fgf21 levels were halved in C;ff dams but unchanged in ff dams (data not shown). Liver Fgf21 transcript abundance followed this same trend, but suppression of *Fgf21* transcript in fasted C;ff liver was even greater with levels just 30% of controls (data not shown). The failure to induce Fgf21 upon fasting during pregnancy may be consistent with the massive up-regulation in Fgf21 expression that has been observed in late-gestation pregnant mice (232). Liver expression of Fgf21 was 60-fold higher and serum Fgf21 was more than 8-fold higher in late-gestation mice than in non-pregnant controls (232). We reasoned that elevated Fgf21 during pregnancy may contribute to impaired glucose tolerance. To test the contribution of Fgf21 to glucose homeostasis during late gestation, we generated mice with liver-specific KO of Fgf21 as well as mice with liver-specific loss of both Fgf21 and Cpt2 (221). When subjected to an oral glucose tolerance test at 17.5 dpc, we observed that loss of

Fgf21 did not affect glucose homeostasis and that double-knockout of Fgf21 and Cpt2 did not modify the enhanced glucose tolerance of liver-specific Cpt2 KO mice (**Fig. 4.5C**). The contribution of elevated Fgf21 to metabolic adaptation during pregnancy remains to be determined.

The fetal response to fasting is Pparα-dependent and regulated by maternal metabolism.

We next turned our attention to another model of impaired fatty acid oxidative metabolism, mice with whole-body deletion of the transcriptional regulator PPARα (220). Many of the genes observed to be transcriptionally regulated in fetal liver in response to impaired mitochondrial pyruvate metabolism or in response to maternal fasting are canonical PPARα target genes. Late-gestation fetuses with heterozygous and homozygous PPARα deletion from PPARα$^{-/-}$ dams exhibited a decrease in body weight comparable to WT litters upon subjecting the dam to 24h food deprivation (**Fig. 4.6A**). Moreover, PPARα$^{+/-}$ and PPARα$^{-/-}$ fetuses from PPARα$^{-/-}$ dams were no smaller than the same fetal genotypes from PPARα$^{+/-}$ dams. To examine the intersection of maternal fasting metabolism and fetal liver response, fasting-regulated gene induction was measured in fed and fasted fetal livers from WT dams, PPARα$^{+/-}$ dams, and PPARα$^{-/-}$ dams (**Fig. 4.6B**). All genes shown in Fig. 4.6B demonstrated PPARα-dependent fasting induction in that PPARα$^{-/-}$ livers failed to induce expression of these genes upon fasting. Interestingly, although not induced by fasting, *Acot1* and *Acot2* were higher in PPARα$^{-/-}$ fed livers than WT or PPARα$^{+/-}$ livers. While the fetal liver transcriptional response to fasting requires PPARα, the effect of the intrauterine environment is also important for eliciting these responses. Remarkably, all genes tested were more robustly induced in PPARα$^{+/-}$ fetal livers from fasted PPARα$^{-/-}$ dams than from fasted PPARα$^{+/-}$ dams. This suggests that a maternally-derived signal from models of impaired fasting can potentiate the fetal liver response to maternal nutrient deprivation. This is consistent

with the $Cpt2^{L-/-}$ model in which fetuses from fasted $Cpt2^{L-/-}$ dams had higher liver expression of certain fasting-regulated transcripts than fetuses from fasted ff control dams (**Fig. 4.3E**).

4.5 Discussion

Eutherian pregnancy is characterized by greater metabolic flexibility than in the non-pregnant state in order to protect fetal growth from maternal nutrient deprivation (1). Here, we have subjected mouse models of impaired carbohydrate and lipid metabolism to metabolic challenge during late-gestation in order to determine both the maternal and fetal effects of impaired mitochondrial oxidative metabolism. Consistent with studies in fasted pregnant rats, we observed decreased fetal body weights, dramatic increases in maternal circulating ketone levels, and increased placental and fetal lipid accretion (29, 75, 92, 200). Our genetic models provide further insight into the metabolic factors behind these outcomes. For example, fasting-induced increases in placental and fetal liver triglyceride content were higher in WT dams relative to Mpc1-deficient dams, and these changes were proportional to maternal circulating free fatty acid and triglyceride concentrations. In addition, in a model of impaired hepatic ketogenesis by liver-specific deletion of Cpt2, fetal liver concentrations of β-hydroxybutyrate were directly related to maternal circulating concentrations, and the capacity for fetal liver fatty acid oxidation made no contribution to ketone levels. The dramatic increase in circulating ketones is one hallmark of the "accelerated starvation" response of pregnancy (6, 186). We demonstrate that maternal liver fatty acid oxidation, in combination with increased serum concentrations of triglyceride, phospholipids, and non-esterified fatty acids (NEFA), may help mediate this metabolic adaptation. Levels of these metabolites increase over the course of gestation, and circulating triglyceride levels, for example, increase more than 250% by the end of pregnancy, which is

almost twice the post-prandial concentration in a non-pregnant individual (17, 185). The increase in concentrations of these lipids and lipid-derived metabolites is so dramatic that overnight fasting (14-18h) in normal late term pregnancy leads to serum metabolite concentrations that rival the effects of 2-3 days of starvation in non-pregnant individuals (186, 187). Fasting during pregnancy results in an earlier than normal shift from glucose to fat utilization by maternal tissues to spare glucose and amino acids for fetal uptake (187), and mitochondrial metabolism is an important regulator of these changes in substrate utilization.

Maternal hormones certainly play a role in the adaptive response to fasting, but accelerated fasting is most apparent during late gestation when the conceptus is large enough to challenge maternal energy reserves. Fetal signals may also contribute, as suppressed insulin and elevated glucagon were measured in fetal circulation upon maternal nutrient deprivation (200). In addition, another endocrine molecule that has been shown to promote the accelerated maternal fasting response during pregnancy is delta-like homolog 1 (DLK1). Loss of DLK1 increased adiposity in females before pregnancy, and circulating levels of DLK1 increased 5-fold in the first two weeks of mouse pregnancy (233). The majority of circulating DLK1 during pregnancy is from the fetus, and females without pregnancy-associated DLK1 failed to up-regulate ketogenesis during a fast (233). However, other secreted molecules that regulate fuel utilization in adult animals may have different roles during pregnancy. For instance, serum Fgf21 concentrations increase 8-fold over the course of mouse gestation (232), but we have found that liver-derived Fgf21 does not alter maternal glucose homeostasis during late gestation. Loss of hepatic fatty acid oxidation by liver-specific deletion of Cpt2, however, does improve maternal glucose tolerance. This is likely due to an impaired capacity for hepatic gluconeogenesis by maternal liver without Cpt2, as enhanced gluconeogenesis during pregnancy may contribute to the transient glucose intolerance and insulin resistance of pregnancy. In addition, long-chain acylcarnitines have been

associated with insulin resistance, but it is unclear if these molecules play a role in promoting insulin resistance or are simply evidence of impaired metabolic plasticity (234). Serum samples from pregnant women undergoing an oral glucose tolerance test around 25 weeks gestation revealed a decrease in several medium- and long-chain acylcarnitine species upon glucose administration, as expected (235). Although acylcarnitine species were not associated with glucose intolerance in this cohort, several triglyceride species were found to be correlated with gestational diabetes status in these women (235). Long-chain acyl-CoAs, diacylglycerides, ceramides, and triglycerides have all been implicated in lipotoxic mechanisms of insulin resistance as these molecules are up-regulated in models of diet-induced obesity as a result of metabolic overload (236). It is interesting that, despite having elevated concentrations of long-chain acylcarnitine species, pregnant mice with liver-specific deletion of Cpt2 have better glucose homeostasis than controls. This finding suggests that hepatic gluconeogenesis may be a larger contributor to glucose intolerance during pregnancy than particular classes of lipids or impaired hepatic fatty acid oxidative metabolism.

Hepatic lipid metabolism is a critical regulator of the maternal response to fasting during pregnancy. Rates of mitochondrial β-oxidation of [U-^{14}C]palmitate to acid-soluble products by mouse liver mitochondria decreased by 50% during late gestation relative to non-pregnant controls (237). Similarly, rates of [^{14}C]CO_2 exhalation from gastric administration of uniformly labeled or 1-^{14}C-labeled fatty acids were also decreased in pregnant dams (237). A challenge of these experiments is the proper dosing of fatty acids with increased maternal body weight and also increased endogenous circulating lipid levels during late gestation. Nevertheless, this study suggests that maternal liver fatty acid oxidation may change over the course of gestation, consistent with a changing role of and demand for lipids and lipid-derived metabolites by the developing fetus. It is well known that fatty acid oxidation fuels gluconeogenesis and that

maternal gluconeogenic capacity increases over the course of gestation. Isotopic labeling studies in pregnant women have demonstrated a 30% increase in total gluconeogenesis from early to late pregnancy (11 to 34 weeks gestation) (15). It is unclear, however, to what extent placental or fetal gluconeogenesis could contribute to meet metabolic demand. A few reports provide evidence for glucose production by the placenta, but the capacity for and regulation of this potential source of increased glucose production during late gestation is not well understood (56, 57). Fetal liver extracts have demonstrated increased PEPCK and glucose-6-phosphatase activity upon fasting. In addition, fetal liver explants demonstrated increased lactate, alanine, serine, and glycerol conversion to glucose (200). This capacity is consistent with our observation that *Pck1* expression in fetal liver increased upon fasting and with increasing gestational age. Furthermore, *Pck1* was still induced in fetal livers with impaired fatty acid oxidation, but it is unclear to what extent fetal liver fatty acid oxidation may contribute to meeting the energetic and reducing power needed to fuel gluconeogenesis. These studies suggest that during late gestation and upon extreme maternal fasting it is possible to prematurely implement fetal gluconeogenesis, a capacity that is normally reserved for the early postnatal period after the maternal fuel supply has been interrupted at birth (24). The increase in *Pck1* expression suggests that disruption of maternal nutrient supply and metabolic communication by a severe fast is sufficient to induce these adaptations in the fetus.

Although deletion of Cpt2 in fetal liver did not affect triglyceride content, acylcarnitine abundance, β-hydroxybutyrate levels, or the fetal liver transcriptional program, it is significant that fetal liver acylcarnitine concentrations largely reflected maternal circulating acylcarnitine abundances. Studies in humans demonstrated that carnitine levels in cord blood are higher than in maternal blood and that pregnant women have lower free carnitine concentrations than non-pregnant women (91, 238). These data are strong evidence for placental transport and fetal accumulation of these molecules. Remarkably, placental carnitine concentrations were found to

be more than 7-fold higher than in heart or any other tissue tested (239). Free carnitine accounts for 85% of placental total carnitines (53% of total placental carnitines in humans (240)), and deletion of the carnitine transporter OCTN2 (Slc22a5) in mouse reduced placental carnitine concentrations to less than 10% of wild-type levels (239). In addition to the placental transport of maternal acylcarnitines, we also observed some species of acylcarnitines that were selectively up-regulated in the fetal liver, for example C4 and C5 short-chain acylcarnitines were increased upon fasting in fetal liver only. These molecules may be derived from amino acid catabolism, and fasting led to significant increases in circulating total amino acid concentrations in both maternal and fetal circulation (200). Related to fetal capacity for amino acid catabolism and biosynthesis, we observed that *Glud1*, which encodes glutamate dehydrogenase, was down-regulated while *Got1*, a cytosolic aspartate aminotransferase, was up-regulated by fasting in fetal liver (**Fig. 4.2A,B**). Counter-regulation of these two enzymatic activities has been previously described in the context of the transition from proliferation to quiescence in order to ensure non-essential amino acid biosynthesis by the transaminases during proliferation (178). As pharmacological inhibition of the mTOR pathway has been linked to increased *Glud1* and decreased transaminase expression (178), the regulation in fetal liver may be consistent with mTOR activation; however, preliminary studies revealed no evidence for mTOR activation in fetal liver upon maternal fasting (data not shown). Moreover, $Mpc1^{KI/KI}$ fetal livers demonstrated a trend toward increased Got1 expression, and this could be related to the elevated aspartate levels observed in this model. GOT1 promoted aspartate consumption in nutrient replete conditions and was required for aspartate production in the context of impaired electron transport chain function (154). Interestingly, the elevated aspartate observed in $Mpc1^{KI/KI}$ fetal livers was decreased back to WT levels in response to maternal fasting.

Importantly, lactate accumulation in Mpc1-deficient fetal tissues was rescued to WT levels upon maternal fasting. Using mouse embryonic fibroblasts with Mpc1 deletion, we demonstrated that the addition of 1mM D,L-β-hydroxybutyrate for 24h was sufficient to rescue lactate accumulation in this culture model. Ketones can serve as alternative oxidative substrates for mitochondrial metabolism during fasting, and concentrations of ketones in the maternal circulation are dramatically up-regulated as part of the accelerated fasting response. We demonstrated that loss of fatty acid oxidation in fetal liver did not affect concentrations of β-hydroxybutyrate (βHB), but that fetal liver concentrations were largely reflective of maternal circulating levels. Consistent with this, maternal fasting was found to increase the capacity for βHB transport in late-gestation microvillous membrane vesicles isolated from rat placenta (241). Towards a mechanism for how the presence of ketones could affect lactate concentrations, a study of first-trimester human trophoblasts demonstrated that ketones decreased glucose uptake in a dose-dependent manner (242). Also, the presence of βHB and acetoacetate could alter NAD^+/NADH redox balance and regulation of lactate dehydrogenase, pyruvate dehydrogenase, and other cellular dehydrogenases. Although the capacity for ketogenesis from medium- and long-chain fatty acids was low in hepatocytes from newborn fetal rat liver, fatty acid oxidation and ketogenesis increased in fasted neonatal liver relative to newborn controls (243). Nevertheless, the capacity to utilize maternally-derived ketones may be intact before birth, and ketones may represent an important oxidative substrate for the fetus during maternal nutrient limitation.

In addition, fetal utilization of lactate could be another way in which steady-state lactate levels are reduced by maternal fasting. Umbilical uptake of oxygen and glucose were found to be 45% and 75% lower, respectively, than the total uterine uptake in sheep, suggesting significant glucose oxidation by the placenta (59). In an ovine model of impaired placental growth, oxidative

metabolism of glucose by placenta was impaired, but lactate efflux to the umbilical vein was increased and fetal lactate consumption increased as a result (60). In late gestation, maternal gluconeogenesis is elevated to ensure adequate glucose supply to the fetal compartment, and lactate is an important gluconeogenic substrate. However, only 40-50% of lactate was used for gluconeogenesis in late-gestation pregnant rats, as compared to 70-80% in non-pregnant rats, suggesting that fetal utilization of lactate may account for the difference (27). Studies in fetal lamb confirm that lactate concentrations are higher in fetal umbilical vein than in fetal artery, again consistent with the fetus being a net consumer of lactate (61). Recent magnetic resonance imaging studies using hyperpolarized [1-^{13}C]pyruvate administered to late-gestation pregnant rats resulted in clear placental localization of signal as well as evidence of conversion to [1-^{13}C]lactate and [1-^{13}C]alanine in maternal organs and in placenta. Importantly, the intensity of the [1-^{13}C]lactate signal from placenta was lower in a rat model of preeclampsia, and this reduction in signal is not due to changes in placental perfusion but rather likely represents impaired placental metabolism of pyruvate (62). Together, these observations challenge the dogma that *in utero* development is characterized by low oxygen tension and is not conducive to mitochondrial oxidative metabolism. While this may be true during early development, once placental exchange function is developed and fetal mitochondrial biogenesis begins (63), the fetus is poised to utilize oxidative metabolism for energy production and anabolism.

Together, our genetic mouse models of impaired mitochondrial pyruvate and fatty acid metabolism demonstrate the importance of mitochondrial oxidative metabolism in regulating both the maternal and fetal response to nutrient deprivation. Despite the nutritionally-sensitive nature of this stage in mammalian development, there exists remarkable metabolic plasticity and crosstalk among these major pathways of central carbon metabolism. Maternal-fetal metabolic communication helps ensure adequate nutrient exchange and is particularly important during

times of nutrient limitation. Miscommunication may result in metabolic complications during pregnancy including gestational diabetes, and promoting healthy maternal-fetal metabolic communication may prove an important therapeutic approach for metabolic disorders of pregnancy.

4.6 Future Directions

To address the sufficiency of β-hydroxybutyrate to suppress fetal lactate accumulation in the Mpc1-deficient mouse model, pregnant dams will be infused with β-hydroxybutyrate (βHB) or PBS using Alzet osmotic minipumps implanted subcutaneously early in gestation (244). We expect the infusion of βHB will largely recapitulate the effects of maternal fasting on fetal metabolism in Mpc1-deficient fetal tissues. The same approach can be used in the liver-specific Cpt2 loss-of-function mouse model, with the expectation that βHB infusion will largely rescue the metabolic and transcriptional defects in fetuses from liver-specific Cpt2 KO dams. Additionally, a dietary rescue approach could be attempted using a diet rich in medium-chain fatty acids to restore ketogenesis in the Cpt2 KO liver, as medium-chain fatty acids do not require the carnitine shuttle system to gain access to the mitochondrial matrix. Finally, we are using a genetic approach to define the contributions of liver fatty acid oxidation to maternal adaptation in Mpc1-deficient pregnant dams by generating double knockout mice such that dams heterozygous for Mpc1 deficiency will also have liver-specific loss of Cpt2. We expect that loss of Cpt2 on top of Mpc1 deficiency may prevent the rescue of fetal lactate concentrations by maternal fasting. Furthermore, heterozygosity for Mpc1 may affect the capacity of other tissues to compensate for the loss of liver fatty acid oxidation.

To further address the metabolic fates of mitochondrial pyruvate, the lab has acquired a hypomorphic allele and a floxed allele of pyruvate carboxylase (Pcx). The loss-of-function allele

and liver-specific deletion of pyruvate carboxylase will be used to probe the developmental and metabolic requirements for mitochondrial pyruvate-mediated anaplerosis during fetal development and the maternal response to fasting. Preliminary data suggests that the whole-body hypomorphic allele results in early postnatal lethality, consistent with the prognosis for human patients with mutations in *PCX* (245-247). This allele may help define the contribution of mitochondrial pyruvate and Pcx-derived oxaloacetate to fetal growth and *de novo* lipogenesis. In addition, this model can be used to determine the contribution of maternal and fetal gluconeogenesis during maternal nutrient deprivation. We expect impaired gluconeogenesis in liver-specific Pcx KO dams, which may result in elevated rates of ketogenesis as a compensatory mechanism.

In addition, we would like to address how the intrauterine environment primes the neonate for early postnatal life. Preliminary studies on the effects of maternal contributions to early postnatal metabolism are addressed in the next section.

4.7 Acknowledgments

Thank you to Ebru Selen Alpergin for conducting and analyzing ^{1}H-NMR spectra on maternal serum, fetal liver, and MEFs, and thanks to Susanna Scafidi for acylcarnitine analysis on maternal blood and fetal liver.

5. Maternal Lipid Metabolism Directs Postnatal Metabolism

Not only does the transition to independent life at birth initiate dramatic changes in neonatal metabolism as compared to fetal metabolism, but maternal whole-body metabolic homeostasis and energy budgets shift during the transition from pregnancy to lactation, too. Here we describe both the maternal and neonatal changes in energy metabolism after parturition and we examine preliminary studies of impaired neonatal metabolism in our mouse models of impaired fatty acid oxidation.

5.1 Maternal Metabolic Changes Support Lactation

After parturition, neonatal mammals receive nutritional support from the mother's milk. While there are vast differences across species in how independent and precocious the neonate is, what the nutrient content of milk is, how milk composition changes over lactation, and how long is the duration of lactation, all mothers must adopt new strategies to meet the metabolic demands of lactation. These strategies may change maternal energy expenditure, mobilization of adipose stores, and metabolic/hormonal communication to coordinate milk production.

Two of the primary hormones that promote and regulate lactation are prolactin and oxytocin, secreted by the anterior and posterior pituitary, respectively (4). Prolactin works in concert with insulin and cortisol to promote milk fat and milk protein production by the secretory cells of the mammary gland. Oxytocin is part of the neuroendocrine loop that promotes milk expression (4). Fgf21 is another secreted molecule recently implicated to play metabolic regulatory roles in pregnancy and lactation based on studies in whole-body Fgf21 knockout mice (248, 249). In mice, hepatic Fgf21 expression increases throughout the course of pregnancy (232), and Fgf21 levels remain 2.4-fold higher than non-pregnant, non-lactating levels by 7 days of lactation and remain high, even three weeks after weaning (249). Fgf21 was required for

pregnancy-induced cardiac remodeling (248), and a comprehensive study of bone remodeling during lactation found that Fgf21 KO mice were protected from loss of bone mass during lactation (249). It is unknown whether Fgf21 could play additional roles in mediating changes in maternal energy expenditure during pregnancy and lactation, although we have shown that liver-derived Fgf21 does not affect maternal glucose homeostasis during late gestation.

In humans, maternal energy expenditure and basal metabolic rate were higher during pregnancy than during lactation, based on longitudinal studies conducted in late-gestation pregnant women and then 3 and 6 months postpartum in both lactating and non-lactating mothers (33). Lactating mothers also had higher energy expenditure and basal metabolic rate than non-lactating mothers, and the higher respiratory quotient and net carbohydrate utilization measured in pregnancy was also sustained during lactation (33). This suggests that the increased energy costs of milk synthesis by mammary gland are largely met with glucose. Maternal blood glucose is the precursor for the synthesis of lactose, the major carbohydrate found in human milk (4). Butte and King offer a comprehensive review on human energy expenditure and energy requirements during lactation (250).

In small mammals, lactation is more energetically expensive than pregnancy (251). In rodents, in particular, hyperphagia meets the increased energy demands of lactation. In addition, rodents exhibit suppressed brown adipose tissue thermogenesis and enhanced mobilization of maternal adipose depots that also contribute to meeting the high metabolic demand of lactation (251). Because marsupials are born at a much earlier stage of development, lactation plays a greater role in marsupial development, emulating later stages of eutherian *in utero* development (45). Remarkably, some pinnipeds do not eat during lactation, and, in these species, mobilization of maternal fat stores is the principal or only route for funding milk production (252, 253). These

examples highlight some of the extreme metabolic adaptations in place to support lactation and its key role in early postnatal development across mammalian species.

Given that the largest proportion of calories in the milk of many species comes from lipids (254), we turn our attention back to maternal adipose tissue and lipid mobilization. Despite the increased metabolic demand of lactation in small mammals, overall efficiency of energy utilization does not change over the course of pregnancy/lactation (251). Brown adipose tissue thermogenic activity, however, is reduced during lactation, as a result of decreased sympathetic activation. Expression of the mitochondrial uncoupling protein, *Ucp1*, was decreased in the brown adipose tissue of mice during early lactation (249). It has been proposed that this "functional atrophy" of brown adipose tissue provides a net savings in energy expenditure that can reduce the energy requirements of lactation (251). Another way to reduce the energy costs of lactation is to mobilize adipose stores to fuel milk production. During pregnancy, the concentrations of circulating lipid metabolites increase over the course of gestation (17). While maternal serum triglyceride concentrations drop after parturition, lactation further decreases circulating triglyceride levels to pre-conception levels by 8 to 12 weeks after birth (185). This suggests that tissue-specific utilization of VLDL for milk synthesis by the mammary gland could underlie the decrease in circulating TG during lactation. The use of preformed fat should be more biochemically efficient for milk production than *de novo* lipogenesis or utilization of dietary fats, for example (250). The life histories, neonatal requirements, and dietary patterns of different species affect the sources and amounts of lipids that contribute to milk production (254).

5.2 Metabolic Adaptations of Early Postnatal Life

While dogma posits that fetal metabolic needs are largely met by glucose, we have observed remarkable metabolic plasticity during late-gestation fetal development that permits compensation by amino acid and lipid utilization, particularly during times of nutrient deprivation (130, 210). Some of these fetal metabolic adaptations hint at an accelerated shift towards a metabolic program that resembles postnatal metabolic strategies. Here we describe some of the key adaptations in neonatal metabolism that promote energy acquisition from a high-fat milk diet.

At birth, maternal and fetal metabolic exchange is immediately interrupted. As such, neonates must rely on glucose mobilized from glycogen stores or produced from gluconeogenesis in the early postnatal period before suckling begins (24). Elevated glucagon (and decreased insulin) is an important metabolic signal that increases neonatal liver glycogenolysis and gluconeogenic flux. The activities of key gluconeogenic enzymes, including pyruvate carboxylase, phosphoenolpyruvate carboxykinase, and glucose-6-phosphatase, increase after birth (24). In neonatal liver, as in adult liver, fatty acid oxidation provides the energy to fuel gluconeogenesis. In the early postnatal period, lipolysis from adipose depots provides this fuel, as demonstrated from increased circulating free fatty acids and ketones after birth, particularly in human neonates with adequate adipose depots at birth (17). Measurement of oleate oxidation from fetal hepatocytes vs fasted newborn hepatocytes demonstrated increased fatty acid oxidation at later postnatal ages. The increase in fatty acid oxidation was concurrent with decreased *de novo* lipogenesis and lower levels of malonyl-CoA, which serves as a negative allosteric regulator of CPT1 of the carnitine shuttle for long-chain fatty acid import by mitochondria (255).

Once milk consumption begins, dietary fats are used to fuel fatty acid oxidation for ketogenesis and to support gluconeogenesis if dietary carbohydrates from milk are low. Importantly, young neonates are heavily reliant on carnitine provided from the mother's milk

until the capacity for carnitine biosynthesis by the liver fully develops (238). The importance of milk in providing carnitine is evident in mice lacking the carnitine transporter OCTN2, which only survive 3 to 4 weeks (at the time of weaning) unless carnitine supplementation is administered (239). These mice deficient in carnitine transport, which limits carnitine availability both from diet and from endogenous synthesis in the liver, have severe hepatic steatosis and cardiomyopathy, as to be expected with severe defects in fatty acid oxidation (239). Dietary sources of carnitine are also important in adult humans, as 75% of carnitine comes from the diet (238), but the dietary significance of carnitine is particularly important during early postnatal development. Systemic levels of carnitine are balanced by ingestion/intestinal uptake; biosynthesis in liver; uptake/release by other tissues; and clearance by kidney. Newborn urine contains higher levels of acetylcarnitine than free carnitine, and this trend is reversed in adults, suggesting that when the neonate is dependent on mother's milk for carnitine, free carnitine concentrations are carefully guarded (256). Carnitine supplementation for neonates with metabolic acidurias may assist in urinary clearance of some of these metabolites as carnitine esters (238). Carnitine supplementation has also been recommended for low birth weight neonates, as carnitine can enhance fatty acid oxidation and increase ketogenesis (238, 256). The importance of ketones as a metabolic substrate for neonates will be addressed in the next section. It would be interesting to determine the effect of carnitine on fatty acid utilization and fetal growth in the Mpc1-deficient mouse model. Our plans to generate Mpc1; Cpt2 double knockout mice may address some of these questions as dams heterozygous for Mpc1 with liver-specific deletion of Cpt2 would be expected to have lower carnitine and impaired ketogenesis. Maternal administration of carnitine would be another way to determine the effects of carnitine on fetal outcomes.

Ketones, products of mitochondrial β-oxidation of fatty acids, are an important oxidizable substrate during times of nutrient deprivation but also throughout early postnatal development as the neonate consumes a high-fat milk diet. We have demonstrated that fetal uptake of β-hydroxybutyrate (βHB) is based on maternal circulating concentrations and that endogenous fatty acid oxidation does not contribute appreciably to βHB levels in fetal liver (210). Administration of a ketogenic diet during gestation can alter fetal and neonatal brain structures (183, 184). Rather unexpectedly, ketogenic feeding of lactating dams was associated with increased risk of fatal ketoacidosis during lactation in wild-type mice, and removal of the suckling neonates was sufficient to reverse and prevent critical ketoacidosis (184). This highlights the extreme metabolic demand that lactation places on maternal metabolism. In terms of neonatal metabolism, ketogenesis from dietary milk is particularly important during the early postnatal period and ketogenic capacity declines at weaning and the transition to a high-carbohydrate diet (144). The developing brain is particularly reliant on ketones for energy production (43), although the contribution of local ketone production vs peripheral ketogenesis is another question of interest in the Wolfgang laboratory. In addition to the utilization of ketones, it has been shown that astrocytes in the developing rat brain have the capacity for long-chain fatty acid oxidation and the expression of genes involved in mitochondrial β-oxidation of long-chain fatty acids are increased over early postnatal development and may be correlated with increased concentrations of long-chain acylcarnitines in brain tissue (257). The genetic requirement for ketone oxidation by peripheral tissues has been characterized using mouse models of tissue-specific deletion of *Oxct1*, the succinyl-CoA transferase that mediates the first step in ketone oxidation (258-260). Remarkably, while whole-body impairment in ketolysis is lethal within 48h of birth, tissue-specific deletion of this enzyme in neurons, cardiomyocytes, or skeletal myocytes is permissive

for neonatal life, and adult tissue-specific Oxct1 KO mice tolerate starvation with only modest increases in ketone levels (260).

Altogether, these observations and genetic models demonstrate the importance of fatty acid oxidation, ketogenesis, and gluconeogenesis during the early postnatal period when neonatal metabolism relies on high-fat milk. To specifically understand the role of liver mitochondrial β-oxidation of long-chain fatty acids during early postnatal metabolism, we have begun to study neonatal mice at postnatal day 2 with liver-specific deletion of carnitine palmitoyltransferase 2, Cpt2, born to and reared by WT or liver-specific Cpt2 KO dams. This is a logical continuation of our studies *in utero* in which we can decipher maternal and fetal effects in response to metabolic challenge. Here, maternal effects and neonate-autonomous effects are being described based on cross-fostering experiments in which pups born to WT dams are switched to being reared by liver-specific KO dams (and *vice versa*) on the day of birth. There are many interesting questions about fetal-neonatal metabolic transitions as well as the transition from pregnancy to lactation that can begin to be addressed using these genetic models.

5.3 Maternal-Dependent Regulation Persists to the Early Postnatal Period

To determine the requirements for hepatic mitochondrial β-oxidation of long-chain fatty acids in early postnatal metabolism, mice with liver-specific deletion of Cpt2 and littermate controls were born to and reared by $Cpt2^{L-/-}$ (C;ff) and ff control dams. By postnatal day 2 (P2), ff and C;ff pups born to C;ff dams were significantly smaller than ff pups born to ff dams (**Fig. 5.1A**). There was also a trend toward lower blood glucose and decreased milk consumption, as measured by stomach weight, in pups reared by C;ff dams (**Fig. 5.1A**). There was a slight but not significant increase in liver triglyceride content in C;ff pups compared to ff controls reared by ff

or C;ff dams (**Fig. 5.1B**). Despite this, livers of P2 C;ff pups were noticeably paler than ff livers, and more lipid-laden as can be seen from histological sections of these livers (**Fig. 5.1C**). Postnatal day 2 was chosen as an endpoint because PPARα$^{-/-}$ mice were found to have marked hepatic lipid accumulation by P2 (227), as we have also observed (**Fig. 5.1B**).

We next measured the gene expression for two genes which are known to be highly up-regulated in adult Cpt2 KO liver upon fasting, *Acot1* and *Fgf21* (213). Acot1 was up-regulated at both the transcript and protein level in C;ff livers (**Fig. 5.1D,E**). This transcriptional response in P2 liver represents the earliest significant difference observed between ff and C;ff livers, as all fetal outcomes measured were unaffected by fetal genotype (210). The up-regulation of Acot1 by neonatal liver is likely PPARα-independent, as PPARα$^{-/-}$ neonates also demonstrated increased expression of *Acot1* (**Fig. 5.1D**). The expression of *Fgf21*, on the other hand, was highly PPARα-dependent, as others have also shown in neonatal liver (227, 261). *Fgf21* expression was barely detectable in PPARα$^{-/-}$ liver, and levels in pups born to C;ff dams were equally low (**Fig. 5.1D**). *Fgf21* expression was slightly higher in C;ff pups relative to ff pups. Remarkably, when pups born to C;ff dams were cross-fostered to ff dams on the day of birth, Fgf21 expression was markedly increased over pups reared by C;ff dams (**Fig. 5.1D**). Similarly, when pups born to ff dams were cross-fostered by C;ff dams, there was a slight suppression in Fgf21 expression (**Fig. 5.1D,E**). Acot1 followed a similar trend in that it was robustly induced in litters born to C;ff dams but cross-fostered to ff dams (**Fig. 5.1E**). These findings suggest that maternal effects communicated via milk can override neonatal transcriptional responses programmed from development *in utero*.

We also measured the abundances of blood acylcarnitines in P2 pups, as is routinely done to screen for inborn errors of metabolism (228). Interestingly, despite differences in liver transcriptional responses between ff and C;ff pups from the same litters, there were no differences

in free carnitine or acetylcarnitine abundances between ff and C;ff pups. This, too, suggests that maternal effects dominate, supplied via milk composition. Even more remarkable is that for cross-fostered litters, despite two days of nutrition from a dam of the opposite genotype, the carnitine concentrations more closely resembled the carnitine abundances of litters from the birth mother (**Fig. 5.1F**). For example, litters born to ff dams did not become carnitine-deficient when fostered by a C;ff dam, and pups born to C;ff dams failed to increase free carnitine concentrations when nursed by ff dams. This may indicate that more time may be necessary to increase or deplete carnitine concentrations in the early postnatal circulation. Interestingly, acetylcarnitine was up-regulated by both cross-fostering conditions relative to birth mother. Neither carnitine nor acetylcarnitine was significantly regulated by PPARα deficiency (**Fig. 5.1F**).

These preliminary studies demonstrate that the fetal transcriptional response can be very different from adult liver, and that maternal effects on neonatal transcription and metabolism are mostly determined by the genotype of the dam providing milk to the neonate rather than the birth dam. An exception to this was neonatal carnitine concentrations which were more reflective of intrauterine environment than current milk provision. Different genes may also display unique patterns of transcriptional regulation based on *in utero* environment vs postnatal nutrition. Interestingly, Fgf21 is suppressed in neonatal fasting liver (261), which is the opposite regulation as in adult liver where fasting dramatically increases expression (213), and this may be partly mediated by histone acetylation and β-hydroxybutyrate-mediated inhibition of histone deacetylase (HDAC3) (227). Immunoblotting for lysine acetylation revealed a slight increase in acetylation of a protein of unknown identity in neonatal liver of pups reared by C;ff dams (**Fig. 5.1E**). Preliminary studies suggest that neonatal genotype did not affect protein acetylation, but it may be of interest to characterize histone acetylation status in these models.

The neonatal liver model of impaired fatty acid oxidation is different from fetal liver because the effects of liver fatty acid oxidation are now apparent as differences in liver triglyceride content and transcriptional differences. It is interesting that PPARα$^{-/-}$ livers exhibited significantly more triglyceride accumulation than Cpt2 KO livers, and PPARα$^{-/-}$ neonates were not carnitine-deficient like pups born to C;ff dams were. One possibility is that the dramatic increase in triglyceride accumulation in PPARα$^{-/-}$ livers may be the result of whole-body impairments in fatty acid oxidation. It would also be of interest to characterize differences in heart and brain metabolism in liver-specific Cpt2 KO neonates, for example. It will be necessary to measure liver β-hydroxybutyrate concentrations in ff and C;ff pups to demonstrate impaired ketogenesis. If C;ff pups fail to generate ketones like C;ff adult liver (as would be expected), this may represent an excellent model in which to characterize the effects of peripheral ketones on brain metabolism and development.

In order to determine the maternal factors affecting neonatal response, it may be necessary to characterize the milk composition of ff and C;ff dams. At the least, it may be interesting to measure acylcarnitine concentrations in milk since free carnitine and long-chain acylcarnitine concentrations are known to be different in maternal serum of ff and C;ff late gestation dams (210). In humans, maternal plasma acylcarnitines are similarly reflected in milk composition, with the exception that maternal serum acylcarnitines are always lower than acylcarnitine concentrations in milk (238). It may also be necessary to determine how long it takes for cross-fostering to reverse some of the metabolic effects such as carnitine levels. In addition, it may be interesting to determine when C;ff pups become carnitine-deficient like C;ff adults, or if milk provision of free carnitine prevents this until weaning. If defects in protein acetylation are detected in C;ff livers, it may be interesting to try metabolic rescue by injection of β-hydroxybutyrate or increasing the medium-chain fatty acid content of the milk. Attempts to

rescue liver-specific Cpt2 KO phenotypes may affect metabolism, post-translational modifications, or transcriptional regulation, and it will be of interest to determine which factors reverse which of these phenotypes. Furthermore, a more global assessment of transcriptional regulation may provide insight into the factors that affect transcriptional responses to impaired mitochondrial oxidative metabolism between different nutritional conditions or even between different developmental stages. By studying transitions in macronutrient metabolism at different stages of life, it may be possible to identify unifying features regulating these metabolic adaptations.

Here, we have demonstrated that early postnatal metabolic responses are sensitive to maternal genotype. Cross-fostering experiments have demonstrated that some, but not all, of the metabolic responses of pups born to dams with impaired lipid metabolism can be reversed. We have defined a useful genetic system to characterize factors that affect neonatal fatty acid metabolism in the transition to independent life at birth. These studies complement our investigations into fetal mitochondrial oxidative metabolism in response to maternal nutrient deprivation and reveal additional mechanisms of metabolic flexibility in response to impaired mitochondrial metabolism.

6. Frontiers in Defining Maternal-Fetal Metabolic Communication

Gestational success requires metabolic, hormonal, and immunological communication between mother and fetus. Using mouse models of impaired mitochondrial pyruvate and fatty acid metabolism we have characterized fetal and maternal responses to nutrient deprivation. The use of genetic models and biochemical approaches to obtain a greater mechanistic understanding of maternal-fetal metabolic communication may inform interventions for common conditions

such as gestational diabetes (201) as well as rare disorders with a genetic component (208). In addition, these same genetic models are providing insight into metabolic adaptations during early postnatal life and how maternal contributions affect neonatal responses. Future studies will include mouse models combining genetic deficiency of both mitochondrial pyruvate and fatty acid metabolism. In addition, metabolic rescue experiments will be employed to determine the sufficiency of particular substrates to reverse the observed phenotypes. Advances in isotopic labeling approaches and imaging technologies *in vivo* will also serve to advance the field of maternal-fetal metabolic communication. Significant metabolic communication and cooperation are necessary between mother and fetus. Fetal demands and maternal countermeasures are always at work to compromise for a balance that will suit both mother and fetus, and there is both harmony and conflict under nearly all maternal-fetal interactions.

Advances in systems biology and longitudinal studies of human pregnancy across large populations with data about neonatal outcomes will also prove instrumental in the next wave of investigations into maternal-fetal metabolic communication. These may inform new animal models and genetic approaches to define and treat metabolic disorders of pregnancy. Moreover, an entirely new field of investigation in fetal-maternal communication includes the study of exosomes, which are membrane-bound extracellular vesicles that contain cytoplasmic components of the cells from which they were released. Exosomes derived from the placenta are evident in the maternal circulation as early as six weeks gestation (262). Placental exosomes may also play an important role in placental development and syncytiotrophoblast fusion (263), and exosomes derived from maternal adipose tissue could mediate cross-tissue communication between the placenta and maternal tissues (264). Exosomes may also be a way of delivering maternal cargo to the fetus; however, placental exosomes have not been identified in the fetal circulation in humans, although exosomes from syncytiotrophoblast and from umbilical cord

mesenchymal stem cells have been detected in umbilical blood (265). Milk exosomes may even contribute to neonatal nutrition and immunity (266). Altogether, exosomes and their cargo may provide an additional means of communication between mother and offspring.

Given that pregnancy may be the most nutritionally sensitive stage in the life cycle, nutritional interventions during pregnancy may have the greatest capacity to benefit maternal, fetal, and infant health. Improved nutrition during gestation and early postnatal life may improve overall health and reduce the likelihood of chronic disease in adulthood. Studies of macronutrient metabolism during pregnancy and lactation may inform therapeutic approaches to improve human health at all stages of life.

Appendix: The Mammalian Malonyl-CoA Synthetase ACSF3 Is Required for Mitochondrial Protein Malonylation and Metabolic Efficiency

Adapted from (222): Bowman CE, Rodriguez S, Selen Alpergin ES, Acoba MG, Zhao L, Hartung T, Claypool SM, Watkins PA, Wolfgang MJ. 2017. The Mammalian Malonyl-CoA Synthetase ACSF3 Is Required for Mitochondrial Protein Malonylation and Metabolic Efficiency. Cell Chem Biol 24:673-684 e674.

SUMMARY

Malonyl-CoA is a central metabolite in mammalian fatty acid biochemistry generated and utilized in the cytoplasm; however, little is known about noncanonical organelle-specific malonyl-CoA metabolism. Intramitochondrial malonyl-CoA is generated by a malonyl-CoA synthetase, ACSF3, that produces malonyl-CoA from malonate, an endogenous competitive inhibitor of succinate dehydrogenase. To determine the metabolic requirement for mitochondrial malonyl-CoA, ACSF3 knockout (KO) cells were generated by CRISPR/Cas-mediated genome editing. ACSF3 KO cells exhibited elevated malonate and impaired mitochondrial metabolism. Unbiased and targeted metabolomics analysis of KO and control cells in the presence or absence of exogenous malonate revealed metabolic changes dependent on either malonate or malonyl-CoA. While ACSF3 was required for the metabolism and therefore detoxification of malonate, ACSF3-derived malonyl-CoA was specifically required for lysine malonylation of mitochondrial proteins. Together, these data describe an essential role for ACSF3 in dictating the metabolic fate of mitochondrial malonate and malonyl-CoA in mammalian metabolism.

INTRODUCTION

Malonyl-CoA is positioned at a central regulatory node in mammalian metabolism to coordinate the synthesis and oxidation of fatty acids. Malonyl-CoA is generated in the cytoplasm and mitochondrial outer membrane by the biotin-dependent carboxylation of acetyl-CoA by the highly regulated Acetyl-CoA Carboxylase (267-271). Malonyl-CoA can then be used by Fatty Acid Synthase (FASN) to generate long-chain fatty acids, or be used for chain-elongation of fatty acids (267). Therefore, malonyl-CoA represents the rate-determining and committed metabolite in *de novo* fatty acid synthesis. Concomitantly, malonyl-CoA acts as an allosteric inhibitor of Carnitine Palmitoyltransferase 1 (CPT1), the rate-setting step in the mitochondrial β-oxidation of long-chain fatty acids; therefore, malonyl-CoA is the metabolite that mediates the basic metabolic logic whereby fatty acid synthesis and oxidation do not occur simultaneously. Both acetyl-CoA and malonyl-CoA are membrane-impermeable and all of the canonical biosynthetic machinery for malonyl-CoA that has been described is localized exclusively to the cytoplasm. Even tissues with limited expression of FASN, such as mammalian muscle, generate cytoplasmic malonyl-CoA to regulate fatty acid oxidation (272, 273). Muscle regulates malonyl-CoA largely by its decarboxylation via Malonyl-CoA Decarboxylase, MLYCD (162, 274). Inborn errors of MLYCD result in a combined malonic and methylmalonic aciduria (275-277). Curiously, MLYCD contains putative peroxisomal and mitochondrial targeting sequences and can be readily found in mitochondria (275, 278-280). How malonyl-CoA, which is membrane-impermeable, can be generated in the mitochondrial matrix has been a longstanding mystery. This has been at least partly resolved by the discovery of a eukaryotic mitochondrial malonyl-CoA synthetase, ACSF3 (281, 282).

ACSF3 was originally described as an orphan member of the Acyl-CoA Synthetase (ACS) family of enzymes (283). Recently, the *Arabidopsis* ACSF3 ortholog, Acyl Activating Enzyme 13, was described as a eukaryotic malonyl-CoA synthetase essential for plant growth and viability, especially in the presence of exogenous malonate (282, 284). Like other acyl-CoA synthetases, ACSF3 ligates Coenzyme A to its co-substrate, malonate, in an ATP-dependent manner (**Figure A.1A**). Human ACSF3 localizes to the mitochondrial matrix to produce malonyl-CoA from malonate within that organelle (281). Mitochondrial malonate is an endogenous metabolite that is a classic competitive inhibitor of succinate dehydrogenase, a component of the tricarboxylic acid (TCA) cycle and Complex II of the electron transport chain (285). As such, malonate is often used as a metabolic toxin to destroy striatal neurons in models of Parkinson's disease (286-288). The severe malonic and methylmalonic aciduria characteristic of MLYCD deficiency is also accompanied by developmental delay, seizure disorders, hypoglycemia, and cardiomyopathy. Recently, patients that presented with combined malonic and methylmalonic aciduria without mutations in *MLYCD* were found to have nonsynonymous mutations in the *ACSF3* gene (289, 290). The similarities in the phenotypes of MLYCD and ACSF3 deficiencies suggest that they exist in the same biochemical pathway. This presents a metabolic rationale for why MLYCD is localized within mitochondria—toxic malonate may be metabolized within mitochondria through the subsequent activities of ACSF3 and MLYCD.

Here we have taken advantage of CRISPR/Cas9-mediated genome editing to mutate ACSF3 in a human cell line that robustly expresses the enzyme. Using a combination of metabolic flux assays and measurement of steady-state metabolite concentrations, we demonstrate the requirement for ACSF3 in mitochondrial metabolism and reveal the metabolic fate of malonate in human cells. Furthermore, we demonstrate that ACSF3-derived malonyl-CoA

is required for mitochondrial protein malonylation, a recently identified posttranslational lysine modification that can affect metabolic enzyme activity to alter cellular metabolism.

RESULTS

Engineering *ACSF3* Genomic Mutations in Human Cells

Human patient fibroblasts can be difficult to obtain and can have limited utility. Engineering mutations in well-characterized human cell lines is advantageous for elucidating the function of enzymes in cellular metabolism and bypasses the transient and often insufficient knockdown by RNA interference. Here we have taken advantage of CRISPR/Cas9-mediated genome engineering to induce mutations in the *ACSF3* gene in human HEK293T cells (130, 131). ACSF3 is a 576 amino acid protein encoded by an 11-exon gene on human chromosome 16. We targeted a site in exon 3, the first protein-coding exon, by transfecting cells with a plasmid co-expressing human codon-optimized Cas9 nuclease and the designed guide RNA targeting *ACSF3*. Concomitantly, control cells were transfected with Cas9 without a guide RNA. Individual clones were selected by limited dilution plating and screened for loss of ACSF3 protein by immunoblotting (**Figure A.1B**). Select clones were analyzed for genomic mutations in *ACSF3* which are the result of non-homologous end-joining repair after Cas9-mediated endonuclease activity (**Figure A.S1A**). Consistent with its biochemical function, ACSF3 knockout (KO) cells have a 5-fold higher concentration of the enzyme's substrate, malonate, relative to control cells (**Figure A.1C**). Total malonyl-CoA and acetyl-CoA abundance was unchanged in ACSF3 KO cells, demonstrating that compartment-specific defects in malonyl-CoA metabolism may not affect the cellular concentration of the enzyme's product (**Figure A.S1B**). Cytoplasmic routes of malonyl-CoA synthesis likely account for a greater proportion of cellular malonyl-CoA than

ACSF3-derived mitochondrial malonyl-CoA. In this way, we have engineered cells with a similar biochemical phenotype to humans with inborn errors in ACSF3 in a cell line that can be easily cultured and manipulated *in vitro*.

ACSF3 is Required for Malonate Oxidation

Loss of ACSF3 resulted in increased steady-state levels of malonate (**Figure A.1C**), but the metabolic fate of malonate in human cells remained unclear. Malonate is an endogenous metabolite that acts as a classic competitive inhibitor of succinate dehydrogenase (285). As such, malonate is cytotoxic by blocking cellular respiration, and the effects of malonate are especially detrimental in cells that rely heavily on oxidative metabolism (286-288). To determine if loss of ACSF3 would exacerbate malonate-induced toxicity, ACSF3 KO and control cells were treated with increasing concentrations of malonate and cell survival was assayed after 72 hours of exposure (**Figure A.S1C**). Malonate impairs proliferation of ACSF3 KO and control cells to the same extent, with only subtle differences in cell viability by genotype across the malonate concentrations tested. This suggests that, while ACSF3 participates in the clearance of mitochondrial malonate, loss of ACSF3 does not affect cell growth under normal culture conditions.

Consistent with the action of malonate as a potent inhibitor of succinate dehydrogenase, exposure of cells to 5 mM malonate for 24 hours dramatically increased steady-state succinate levels, and ACSF3 KO cells had 1.5-fold higher succinate accumulation than control cells upon malonate exposure (**Figure A.1D**). In the absence of exogenous malonate, steady-state intracellular succinate concentrations were not different between ACSF3 KO and control cells, likely due to the ability of succinate to exit cells via the dicarboxylic acid transporter. Consistent with this, we observed that succinate secretion increased in a dose-dependent manner with

increasing malonate exposure in both control and ACSF3 KO cells (**Figure** A.**1D**). At baseline, ACSF3 KO cells had higher malonate levels, providing evidence that the endogenous malonate-clearance machinery may operate at low concentrations of substrate.

To determine the ACSF3-dependent metabolic fate of malonate, ACSF3 KO and control cells were labeled with [1,3-^{13}C]malonate, and isotopomer distribution into short-chain acyl-carnitines, TCA cycle intermediates, and select amino acids was determined by LC-MS/MS (**Figure A.1E**). ACSF3 KO cells had less m+1 labeled acetyl-L-carnitine, indicative of less acetyl-CoA formation from labeled malonate, which results from malonyl-CoA decarboxylase activity on labeled malonyl-CoA in either the cytoplasm or mitochondria. The abundances of m+1 mass isotopomers of TCA cycle intermediates were decreased in ACSF3 KO cells, suggestive of a decrease in malonyl-CoA-derived acetyl-CoA entering the TCA cycle in the absence of ACSF3. These data provide evidence that malonate can be metabolized by mammalian cells in a manner that depends on its activation to malonyl-CoA by ACSF3.

Loss of ACSF3 Perturbs Mitochondrial Metabolism

In addition to decreased labeling of TCA cycle intermediates from malonate in ACSF3 KO cells, the total abundances of α-ketoglutarate and fumarate were decreased while malate and citrate concentrations were unchanged by loss of ACSF3 (**Figure A.S1D**). Again, in the presence of exogenous malonate, cellular succinate increased in ACSF3 KO cells, consistent with the action of malonate as a succinate dehydrogenase inhibitor. To determine how impaired mitochondrial malonate metabolism would affect overall mitochondrial function, cellular oxygen consumption was measured in the presence of 10 mM glucose, 2 mM glutamine, and 1 mM pyruvate. ACSF3 KO cells exhibited significantly lower basal respiration than control cells, as well as lower CCCP-stimulated maximal respiration, with no difference in non-mitochondrial respiration

(**Figure A.2A**). These data demonstrate an ACSF3-dependent defect in mitochondrial oxidative metabolism.

To test for differences in substrate-specific oxidative metabolism, glucose, glutamine, and alanine oxidation rates in ACSF3 KO and control cells were determined with radiolabeled substrates (**Figure A.2B**). Rates of oxidation of [U-^{14}C]D-glucose to $^{14}CO_2$ in ACSF3 KO cells were 65-75% of control cells, and the complete oxidation of [U-^{14}C]L-glutamine and [U-^{14}C]L-alanine was similarly impaired (**Figure A.2B**). These defects in catabolic substrate utilization suggest a general impairment of mitochondrial metabolism in ACSF3 KO cells, consistent with a model of malonate-induced mitochondrial toxicity.

To determine whether the generalized impairment of mitochondrial metabolism in ACSF3 KO cells was a result of reduced mitochondrial content, immunoblotting for several mitochondrial proteins was conducted on ACSF3 KO and control cells (**Figure A.2C**). While the abundance of the outer mitochondrial membrane voltage-dependent anion channel (VDAC) and the matrix enzyme aconitase (ACO2) was unchanged between ACSF3 KO and control cells, several subtle differences were observed among inner mitochondrial membrane proteins that are components of the oxidative phosphorylation machinery. Among these, the abundances of a Complex I subunit (NDUFB8) and a Complex III subunit (UQCRC2) were significantly lower in ACSF3 KO cells while ATP synthase subunit ATP5A expression was unchanged (**Figure A.2C**). We next tested for complex-specific differences in respiratory chain function between ACSF3 KO and control cells in isolated mitochondria. No differences were observed in the individual activities of Complex I, Complex II, Complex IV, or Complex V (**Figure A.S2A, A.S3B**). These data suggest that the subtle differences in mitochondrial protein abundance were not contributing to the overall defects in mitochondrial metabolism observed in ACSF3 KO cells and the

suppression in oxidative metabolism was due mainly to the competitive inhibition of SDH by malonate.

Impaired Mitochondrial Malonate Metabolism Affects Cellular Energy Status and Impairs *De Novo* Lipogenesis

To determine how impaired mitochondrial oxidative metabolism in ACSF3 KO cells affected cellular energy status, we tested the phosphorylation status of acetyl-CoA carboxylase (ACC). ACC is a substrate of the canonical energy-sensing AMP-activated protein kinase (AMPK), whose activity generates cytoplasmic malonyl-CoA. ACSF3 KO cells had more phosphorylated ACC (Ser79) than control cells (**Figure A.3A**), with no difference in total ACC expression (**Figure A.S2C**). Since malonate inhibits succinate dehydrogenase, we reasoned that malonate treatment might also affect cellular energy status and therefore AMPK signaling. The degree of ACC phosphorylation in both ACSF3 KO and control cells was unchanged by malonate exposure (**Figure A.3A**).

Because phosphorylation and inactivation of ACC affects cytoplasmic production of malonyl-CoA and, therefore, *de novo* lipogenesis, we next measured the flux of radiolabeled substrates into total cellular lipids. Consistent with the phosphorylation status of ACC, [^{3}H]acetate incorporation into lipid was decreased in ACSF3 KO cells relative to controls (**Figure A.3B**). Interestingly, the presence of malonate significantly decreased lipid synthesis from acetate in control cells while ACSF3 KO cells were unaffected by malonate exposure. This observation supports a role for ACSF3 in promoting malonate clearance to prevent a mitochondrial bioenergetic stress. While acetate incorporation into lipid does not require mitochondrial metabolism to generate acetyl-CoA, the synthesis of cellular lipids from the oxidative metabolism of glucose, glutamine, and alanine requires mitochondrial production of citrate. Consistent with

impaired oxidation of these substrates in ACSF3 KO cells (**Figure A.2B**), the flux into total cellular lipids was decreased to a similar degree (**Figure A.3C, Figure A.S2D**). These deficits provide further evidence of suppressed mitochondrial metabolic capacity upon loss of ACSF3.

Protein Lipoylation is Unaffected by ACSF3 Deficiency

Mitochondrial malonyl-CoA derived from ACSF3 has been implicated as a significant source of carbon for type II fatty acid synthesis in the mitochondrial matrix (281, 284). The octanoyl-ACP (acyl-carrier protein) produced by *de novo* fatty acid synthesis in the mitochondrial matrix is a substrate for the synthesis of lipoic acid, an essential cofactor for α-ketoacid dehydrogenase complexes (reviewed in (291, 292)). To test the contribution of ACSF3-derived malonyl-CoA to total cellular lipids, cells were labeled with [2-^{14}C]malonate and contribution to the total lipid fraction was determined (**Figure A.3D**). ACSF3 KO cells had significantly lower malonate incorporation into lipid than control cells, consistent with a requirement for ACSF3 in malonate metabolism. In order to more specifically evaluate protein lipoylation status, immunoblotting of ACSF3 KO and control cell lysates was performed with an antibody that recognizes lipoylated residues (**Figure A.3E**). No defects in lipoylation of DLAT (E2 of pyruvate dehydrogenase) or DLST (E2 of α-ketoglutarate dehydrogenase) were detected in ACSF3 KO cells, suggesting that lipoic acid deficiency is not contributing to the impaired mitochondrial metabolic phenotypes in ACSF3 KO cells.

Unbiased Metabolomics of ACSF3 KO Cells Reveal Malonate- and Malonyl-CoA-Dependent Metabolic Alterations

To gain a more global understanding of how ACSF3 regulates cellular metabolism, we performed unbiased global steady-state metabolomics on ACSF3 KO and control cells in the presence or

absence of 5 mM malonate for 24 hours. No signs of toxicity were observed at this concentration of malonate (**Figure A.S1C**). There were 355 unique metabolites detected, and 186 were changed greater than two-fold in either direction by genotype or malonate treatment or both. Metabolic alterations that were dependent upon malonate inhibition of SDH were clearly present (**Figure A.3F; Table A.S1**). However, these steady-state data demonstrate broad metabolic changes that cannot be easily explained by SDH inhibition alone and likely reflect both malonate- and malonyl-CoA-dependence. The differences observed by the loss of ACSF3 and exogenous malonate reveal intriguing and unique metabolic effects of the reaction's substrate and product.

ACSF3 Is Required for Mitochondrial Protein Malonylation

The complexity of metabolic changes observed in ACSF3 KO cells suggests a more complex role for malonate than inhibition of SDH alone. Malonate and other structurally similar dicarboxylic acids traverse membranes via dedicated transporters in a concentration-dependent manner. ACSF3-derived mitochondrial malonyl-CoA, however, is trapped within that organelle. To further delineate the fate of malonate and mitochondrial malonyl-CoA, cells were labeled with [2-^{14}C]malonate and a biphasic extraction protocol was used to separate and recover polar, non-polar, protein, and nucleic acid fractions (293). ACSF3 KO cells had higher [2-^{14}C]malonate accumulation than control cells (total counts) and higher ^{14}C signal in the polar metabolite fraction (**Figure A.4A**), consistent with the elevated steady-state malonate concentrations observed in ACSF3 KO cells (**Figure A.1C**). Interestingly, although malonate incorporation into protein only accounted for ~5% of total label incorporation in control cells (**Figure A.S2E**), ACSF3 KO cells had significantly lower malonate incorporation into protein (~1% of total label incorporation). These results suggest that the ACSF3-dependent incorporation of malonate into the protein fraction may be part of an adaptive response to cellular malonate exposure.

Furthermore, an inability to direct malonate toward this fate may account for some of the metabolic derangements observed in ACSF3 KO cells, particularly in the presence of exogenous malonate.

Protein malonylation has been recognized as a dynamically regulated posttranslational lysine modification that can affect mitochondrial and nucleocytoplasmic proteins (294-296), and malonyl-CoA is the likely substrate for protein malonylation (297-299). Using an antibody that specifically recognizes malonylated lysine residues, we immunoblotted for this modification in whole cell lysates and after enriching for mitochondria. Exogenous malonate treatment robustly increased mitochondrial protein malonylation and the majority of protein malonylation signal was localized to mitochondria (**Figure A.4B**). Importantly, ACSF3 was required for mitochondrial protein malonylation, and transient re-expression of ACSF3 was sufficient to rescue the impaired mitochondrial malonylation in ACSF3 KO cells (**Figure A.4B**). Transient re-expression of ACSF3 in KO cells did not alter the observed differences in protein abundance of particular inner mitochondrial membrane components of the oxidative phosphorylation machinery (**Figure A.4B**). Interestingly, immunoprecipitation of a mitochondrially-targeted YFP and immunoblotting for malonylated lysine residues demonstrated that a heterologous protein can be malonylated in the mitochondrial matrix of control cells but not in ACSF3 KO cells (**Figure A.S3**). This suggests that protein malonylation may be proportional to malonyl-CoA concentrations, as others have suggested (300), and that ACSF3 is the principal source of mitochondrial malonyl-CoA in cells treated with malonate.

Mitochondrial Protein Malonylation Is a Stable Posttranslational Modification that Alters Cellular Metabolism

We next sought to define the metabolic effects of mitochondrial protein malonylation through a malonate washout paradigm where cells were cultured in the presence of 5 mM malonate for 24 hours before a washout with malonate-free growth media for up to 24 hours. We observed that mitochondrial protein malonylation is a stable modification that persists after removing malonate from the media (**Figure A.5A**). To understand potential roles of mitochondrial malonylation, we performed a malonate washout experiment with steady-state metabolite concentrations determined by ^{1}H-NMR over the time course. Cellular succinate concentrations decreased rapidly (within 3h) after removal of exogenous malonate, consistent with the acute and reversible inhibition of SDH by malonate (**Figure A.5B**). Across the same time course, cellular lactate and pyruvate increased, while threonine concentrations remained consistently lower in ACSF3 KO cells, independent of time from malonate washout (**Figure A.5B**). These data further demonstrate malonate-dependent and malonyl-CoA-dependent effects of ACSF3 deficiency.

ACSF3 Enables Metabolite-Specific Mitochondrial Protein Acylation

We reasoned that global changes in protein malonylation may affect other lysine acyl modifications that are altered by cellular metabolism. Despite the defects in mitochondrial metabolism in ACSF3 KO cells related to SDH inhibition by malonate, neither malonate treatment nor loss of ACSF3 dramatically affected mitochondrial lysine acetylation (**Figure A.6A**). The removal of the malonyl-lysine modification is catalyzed by the mitochondrial sirtuin SIRT5 (294, 295), which also removes the structurally similar succinyl-lysine modification (295, 301). The loss of Sirt5 enhances both malonylation and succinylation and has clear metabolic effects (296, 301). We hypothesized that the increase in cellular succinate upon SDH inhibition

by malonate may concurrently increase lysine succinylation and malonylation. Surprisingly, exogenous malonate did not affect mitochondrial protein succinylation, and ACSF3 KO and control cells exhibited no differences in mitochondrial protein succinylation (**Figure A.6B, A.6C**). In order to increase succinate and succinyl-CoA concentrations by an orthogonal method, cells were treated with the SDH suicide inhibitor, 3-nitropropanoate (3-NP). Cellular succinate concentrations were dramatically increased by 3-NP (**Figure A.S5**) and corresponded with increased mitochondrial protein succinylation independent of ACSF3 (**Figure A.6C**). Lysine succinylation and malonylation may occur on the same residues, so we also treated cells with both 3-NP and malonate simultaneously to test whether there is a propensity for one modification over the other. The presence of both malonate and 3-NP decreased the intensity of the malonyl-lysine and succinyl-lysine signals relative to their respective controls with only one inhibitor (**Figure A.6B, A.6C**). These results show that ACSF3, by being required for protein malonylation, participates in the metabolite-specific acylation of mitochondrial proteins.

Tissue-specific Differences in Mitochondrial Protein Malonylation Reflect Acsf3 Abundance

ACSF3 expression across tissues and under different physiological conditions may provide insight into the regulation of mitochondrial malonate metabolism *in vivo*. *ACSF3* mRNA is highly expressed in mitochondria-rich tissues in mouse such as brown adipose tissue (BAT), soleus muscle, kidney, and liver (85). Others have shown that protein malonylation is higher in fed liver than fasted liver (296), and obese leptin-deficient *ob/ob* mice exhibit a dramatic increase in hepatic protein malonylation (302). Both fed liver and *ob/ob* liver are characterized by high rates of *de novo* fatty acid synthesis and, therefore, elevated cytoplasmic malonyl-CoA. We posit that hydrolysis of cytoplasmic malonyl-CoA and transport into the mitochondrial matrix could

represent a significant source of malonate for ACSF3-derived malonyl-CoA that can be metabolized or modify mitochondrial proteins.

In four mitochondria-rich tissues (liver, kidney, heart, and BAT), we observed different levels of mitochondrial protein malonylation that positively correlated with Acsf3 expression (**Figure A.7A**). Malonylation of mitochondrial proteins was most robust in BAT, kidney, and liver. We confirm the findings of Du *et al*. that showed increased total protein malonylation in livers of *ob/ob* mice; and furthermore, we demonstrate that mitochondrial proteins from *ob/ob* mice have higher lysine malonylation than wild-type (WT) mitochondrial extracts (**Figure A.7B**) (302). Interestingly, mitochondrial protein succinylation was the same in WT and *ob/ob* liver (**Figure A.7B**), suggesting that the regulation observed in *ob/ob* mice is metabolite-specific. In BAT, both malonylation and succinylation of mitochondrial proteins was reduced in *ob/ob* mice relative to WT consistent with diminished nonshivering thermogenesis and BAT function in this model. Here we demonstrate that mitochondrial protein malonylation is positively correlated with Acsf3 expression and that alterations in lysine acylation in *ob/ob* mice may reflect tissue- and metabolite-specific differences relevant to the physiology of these tissues.

DISCUSSION

Cytoplasmic malonyl-CoA is a well-characterized metabolite that simultaneously drives *de novo* fatty acid synthesis while inhibiting the rate-setting step in mitochondrial β-oxidation of long-chain fatty acids (reviewed in (268-271)). The role and requirement for malonyl-CoA in the mitochondrial matrix is poorly understood, yet two enzymes have (so far) been identified as participants in the metabolism of this metabolite. Acyl-CoA synthetase family member 3 (ACSF3) uses ATP and Coenzyme A to activate malonate to malonyl-CoA within the mitochondrial matrix (281-283), and mitochondrially-localized malonyl-CoA decarboxylase (MLYCD) can decarboxylate malonyl-CoA to generate acetyl-CoA and CO_2. Malonate is an endogenous metabolic intermediate and a well-characterized competitive inhibitor of succinate dehydrogenase (SDH) (285). As such, malonate is cytotoxic by blocking the TCA cycle and cellular respiration. We propose that ACSF3 and MLYCD work in concert to clear malonate from mammalian mitochondria. In addition, another fate of mitochondrial malonyl-CoA is modification of lysine residues of mitochondrial proteins. To this end, we have shown that mammalian cells are capable of metabolizing labeled malonate in an ACSF3-dependent manner and that ACSF3 is required for mitochondrial protein malonylation.

Acetyl-CoA derived from MLYCD-catalyzed decarboxylation of mitochondrial malonyl-CoA can enter the TCA cycle and be fully oxidized, analogous to some bacterial species (303, 304). Indeed, in legume plants, rhizobacteria are significant utilizers of malonate; however, the exact molecular source of malonate in eukaryotic cells is not well defined. We suggest that much of the mitochondrial malonate may derive from hydrolysis of cytoplasmic malonyl-CoA and subsequent transport into the mitochondrial matrix via dicarboxylic acid transporters of the inner mitochondrial membrane. In this way, ACSF3 may play a critical role in metabolic proofreading of a toxic side reaction (305). In plants and in pig heart, malonate was shown to be generated

from the decarboxylation of oxaloacetate (306, 307). Additionally, some bacterial species can generate malonate from pyrimidines (308). Interestingly, several pyrimidine-related metabolites were up-regulated in ACSF3 KO cells (**Table A.S1**). It has also been proposed that malonate can be formed from the oxidation of malondialdehyde, a product of lipid peroxidation, that is often used as an indicator of oxidative stress (282, 309). Alternatively, prior to the identification of ACSF3 as the eukaryotic malonyl-CoA synthetase, it was proposed that malonyl-CoA could be non-specifically synthesized by propionyl-CoA carboxylase from acetyl-CoA in the mitochondrial matrix, albeit at a much lower rate than propionyl-CoA carboxylation (310, 311). Although the relative contributions of each of these potential sources of mitochondrial malonate remains to be determined, our model describes the roles for ACSF3 and MLYCD in regulating mitochondrial malonate concentrations. Consistent with our model, mutations in human ACSF3 or MLYCD result in toxic accumulation of malonate and systemic metabolic acidosis (289, 290).

To further determine the metabolic role of ACSF3 in mammalian cells, we generated an ACSF3 loss-of-function genetic model in cultured cells by CRISPR/Cas9-mediated genome editing. Prior to recent advances in genome editing in mammalian cells, the use of patient primary cells has been the preferred model to study inborn errors of metabolism and to determine the molecular mechanisms behind human disease. However, these cultured patient fibroblasts or lymphoblasts often do not sufficiently express the genes of interest to determine the consequence of the mutations (312). Here we demonstrate the utility of generating stable mutations in well-defined cultured cells to accomplish this same purpose. ACSF3 knockout (KO) cells have elevated steady-state malonate and succinate concentrations (**Figure A.1C** and **Table A.S1**), consistent with the biochemical function of ACSF3 and the inhibitory role of its substrate malonate. Although methods are currently lacking to measure concentrations of malonate and malonyl-CoA with subcellular resolution (313), mitochondrial protein malonylation may be a

reasonable proxy for mitochondrial matrix malonyl-CoA concentrations. Indeed, fibroblasts from patients with MLYCD deficiency had higher protein malonylation, consistent with an inability to catabolize malonyl-CoA to acetyl-CoA (298, 300). Elevated protein malonylation in MLYCD-deficient cells also corresponded with impaired mitochondrial function, and here we demonstrate that a lack of mitochondrial protein malonylation in ACSF3-deficient cells also correlated with impaired mitochondrial function. The similar metabolic phenotypes observed in MLYCD- and ACSF3-deficient cells corroborate the similar clinical presentation of ACSF3 and MLYCD mutations in combined malonic and methylmalonic aciduria (CMAMMA).

Elevated levels of malonate in plasma (2-10 μM) and urine (15-70 μM) have been described in patients with mutations in ACSF3 (290). Loss of the plant homolog of ACSF3 also resulted in dramatically elevated malonate concentrations in plant shoots as well as a dose-dependent increase in both malonate and succinate upon treatment with exogenous malonate (282). In a similar manner, we expected cells deficient in ACSF3 to be more sensitive to malonate-induced cytotoxicity. Surprisingly, ACSF3-deficient cells were as sensitive to increasing concentrations of malonate as control cells. The doses of malonate tested are comparable to the concentrations used to treat plants (282) and lower than the concentrations used to induce cytotoxicity in neuronal cultures (10-75 mM) (288, 314); however, it is possible that these doses simply overwhelm the endogenous malonate-clearance machinery. Like other metabolite proofreading systems, we suggest that mitochondrial malonate metabolism operates at low levels of substrate (305), and, consistent with this, malonyl-CoA concentrations were lower than other short-chain acyl-CoAs *in vivo* (315). Additionally, in cell culture models, the culture media represents a significant metabolic sink, and toxic intermediates may be secreted into the media instead of being accumulated to the same extent as might occur *in vivo*. Specifically, we propose that malonate-induced inhibition of SDH does not result in dramatic accumulation of

succinate because this metabolite is free to exit the cell via dicarboxylic acid transporters. Nevertheless, the observation that there is no difference in malonate-induced cytotoxicity between ACSF3 KO and control cells facilitates interpretation of differences in metabolic flux data and steady-state metabolite concentrations, as these are not complicated by differences in cell viability.

ACSF3 KO cells demonstrate impaired mitochondrial metabolism as evidenced by decreased oxygen consumption and impaired flux of glucose and glutamine to CO_2 and to total cellular lipids. Additionally, steady-state concentrations of several TCA cycle intermediates were slightly decreased in ACSF3 KO cells relative to controls. This generalized impairment of mitochondrial flux is not the result of defective protein lipoylation, as ACSF3 KO cells have normal levels of lipoylated proteins. Instead, we hypothesize that malonate-induced toxicity accounts for the impaired mitochondrial metabolism observed in ACSF3 KO cells, and impaired mitochondrial protein malonylation may also contribute to the observed impairments. Widespread changes in malonylation as a result of ACSF3 deficiency could have the capacity to broadly affect several metabolic pathways, and metabolites identified from our steady-state metabolomic analysis as being regulated in a malonyl-CoA-dependent manner could represent candidate pathways that are regulated by malonylation.

ACSF3 is a recently identified mitochondrial malonyl-CoA synthetase. Patients with mutations in ACSF3 or MLYCD display genetic concordance with systemic malonic aciduria and clinical features such as developmental delay, seizure disorders, hypoglycemia, and cardiomyopathy (289, 290), although the tissue-autonomous role for mitochondrial malonate metabolism is unknown. While there is much to be learned about the role and requirement for ACSF3 *in vivo*, we have generated ACSF3-deficient human cells using CRISPR/Cas9-mediated genome engineering to begin deciphering the cell-autonomous requirements for mitochondrial

malonate metabolism. Using a combination of metabolic flux assays and measurement of steady-state metabolite concentrations, we have shown that malonate can be oxidized by mammalian cells and that ACSF3 plays an important role in preventing malonate-induced impairment of mitochondrial metabolism. Our approach is broadly applicable to target other metabolic enzymes implicated in human disease and may yield mechanistic insight into metabolic regulation in health and disease.

SIGNIFICANCE

The regulation of cytoplasmic malonyl-CoA to promote fatty acid synthesis and inhibit mitochondrial β-oxidation of long-chain fatty acids is well described, but the source and metabolic fate of mitochondrial malonyl-CoA has remained a mystery until the recent identification of a mitochondrial malonyl-CoA synthetase, ACSF3. By engineering loss-of-function mutations in ACSF3 in cultured human cells, we defined the requirement for mitochondrial malonate metabolism and gained mechanistic insight into disease-causing genetic deficiencies in malonyl-CoA metabolism. Malonate is an endogenous metabolite that potently inhibits succinate dehydrogenase, and we demonstrated that ACSF3 is required for malonate detoxification to promote mitochondrial metabolic flux. Malonate can be oxidized by human cells via the subsequent activities of ACSF3 and mitochondrial malonyl-CoA decarboxylase. ACSF3-deficient cells exhibited elevated malonate concentrations and impaired mitochondrial metabolism. A combination of steady-state metabolite measurements and metabolic flux studies was used to describe malonate- and malonyl-CoA-dependent metabolic alterations. Lysine malonylation of mitochondrial proteins was identified as another significant fate of ACSF3-derived malonyl-CoA. ACSF3 was specifically required for malonylation but did not affect lysine

acetylation or succinylation. ACSF3-deficient cells represent an excellent model system to define the regulation and metabolic consequences of mitochondrial protein malonylation to delineate the metabolic underpinnings of human metabolic disease.

Acknowledgments: We would like to thank Natasha Zachara for essential reagents. This work was supported in part by a National Institutes of Health grant R01NS072241 to M.J.W. and R01HL108882 to S.M.C. and a pilot grant from the National Organization of Rare Disease to M.J.W. C.E.B. was supported in part by a fellowship from the American Heart Association 15PRE25090309. M.G.A. was supported in part by a fellowship from the American Heart Association 16PRE31140006.

EXPERIMENTAL MODEL AND SUBJECT DETAILS

Cell Lines

HEK293T cells were grown in DMEM supplemented with 10% bovine calf serum and 1% pen/strep antibiotic (Invitrogen) at 37°C in a humidity-controlled incubator at 10% CO_2. As described in Method Details, ACSF3 KO cells were generated by transfecting hCas9 and the hACSF3 gRNA or hCas9 alone and deriving individual clones that were screened by immunoblotting and sequencing the *ACSF3* target site.

Mice

All procedures were performed in accordance with the NIH's *Guide for the Care and Use of Laboratory Animals* and under the approval of the Johns Hopkins Medical School Animal Care

and Use Committee. Male, 8-week-old, chow-fed, wild-type and *ob/ob* mice (C57BL/6J) were housed in a facility with ventilated racks on a 14h light/10h dark cycle with *ad libitum* access to a standard rodent chow (2018SX;Teklad Global; 18% protein).

METHOD DETAILS

CRISPR/Cas9 Cloning Strategy

Human codon-optimized Cas9 expression vector was obtained from Addgene, plasmid #41815 (131), and hCas9 was cloned into a pEF6 expression vector, downstream and in-frame with a nuclear-localized YFP, linked by a viral 2A bicistronic peptide, such that nls-YFP and Cas9 are expressed in approximate equimolar quantities. A guide RNA (gRNA) targeting human *ACSF3* (**Figure S1A**) was designed according to the recommendations of Mali *et al.* (131) and was computed as a candidate unique gRNA target. The gRNA, including the U6 promoter, was synthesized as a 500bp gBlocks fragment (Integrated DNA Technologies) and was cloned into the pEF6-nls-YFP-2A-Cas9 vector by In-Fusion Cloning (Clontech), as previously described (130).

Derivation of ACSF3 *KO clones*

HEK293T cells were grown in DMEM supplemented with 10% bovine calf serum and 1% pen/strep antibiotic (Invitrogen) at 37°C in a humidity-controlled incubator at 10% CO_2. Cells were transfected with plasmid expressing both hCas9 and the hACSF3 gRNA or hCas9 alone using Fugene HD (Promega) transfection reagent according to manufacturer's instructions. Selection with 7.5 µg/mL blasticidin was started 48 hours post-transfection and continued for two weeks. Individual clones were selected by limited dilution plating and screened for loss of

ACSF3 protein by immunoblotting. For transient addback experiments, ACSF3 KO cells were transfected with a human ACSF3 expression vector and control cells were transfected with a plasmid encoding mitochondrially-targeted YFP (Clontech). Assays were conducted 48-72 h post-transfection. For cell viability assay, cells were counted, plated in 96-well format, and treated with 0, 2.5, 5, or 10 mM malonate (Sigma-Aldrich) for 72 hours, and cell viability was determined by CellTiter 96 Aqueous One Solution tetrazolium-based cell proliferation assay (Promega).

Characterization of ACSF3 *Mutations*

Genotyping primers were designed to span the gRNA target in exon 3 of *ACSF3* (F: 5'ACACAGAGGAAGTGGTCTTCT3'/ R:5'CGTTAGCGCATAGGAAGGAGA3') and PCR was conducted on genomic DNA from *ACSF3* KO clones by standard methods. PCR products were separated on agarose gels, and bands were excised, gel-extracted, and cloned into pCRII vector (Invitrogen) for Sanger sequencing.

Measurement of Cellular Oxygen Consumption

Oxygen consumption was measured using the Seahorse XF^{e}96 extracellular flux analyzer (Seahorse Bioscience). 24,000 cells were plated in poly-L-lysine-coated 96-well microplates 18h before assaying cellular respiration. Cells were incubated with Seahorse base medium supplemented with 10mM glucose, 2 mM glutamine, 1 mM pyruvate for 1h before starting the assay. Oxygen consumption was measured repeatedly over the course of the experiment as the following inhibitors were added sequentially at the specified concentrations: 2 μM oligomycin A, 250 nM CCCP, 0.5 μM rotenone/0.5 μM antimycin A. Cell number was determined by

CyQUANT (Invitrogen) staining of cellular nucleic acids and was used to normalize oxygen consumption rate in pmol/min.

Mitochondrial Isolation and Functional Assays

Mitochondria were isolated as previously described (316). Briefly, cells were scraped into cold isolation buffer (10 mM Tris, 10 mM MOPS, 1 mM EGTA, 200 mM sucrose, supplemented with 20 mM nicotinamide, pH 7.4) and homogenized on ice with a glass homogenizer for 45 strokes before centrifuging at 600g, resuspending the pellet, and centrifuging again at 600g. All centrifugation steps were for 10 min at 4°C. The supernatant was transferred to new tubes and centrifuged at 7,000g. The supernatant was discarded and the pellet was resuspended, and centrifuged at 7,000g followed by a resuspension of the pellet and centrifugation at 10,000g. The mitochondrial pellet was resuspended in lysis buffer, sonicated, and protein concentration determined by BCA assay prior to SDS-PAGE and immunoblotting.

For in-gel assays of respiratory complex function, mitochondria were solubilized in 1.25% digitonin in basic lysis buffer (20mM HEPE-KOH, pH 7.4, 100mM NaCl, 20mM imidazole, 1mM $CaCl_2$, 10% glycerol) with protease inhibitors (1mM PMSF, 10µM leupeptin, 2µM pepstatin A) on ice for 30 min. Insoluble material was pelleted at 21,000g for 30min at 4°C and supernatant was combined with 10X native sample buffer (5% Coomassie Brilliant Blue G-250, 0.5M 6-aminocaproic acid, 100mM BisTris-HCl, pH 7.0). 150µg of solubilized mitochondria were loaded per well and separated on 5-12% or 6-16% BisTris acrylamide gels. For Complex I NADH Nitrotetrazolium blue (NTB) reductase activity assay, gels were incubated in 2.5mg/mL NTB, 0.1mg/mL NADH, and 5mM Tris-HCl, pH 7.4 for 2h at room temperature, then fixed in 50% (v/v) methanol, 10% (v/v) acetic acid and destained. For Complex IV cytochrome c oxidase activity, native gels were incubated in 0.5mg/mL diaminobenzidine,

0.025mM equine heart cytochrome c, 50mM potassium phosphate, pH 7.4 for 5h at room temperature, protected from light, then fixed in 50% (v/v) methanol, 10% (v/v) acetic acid and destained. For Complex V ATP hydrolysis activity, native gels were equilibrated in 270mM glycine, 35mM Tris-HCl for 1h at room temperature, then switched to assay buffer containing 270mM glycine, 35mM Tris-HCl with 14mM $MgSO_4$, 0.2% $Pb(NO_3)_2$, and 8mM ATP, and incubated overnight. Gels were fixed in 50% (v/v) methanol and destained before imaging. Complex II activity was assayed by immunoaffinity microplate-based colorimetric assay (Abcam ab109908). Mitochondria were solubilized as per manufacturer's recommendations and 50µg of mitochondria were used per well. Activity is quantified as the rate of decrease in absorbance at 600nm as the production of ubiquinol reduces the blue dye DCPIP to a colorless product.

Immunoblotting

Cells were harvested in lysis buffer (50 mM Tris-HCl, pH 7.5, 150 mM NaCl, 1% Triton X-100) with protease inhibitor cocktail (Roche) followed by brief sonication and pelleting of cellular debris at 12,000g (5 min at 4°C). 20 mM nicotinamide was included in the lysis buffer for immunoblotting for lysine acylation. Protein concentration of lysate was determined by bicinchoninic acid (BCA) assay (Thermo Scientific), and 30µg of cell lysate was separated by Tris-Glycine SDS-PAGE (12% polyacrylamide). Proteins were transferred to PVDF membranes (Immobilon), blocked in 5% nonfat-milk TBST, and incubated with primary antibodies overnight. Primary antibodies used include: ACSF3 rabbit polyclonal at 1:1000 (ThermoFisher PA5-25803), heat shock chaperone 70 (HSC70) mouse monoclonal at 1:1000 (Santa Cruz sc-7298), MitoProfile total OXPHOS mouse monoclonal antibody cocktail at 1:500 (Abcam ab110413), voltage-dependent anion channel 1 (VDAC1) rabbit polyclonal at 1:1000 (Calbiochem AB10527), aconitase 2 (ACO2) rabbit polyclonal at 1:1000 (Cell Signaling 6922), α-lipoic acid

rabbit polyclonal at 1:1000 (Calbiochem #437695), phospho-ACC (Ser79) rabbit polyclonal at 1:1000 (Cell Signaling 11818), total ACC rabbit polyclonal at 1:1000 (Cell Signaling 3676), malonyl-lysine rabbit monoclonal mix at 1:1000 (Cell Signaling 14942), acetyl-lysine rabbit polyclonal at 1:1000 (Cell Signaling 9441), succinyl-lysine rabbit polyclonal at 1:1000 (PTM Biolabs 401), GFP mouse monoclonal at 1:1000 (Santa Cruz sc-9996). Cy3-conjugated anti-mouse secondary antibodies (Invitrogen M30010) at 1:1500 or horseradish peroxidase (HRP)-conjugated anti-mouse (GE Healthcare NA931V) or anti-rabbit secondary antibodies (GE Healthcare NA934V) at 1:2000 were incubated with washed membranes, and proteins were visualized with Amersham Prime enhanced chemiluminescent substrate (GE Healthcare) or epifluorescence on an Alpha Innotech MultiImage III instrument. Protein abundance was quantified using Alpha Innotech FluorChem Q software (Santa Clara, CA) and was normalized to HSC70 expression. For amido black total protein staining, PVDF membranes were incubated in 0.1% naphthol blue black (w/v), 10% methanol (v/v), 2% acetic acid (v/v) for 5 min and destained in 10% acetic acid (v/v), 25% isopropanol (v/v) for 1 min before imaging. For GFP immunoprecipitation (IP), cells were lysed in lysis buffer with 20 mM nicotinamide, and 800 µg of protein was incubated with 10 µL of GFP nanobody magnetic beads (Allele Biotechnology) for 4h at 4°C in 400 µL final volume binding buffer (10 mM Tris HCl, 150 mM NaCl, 20 mM nicotinamide). Beads were washed once in binding buffer and twice in wash buffer (10 mM Tris HCl, 500 mM NaCl, 20 mM nicotinamide) before eluting with 40 µL elution buffer (200 mM glycine, pH 2.5) and neutralizing with 4 µL 1M Tris. IP samples from an equivalent of 200 µg cell lysate were resolved by SDS-PAGE as described above.

Radiolabeled Substrate Metabolic Flux Assays

For glucose oxidation assays, cells were incubated in stoppered T-25 flasks with 0.1μCi/flask [U-^{14}C]D-glucose (Moravek Biochemicals) in serum-free DMEM containing 2.5 mM glucose, 2 mM glutamine, 0.5 mM pyruvate for 4 h. $^{14}CO_2$ was trapped on a filter paper suspended in the headspace of the flask by addition of 200μL 70% perchloric acid to the flask and 150μL 1M NaOH to the filter paper and incubating the samples at 55°C for 1 h. The filter paper was placed in scintillation fluid and counted, and counts were normalized to total protein. Glutamine and alanine oxidation assays were performed as described for glucose except 0.2μCi/flask [U-^{14}C]L-glutamine (New England Nuclear Radiochemicals/PerkinElmer) with 0.5 mM cold glutamine or 0.2μCi/flask [U-^{14}C]L-alanine (Moravek Biochemicals) with 0.1 mM cold alanine were used, respectively.

To determine substrate incorporation into the total lipid fraction, cells were plated in 24-well dishes and labeled with ^{14}C-labeled substrate for 4h. Total lipids were extracted with 2:1 chloroform:methanol via the Folch method (132), and radioactivity was counted by liquid scintillation. For [^{3}H]acetate incorporation, cells were labeled for 4h with 0.2μCi/well in DMEM supplemented with 10% bovine calf serum. For glucose, glutamine, and alanine incorporation, 0.2μCi/mL of radioactivity was used with the same media compositions as used for oxidation assays. For [2-^{14}C]malonate incorporation, cells were labeled for 4h with 0.2μC/well in 0.1mM unlabeled malonate. All counts were normalized to total protein as determined by BCA assay (Thermo Scientific). In order to separate and recover polar, non-polar, protein, and nucleic acid fractions from cells labeled with 0.2μCi/well [2-^{14}C]malonate (0.1mM unlabeled malonate) for 4h, a biphasic extraction protocol was used (293).

Metabolite Extraction and Analysis

For LC-QTOF, control and ACSF3 KO cells were exposed to 0 or 5 mM malonate for 24h prior to collection of cell extracts in ice-cold HPLC-grade 80:20 methanol: water and rapid quenching in liquid nitrogen. Cellular debris was pelleted by centrifugation, and the supernatant was dried by vacuum centrifugation prior to resuspension and unbiased metabolomics analysis by LC-QTOF (130, 134).

For stable isotope labeling experiments, cells (5E6 cells plated 24h before labeling) were incubated with 2.5 mM [1,3-^{13}C]malonate (Sigma-Aldrich) for 4 hours and washed twice in PBS before cell extracts were collected in ice-cold 80:20 methanol:water with rapid quenching in liquid nitrogen. The abundance and isotopic enrichment of select water-soluble metabolites (including short-chain acyl-carnitines, TCA cycle intermediates, and select amino acids) were quantified by LC-MS/MS on an Agilent 6490 triple-quadropole system (Agilent Technologies, Santa Clara, CA), as previously described (130). Briefly, the MS/MS experiment was performed in positive/negative switching electrospray mode, as described previously (133), and all data processing was performed with the Mass Hunter Quantitative Analysis software package. Raw metabolite abundances were normalized to protein content.

For capillary electrophoresis-MS (CE-MS), cells were washed with 5% mannitol and extracted with methanol spiked with an internal standard solution as specified by Human Metabolome Technologies. Insoluble material was pelleted and supernatant was filtered through centrifugal filters. Filtrate was dried under vacuum and resuspended for analysis by CE-TOF MS for cationic metabolites and CE-QqQ MS for anionic metabolites. Metabolite abundances were normalized to protein content.

For ^{1}H-NMR, cells were washed with ice-cold PBS and scraped into ice-cold methanol and snap frozen in liquid nitrogen before two additional freeze-thaw rounds with methanol

extraction. For ^{1}H-NMR of culture medium for succinate measurements, 600µL of media was extracted with twice the volume ice-cold methanol, snap frozen in liquid nitrogen and thawed. Cell extracts and media samples were subjected to a final spin at 15,000g for 1 min at 4°C, then the supernatant was dried under vacuum and the extract resuspended in 20 mM phosphate buffer, pH 7.4 ± 0.1, with 0.1 mM TMSP as an internal reference and 0.1 mM sodium azide. ^{1}H spectra were recorded on a Bruker Avance III 500MHz (Bruker Instruments, Germany) NMR spectrometer, operating at 499.9MHz and equipped with room temperature quadruple nuclei probe. Typical ^{1}H spectra were acquired using presaturation solvent suppression pulse sequence (noesyprld). Acquisition parameters were set as follows; spectral width of 8012.820 with a 64K data points, 512 scans, with a relaxation delay of 7s for a total collection time of 1.14h. Samples were automatically tuned and match, and shimmed to TMSP signal. Spectra were exported into Bruker format and were processed with Chenomx NMR Suit 8.2 Professional (Chenomx Inc, Edmonton, Alberta, Canada). TMSP signal (0.0 ppm) was used as a reference peak, spectra manually phase corrected and spline function was applied for the baseline correction. Metabolites were profiled and quantified using built-in Chenomx 500MHz library. Metabolite concentrations were normalized to protein content.

Protein Malonylation in Mouse Tissue Lysates

Mitochondria were isolated based on Frezza *et al*. 2007, and tissue lysates and mitochondrial extracts were prepared in RIPA buffer (50mM Tris-HCl, pH 7.4, 150mM NaCl, 1mM EDTA, 1% Triton X-100, 0.25% deoxycholate) with protease inhibitor, supplemented with 20mM nicotinamide, followed by pelleting of insoluble material at 13,000g for 15 min at 4°C.

QUANTIFICATION AND STATISTICAL ANALYSIS

Student's t-test was used to evaluate statistical significance for quantitation of metabolic flux assays and quantitation of immunoblots between control and ACSF3 KO cells. Repeated measures ANOVA with Bonferroni post-tests were used to test statistical significance in cellular oxygen consumption experiments and ^{1}H-NMR time course. For steady-state metabolomics analysis, two-way ANOVA was conducted using the freely available, web-based MetATT metabolomics tool for two-factor datasets (317). Statistical details of individual experiments can be found in Figure Legends.

Table 2.1. Primer sequences

Gene	RefSeq ID	Forward primer (5'→3')	Reverse primer (5'→3')
18S rRNA	NR_003278.3	GCAATTATTCCCCATGAACG	GGCCTCACTAAACCATCCAA
Rpl22	NM_009079.3	AGCAGGTTTTGAAGTTCACCC	CAGCTTTCCCATTCACCTTGA
B-actin	NM_007393.5	GGCTGTATTCCCCTCCATCG	CCAGTTGGTAACAATGCCATGT
Gapdh	NM_001289726.1	AGGTCGGTGTGAACGGATTTG	TGTAGACCATGTAGTTGAGGTCA
Mpc1	NM_018819.4	ATGTCCGGAGCAAGGACTTC	ACAGAGGGCGAAAGTCATCC
Mpc2	NM_027430.2	AATGGGGATTGGTGTGTGCT	TGACCAAATAAACCCTGTAGCCA
mt-Nd1	NC_005089.1	AATCGCCATAGCCTTCCTAACAT	GGCGTCTGCAAATGGTTGTAA
nuc-H19	NC_000073.6	GTACCCACCTGTCGTCC	GTCCACGAGACCAATGACTG
nuc-Chr12	NC_000078.6	GGGCTGACCTAAATGTGGCT	CTCCCTCGTTTTCAGACCCC
Pck1	NM_011044.2	GGAAGGACAAAGATGGCAAGTTC	AGGCGTTTTCCTTAGGGATGTAG
Pck2	NM_028994.2	ATGGCTGCTATGTACCTCCC	GCCACAAAGTCTCGAACTCC

Table 2.S1

Metabolites significantly regulated by Mpc1 deficiency in e17.5 brain or liver. Values shown are fold-change over WT and p-value as determined by Welch's two-sample t-test (n=8).

Metabolites significantly regulated by Mpc1 deficiency in e17.5 brain		
Biochemical Name	Mpc1 KI/WT	p-value
hypotaurine	15.51	0.0000
pyruvate	5.04	0.0000
4-imidazoleacetate	3.16	0.0000
phenyllactate (PLA)	2.98	0.0001
histamine	2.77	0.0113
sphingomyelin (d18:1/15:0, d16:1/17:0)*	2.35	0.0025
N-acetylglycine	2.34	0.0000
N-acetylhistidine	2.30	0.0000
sarcosine (N-Methylglycine)	2.24	0.0000
serine	2.19	0.0000
sphingomyelin (d18:1/14:0, d16:1/16:0)*	2.06	0.0007
4-vinylphenol sulfate	2.00	0.0210
proline	1.98	0.0000
glycine	1.94	0.0000
guanidinoacetate	1.93	0.0003
lactate	1.89	0.0000
phenylacetylglycine	1.88	0.0009
3-indoxyl sulfate	1.88	0.0033

N-acetylserine	1.84	0.0000
imidazole propionate	1.84	0.0013
aspartate	1.83	0.0000
anserine	1.83	0.0000
1-palmitoyl-2-linoleoyl-GPE (16:0/18:2)	1.81	0.0025
catechol sulfate	1.80	0.0028
beta-alanine	1.78	0.0000
hippurate	1.76	0.0396
N6-acetyllysine	1.75	0.0219
phenol sulfate	1.72	0.0150
4-acetamidobutanoate	1.71	0.0000
cysteine	1.68	0.0000
cysteine sulfinic acid	1.67	0.0413
2-aminophenol sulfate	1.63	0.0137
methylsuccinate	1.61	0.0000
carnosine	1.61	0.0081
isovalerylcarnitine	1.60	0.0036
ethylmalonate	1.59	0.0000
2-methylcitrate/homocitrate	1.59	0.0001
N-acetyltaurine	1.55	0.0002
gamma-glutamyl-epsilon-lysine	1.55	0.0009
orotate	1.55	0.0001
1-methylimidazoleacetate	1.54	0.0004
beta-hydroxyisovalerate	1.54	0.0001
palmitoyl dihydrosphingomyelin (d18:0/16:0)*	1.54	0.0211
beta-hydroxyisovaleroylcarnitine	1.52	0.0001
3-ureidopropionate	1.52	0.0037
4-hydroxyphenylpyruvate	1.49	0.0091
N-acetylalanine	1.48	0.0010
N-formylmethionine	1.48	0.0001
N-acetylvaline	1.46	0.0003
N-acetylmethionine	1.46	0.0001
1,2-dioleoyl-GPS (18:1/18:1)	1.46	0.0087
N-acetylthreonine	1.45	0.0001
betaine	1.42	0.0011
methylmalonate (MMA)	1.42	0.0013
N-acetylphenylalanine	1.41	0.0001
N-methylproline	1.41	0.0071
pyrraline	1.41	0.0027

N-acetylputrescine	1.38	0.0015
1-stearoyl-2-linoleoyl-GPE (18:0/18:2)*	1.38	0.0116
N-acetylarginine	1.36	0.0040
trigonelline (N'-methylnicotinate)	1.35	0.0032
N-glycolylneuraminate	1.35	0.0360
1-oleoyl-GPE (18:1)	1.34	0.0434
sphinganine	1.34	0.0352
succinylcarnitine	1.33	0.0275
arginine	1.32	0.0102
3-hydroxyisobutyrate	1.29	0.0150
2-hydroxyglutarate	1.26	0.0006
N-acetyltyrosine	1.25	0.0488
argininosuccinate	1.25	0.0243
1,2-dioleoyl-GPC (18:1/18:1)*	1.25	0.0411
carnitine	1.20	0.0373
1-palmitoyl-2-linoleoyl-GPC (16:0/18:2)	1.20	0.0403
lysine	1.18	0.0038
prolylglycine	1.18	0.0001
acetylcarnitine	1.18	0.0353
1-palmitoleoyl-GPC (16:1)*	1.17	0.0403
N-acetyl-aspartyl-glutamate (NAAG)	1.16	0.0177
N-acetylglucosaminylasparagine	1.09	0.0027
glycerophosphoglycerol	0.93	0.0174
ribitol	0.90	0.0107
glycerate	0.89	0.0076
gulonic acid*	0.88	0.0157
allantoin	0.87	0.0138
tartronate (hydroxymalonate)	0.87	0.0363
myo-inositol	0.86	0.0227
oxalate (ethanedioate)	0.86	0.0023
trans-4-hydroxyproline	0.84	0.0054
glucosamine-6-phosphate	0.84	0.0469
adenosine 5'-diphosphate (ADP)	0.84	0.0295
1-methylnicotinamide	0.84	0.0462
gamma-aminobutyrate (GABA)	0.82	0.0064
erythronate*	0.82	0.0001
leucine	0.81	0.0105
oleoyl ethanolamide	0.81	0.0005
palmitoyl ethanolamide	0.80	0.0001

2'-deoxycytidine	0.79	0.0087
threonate	0.79	0.0003
valine	0.78	0.0149
gamma-glutamylisoleucine*	0.78	0.0228
glycerophosphoethanolamine	0.78	0.0001
hexanoylcarnitine	0.77	0.0170
citrate	0.76	0.0077
pseudouridine	0.76	0.0000
N-palmitoyltaurine	0.75	0.0134
spermidine	0.74	0.0002
mannitol/sorbitol	0.73	0.0017
palmitoylcarnitine	0.73	0.0030
glutamate	0.72	0.0000
glutamate, gamma-methyl ester	0.72	0.0012
gamma-glutamylvaline	0.72	0.0034
isocitrate	0.71	0.0012
docosapentaenoate (n6 DPA; 22:5n6)	0.71	0.0275
stearoylcarnitine	0.71	0.0061
glutathione, oxidized (GSSG)	0.70	0.0001
5-oxoproline	0.70	0.0314
galactose 1-phosphate	0.70	0.0188
galactonate	0.70	0.0036
laurylcarnitine	0.70	0.0014
citrulline	0.69	0.0063
2-aminoheptanoate	0.69	0.0003
octanoylcarnitine	0.69	0.0033
glycerophosphorylcholine (GPC)	0.69	0.0000
glycerol	0.69	0.0045
2-aminoadipate	0.68	0.0207
kynurenine	0.67	0.0033
S-adenosylhomocysteine (SAH)	0.67	0.0078
ascorbate (Vitamin C)	0.67	0.0061
1-methylhistidine	0.66	0.0000
cystathionine	0.66	0.0024
ophthalmate	0.66	0.0202
myristoleoylcarnitine*	0.66	0.0003
2-aminobutyrate	0.65	0.0039
gamma-glutamylmethionine	0.65	0.0376
succinate	0.65	0.0012

myristoylcarnitine	0.65	0.0000
gamma-glutamylleucine	0.62	0.0006
tryptophan	0.60	0.0000
isoleucine	0.60	0.0015
3-methyl-2-oxovalerate	0.60	0.0059
methionine sulfone	0.60	0.0008
S-methylglutathione	0.60	0.0170
homocitrulline	0.59	0.0005
glutathione, reduced (GSH)	0.58	0.0013
gamma-glutamylthreonine*	0.56	0.0004
gamma-glutamylglutamine	0.54	0.0001
glycerol 3-phosphate	0.54	0.0001
S-methylcysteine	0.53	0.0018
N-delta-acetylornithine	0.53	0.0000
3-methylhistidine	0.47	0.0000
3-methoxytyrosine	0.45	0.0000
nicotinamide adenine dinucleotide reduced (NADH)	0.45	0.0001
2-hydroxyadipate	0.42	0.0003
glutamine	0.39	0.0000
alanine	0.32	0.0000
Metabolites significantly regulated by Mpc1 deficiency in e17.5 liver		
Biochemical Name	Mpc1 KI/WT	p-value
3-methylglutarylcarnitine (2)	3.68	0.0003
heme	2.99	0.0005
pyruvate	2.61	0.0017
4-imidazoleacetate	2.41	0.0021
sphingomyelin (d18:1/14:0, d16:1/16:0)*	2.41	0.0000
1-linoleoyl-GPE (18:2)*	2.35	0.0024
1-arachidonylglycerol (20:4)	2.35	0.0079
palmitoyl dihydrosphingomyelin (d18:0/16:0)*	2.30	0.0000
histamine	2.19	0.0002
1-palmitoyl-2-linoleoyl-GPG (16:0/18:2)	2.16	0.0000
1-arachidonoyl-GPE (20:4)*	2.10	0.0069
biliverdin	2.03	0.0283
sphingomyelin (d18:1/15:0, d16:1/17:0)*	2.00	0.0000
docosahexaenoate (DHA; 22:6n3)	1.96	0.0066
sphingomyelin (d18:1/17:0, d17:1/18:0, d19:1/16:0)	1.96	0.0000

2-arachidonoylglycerol (20:4)	1.95	0.0424
indolepropionate	1.94	0.0371
sphinganine	1.92	0.0004
1-stearoyl-GPS (18:0)*	1.90	0.0090
stearoyl sphingomyelin (d18:1/18:0)	1.90	0.0000
adenosine 3',5'-diphosphate	1.84	0.0230
1-docosahexaenoyl-GPE (22:6)*	1.80	0.0267
eicosapentaenoate (EPA; 20:5n3)	1.77	0.0023
N-acetylhistidine	1.73	0.0049
methylsuccinate	1.72	0.0035
1-palmitoyl-2-linoleoyl-GPE (16:0/18:2)	1.69	0.0003
1-stearoyl-2-arachidonoyl-GPS (18:0/20:4)	1.67	0.0003
sphingomyelin (d18:1/20:0, d16:1/22:0)*	1.66	0.0000
N-acetyltaurine	1.64	0.0012
gamma-carboxyglutamate	1.62	0.0005
1-stearoyl-2-linoleoyl-GPE (18:0/18:2)*	1.62	0.0005
1-palmitoyl-2-arachidonoyl-GPE (16:0/20:4)*	1.60	0.0000
p-cresol-glucuronide*	1.56	0.0479
1-oleoyl-GPE (18:1)	1.55	0.0164
N-acetylmethionine sulfoxide	1.53	0.0211
gamma-glutamylglycine	1.53	0.0350
1-palmitoyl-GPE (16:0)	1.53	0.0058
2-palmitoleoyl-GPC (16:1)*	1.51	0.0377
sphingomyelin (d18:1/18:1, d18:2/18:0)	1.50	0.0004
palmitoyl sphingomyelin (d18:1/16:0)	1.49	0.0000
N-acetylphenylalanine	1.48	0.0009
phenylacetylglycine	1.48	0.0300
ethylmalonate	1.48	0.0000
1-oleoyl-2-linoleoyl-GPE (18:1/18:2)*	1.45	0.0008
flavin adenine dinucleotide (FAD)	1.45	0.0185
N-acetylglycine	1.44	0.0040
guanosine 5'- monophosphate (5'-GMP)	1.43	0.0007
1-stearoyl-GPE (18:0)	1.42	0.0020
histidine	1.41	0.0498
glycine	1.40	0.0015
1-stearoyl-2-arachidonoyl-GPE (18:0/20:4)	1.40	0.0014
1,2-dilinoleoyl-GPC (18:2/18:2)	1.40	0.0003
N-palmitoyl-sphingosine (d18:1/16:0)	1.40	0.0175
sphingomyelin (d18:1/22:1, d18:2/22:0, d16:1/24:1)*	1.40	0.0016

1-stearoyl-2-oleoyl-GPS (18:0/18:1)	1.39	0.0153
N-acetyltyrosine	1.38	0.0445
1-stearoyl-2-arachidonoyl-GPI (18:0/20:4)	1.38	0.0104
sulfate*	1.38	0.0106
phosphoethanolamine	1.37	0.0061
1-stearoyl-2-linoleoyl-GPC (18:0/18:2)*	1.36	0.0084
serine	1.35	0.0022
3-indoxyl sulfate	1.35	0.0453
1-methylhistamine	1.34	0.0241
1-stearoyl-2-arachidonoyl-GPC (18:0/20:4)	1.34	0.0228
1-(1-enyl-palmitoyl)-2-arachidonoyl-GPE (P-16:0/20:4)*	1.33	0.0046
1-palmitoleoyl-2-linoleoyl-GPC (16:1/18:2)*	1.32	0.0028
1-(1-enyl-palmitoyl)-2-linoleoyl-GPE (P-16:0/18:2)*	1.32	0.0124
sphingomyelin (d18:2/24:1, d18:1/24:2)*	1.31	0.0082
1-linoleoyl-2-arachidonoyl-GPC (18:2/20:4)*	1.30	0.0006
anserine	1.29	0.0244
adenosine 5'-diphosphate (ADP)	1.29	0.0116
1-oleoyl-2-linoleoyl-GPC (18:1/18:2)*	1.25	0.0010
1,2-dipalmitoyl-GPC (16:0/16:0)	1.24	0.0034
1-palmitoyl-2-linoleoyl-GPC (16:0/18:2)	1.23	0.0024
1-palmitoyl-2-oleoyl-GPE (16:0/18:1)	1.23	0.0362
sphingomyelin (d18:2/16:0, d18:1/16:1)*	1.23	0.0013
pyridoxamine phosphate	1.23	0.0131
proline	1.22	0.0366
lactate	1.21	0.0015
palmitoyl ethanolamide	1.21	0.0360
beta-hydroxyisovaleroylcarnitine	1.18	0.0185
adenosine 5'-monophosphate (AMP)	1.18	0.0207
1-palmitoyl-2-arachidonoyl-GPC (16:0/20:4)	1.16	0.0154
N-acetylglucosaminylasparagine	1.12	0.0104
carnitine	0.87	0.0149
methionine sulfoxide	0.86	0.0373
threonate	0.85	0.0158
2'-deoxyuridine	0.84	0.0390
pro-hydroxy-pro	0.81	0.0451
2-aminoheptanoate	0.81	0.0030
glutamate	0.79	0.0304
thiamin diphosphate	0.79	0.0091

erythronate*	0.78	0.0008
tryptophan	0.77	0.0073
trans-4-hydroxyproline	0.77	0.0003
ribitol	0.77	0.0022
erythritol	0.77	0.0029
alanine	0.76	0.0005
1-methylhistidine	0.76	0.0022
citrulline	0.76	0.0003
5-methylthioadenosine (MTA)	0.75	0.0012
mannitol/sorbitol	0.75	0.0244
glycerol	0.75	0.0115
oxalate (ethanedioate)	0.75	0.0000
N6,N6,N6-trimethyllysine	0.74	0.0023
3-methoxytyrosine	0.74	0.0496
putrescine	0.74	0.0249
gamma-glutamylisoleucine*	0.74	0.0006
gamma-glutamylleucine	0.73	0.0076
orotate	0.73	0.0499
2'-deoxycytidine	0.73	0.0236
glycerol 3-phosphate	0.72	0.0279
thymidine	0.72	0.0363
orotidine	0.71	0.0003
pseudouridine	0.71	0.0000
S-adenosylhomocysteine (SAH)	0.70	0.0226
5-methyl-2'-deoxycytidine	0.70	0.0118
ergothioneine	0.70	0.0004
homocitrulline	0.69	0.0017
gamma-glutamylvaline	0.69	0.0002
N6-succinyladenosine	0.69	0.0403
N4-acetylcytidine	0.68	0.0010
2-aminobutyrate	0.67	0.0475
creatine	0.67	0.0000
N-acetylglucosamine 6-phosphate	0.67	0.0344
maleate	0.67	0.0001
nicotinamide adenine dinucleotide (NAD+)	0.67	0.0156
dimethylglycine	0.66	0.0000
N-delta-acetylornithine	0.66	0.0001
arabitol/xylitol	0.66	0.0085
methionine sulfone	0.65	0.0005

cysteine-glutathione disulfide	0.64	0.0182
gamma-glutamylthreonine*	0.64	0.0085
gamma-glutamyltryptophan	0.64	0.0119
alpha-ketoglutarate	0.62	0.0001
2-hydroxyglutarate	0.62	0.0091
S-methylglutathione	0.61	0.0139
gamma-glutamylalanine	0.61	0.0010
fumarate	0.61	0.0000
3-methylhistidine	0.60	0.0014
alpha-hydroxyisocaproate	0.59	0.0376
malate	0.59	0.0001
gulonic acid*	0.59	0.0000
ophthalmate	0.57	0.0398
argininosuccinate	0.56	0.0007
N-acetyl-glucosamine 1-phosphate	0.55	0.0102
5-ketogluconate	0.55	0.0000
creatinine	0.54	0.0000
pipecolate	0.53	0.0006
glutamine	0.51	0.0152
isovalerylcarnitine	0.50	0.0414
glutarylcarnitine (C5)	0.49	0.0104
3-methylglutarylcarnitine (1)	0.43	0.0003
pregn steroid monosulfate*	0.43	0.0000
N-carbamoylaspartate	0.37	0.0013
creatine phosphate	0.33	0.0011
isobutyrylcarnitine	0.31	0.0015

Table 4.1 Primers for maternal-fetal metabolic communication study

Gene	RefSeq ID	Forward primer (5'→3')	Reverse primer (5'→3')
Acadl	NM_007381.4	TTTCCTCGGAGCATGACATTTT	GCCAGCTTTTTCCCAGACCT
Acadm	NM_007382.5	AACACTTACTATGCCTCGATTGCA	CCATAGCCTCCGAAAATCTGAA
Acot1	NM_012006.2	AACATCACCTTTGGAGGGGAG	TCCCCAACCTCCAAACCATCA
Acot2	NM_134188.3	AGTCAACGACGCAAAATGGTG	GCTCTTCCAATCCTGTTGGC
Acox1	NM_015729.3	ACGCCACTTCCTTGCTCTTC	AGATTGGTAGAAATTGCTGCAAA
Acsl1	NM_001302163.1	ATCTGGTGGAACGAGGCAAG	TCCTTTGGGGTTGCCTGTAG
Bdh1	NM_175177.4	TGACACCCGTCGGACCTAC	TTCTCAGTCGGTCACTCTTCA
Cpt1a	NM_013495.2	CCATCCTGTCCTGACAAGGTTTAG	CCTCACTTCTGTTACAGCTAGCAC
Cpt1b	NM_009948.2	GGTCCCATAAGAAACAAGACCTCC	CAGAAAGTACCTCAGCCAGGAAAG
Cpt2	NM_009949.2	CAACTCGTATACCCAAACCCAGTC	GTTCCCATCTTGATCGAGGACATC
Ehhadh	NM_023737.3	CAGATGAAGCACTCAAGCTTG	ACCTTGGCAATGGCTTCTGCA
Fabp3	NM_010174.1	AGTCACTGGTGACGCTGGACG	AGGCAGCATGGTGCTGAGCTG
Fasn	NM_007988.3	GCTGCGGAAACTTCAGGAAAT	AGAGACGTGTCACTCCTGGACTT
Fgf21	NM_020013.4	CCTCTAGGTTTCTTTGCCAACAG	AAGCTGCAGGCCTCAGGAT
Glud1	NM_008133.4	ACTCTGGCTTGGCCTACACAATG	CGGCTGTGAGCTGTCTATGTGAA
Got1	NM_010324.2	CATCAGTCTTTGCCCAGGTTC	GCTGAGATTCATCTGTGCGGTA
Got2	NM_010325.2	TCACCGGCCTAAAGCCAGA	TGAATGGCATGGGCAAGGTA
Gpt1	NM_182805.3	CGTGGTGGCTATGTGGAAGT	CTCCTGCCTCTCTGCTTGAAA
Gpt2	NM_173866.3	TGATGGCACTCTGCACCTAC	GCACTGTAAGATCCCAAGCTG
Hadha	NM_178878.2	TGCATTTGCCGCAGCTTTAC	GTTGGCCCAGATTTCGTTCA
Mpc1	NM_018819.4	ATGTCCGGAGCAAGGACTTC	ACAGAGGGCGAAAGTCATCC
Mpc2	NM_027430.2	AATGGGGATTGGTGTGTGCT	TGACCAAATAAACCCTGTAGCCA
Pck1	NM_011044.2	GGAAGGACAAAGATGGCAAGTTC	AGGCGTTTTCCTTAGGGATGTAG
Pck2	NM_028994.3	ATGGCTGCTATGTACCTCCC	GCCACAAAGTCTCGAACTCC
Pcx	NM_001162946.1	GGAGCTTATCCCGAACATCC	CGGAAGACGTCCATACCATTC
Pdk4	NM_013743.2	ATCTAACATCGCCAGAATTAAACC	GGAACGTACACAATGTGGATTG
Pgc1α	NM_008904.2	CAACATGCTCAAGCCAAACCAACA	CGCTCAATAGTCTTGTTCTCAAATGGG
PPARα	NM_011144.6	GCGTACGGCAATGGCTTTAT	GAACGGCTTCCTCAGGTTCTT
Scd1	NM_009127.4	CCCTGCGGATCTTCCTTATC	TGTGTTTCTGAGAACTTGTGGTG
Trib3	NM_175093.2	GGCCTTATATCCTTTTGGAACGA	CGCTGGCAGGGTACACCTT
Reference genes:			
Rpl22	NM_009079.3	AGCAGGTTTTGAAGTTCACCC	CAGCTTTCCCATTCACCTTGA
Gapdh	NM_001289726.1	AGGTCGGTGTGAACGGATTTG	TGTAGACCATGTAGTTGAGGTCA
18S	NR_003278.3	GCAATTATTCCCCATGAACG	GGCCTCACTAAACCATCCAA
B-actin	NM_007393.5	GGCTGTATTCCCCTCCATCG	CCAGTTGGTAACAATGCCATGT

Table A.S1. Malonate- and Malonyl-CoA-Dependent Metabolic Alterations in ACSF3 KO Cells Revealed by Steady-State Metabolite Abundances

Average metabolite abundances expressed as fold change relative to untreated control cells, displayed as "average (SEM)", n=10 per condition. Select metabolites are organized by molecular class or metabolic pathway and are ranked by most highly up-regulated in KO cells to most down-regulated in KO cells under baseline conditions (0mM malonate). Also shown is fold change of metabolite abundance of control and ACSF3 KO cells after 24 hour exposure to 5 mM malonate relative to untreated control cells. Statistical significance of genotype effects, malonate treatment, and/or interaction between genotype and treatment determined by two-way ANOVA and indicated in rightmost columns (* $p<0.01$, ** $p<0.001$).

Compound Name	Control	ACSF3 KO	Control + Malonate	ACSF3 KO + Malonate	Genotype	Malonate	Interaction
Malonate	1.00 (0.27)	4.86 (0.63)	772.8 (37.8)	1304 (159)	*	**	*
TCA Cycle Intermediates							
Succinate	1.00 (0.13)	1.21 (0.08)	26.81 (1.50)	39.38 (2.65)	**	**	*
Citrate	1.00 (0.09)	1.00 (0.10)	0.83 (0.06)	0.59 (0.10)		*	
Isocitrate	1.00 (0.07)	0.74 (0.04)	0.76 (0.04)	0.64 (0.01)	**	*	
cis-Aconitate	1.00 (0.02)	0.59 (0.05)	0.52 (0.01)	0.37 (0.04)	**	**	*
Amino Acid Metabolism							
Glutamine	1.00 (0.18)	3.82 (0.42)	0.74 (0.32)	4.84 (0.32)	**		
Histidinol	1.00 (0.14)	1.15 (0.29)	0.15 (0.22)	1.27 (0.22)	*		
Histidinal	1.00 (0.17)	1.14 (0.30)	0.13 (0.23)	1.26 (0.23)	*		
Glutamate	1.00 (0.03)	0.99 (0.01)	0.76 (0.01)	0.98 (0.01)	**	**	**
Imidazole-4-acetate	1.00 (0.12)	0.81 (0.22)	0.26 (0.34)	1.78 (0.34)	*		*
Leucine / Isoleucine	1.00 (0.04)	0.74 (0.06)	1.17 (0.03)	0.80 (0.09)	**		
Glycine	1.00 (0.06)	0.72 (0.03)	1.20 (0.03)	0.79 (0.03)	**	*	
Valine	1.00 (0.03)	0.71 (0.05)	0.94 (0.06)	0.63 (0.06)	**		
Glutathione	1.00 (0.04)	0.68 (0.07)	1.08 (0.08)	0.68 (0.08)	**		
Methionine	1.00 (0.04)	0.64 (0.04)	1.36 (0.07)	0.82 (0.07)	**	**	
Proline	1.00 (0.03)	0.63 (0.04)	1.06 (0.02)	0.47 (0.02)	**		*
Tryptophan	1.00 (0.04)	0.62 (0.04)	1.07 (0.10)	0.65 (0.10)	**		
Phenylalanine	1.00 (0.03)	0.62 (0.04)	1.10 (0.08)	0.66 (0.08)	**		
Asparagine	1.00 (0.07)	0.60 (0.06)	0.91 (0.16)	1.54 (0.16)		**	**

Lysine	1.00	(0.05)	0.59	(0.05)	0.81	(0.10)	0.63	(0.10)	**		
Threonine	1.00	(0.03)	0.50	(0.06)	1.12	(0.05)	0.57	(0.05)	**		
Serine	1.00	(0.04)	0.46	(0.02)	1.25	(0.14)	2.70	(0.14)	**	**	**
Hypotaurine	1.00	(0.08)	0.42	(0.01)	1.30	(0.02)	0.47	(0.02)	**	*	
4-Hydroxyphenylacetaldehyde/ Phenylacetic acid	1.00	(0.20)	0.38	(0.01)	0.46	(0.02)	0.16	(0.02)	**	*	
Alanine	1.00	(0.02)	0.33	(0.07)	1.45	(0.02)	0.88	(0.05)	**	**	

Compound Name	Control		ACSF3 KO		Control + Malonate		ACSF3 KO + Malonate		Genotype	Malonate	Interaction
Carbohydrate / Nucleotide Metabolism											
2-Deoxy-ribose 1-phosphate	1.00	(0.12)	2.78	(0.53)	1.29	(0.11)	3.98	(0.59)	**		
Ribitol	1.00	(0.07)	0.86	(0.11)	1.13	(0.06)	0.46	(0.06)	**		*
Deoxyribose	1.00	(0.02)	0.49	(0.02)	1.07	(0.02)	0.61	(0.02)	**	**	
AMP	1.00	(0.05)	1.69	(0.13)	0.75	(0.06)	1.32	(0.15)	**	*	
ADP	1.00	(0.07)	1.29	(0.07)	1.04	(0.09)	0.70	(0.05)		**	**
UDP	1.00	(0.14)	1.66	(0.32)	5.97	(0.61)	1.32	(0.29)	**	**	**
UMP	1.00	(0.11)	0.46	(0.08)	0.46	(0.11)	0.37	(0.06)	*	*	
2'-Deoxyinosine 5'-phosphate	1.00	(0.19)	0.16	(0.02)	0.84	(0.19)	0.16	(0.03)	**		
UDP-glucose / UDP-galactose	1.00	(0.15)	1.55	(0.39)	5.38	(0.36)	1.88	(0.51)	**	**	**
UDP-glucuronate/ UDP-galacturonate/UDP-iduronate	1.00	(0.32)	1.24	(0.47)	17.32	(4.49)	1.00	(0.33)	*	*	*
Cytidine	1.00	(0.12)	1.68	(0.15)	1.47	(0.16)	2.70	(0.17)	**	**	
Deoxycytidine	1.00	(0.05)	0.90	(0.10)	1.23	(0.04)	0.51	(0.03)	**		**
Adenine	1.00	(0.09)	0.73	(0.10)	0.15	(0.03)	0.20	(0.05)		**	
3-Ureidopropionate	1.00	(0.07)	0.59	(0.06)	1.01	(0.10)	1.54	(0.16)		**	**
Uridine / Pseudouridine	1.00	(0.21)	0.56	(0.14)	0.74	(0.14)	0.31	(0.09)	*		
5-Methylcytosine	1.00	(0.17)	1.14	(0.30)	0.13	(0.03)	1.26	(0.23)	*		
1-Methyladenosine	1.00	(0.15)	0.46	(0.03)	1.03	(0.08)	0.63	(0.06)	**		
Methylglyoxal / Propenoate	1.00	(0.23)	0.90	(0.28)	44.43	(2.58)	65.42	(4.40)	**	**	*
Lipid Metabolism											
5-Phosphomevalonate	1.00	(0.12)	2.80	(0.54)	1.30	(0.11)	4.02	(0.60)	**		
Glycerol 3-phosphate	1.00	(0.19)	2.76	(0.43)	1.25	(0.22)	0.90	(0.08)		*	*
sn-glycero-3-Phosphoethanolamine	1.00	(0.08)	1.97	(0.11)	2.11	(0.16)	2.08	(0.07)	**	**	**
Glycerol	1.00	(0.06)	0.75	(0.09)	1.13	(0.06)	0.40	(0.05)	**		*
2-Arachidonoylglycerol	1.00	(0.07)	0.30	(0.04)	0.69	(0.06)	0.21	(0.01)	**	**	

Vitamin/Cofactor Metabolism											
Pantothenate	1.00	(0.03)	0.66	(0.06)	0.78	(0.02)	0.54	(0.04)	**	**	
Biotin	1.00	(0.07)	0.64	(0.11)	0.35	(0.04)	0.93	(0.12)			**

Table A.S2 Key Resources Table

REAGENT or RESOURCE	SOURCE	IDENTIFIER
Antibodies		
Acyl-CoA synthetase family member 3 (ACSF3), rabbit polyclonal	ThermoFisher	Cat#PA5-25803; RRID: AB_2543303
Heat shock chaperone 70 (HSC70), mouse monoclonal	Santa Cruz	Cat#sc-7298; RRID: AB_627761
MitoProfile total OXPHOS, mouse monoclonal antibody mix	Abcam	Cat#ab110413; RRID: AB_2629281
Voltage-dependent anion channel 1 (VDAC1), rabbit polyclonal	Calbiochem	Cat#AB10527; RRID: AB_10806766
Aconitase 2 (ACO2), rabbit polyclonal	Cell Signaling	Cat#6922; RRID: AB_10828218
α-lipoic acid, rabbit polyclonal	Calbiochem	Cat#437695; RRID: AB_212120
Phospho-acetyl-CoA carboxylase (ACC) (Ser79), rabbit polyclonal	Cell Signaling	Cat#11818
Total ACC, rabbit polyclonal	Cell Signaling	Cat#3676; RRID: AB_2219397
α-malonyl-lysine, rabbit monoclonal antibody mix	Cell Signaling	Cat#14942
α-acetyl-lysine, rabbit polyclonal	Cell Signaling	Cat#9441; RRID: AB_331806
α-succinyl-lysine, rabbit polyclonal	PTM Biolabs	Cat#401
GFP, mouse monoclonal	Santa Cruz	Cat#sc-9996; RRID: AB_627695
Cy3-conjugated anti-mouse secondary antibody	Invitrogen	Cat#M30010; RRID: AB_2536619
Horseradish peroxidase (HRP)-conjugated anti-mouse secondary antibody	GE Healthcare	Cat#NA931V
HRP-conjugated anti-rabbit secondary antibody	GE Healthcare	Cat#NA934V
GFP nanobody magnetic beads	Allele Biotechnology	Cat#ABP-NAB-GFPM050
Chemicals, Peptides, and Recombinant Proteins		
Malonate	Sigma-Aldrich	M1296; CAS: 141-82-2
[U-^{14}C]D-glucose	Moravek Biochemicals	MC144W
[U-^{14}C]L-glutamine	New England Nuclear/PerkinElmer	NEC451050UC
[U-^{14}C]L-alanine	Moravek Biochemicals	MC132
[^{3}H]acetate	New England Nuclear/PerkinElmer	NET003025MC
[2-^{14}C]malonate	Moravek Biochemicals	MC312
[1,3-^{13}C]malonate	Sigma-Aldrich	490199; CAS: 99524-14-8
3-Nitropropionic acid	Sigma-Aldrich	N5636; CAS: 504-88-1

Critical Commercial Assays		
CellTiter 96 Aqueous One Cell Proliferation Assay	Promega	Cat#G3582
Amersham Prime Enhanced Chemiluminescent Substrate	GE Healthcare	Cat#RPN2232
XF^{e}96 Extracellular Flux Assay Kit	Seahorse Bioscience	Cat#102601-100
CyQUANT Cell Proliferation Assay Kit	Invitrogen	Cat#C7026
Complex II Enzyme Activity Microplate Assay	Abcam	Cat#ab109908
Experimental Models: Cell Lines		
Human: HEK293T	ATCC	Cat#CRL-3216; RRID: CVCL_0063
Experimental Models: Organisms/Strains		
Mouse: Wild-type C57BL/6J	The Jackson Laboratory	RRID: IMSR_JAX:000664
Mouse: *ob/ob* obese, leptin-deficient: B6.Cg-*Lep*^{ob}/J	The Jackson Laboratory	RRID: IMSR_JAX:000632
Oligonucleotides		
ACSF3 Forward: 5'-ACACAGAGGAAGTGGTCTTCT-3'	This paper	N/A
ACSF3 Reverse: 5'-CGTTAGCGCATAGGAAGGAGA-3'	This paper	N/A
Recombinant DNA		
Human codon-optimized Cas9 expression vector	Mali et al., 2013	Addgene Plasmid #41815
pEF6-nls-YFP-2A-Cas9 for bicistronic expression of nuclear YFP and Cas9	Bowman et al., 2016	N/A
Mitochondrially-targeted YFP expression vector (pEYFP-Mito)	Clontech	Cat#6115
Cytoplasmic YFP expression vector (pEYFP-C1)	Clontech	Cat#6341
Other		
FuGENE HD Transfection Reagent	Promega	Cat#E2311
In-Fusion HD Cloning Enzyme	Clontech	Cat#639636

References

1. **Prentice AM, Goldberg GR.** 2000. Energy adaptations in human pregnancy: limits and long-term consequences. Am J Clin Nutr **71:**1226S-1232S.
2. **Elliot MG, Crespi BJ.** 2008. Placental invasiveness and brain-body allometry in eutherian mammals. J Evol Biol **21:**1763-1778.
3. **Grosser O.** 1909. Vergleichende Anatomie und Entwicklungsgeschichte der Eihaute und der Placenta. Wilhelm Braumuller, Vienna.
4. **Blackburn ST.** 2007. Maternal, Fetal, and Neonatal Physiology: A Clinical Perspective, Third ed. Saunders Elsevier.
5. **Yamashita H, Shao J, Friedman JE.** 2000. Physiologic and molecular alterations in carbohydrate metabolism during pregnancy and gestational diabetes mellitus. Clin Obstet Gynecol **43:**87-98.
6. **Freinkel N.** 1980. Banting Lecture 1980. Of pregnancy and progeny. Diabetes **29:**1023-1035.
7. **Butte NF, Wong WW, Treuth MS, Ellis KJ, O'Brian Smith E.** 2004. Energy requirements during pregnancy based on total energy expenditure and energy deposition. Am J Clin Nutr **79:**1078-1087.
8. **Kopp-Hoolihan LE, van Loan MD, Wong WW, King JC.** 1999. Longitudinal assessment of energy balance in well-nourished, pregnant women. Am J Clin Nutr **69:**697-704.
9. **Dewar AD.** 1953. Total metabolism of the mouse after pseudoparturition and parturition. Q J Exp Physiol Cogn Med Sci **38:**263-294.
10. **Haig D.** 1993. Genetic conflicts in human pregnancy. Q Rev Biol **68:**495-532.
11. **Haig D.** 1996. Altercation of generations: genetic conflicts of pregnancy. Am J Reprod Immunol **35:**226-232.
12. **Tunster SJ, Jensen AB, John RM.** 2013. Imprinted genes in mouse placental development and the regulation of fetal energy stores. Reproduction **145:**R117-137.
13. **Moore T, Haig D.** 1991. Genomic imprinting in mammalian development: a parental tug-of-war. Trends Genet **7:**45-49.
14. **Battaglia FC, Meschia G.** 1978. Principal substrates of fetal metabolism. Physiol Rev **58:**499-527.
15. **Kalhan S, Rossi K, Gruca L, Burkett E, O'Brien A.** 1997. Glucose turnover and gluconeogenesis in human pregnancy. J Clin Invest **100:**1775-1781.
16. **Longo LD.** 1983. Maternal blood volume and cardiac output during pregnancy: a hypothesis of endocrinologic control. Am J Physiol **245:**R720-729.
17. **Haggarty P.** 2010. Fatty acid supply to the human fetus. Annu Rev Nutr **30:**237-255.
18. **Even MD, Laughlin MH, Krause GF, vom Saal FS.** 1994. Differences in blood flow to uterine segments and placentae in relation to sex, intrauterine location and side in pregnant rats. J Reprod Fertil **102:**245-252.
19. **Coe BL, Kirkpatrick JR, Taylor JA, vom Saal FS.** 2008. A new 'crowded uterine horn' mouse model for examining the relationship between foetal growth and adult obesity. Basic Clin Pharmacol Toxicol **102:**162-167.
20. **Knopp RH, Herrera E, Freinkel N.** 1970. Carbohydrate metabolism in pregnancy. 8. Metabolism of adipose tissue isolated from fed and fasted pregnant rats during late gestation. J Clin Invest **49:**1438-1446.
21. **Elliott JA.** 1975. The effect of pregnancy on the control of lipolysis in fat cells isolated from human adipose tissue. Eur J Clin Invest **5:**159-163.

22. **Herrera E, Amusquivar E, Lopez-Soldado I, Ortega H.** 2006. Maternal lipid metabolism and placental lipid transfer. Horm Res **65 Suppl 3:**59-64.
23. **Hytten FE.** 1981. Weight gain in pregnancy--30 year of research. S Afr Med J **60:**15-19.
24. **Girard J, Ferre P, Pegorier JP, Duee PH.** 1992. Adaptations of glucose and fatty acid metabolism during perinatal period and suckling-weaning transition. Physiol Rev **72:**507-562.
25. **Widdowson EM.** 1968. Growth and composition of the fetus and newborn., p 1-49. *In* Assali NS (ed), The Biology of Gestation, vol 2. Academic, New York.
26. **Morrison SD.** 1956. The total energy and water metabolism during pregnancy in the rat. J Physiol **134:**650-664.
27. **Valcarce C, Cuezva JM, Medina JM.** 1985. Increased Gluconeogenesis in the Rat at Term Gestation. Life Sci **37:**553-560.
28. **Richard D, Trayhurn P.** 1985. Energetic efficiency during pregnancy in mice fed ad libitum or pair-fed to the normal energy intake of unmated animals. J Nutr **115:**593-600.
29. **Edson JL, Hudson DG, Hull D.** 1975. Evidence of increased fatty acid transfer across the placenta during a maternal fast in rabbits. Biol Neonate **27:**50-55.
30. **Nagy LE, King JC.** 1984. Postprandial energy expenditure and respiratory quotient during early and late pregnancy. Am J Clin Nutr **40:**1258-1263.
31. **Forsum E, Lof M.** 2007. Energy metabolism during human pregnancy. Annu Rev Nutr **27:**277-292.
32. **Catalano PM, Roman-Drago NM, Amini SB, Sims EA.** 1998. Longitudinal changes in body composition and energy balance in lean women with normal and abnormal glucose tolerance during pregnancy. Am J Obstet Gynecol **179:**156-165.
33. **Butte NF, Hopkinson JM, Mehta N, Moon JK, Smith EO.** 1999. Adjustments in energy expenditure and substrate utilization during late pregnancy and lactation. Am J Clin Nutr **69:**299-307.
34. **Silva JF, Serakides R.** 2016. Intrauterine trophoblast migration: A comparative view of humans and rodents. Cell Adh Migr **10:**88-110.
35. **Coan PM, Ferguson-Smith AC, Burton GJ.** 2004. Developmental dynamics of the definitive mouse placenta assessed by stereology. Biol Reprod **70:**1806-1813.
36. **Rossant J, Cross JC.** 2001. Placental development: lessons from mouse mutants. Nat Rev Genet **2:**538-548.
37. **Dilworth MR, Sibley CP.** 2013. Review: Transport across the placenta of mice and women. Placenta **34 Suppl:**S34-39.
38. **Sandovici I, Hoelle K, Angiolini E, Constancia M.** 2012. Placental adaptations to the maternal-fetal environment: implications for fetal growth and developmental programming. Reprod Biomed Online **25:**68-89.
39. **Grigsby PL.** 2016. Animal Models to Study Placental Development and Function throughout Normal and Dysfunctional Human Pregnancy. Semin Reprod Med **34:**11-16.
40. **Duyne CMV, Parker HR, Havel RJ, Holm LW.** 1960. Free fatty acid metabolism in fetal and newborn sheep. American Journal of Physiology-Legacy Content **199:**987-990.
41. **Kety SS.** 1957. The general metabolism of the brain *in vivo*, p 221-237. *In* Richter D (ed), Metabolism of the nervous system. Pergamon, London.
42. **Rolfe DF, Brown GC.** 1997. Cellular energy utilization and molecular origin of standard metabolic rate in mammals. Physiol Rev **77:**731-758.
43. **Cremer JE.** 1982. Substrate utilization and brain development. J Cereb Blood Flow Metab **2:**394-407.

44. **Lynen F.** 1957. Fatty acid metabolism, p 381-395. *In* Richter D (ed), Metabolism of the nervous system. Pergamon, London.
45. **Abbot P, Rokas A.** 2017. Mammalian pregnancy. Curr Biol **27:**R127-r128.
46. **Guernsey MW, Chuong EB, Cornelis G, Renfree MB, Baker JC.** 2017. Molecular conservation of marsupial and eutherian placentation and lactation. Elife **6**.
47. **Lopaschuk GD, Spafford MA, Marsh DR.** 1991. Glycolysis is predominant source of myocardial ATP production immediately after birth. American Journal of Physiology - Heart and Circulatory Physiology **261:**H1698-H1705.
48. **Fisher DJ, Heymann MA, Rudolph AM.** 1981. Myocardial consumption of oxygen and carbohydrates in newborn sheep. Pediatr Res **15:**843-846.
49. **Arizmendi C, Medina JM.** 1983. Lactate as an oxidizable substrate for rat brain in vitro during the perinatal period. Biochem J **214:**633-635.
50. **Faubert B, Li KY, Cai L, Hensley CT, Kim J, Zacharias LG, Yang C, Do QN, Doucette S, Burguete D, Li H, Huet G, Yuan Q, Wigal T, Butt Y, Ni M, Torrealba J, Oliver D, Lenkinski RE, Malloy CR, Wachsmann JW, Young JD, Kernstine K, DeBerardinis RJ.** 2017. Lactate Metabolism in Human Lung Tumors. Cell **171:**358-371.e359.
51. **Hui S, Ghergurovich JM, Morscher RJ, Jang C, Teng X, Lu W, Esparza LA, Reya T, Le Z, Yanxiang Guo J, White E, Rabinowitz JD.** 2017. Glucose feeds the TCA cycle via circulating lactate. Nature **551:**115-118.
52. **Illsley NP.** 2000. Glucose transporters in the human placenta. Placenta **21:**14-22.
53. **Gaither K, Quraishi AN, Illsley NP.** 1999. Diabetes alters the expression and activity of the human placental GLUT1 glucose transporter. J Clin Endocrinol Metab **84:**695-701.
54. **Barker DJ, Gluckman PD, Godfrey KM, Harding JE, Owens JA, Robinson JS.** 1993. Fetal nutrition and cardiovascular disease in adult life. Lancet **341:**938-941.
55. **Matsubara S, Sato I.** 2000. Glucose production and glucose-6-phosphatase in the human placenta. Placenta **21:**591-593.
56. **Leonce J, Brockton N, Robinson S, Venkatesan S, Bannister P, Raman V, Murphy K, Parker K, Pavitt D, Teoh TG, Regan L, Burchell A, Steer P, Johnston DG.** 2006. Glucose production in the human placenta. Placenta **27 Suppl A:**S103-108.
57. **Prendergast CH, Parker KH, Gray R, Venkatesan S, Bannister P, Castro-Soares J, Murphy KW, Beard RW, Regan L, Robinson S, Steer P, Halliday D, Johnston DG.** 1999. Glucose production by the human placenta in vivo. Placenta **20:**591-598.
58. **Akison LK, Nitert MD, Clifton VL, Moritz KM, Simmons DG.** 2017. Review: Alterations in placental glycogen deposition in complicated pregnancies: Current preclinical and clinical evidence. Placenta **54:**52-58.
59. **Meschia G, Battaglia FC, Hay WW, Sparks JW.** 1980. Utilization of substrates by the ovine placenta in vivo. Fed Proc **39:**245-249.
60. **Owens JA, Falconer J, Robinson JS.** 1987. Effect of restriction of placental growth on fetal and utero-placental metabolism. J Dev Physiol **9:**225-238.
61. **Sparks JW, Hay WW, Bonds D, Meschia G, Battaglia FC.** 1982. Simultaneous measurements of lactate turnover rate and umbilical lactate uptake in the fetal lamb. J Clin Invest **70:**179-192.
62. **Markovic S, Fages A, Roussel T, Hadas R, Brandis A, Neeman M, Frydman L.** 2018. Placental physiology monitored by hyperpolarized dynamic (13)C magnetic resonance. Proc Natl Acad Sci U S A doi:10.1073/pnas.1715175115.
63. **Baker C, Ebert S.** 2013. Development of aerobic metabolism in utero: Requirement for mitochondrial function during embryonic and fetal periods. OA Biotechnology **2**.

64. **Cetin I, de Santis MS, Taricco E, Radaelli T, Teng C, Ronzoni S, Spada E, Milani S, Pardi G.** 2005. Maternal and fetal amino acid concentrations in normal pregnancies and in pregnancies with gestational diabetes mellitus. Am J Obstet Gynecol **192:**610-617.
65. **Jansson T.** 2001. Amino acid transporters in the human placenta. Pediatr Res **49:**141-147.
66. **Carter AM.** 2012. Evolution of placental function in mammals: the molecular basis of gas and nutrient transfer, hormone secretion, and immune responses. Physiol Rev **92:**1543-1576.
67. **Lager S, Powell TL.** 2012. Regulation of nutrient transport across the placenta. J Pregnancy **2012:**179827.
68. **Vaughan OR, Rosario FJ, Powell TL, Jansson T.** 2017. Regulation of Placental Amino Acid Transport and Fetal Growth. Prog Mol Biol Transl Sci **145:**217-251.
69. **Panitchob N, Widdows KL, Crocker IP, Johnstone ED, Please CP, Sibley CP, Glazier JD, Lewis RM, Sengers BG.** 2016. Computational modelling of placental amino acid transfer as an integrated system. Biochim Biophys Acta **1858:**1451-1461.
70. **Roos S, Powell TL, Jansson T.** 2009. Placental mTOR links maternal nutrient availability to fetal growth. Biochem Soc Trans **37:**295-298.
71. **Abu-Elheiga L, Matzuk MM, Kordari P, Oh W, Shaikenov T, Gu Z, Wakil SJ.** 2005. Mutant mice lacking acetyl-CoA carboxylase 1 are embryonically lethal. Proc Natl Acad Sci U S A **102:**12011-12016.
72. **Chirala SS, Chang H, Matzuk M, Abu-Elheiga L, Mao J, Mahon K, Finegold M, Wakil SJ.** 2003. Fatty acid synthesis is essential in embryonic development: Fatty acid synthase null mutants and most of the heterozygotes die in utero. Proceedings of the National Academy of Sciences **100:**6358-6363.
73. **Mao J, DeMayo FJ, Li H, Abu-Elheiga L, Gu Z, Shaikenov TE, Kordari P, Chirala SS, Heird WC, Wakil SJ.** 2006. Liver-specific deletion of acetyl-CoA carboxylase 1 reduces hepatic triglyceride accumulation without affecting glucose homeostasis. Proc Natl Acad Sci U S A **103:**8552-8557.
74. **Chakravarthy MV, Pan Z, Zhu Y, Tordjman K, Schneider JG, Coleman T, Turk J, Semenkovich CF.** 2005. "New" hepatic fat activates PPARalpha to maintain glucose, lipid, and cholesterol homeostasis. Cell Metab **1:**309-322.
75. **Shafrir E, Khassis S.** 1982. Maternal-fetal fat transport versus new fat synthesis in the pregnant diabetic rat. Diabetologia **22:**111-117.
76. **Clandinin MT, Chappell JE, Heim T, Swyer PR, Chance GW.** 1981. Fatty acid accretion in fetal and neonatal liver: Implications for fatty acid requirements. Early Hum Dev **5:**7-14.
77. **Elphick MC, Filshie GM, Hull D.** 1978. The passage of fat emulsion across the human placenta. Br J Obstet Gynaecol **85:**610-618.
78. **Naoum HG, De Chazal RC, Eaton BM, Contractor SF.** 1987. Characterization and specificity of lipoprotein binding to term human placental membranes. Biochim Biophys Acta **902:**193-199.
79. **Wittmaack FM, Gafvels ME, Bronner M, Matsuo H, McCrae KR, Tomaszewski JE, Robinson SL, Strickland DK, Strauss JF, 3rd.** 1995. Localization and regulation of the human very low density lipoprotein/apolipoprotein-E receptor: trophoblast expression predicts a role for the receptor in placental lipid transport. Endocrinology **136:**340-348.
80. **Kaminsky S, Sibley CP, Maresh M, Thomas CR, D'Souza SW.** 1991. The effects of diabetes on placental lipase activity in the rat and human. Pediatr Res **30:**541-543.

81. **Bonet B, Brunzell JD, Gown AM, Knopp RH.** 1992. Metabolism of very-low-density lipoprotein triglyceride by human placental cells: the role of lipoprotein lipase. Metabolism **41:**596-603.
82. **Thomas CR, Lowy C.** 1987. The interrelationships between circulating maternal esterified and non-esterified fatty acids in pregnant guinea pigs and their relative contributions to the fetal circulation. J Dev Physiol **9:**203-214.
83. **Duttaroy AK.** 2009. Transport of fatty acids across the human placenta: a review. Prog Lipid Res **48:**52-61.
84. **Larque E, Demmelmair H, Berger B, Hasbargen U, Koletzko B.** 2003. In vivo investigation of the placental transfer of (13)C-labeled fatty acids in humans. J Lipid Res **44:**49-55.
85. **Ellis JM, Bowman CE, Wolfgang MJ.** 2015. Metabolic and Tissue-Specific Regulation of Acyl-CoA Metabolism. PLoS One **10:**e0116587.
86. **Coleman RA, Lewin TM, Van Horn CG, Gonzalez-Baró MR.** 2002. Do acyl-CoA synthetases regulate fatty acid entry into synthetic versus degradative pathways? J Nutr **132:**2123-2126.
87. **Tong F, Black PN, Coleman RA, DiRusso CC.** 2006. Fatty acid transport by vectorial acylation in mammals: roles played by different isoforms of rat long-chain acyl-CoA synthetases. Arch Biochem Biophys **447:**46-52.
88. **Ellis JM, Frahm JL, Li LO, Coleman RA.** 2010. Acyl-coenzyme A synthetases in metabolic control. Curr Opin Lipidol **21:**212-217.
89. **Duttaroy AK, Crozet D, Taylor J, Gordon MJ.** 2003. Acyl-CoA thioesterase activity in human placental choriocarcinoma (BeWo), cells: effects of fatty acids. Prostaglandins Leukot Essent Fatty Acids **68:**43-48.
90. **Wu X, Huang W, Prasad PD, Seth P, Rajan DP, Leibach FH, Chen J, Conway SJ, Ganapathy V.** 1999. Functional characteristics and tissue distribution pattern of organic cation transporter 2 (OCTN2), an organic cation/carnitine transporter. J Pharmacol Exp Ther **290:**1482-1492.
91. **Hahn P, Skala JP, Seccombe DW, Frohlich J, Penn-Walker D, Novak M, Hynie I, Towell ME.** 1977. Carnitine content of blood and amniotic fluid. Pediatr Res **11:**878-880.
92. **Diamant YZ, Diamant S, Freinkel N.** 1980. Lipid deposition and metabolism in rat placenta during gestation. Placenta **1:**319-325.
93. **Perazzolo S, Hirschmugl B, Wadsack C, Desoye G, Lewis RM, Sengers BG.** 2017. The influence of placental metabolism on fatty acid transfer to the fetus. J Lipid Res **58:**443-454.
94. **Hay WW, Jr., Sparks JW, Battaglia FC, Meschia G.** 1984. Maternal-fetal glucose exchange: necessity of a three-pool model. Am J Physiol **246:**E528-534.
95. **Shekhawat P, Bennett MJ, Sadovsky Y, Nelson DM, Rakheja D, Strauss AW.** 2003. Human placenta metabolizes fatty acids: implications for fetal fatty acid oxidation disorders and maternal liver diseases. Am J Physiol Endocrinol Metab **284:**E1098-1105.
96. **Oey NA, den Boer ME, Ruiter JP, Wanders RJ, Duran M, Waterham HR, Boer K, van der Post JA, Wijburg FA.** 2003. High activity of fatty acid oxidation enzymes in human placenta: implications for fetal-maternal disease. J Inherit Metab Dis **26:**385-392.
97. **Carnielli VP, Wattimena DJ, Luijendijk IH, Boerlage A, Degenhart HJ, Sauer PJ.** 1996. The very low birth weight premature infant is capable of synthesizing arachidonic and docosahexaenoic acids from linoleic and linolenic acids. Pediatr Res **40:**169-174.

98. **Nguyen LN, Ma D, Shui G, Wong P, Cazenave-Gassiot A, Zhang X, Wenk MR, Goh EL, Silver DL.** 2014. Mfsd2a is a transporter for the essential omega-3 fatty acid docosahexaenoic acid. Nature **509:**503-506.
99. **Ben-Zvi A, Lacoste B, Kur E, Andreone BJ, Mayshar Y, Yan H, Gu C.** 2014. Mfsd2a is critical for the formation and function of the blood-brain barrier. Nature **509:**507-511.
100. **Prieto-Sanchez MT, Ruiz-Palacios M, Blanco-Carnero JE, Pagan A, Hellmuth C, Uhl O, Peissner W, Ruiz-Alcaraz AJ, Parrilla JJ, Koletzko B, Larque E.** 2016. Placental MFSD2a transporter is related to decreased DHA in cord blood of women with treated gestational diabetes. Clin Nutr doi:10.1016/j.clnu.2016.01.014.
101. **Chambaz J, Ravel D, Manier MC, Pepin D, Mulliez N, Bereziat G.** 1985. Essential fatty acids interconversion in the human fetal liver. Biol Neonate **47:**136-140.
102. **Poisson JP, Dupuy RP, Sarda P, Descomps B, Narce M, Rieu D, Crastes de Paulet A.** 1993. Evidence that liver microsomes of human neonates desaturate essential fatty acids. Biochim Biophys Acta **1167:**109-113.
103. **Salem N, Jr., Wegher B, Mena P, Uauy R.** 1996. Arachidonic and docosahexaenoic acids are biosynthesized from their 18-carbon precursors in human infants. Proc Natl Acad Sci U S A **93:**49-54.
104. **Pauter AM, Trattner S, Gonzalez-Bengtsson A, Talamonti E, Asadi A, Dethlefsen O, Jacobsson A.** 2017. Both maternal and offspring Elovl2 genotypes determine systemic DHA levels in perinatal mice. J Lipid Res **58:**111-123.
105. **Kahn SE, Hull RL, Utzschneider KM.** 2006. Mechanisms linking obesity to insulin resistance and type 2 diabetes. Nature **444:**840-846.
106. **Hanahan D, Weinberg RA.** 2011. Hallmarks of cancer: the next generation. Cell **144:**646-674.
107. **Halestrap AP, Scott RD, Thomas AP.** 1980. Mitochondrial pyruvate transport and its hormonal regulation. Int J Biochem **11:**97-105.
108. **Halestrap AP.** 2012. The mitochondrial pyruvate carrier: has it been unearthed at last? Cell Metab **16:**141-143.
109. **Schell JC, Rutter J.** 2013. The long and winding road to the mitochondrial pyruvate carrier. Cancer Metab **1:**6.
110. **Klingenberg M.** 1970. Mitochondria metabolite transport. FEBS Lett **6:**145-154.
111. **Papa S, Francavilla A, Paradies G, Meduri B.** 1971. The transport of pyruvate in rat liver mitochondria. FEBS Lett **12:**285-288.
112. **Halestrap AP, Denton RM.** 1974. Specific inhibition of pyruvate transport in rat liver mitochondria and human erythrocytes by alpha-cyano-4-hydroxycinnamate. Biochem J **138:**313-316.
113. **Halestrap AP.** 1978. Pyruvate and ketone-body transport across the mitochondrial membrane. Exchange properties, pH-dependence and mechanism of the carrier. Biochem J **172:**377-387.
114. **Nalecz MJ, Nalecz KA, Broger C, Bolli R, Wojtczak L, Azzi A.** 1986. Extraction, partial purification and functional reconstitution of two mitochondrial carriers transporting keto acids: 2-oxoglutarate and pyruvate. FEBS Lett **196:**331-336.
115. **Brailsford MA, Thompson AG, Kaderbhai N, Beechey RB.** 1986. The extraction and reconstitution of the alpha-cyanocinnamate-sensitive pyruvate transporter from castor bean mitochondria. Biochem Biophys Res Commun **140:**1036-1042.
116. **Bolli R, Nalecz KA, Azzi A.** 1989. Monocarboxylate and alpha-ketoglutarate carriers from bovine heart mitochondria. Purification by affinity chromatography on immobilized 2-cyano-4-hydroxycinnamate. J Biol Chem **264:**18024-18030.

117. **Capuano F, Di Paola M, Azzi A, Papa S.** 1990. The monocarboxylate carrier from rat liver mitochondria. Purification and kinetic characterization in a reconstituted system. FEBS Lett **261:**39-42.
118. **Palmieri F, Pierri CL.** 2010. Mitochondrial metabolite transport. Essays Biochem **47:**37-52.
119. **Hildyard JC, Halestrap AP.** 2003. Identification of the mitochondrial pyruvate carrier in Saccharomyces cerevisiae. Biochem J **374:**607-611.
120. **Todisco S, Agrimi G, Castegna A, Palmieri F.** 2006. Identification of the mitochondrial NAD+ transporter in Saccharomyces cerevisiae. J Biol Chem **281:**1524-1531.
121. **Herzig S, Raemy E, Montessuit S, Veuthey JL, Zamboni N, Westermann B, Kunji ER, Martinou JC.** 2012. Identification and functional expression of the mitochondrial pyruvate carrier. Science **337:**93-96.
122. **Bricker DK, Taylor EB, Schell JC, Orsak T, Boutron A, Chen YC, Cox JE, Cardon CM, Van Vranken JG, Dephoure N, Redin C, Boudina S, Gygi SP, Brivet M, Thummel CS, Rutter J.** 2012. A mitochondrial pyruvate carrier required for pyruvate uptake in yeast, Drosophila, and humans. Science **337:**96-100.
123. **Timon-Gomez A, Proft M, Pascual-Ahuir A.** 2013. Differential regulation of mitochondrial pyruvate carrier genes modulates respiratory capacity and stress tolerance in yeast. PLoS One **8:**e79405.
124. **Bender T, Pena G, Martinou JC.** 2015. Regulation of mitochondrial pyruvate uptake by alternative pyruvate carrier complexes. The EMBO Journal **34:**911-924.
125. **Nagampalli RSK, Quesnay JEN, Adamoski D, Islam Z, Birch J, Sebinelli HG, Girard R, Ascencao CFR, Fala AM, Pauletti BA, Consonni SR, de Oliveira JF, Silva ACT, Franchini KG, Leme AFP, Silber AM, Ciancaglini P, Moraes I, Dias SMG, Ambrosio ALB.** 2018. Human mitochondrial pyruvate carrier 2 as an autonomous membrane transporter. Sci Rep **8:**3510.
126. **Brivet M, Garcia-Cazorla A, Lyonnet S, Dumez Y, Nassogne MC, Slama A, Boutron A, Touati G, Legrand A, Saudubray JM.** 2003. Impaired mitochondrial pyruvate importation in a patient and a fetus at risk. Mol Genet Metab **78:**186-192.
127. **Jiang M, Gu X, Feng X, Fan Z, Ding F, Liu Y.** 2009. The molecular characterization of the brain protein 44-like (Brp44l) gene of Gekko japonicus and its expression changes in spinal cord after tail amputation. Mol Biol Rep **36:**215-220.
128. **Da Cruz S, Xenarios I, Langridge J, Vilbois F, Parone PA, Martinou JC.** 2003. Proteomic analysis of the mouse liver mitochondrial inner membrane. J Biol Chem **278:**41566-41571.
129. **Rardin MJ, Newman JC, Held JM, Cusack MP, Sorensen DJ, Li B, Schilling B, Mooney SD, Kahn CR, Verdin E, Gibson BW.** 2013. Label-free quantitative proteomics of the lysine acetylome in mitochondria identifies substrates of SIRT3 in metabolic pathways. Proc Natl Acad Sci U S A **110:**6601-6606.
130. **Bowman CE, Zhao L, Hartung T, Wolfgang MJ.** 2016. Requirement for the Mitochondrial Pyruvate Carrier in Mammalian Development Revealed by a Hypomorphic Allelic Series. Mol Cell Biol **36:**2089-2104.
131. **Mali P, Yang L, Esvelt KM, Aach J, Guell M, DiCarlo JE, Norville JE, Church GM.** 2013. RNA-guided human genome engineering via Cas9. Science **339:**823-826.
132. **Folch J, Lees M, Sloane Stanley GH.** 1957. A simple method for the isolation and purification of total lipides from animal tissues. The Journal of biological chemistry **226:**497-509.

133. **Alves TC, Pongratz RL, Zhao X, Yarborough O, Sereda S, Shirihai O, Cline GW, Mason G, Kibbey RG.** 2015. Integrated, Step-Wise, Mass-Isotopomeric Flux Analysis of the TCA Cycle. Cell Metab **22:**936-947.
134. **Ellis JM, Wong GW, Wolfgang MJ.** 2013. Acyl coenzyme A thioesterase 7 regulates neuronal fatty acid metabolism to prevent neurotoxicity. Mol Cell Biol **33:**1869-1882.
135. **Lee J, Wolfgang MJ.** 2012. Metabolomic profiling reveals a role for CPT1c in neuronal oxidative metabolism. BMC Biochem **13:**23.
136. **Passonneau JV, Lauderdale VR.** 1974. A comparison of three methods of glycogen measurement in tissues. Anal Biochem **60:**405-412.
137. **Zhang P.** 2012. Analysis of mouse liver glycogen content. Bio-Protocol **Vol 2:10, www.bio-protocol.org/e186**.
138. **Vigueira PA, McCommis KS, Schweitzer GG, Remedi MS, Chambers KT, Fu X, McDonald WG, Cole SL, Colca JR, Kletzien RF, Burgess SC, Finck BN.** 2014. Mitochondrial pyruvate carrier 2 hypomorphism in mice leads to defects in glucose-stimulated insulin secretion. Cell Reports **7:**2042-2053.
139. **Vanderperre B, Bender T, Kunji ER, Martinou JC.** 2014. Mitochondrial pyruvate import and its effects on homeostasis. Curr Opin Cell Biol **33c:**35-41.
140. **DeBerardinis RJ, Lum JJ, Hatzivassiliou G, Thompson CB.** 2008. The biology of cancer: metabolic reprogramming fuels cell growth and proliferation. Cell Metab **7:**11-20.
141. **Vander Heiden MG, Cantley LC, Thompson CB.** 2009. Understanding the Warburg effect: the metabolic requirements of cell proliferation. Science **324:**1029-1033.
142. **Ward PS, Thompson CB.** 2012. Metabolic reprogramming: a cancer hallmark even warburg did not anticipate. Cancer Cell **21:**297-308.
143. **Reamy AA, Wolfgang MJ.** 2011. Carnitine palmitoyltransferase-1c gain-of-function in the brain results in postnatal microencephaly. J Neurochem **118:**388-398.
144. **Girard J, Duee PH, Ferre P, Pegorier JP, Escriva F, Decaux JF.** 1985. Fatty acid oxidation and ketogenesis during development. Reprod Nutr Dev **25:**303-319.
145. **Nyman LR, Cox KB, Hoppel CL, Kerner J, Barnoski BL, Hamm DA, Tian L, Schoeb TR, Wood PA.** 2005. Homozygous carnitine palmitoyltransferase 1a (liver isoform) deficiency is lethal in the mouse. Mol Genet Metab **86:**179-187.
146. **Ji S, You Y, Kerner J, Hoppel CL, Schoeb TR, Chick WS, Hamm DA, Sharer JD, Wood PA.** 2008. Homozygous carnitine palmitoyltransferase 1b (muscle isoform) deficiency is lethal in the mouse. Mol Genet Metab **93:**314-322.
147. **Herrera E, Amusquivar E.** 2000. Lipid metabolism in the fetus and the newborn. Diabetes Metab Res Rev **16:**202-210.
148. **Vincent EE, Sergushichev A, Griss T, Gingras MC, Samborska B, Ntimbane T, Coelho PP, Blagih J, Raissi TC, Choiniere L, Bridon G, Loginicheva E, Flynn BR, Thomas EC, Tavare JM, Avizonis D, Pause A, Elder DJ, Artyomov MN, Jones RG.** 2015. Mitochondrial Phosphoenolpyruvate Carboxykinase Regulates Metabolic Adaptation and Enables Glucose-Independent Tumor Growth. Mol Cell **60:**195-207.
149. **Leithner K, Hrzenjak A, Trotzmuller M, Moustafa T, Kofeler HC, Wohlkoenig C, Stacher E, Lindenmann J, Harris AL, Olschewski A, Olschewski H.** 2015. PCK2 activation mediates an adaptive response to glucose depletion in lung cancer. Oncogene **34:**1044-1050.
150. **Montal ED, Dewi R, Bhalla K, Ou L, Hwang BJ, Ropell AE, Gordon C, Liu WJ, DeBerardinis RJ, Sudderth J, Twaddel W, Boros LG, Shroyer KR, Duraisamy S, Drapkin R, Powers RS, Rohde JM, Boxer MB, Wong KK, Girnun GD.** 2015.

PEPCK Coordinates the Regulation of Central Carbon Metabolism to Promote Cancer Cell Growth. Mol Cell **60:**571-583.

151. **Mendez-Lucas A, Hyrossova P, Novellasdemunt L, Vinals F, Perales JC.** 2014. Mitochondrial phosphoenolpyruvate carboxykinase (PEPCK-M) is a pro-survival, endoplasmic reticulum (ER) stress response gene involved in tumor cell adaptation to nutrient availability. J Biol Chem **289:**22090-22102.
152. **Vitvitsky V, Garg SK, Banerjee R.** 2011. Taurine biosynthesis by neurons and astrocytes. J Biol Chem **286:**32002-32010.
153. **Aruoma OI, Halliwell B, Hoey BM, Butler J.** 1988. The antioxidant action of taurine, hypotaurine and their metabolic precursors. Biochem J **256:**251-255.
154. **Birsoy K, Wang T, Chen WW, Freinkman E, Abu-Remaileh M, Sabatini DM.** 2015. An Essential Role of the Mitochondrial Electron Transport Chain in Cell Proliferation Is to Enable Aspartate Synthesis. Cell **162:**540-551.
155. **Celis K, Shuldiner S, Haverfield EV, Cappell J, Yang R, Gong DW, Chung WK.** 2015. Loss of function mutation in glutamic pyruvate transaminase 2 (GPT2) causes developmental encephalopathy. J Inherit Metab Dis **38:**941-948.
156. **Maj MC, MacKay N, Levandovskiy V, Addis J, Baumgartner ER, Baumgartner MR, Robinson BH, Cameron JM.** 2005. Pyruvate dehydrogenase phosphatase deficiency: identification of the first mutation in two brothers and restoration of activity by protein complementation. J Clin Endocrinol Metab **90:**4101-4107.
157. **Cameron JM, Maj M, Levandovskiy V, Barnett CP, Blaser S, Mackay N, Raiman J, Feigenbaum A, Schulze A, Robinson BH.** 2009. Pyruvate dehydrogenase phosphatase 1 (PDP1) null mutation produces a lethal infantile phenotype. Hum Genet **125:**319-326.
158. **Marin-Valencia I, Roe CR, Pascual JM.** 2010. Pyruvate carboxylase deficiency: mechanisms, mimics and anaplerosis. Mol Genet Metab **101:**9-17.
159. **Gray LR, Tompkins SC, Taylor EB.** 2014. Regulation of pyruvate metabolism and human disease. Cell Mol Life Sci **71:**2577-2604.
160. **Johnson MT, Mahmood S, Hyatt SL, Yang HS, Soloway PD, Hanson RW, Patel MS.** 2001. Inactivation of the murine pyruvate dehydrogenase (Pdha1) gene and its effect on early embryonic development. Mol Genet Metab **74:**293-302.
161. **Rodriguez S, Wolfgang MJ.** 2012. Targeted chemical-genetic regulation of protein stability in vivo. Chem Biol **19:**391-398.
162. **Rodriguez S, Ellis JM, Wolfgang MJ.** 2014. Chemical-genetic induction of Malonyl-CoA decarboxylase in skeletal muscle. BMC Biochem **15:**20.
163. **Bellingham AJ, Detter JC, Lenfant C.** 1971. Regulatory mechanisms of hemoglobin oxygen affinity in acidosis and alkalosis. J Clin Invest **50:**700-706.
164. **Baron MH, Vacaru A, Nieves J.** 2013. Erythroid development in the mammalian embryo. Blood Cells Mol Dis **51:**213-219.
165. **Bobrow CS, Soothill PW.** 1999. Causes and consequences of fetal acidosis. Arch Dis Child Fetal Neonatal Ed **80:**F246-249.
166. **Khacho M, Tarabay M, Patten D, Khacho P, MacLaurin JG, Guadagno J, Bergeron R, Cregan SP, Harper ME, Park DS, Slack RS.** 2014. Acidosis overrides oxygen deprivation to maintain mitochondrial function and cell survival. Nat Commun **5:**3550.
167. **Warburg O.** 1956. On the origin of cancer cells. Science **123:**309-314.
168. **Lunt SY, Vander Heiden MG.** 2011. Aerobic glycolysis: meeting the metabolic requirements of cell proliferation. Annu Rev Cell Dev Biol **27:**441-464.
169. **Wallace DC.** 2012. Mitochondria and cancer. Nat Rev Cancer **12:**685-698.

170. **Lee WT, St John J.** 2015. The control of mitochondrial DNA replication during development and tumorigenesis. Ann N Y Acad Sci **1350:**95-106.
171. **Cavalli LR, Varella-Garcia M, Liang BC.** 1997. Diminished tumorigenic phenotype after depletion of mitochondrial DNA. Cell Growth Differ **8:**1189-1198.
172. **Dickinson A, Yeung KY, Donoghue J, Baker MJ, Kelly RD, McKenzie M, Johns TG.** 2013. The regulation of mitochondrial DNA copy number in glioblastoma cells. **20:**1644-1653.
173. **Schubert S, Heller S, Loffler B, Schafer I, Seibel M, Villani G, Seibel P.** 2015. Generation of Rho Zero Cells: Visualization and Quantification of the mtDNA Depletion Process. Int J Mol Sci **16:**9850-9865.
174. **Vacanti NM, Divakaruni AS, Green CR, Parker SJ, Henry RR, Ciaraldi TP, Murphy AN, Metallo CM.** 2014. Regulation of substrate utilization by the mitochondrial pyruvate carrier. Mol Cell **56:**425-435.
175. **Yang C, Ko B, Hensley CT, Jiang L, Wasti AT, Kim J, Sudderth J, Calvaruso MA, Lumata L, Mitsche M, Rutter J, Merritt ME, DeBerardinis RJ.** 2014. Glutamine Oxidation Maintains the TCA Cycle and Cell Survival during Impaired Mitochondrial Pyruvate Transport. Mol Cell **56:**414-424.
176. **Gray LR, Sultana MR, Rauckhorst AJ, Oonthonpan L, Tompkins SC, Sharma A, Fu X, Miao R, Pewa AD, Brown KS, Lane EE, Dohlman A, Zepeda-Orozco D, Xie J, Rutter J, Norris AW, Cox JE, Burgess SC, Potthoff MJ, Taylor EB.** 2015. Hepatic Mitochondrial Pyruvate Carrier 1 Is Required for Efficient Regulation of Gluconeogenesis and Whole-Body Glucose Homeostasis. Cell Metab **22:**669-681.
177. **McCommis KS, Chen Z, Fu X, McDonald WG, Colca JR, Kletzien RF, Burgess SC, Finck BN.** 2015. Loss of Mitochondrial Pyruvate Carrier 2 in the Liver Leads to Defects in Gluconeogenesis and Compensation via Pyruvate-Alanine Cycling. Cell Metab **22:**682-694.
178. **Coloff JL, Murphy JP, Braun CR, Harris IS, Shelton LM, Kami K, Gygi SP, Selfors LM, Brugge JS.** 2016. Differential Glutamate Metabolism in Proliferating and Quiescent Mammary Epithelial Cells. Cell Metab doi:10.1016/j.cmet.2016.03.016.
179. **Weinberg F, Hamanaka R, Wheaton WW, Weinberg S, Joseph J, Lopez M, Kalyanaraman B, Mutlu GM, Budinger GR, Chandel NS.** 2010. Mitochondrial metabolism and ROS generation are essential for Kras-mediated tumorigenicity. Proc Natl Acad Sci U S A **107:**8788-8793.
180. **Krebs HA.** 1935. Metabolism of amino-acids: The synthesis of glutamine from glutamic acid and ammonia, and the enzymic hydrolysis of glutamine in animal tissues. Biochem J **29:**1951-1969.
181. **Fahien LA, Macdonald MJ.** 2011. The complex mechanism of glutamate dehydrogenase in insulin secretion. Diabetes **60:**2450-2454.
182. **Muoio DM.** 2014. Metabolic Inflexibility: When Mitochondrial Indecision Leads to Metabolic Gridlock. Cell **159:**1253-1262.
183. **Vanderperre B, Herzig S, Krznar P, Horl M, Ammar Z, Montessuit S, Pierredon S, Zamboni N, Martinou JC.** 2016. Embryonic Lethality of Mitochondrial Pyruvate Carrier 1 Deficient Mouse Can Be Rescued by a Ketogenic Diet. PLoS Genet **12:**e1006056.
184. **Sussman D, Ellegood J, Henkelman M.** 2013. A gestational ketogenic diet alters maternal metabolic status as well as offspring physiological growth and brain structure in the neonatal mouse. BMC Pregnancy Childbirth **13:**198.

185. **Darmady JM, Postle AD.** 1982. Lipid metabolism in pregnancy. Br J Obstet Gynaecol **89:**211-215.
186. **Boden G.** 1996. Fuel metabolism in pregnancy and in gestational diabetes mellitus. Obstet Gynecol Clin North Am **23:**1-10.
187. **Metzger BE, Ravnikar V, Vileisis RA, Freinkel N.** 1982. "Accelerated starvation" and the skipped breakfast in late normal pregnancy. Lancet **1:**588-592.
188. **Painter RC, Roseboom TJ, Bleker OP.** 2005. Prenatal exposure to the Dutch famine and disease in later life: an overview. Reprod Toxicol **20:**345-352.
189. **Wu L, Feng X, He A, Ding Y, Zhou X, Xu Z.** 2017. Prenatal exposure to the Great Chinese Famine and mid-age hypertension. PLoS One **12:**e0176413.
190. **Savitri AI, Yadegari N, Bakker J, van Ewijk RJ, Grobbee DE, Painter RC, Uiterwaal CS, Roseboom TJ.** 2014. Ramadan fasting and newborn's birth weight in pregnant Muslim women in The Netherlands. Br J Nutr **112:**1503-1509.
191. **Gur EB, Turan GA, Ince O, Karadeniz M, Tatar S, Kasap E, Sahin N, Guclu S.** 2015. Effect of Ramadan fasting on metabolic markers, dietary intake and abdominal fat distribution in pregnancy. Hippokratia **19:**298-303.
192. **Karateke A, Kaplanoglu M, Avci F, Kurt RK, Baloglu A.** 2015. The effect of Ramadan fasting on fetal development. Pak J Med Sci **31:**1295-1299.
193. **Dikensoy E, Balat O, Cebesoy B, Ozkur A, Cicek H, Can G.** 2009. The effect of Ramadan fasting on maternal serum lipids, cortisol levels and fetal development. Arch Gynecol Obstet **279:**119-123.
194. **Langley-Evans SC, Phillips GJ, Benediktsson R, Gardner DS, Edwards CR, Jackson AA, Seckl JR.** 1996. Protein intake in pregnancy, placental glucocorticoid metabolism and the programming of hypertension in the rat. Placenta **17:**169-172.
195. **Stettler N, Zemel BS, Kumanyika S, Stallings VA.** 2002. Infant weight gain and childhood overweight status in a multicenter, cohort study. Pediatrics **109:**194-199.
196. **Zheng X, Wang Y, Ren W, Luo R, Zhang S, Zhang JH, Zeng Q.** 2012. Risk of metabolic syndrome in adults exposed to the great Chinese famine during the fetal life and early childhood. Eur J Clin Nutr **66:**231-236.
197. **Hult M, Tornhammar P, Ueda P, Chima C, Bonamy AK, Ozumba B, Norman M.** 2010. Hypertension, diabetes and overweight: looming legacies of the Biafran famine. PLoS One **5:**e13582.
198. **Li C, Lumey LH.** 2017. Exposure to the Chinese famine of 1959-61 in early life and long-term health conditions: a systematic review and meta-analysis. Int J Epidemiol **46:**1157-1170.
199. **Diamant YZ, Shafrir E.** 1978. Placental enzymes of glycolysis, gluconeogenesis and lipogenesis in the diabetic rat and in starvation. Comparison with maternal and foetal liver. Diabetologia **15:**481-485.
200. **Girard JR, Ferre P, Gilbert M, Kervran A, Assan R, Marliss EB.** 1977. Fetal metabolic response to maternal fasting in the rat. Am J Physiol **232:**E456-463.
201. **DeSisto CL, Kim SY, Sharma AJ.** 2014. Prevalence Estimates of Gestational Diabetes Mellitus in the United States, Pregnancy Risk Assessment Monitoring System (PRAMS), 2007-2010. Prev Chronic Dis **11:**E104.
202. **Anonymous.** 2014. Diagnosis and Classification of Diabetes Mellitus. Diabetes Care **37:**S81-S90.
203. **Catalano PM, Tyzbir ED, Wolfe RR, Calles J, Roman NM, Amini SB, Sims EA.** 1993. Carbohydrate metabolism during pregnancy in control subjects and women with gestational diabetes. Am J Physiol **264:**E60-67.

204. **Catalano PM, Huston L, Amini SB, Kalhan SC.** 1999. Longitudinal changes in glucose metabolism during pregnancy in obese women with normal glucose tolerance and gestational diabetes mellitus. Am J Obstet Gynecol **180:**903-916.
205. **Barbour LA, Shao J, Qiao L, Pulawa LK, Jensen DR, Bartke A, Garrity M, Draznin B, Friedman JE.** 2002. Human placental growth hormone causes severe insulin resistance in transgenic mice. Am J Obstet Gynecol **186:**512-517.
206. **Kalkhoff RK, Kissebah AH, Kim HJ.** 1978. Carbohydrate and lipid metabolism during normal pregnancy: relationship to gestational hormone action. Semin Perinatol **2:**291-307.
207. **Dickens LT, Naylor RN.** 2018. Clinical Management of Women with Monogenic Diabetes During Pregnancy. Curr Diab Rep **18:**12.
208. **Liu J, Ghaziani TT, Wolf JL.** 2017. Acute Fatty Liver Disease of Pregnancy: Updates in Pathogenesis, Diagnosis, and Management. Am J Gastroenterol **112:**838-846.
209. **Kurtz DM, Rinaldo P, Rhead WJ, Tian L, Millington DS, Vockley J, Hamm DA, Brix AE, Lindsey JR, Pinkert CA, O'Brien WE, Wood PA.** 1998. Targeted disruption of mouse long-chain acyl-CoA dehydrogenase gene reveals crucial roles for fatty acid oxidation. Proc Natl Acad Sci U S A **95:**15592-15597.
210. **Bowman C, Selen Alpergin ES, Scafidi S, Wolfgang MJ.** 2018. Mitochondrial oxidative metabolism regulates late-gestation maternal-fetal metabolic communication. *In Preparation*.
211. **Gonzalez-Hurtado E, Lee J, Choi J, Selen Alpergin ES, Collins SL, Horton MR, Wolfgang MJ.** 2017. The Loss Of Macrophage Fatty Acid Oxidation Does Not Potentiate Systemic Metabolic Dysfunction. Am J Physiol Endocrinol Metab doi:10.1152/ajpendo.00408.2016**:**ajpendo 00408 02016.
212. **Lee J, Choi J, Aja S, Scafidi S, Wolfgang MJ.** 2016. Loss of Adipose Fatty Acid Oxidation Does Not Potentiate Obesity at Thermoneutrality. Cell Rep **14:**1308-1316.
213. **Lee J, Choi J, Scafidi S, Wolfgang MJ.** 2016. Hepatic Fatty Acid Oxidation Restrains Systemic Catabolism during Starvation. Cell Rep **16:**201-212.
214. **Lee J, Ellis JM, Wolfgang MJ.** 2015. Adipose fatty acid oxidation is required for thermogenesis and potentiates oxidative stress-induced inflammation. Cell Rep **10:**266-279.
215. **Nomura M, Liu J, Rovira, II, Gonzalez-Hurtado E, Lee J, Wolfgang MJ, Finkel T.** 2016. Fatty acid oxidation in macrophage polarization. Nat Immunol **17:**216-217.
216. **Gonzalez-Hurtado E, Lee J, Choi J, Wolfgang MJ.** 2017. Fatty acid oxidation is required for active and quiescent brown adipose tissue maintenance and thermogenic programing. Mol Metab doi:10.1016/j.molmet.2017.11.004.
217. **Kim SP, Li Z, Zoch ML, Frey JL, Bowman CE, Kushwaha P, Ryan KA, Goh BC, Scafidi S, Pickett JE, Faugere MC, Kershaw EE, Thorek DLJ, Clemens TL, Wolfgang MJ, Riddle RC.** 2017. Fatty acid oxidation by the osteoblast is required for normal bone acquisition in a sex- and diet-dependent manner. JCI Insight **2**.
218. **Postic C, Shiota M, Niswender KD, Jetton TL, Chen Y, Moates JM, Shelton KD, Lindner J, Cherrington AD, Magnuson MA.** 1999. Dual roles for glucokinase in glucose homeostasis as determined by liver and pancreatic beta cell-specific gene knock-outs using Cre recombinase. J Biol Chem **274:**305-315.
219. **Lee J, Choi J, Selen Alpergin ES, Zhao L, Hartung T, Scafidi S, Riddle RC, Wolfgang MJ.** 2017. Loss of Hepatic Mitochondrial Long-Chain Fatty Acid Oxidation Confers Resistance to Diet-Induced Obesity and Glucose Intolerance. Cell Rep **20:**655-667.

220. **Lee SS, Pineau T, Drago J, Lee EJ, Owens JW, Kroetz DL, Fernandez-Salguero PM, Westphal H, Gonzalez FJ.** 1995. Targeted disruption of the alpha isoform of the peroxisome proliferator-activated receptor gene in mice results in abolishment of the pleiotropic effects of peroxisome proliferators. Mol Cell Biol **15:**3012-3022.
221. **Potthoff MJ, Inagaki T, Satapati S, Ding X, He T, Goetz R, Mohammadi M, Finck BN, Mangelsdorf DJ, Kliewer SA, Burgess SC.** 2009. FGF21 induces PGC-1alpha and regulates carbohydrate and fatty acid metabolism during the adaptive starvation response. Proc Natl Acad Sci U S A **106:**10853-10858.
222. **Bowman CE, Rodriguez S, Selen Alpergin ES, Acoba MG, Zhao L, Hartung T, Claypool SM, Watkins PA, Wolfgang MJ.** 2017. The Mammalian Malonyl-CoA Synthetase ACSF3 Is Required for Mitochondrial Protein Malonylation and Metabolic Efficiency. Cell Chem Biol **24:**673-684 e674.
223. **Chace DH, Hillman SL, Van Hove JL, Naylor EW.** 1997. Rapid diagnosis of MCAD deficiency: quantitative analysis of octanoylcarnitine and other acylcarnitines in newborn blood spots by tandem mass spectrometry. Clin Chem **43:**2106-2113.
224. **Sandlers Y, Moser AB, Hubbard WC, Kratz LE, Jones RO, Raymond GV.** 2012. Combined extraction of acyl carnitines and 26:0 lysophosphatidylcholine from dried blood spots: prospective newborn screening for X-linked adrenoleukodystrophy. Mol Genet Metab **105:**416-420.
225. **Li X, Li Y, Han G, Li X, Ji Y, Fan Z, Zhong Y, Cao J, Zhao J, Mariusz G, Zhang M, Wen J, Nesland JM, Suo Z.** 2016. Establishment of mitochondrial pyruvate carrier 1 (MPC1) gene knockout mice with preliminary gene function analyses. Oncotarget **7:**79981-79994.
226. **Zou S, Lang T, Zhang B, Huang K, Gong L, Luo H, Xu W, He X.** 2018. Fatty acid oxidation alleviates the energy deficiency caused by the loss of MPC1 in MPC1(+/-) mice. Biochem Biophys Res Commun **495:**1008-1013.
227. **Rando G, Tan CK, Khaled N, Montagner A, Leuenberger N, Bertrand-Michel J, Paramalingam E, Guillou H, Wahli W.** 2016. Glucocorticoid receptor-PPARalpha axis in fetal mouse liver prepares neonates for milk lipid catabolism. Elife **5**.
228. **Rinaldo P, Cowan TM, Matern D.** 2008. Acylcarnitine profile analysis. Genet Med **10:**151-156.
229. **Markan KR, Naber MC, Ameka MK, Anderegg MD, Mangelsdorf DJ, Kliewer SA, Mohammadi M, Potthoff MJ.** 2014. Circulating FGF21 is liver derived and enhances glucose uptake during refeeding and overfeeding. Diabetes **63:**4057-4063.
230. **Badman MK, Pissios P, Kennedy AR, Koukos G, Flier JS, Maratos-Flier E.** 2007. Hepatic fibroblast growth factor 21 is regulated by PPARalpha and is a key mediator of hepatic lipid metabolism in ketotic states. Cell Metab **5:**426-437.
231. **Inagaki T, Dutchak P, Zhao G, Ding X, Gautron L, Parameswara V, Li Y, Goetz R, Mohammadi M, Esser V, Elmquist JK, Gerard RD, Burgess SC, Hammer RE, Mangelsdorf DJ, Kliewer SA.** 2007. Endocrine regulation of the fasting response by PPARalpha-mediated induction of fibroblast growth factor 21. Cell Metab **5:**415-425.
232. **Cui Y, Giesy SL, Hassan M, Davis K, Zhao S, Boisclair YR.** 2014. Hepatic FGF21 production is increased in late pregnancy in the mouse. Am J Physiol Regul Integr Comp Physiol **307:**R290-298.
233. **Cleaton MA, Dent CL, Howard M, Corish JA, Gutteridge I, Sovio U, Gaccioli F, Takahashi N, Bauer SR, Charnock-Jones DS, Powell TL, Smith GC, Ferguson-Smith AC, Charalambous M.** 2016. Fetus-derived DLK1 is required for maternal

metabolic adaptations to pregnancy and is associated with fetal growth restriction. Nat Genet **48:**1473-1480.

234. **Schooneman MG, Vaz FM, Houten SM, Soeters MR.** 2013. Acylcarnitines: reflecting or inflicting insulin resistance? Diabetes **62:**1-8.
235. **Gelaye B, Clish CB, Denis M, Larrabure G, Tadesse MG, Deik A, Pierce K, Bullock K, Dennis C, Enquobahrie DA, Williams MA.** 2018. Metabolomics signatures associated with an oral glucose challenge in pregnant women. Diabetes Metab doi:10.1016/j.diabet.2018.01.004.
236. **Muoio DM, Newgard CB.** 2008. Mechanisms of disease: Molecular and metabolic mechanisms of insulin resistance and beta-cell failure in type 2 diabetes. Nat Rev Mol Cell Biol **9:**193-205.
237. **Grimbert S, Fromenty B, Fisch C, Letteron P, Berson A, Durand-Schneider AM, Feldmann G, Pessayre D.** 1993. Decreased mitochondrial oxidation of fatty acids in pregnant mice: possible relevance to development of acute fatty liver of pregnancy. Hepatology **17:**628-637.
238. **Kepka A, Chojnowska S, Okungbowa OE, Zwierz K.** 2014. The role of carnitine in the perinatal period. Dev Period Med **18:**417-425.
239. **Shekhawat PS, Yang HS, Bennett MJ, Carter AL, Matern D, Tamai I, Ganapathy V.** 2004. Carnitine content and expression of mitochondrial beta-oxidation enzymes in placentas of wild-type (OCTN2(+/+)) and OCTN2 Null (OCTN2(-/-)) Mice. Pediatr Res **56:**323-328.
240. **Oey NA, van Vlies N, Wijburg FA, Wanders RJ, Attie-Bitach T, Vaz FM.** 2006. L-carnitine is synthesized in the human fetal-placental unit: potential roles in placental and fetal metabolism. Placenta **27:**841-846.
241. **Alonso de la Torre SR, Serrano MA, Medina JM.** 1992. Carrier-mediated beta-D-hydroxybutyrate transport in brush-border membrane vesicles from rat placenta. Pediatr Res **32:**317-323.
242. **Shubert PJ, Gordon MC, Landon MB, Gabbe SG, Kniss DA.** 1996. Ketoacids attenuate glucose uptake in human trophoblasts isolated from first-trimester chorionic villi. Am J Obstet Gynecol **175:**56-62.
243. **Ferre P, Satabin P, Decaux JF, Escriva F, Girard J.** 1983. Development and regulation of ketogenesis in hepatocytes isolated from newborn rats. Biochem J **214:**937-942.
244. **Lim S, Chesser AS, Grima JC, Rappold PM, Blum D, Przedborski S, Tieu K.** 2011. D-beta-hydroxybutyrate is protective in mouse models of Huntington's disease. PLoS One **6:**e24620.
245. **Bartlett K, Ghneim HK, Stirk JH, Dale G, Alberti KG.** 1984. Pyruvate carboxylase deficiency. J Inherit Metab Dis **7 Suppl 1:**74-78.
246. **Atkin BM, Buist NR, Utter MF, Leiter AB, Banker BQ.** 1979. Pyruvate carboxylase deficiency and lactic acidosis in a retarded child without Leigh's disease. Pediatr Res **13:**109-116.
247. **Haworth JC, Robinson BH, Perry TL.** 1981. Lactic acidosis due to pyruvate carboxylase deficiency. J Inherit Metab Dis **4:**57-58.
248. **Redondo-Angulo I, Mas-Stachurska A, Sitges M, Tinahones FJ, Giralt M, Villarroya F, Planavila A.** 2017. Fgf21 is required for cardiac remodeling in pregnancy. Cardiovasc Res doi:10.1093/cvr/cvx088.
249. **Bornstein S, Brown SA, Le PT, Wang X, DeMambro V, Horowitz MC, MacDougald O, Baron R, Lotinun S, Karsenty G, Wei W, Ferron M, Kovacs CS, Clemmons D,**

Wan Y, Rosen CJ. 2014. FGF-21 and skeletal remodeling during and after lactation in C57BL/6J mice. Endocrinology **155:**3516-3526.

250. **Butte NF, King JC.** 2005. Energy requirements during pregnancy and lactation. Public Health Nutr **8:**1010-1027.
251. **Trayhurn P.** 1989. Thermogenesis and the energetics of pregnancy and lactation. Can J Physiol Pharmacol **67:**370-375.
252. **Fedak MA, Anderson SS.** 1982. The energetics of lactation: accurate measurements from a large wild mammal, the Grey seal (Halichoerus grypus). J Zool **198:**473-479.
253. **Fowler M, Champagne C, Crocker D.** 2018. Adiposity and fat metabolism during combined fasting and lactation in elephant seals. J Exp Biol **221**.
254. **Skibiel AL, Downing LM, Orr TJ, Hood WR.** 2013. The evolution of the nutrient composition of mammalian milks. J Anim Ecol **82:**1254-1264.
255. **Prip-Buus C, Pegorier JP, Duee PH, Kohl C, Girard J.** 1990. Evidence that the sensitivity of carnitine palmitoyltransferase I to inhibition by malonyl-CoA is an important site of regulation of hepatic fatty acid oxidation in the fetal and newborn rabbit. Perinatal development and effects of pancreatic hormones in cultured rabbit hepatocytes. Biochem J **269:**409-415.
256. **Novak M, Wieser PB, Buch M, Hahn P.** 1979. Acetylcarnitine and free carnitine in body fluids before and after birth. Pediatr Res **13:**10-15.
257. **Jernberg JN, Bowman CE, Wolfgang MJ, Scafidi S.** 2017. Developmental regulation and localization of carnitine palmitoyltransferases (CPTs) in rat brain. J Neurochem **142:**407-419.
258. **Cotter DG, d'Avignon DA, Wentz AE, Weber ML, Crawford PA.** 2011. Obligate role for ketone body oxidation in neonatal metabolic homeostasis. J Biol Chem **286:**6902-6910.
259. **Cotter DG, Ercal B, d'Avignon DA, Dietzen DJ, Crawford PA.** 2013. Impact of peripheral ketolytic deficiency on hepatic ketogenesis and gluconeogenesis during the transition to birth. J Biol Chem **288:**19739-19749.
260. **Cotter DG, Schugar RC, Wentz AE, d'Avignon DA, Crawford PA.** 2013. Successful adaptation to ketosis by mice with tissue-specific deficiency of ketone body oxidation. Am J Physiol Endocrinol Metab **304:**E363-374.
261. **Hondares E, Rosell M, Gonzalez FJ, Giralt M, Iglesias R, Villarroya F.** 2010. Hepatic FGF21 expression is induced at birth via PPARalpha in response to milk intake and contributes to thermogenic activation of neonatal brown fat. Cell Metab **11:**206-212.
262. **Mitchell MD, Peiris HN, Kobayashi M, Koh YQ, Duncombe G, Illanes SE, Rice GE, Salomon C.** 2015. Placental exosomes in normal and complicated pregnancy. Am J Obstet Gynecol **213:**S173-181.
263. **Record M.** 2014. Intercellular communication by exosomes in placenta: a possible role in cell fusion? Placenta **35:**297-302.
264. **Jayabalan N, Nair S, Nuzhat Z, Rice GE, Zuniga FA, Sobrevia L, Leiva A, Sanhueza C, Gutierrez JA, Lappas M, Freeman DJ, Salomon C.** 2017. Cross Talk between Adipose Tissue and Placenta in Obese and Gestational Diabetes Mellitus Pregnancies via Exosomes. Front Endocrinol (Lausanne) **8:**239.
265. **Adam S, Elfeky O, Kinhal V, Dutta S, Lai A, Jayabalan N, Nuzhat Z, Palma C, Rice GE, Salomon C.** 2017. Review: Fetal-maternal communication via extracellular vesicles - Implications for complications of pregnancies. Placenta **54:**83-88.

266. **Zempleni J, Aguilar-Lozano A, Sadri M, Sukreet S, Manca S, Wu D, Zhou F, Mutai E.** 2017. Biological Activities of Extracellular Vesicles and Their Cargos from Bovine and Human Milk in Humans and Implications for Infants. J Nutr **147:**3-10.
267. **Kerner J, Minkler PE, Lesnefsky EJ, Hoppel CL.** 2014. Fatty acid chain elongation in palmitate-perfused working rat heart: mitochondrial acetyl-CoA is the source of two-carbon units for chain elongation. J Biol Chem **289:**10223-10234.
268. **Foster DW.** 2012. Malonyl-CoA: the regulator of fatty acid synthesis and oxidation. J Clin Invest **122:**1958-1959.
269. **Ruderman NB, Saha AK, Kraegen EW.** 2003. Minireview: malonyl CoA, AMP-activated protein kinase, and adiposity. Endocrinology **144:**5166-5171.
270. **Wolfgang MJ, Lane MD.** 2006. The role of hypothalamic malonyl-CoA in energy homeostasis. J Biol Chem **281:**37265-37269.
271. **Saggerson D.** 2008. Malonyl-CoA, a key signaling molecule in mammalian cells. Annu Rev Nutr **28:**253-272.
272. **Funai K, Song H, Yin L, Lodhi IJ, Wei X, Yoshino J, Coleman T, Semenkovich CF.** 2013. Muscle lipogenesis balances insulin sensitivity and strength through calcium signaling. J Clin Invest **123:**1229-1240.
273. **Pender C, Trentadue AR, Pories WJ, Dohm GL, Houmard JA, Youngren JF.** 2006. Expression of genes regulating malonyl-CoA in human skeletal muscle. J Cell Biochem **99:**860-867.
274. **Saha AK, Schwarsin AJ, Roduit R, Masse F, Kaushik V, Tornheim K, Prentki M, Ruderman NB.** 2000. Activation of malonyl-CoA decarboxylase in rat skeletal muscle by contraction and the AMP-activated protein kinase activator 5-aminoimidazole-4-carboxamide-1-beta -D-ribofuranoside. J Biol Chem **275:**24279-24283.
275. **FitzPatrick DR, Hill A, Tolmie JL, Thorburn DR, Christodoulou J.** 1999. The molecular basis of malonyl-CoA decarboxylase deficiency. Am J Hum Genet **65:**318-326.
276. **Gao J, Waber L, Bennett MJ, Gibson KM, Cohen JC.** 1999. Cloning and mutational analysis of human malonyl-coenzyme A decarboxylase. J Lipid Res **40:**178-182.
277. **Wightman PJ, Santer R, Ribes A, Dougherty F, McGill N, Thorburn DR, FitzPatrick DR.** 2003. MLYCD mutation analysis: evidence for protein mistargeting as a cause of MLYCD deficiency. Hum Mutat **22:**288-300.
278. **Kerner J, Hoppel CL.** 2002. Radiochemical malonyl-CoA decarboxylase assay: activity and subcellular distribution in heart and skeletal muscle. Anal Biochem **306:**283-289.
279. **Sambandam N, Steinmetz M, Chu A, Altarejos JY, Dyck JR, Lopaschuk GD.** 2004. Malonyl-CoA decarboxylase (MCD) is differentially regulated in subcellular compartments by 5'AMP-activated protein kinase (AMPK). Studies using H9c2 cells overexpressing MCD and AMPK by adenoviral gene transfer technique. Eur J Biochem **271:**2831-2840.
280. **Laurent G, German NJ, Saha AK, de Boer VC, Davies M, Koves TR, Dephoure N, Fischer F, Boanca G, Vaitheesvaran B, Lovitch SB, Sharpe AH, Kurland IJ, Steegborn C, Gygi SP, Muoio DM, Ruderman NB, Haigis MC.** 2013. SIRT4 coordinates the balance between lipid synthesis and catabolism by repressing malonyl CoA decarboxylase. Mol Cell **50:**686-698.
281. **Witkowski A, Thweatt J, Smith S.** 2011. Mammalian ACSF3 protein is a malonyl-CoA synthetase that supplies the chain extender units for mitochondrial fatty acid synthesis. J Biol Chem **286:**33729-33736.

282. **Chen H, Kim HU, Weng H, Browse J.** 2011. Malonyl-CoA synthetase, encoded by ACYL ACTIVATING ENZYME13, is essential for growth and development of Arabidopsis. Plant Cell **23:**2247-2262.
283. **Watkins PA, Maiguel D, Jia Z, Pevsner J.** 2007. Evidence for 26 distinct acyl-coenzyme A synthetase genes in the human genome. J Lipid Res **48:**2736-2750.
284. **Guan X, Nikolau BJ.** 2016. AAE13 encodes a dual-localized malonyl-CoA synthetase that is crucial for mitochondrial fatty acid biosynthesis. Plant J **85:**581-593.
285. **Quastel JH, Wooldridge WR.** 1928. Some properties of the dehydrogenating enzymes of bacteria. Biochem J **22:**689-702.
286. **Beal MF, Brouillet E, Jenkins B, Henshaw R, Rosen B, Hyman BT.** 1993. Age-dependent striatal excitotoxic lesions produced by the endogenous mitochondrial inhibitor malonate. J Neurochem **61:**1147-1150.
287. **Zeevalk GD, Manzino L, Hoppe J, Sonsalla P.** 1997. In vivo vulnerability of dopamine neurons to inhibition of energy metabolism. Eur J Pharmacol **320:**111-119.
288. **Moy LY, Zeevalk GD, Sonsalla PK.** 2000. Role for dopamine in malonate-induced damage in vivo in striatum and in vitro in mesencephalic cultures. J Neurochem **74:**1656-1665.
289. **Alfares A, Nunez LD, Al-Thihli K, Mitchell J, Melancon S, Anastasio N, Ha KC, Majewski J, Rosenblatt DS, Braverman N.** 2011. Combined malonic and methylmalonic aciduria: exome sequencing reveals mutations in the ACSF3 gene in patients with a non-classic phenotype. J Med Genet **48:**602-605.
290. **Sloan JL, Johnston JJ, Manoli I, Chandler RJ, Krause C, Carrillo-Carrasco N, Chandrasekaran SD, Sysol JR, O'Brien K, Hauser NS, Sapp JC, Dorward HM, Huizing M, Barshop BA, Berry SA, James PM, Champaigne NL, de Lonlay P, Valayannopoulos V, Geschwind MD, Gavrilov DK, Nyhan WL, Biesecker LG, Venditti CP.** 2011. Exome sequencing identifies ACSF3 as a cause of combined malonic and methylmalonic aciduria. Nat Genet **43:**883-886.
291. **Hiltunen JK, Schonauer MS, Autio KJ, Mittelmeier TM, Kastaniotis AJ, Dieckmann CL.** 2009. Mitochondrial fatty acid synthesis type II: more than just fatty acids. J Biol Chem **284:**9011-9015.
292. **Hiltunen JK, Autio KJ, Schonauer MS, Kursu VA, Dieckmann CL, Kastaniotis AJ.** 2010. Mitochondrial fatty acid synthesis and respiration. Biochim Biophys Acta **1797:**1195-1202.
293. **Hosios AM, Hecht VC, Danai LV, Johnson MO, Rathmell JC, Steinhauser ML, Manalis SR, Vander Heiden MG.** 2016. Amino Acids Rather than Glucose Account for the Majority of Cell Mass in Proliferating Mammalian Cells. Dev Cell **36:**540-549.
294. **Peng C, Lu Z, Xie Z, Cheng Z, Chen Y, Tan M, Luo H, Zhang Y, He W, Yang K, Zwaans BM, Tishkoff D, Ho L, Lombard D, He TC, Dai J, Verdin E, Ye Y, Zhao Y.** 2011. The first identification of lysine malonylation substrates and its regulatory enzyme. Mol Cell Proteomics **10:**M111.012658.
295. **Du J, Zhou Y, Su X, Yu JJ, Khan S, Jiang H, Kim J, Woo J, Kim JH, Choi BH, He B, Chen W, Zhang S, Cerione RA, Auwerx J, Hao Q, Lin H.** 2011. Sirt5 is a NAD-dependent protein lysine demalonylase and desuccinylase. Science **334:**806-809.
296. **Nishida Y, Rardin MJ, Carrico C, He W, Sahu AK, Gut P, Najjar R, Fitch M, Hellerstein M, Gibson BW, Verdin E.** 2015. SIRT5 Regulates both Cytosolic and Mitochondrial Protein Malonylation with Glycolysis as a Major Target. Mol Cell **59:**321-332.

297. **Hirschey MD, Zhao Y.** 2015. Metabolic regulation by lysine malonylation, succinylation and glutarylation. Mol Cell Proteomics doi:10.1074/mcp.R114.046664.
298. **Colak G, Pougovkina O, Dai L, Tan M, Te Brinke H, Huang H, Cheng Z, Park J, Wan X, Liu X, Yue WW, Wanders RJ, Locasale JW, Lombard DB, de Boer VC, Zhao Y.** 2015. Proteomic and Biochemical Studies of Lysine Malonylation Suggest Its Malonic Aciduria-associated Regulatory Role in Mitochondrial Function and Fatty Acid Oxidation. Mol Cell Proteomics **14:**3056-3071.
299. **Kulkarni RA, Worth AJ, Zengeya TT, Shrimp JH, Garlick JM, Roberts AM, Montgomery DC, Sourbier C, Gibbs BK, Mesaros C, Tsai YC, Das S, Chan KC, Zhou M, Andresson T, Weissman AM, Linehan WM, Blair IA, Snyder NW, Meier JL.** 2017. Discovering Targets of Non-enzymatic Acylation by Thioester Reactivity Profiling. Cell Chem Biol **24:**231-242.
300. **Pougovkina O, Te Brinke H, Wanders RJ, Houten SM, de Boer VC.** 2014. Aberrant protein acylation is a common observation in inborn errors of acyl-CoA metabolism. J Inherit Metab Dis **37:**709-714.
301. **Rardin MJ, He W, Nishida Y, Newman JC, Carrico C, Danielson SR, Guo A, Gut P, Sahu AK, Li B, Uppala R, Fitch M, Riiff T, Zhu L, Zhou J, Mulhern D, Stevens RD, Ilkayeva OR, Newgard CB, Jacobson MP, Hellerstein M, Goetzman ES, Gibson BW, Verdin E.** 2013. SIRT5 regulates the mitochondrial lysine succinylome and metabolic networks. Cell Metab **18:**920-933.
302. **Du Y, Cai T, Li T, Xue P, Zhou B, He X, Wei P, Liu P, Yang F, Wei T.** 2015. Lysine malonylation is elevated in type 2 diabetic mouse models and enriched in metabolic associated proteins. Mol Cell Proteomics **14:**227-236.
303. **An JH, Kim YS.** 1998. A gene cluster encoding malonyl-CoA decarboxylase (MatA), malonyl-CoA synthetase (MatB) and a putative dicarboxylate carrier protein (MatC) in Rhizobium trifolii--cloning, sequencing, and expression of the enzymes in Escherichia coli. European journal of biochemistry / FEBS **257:**395-402.
304. **Lee HY, An JH, Kim YS.** 2000. Identification and characterization of a novel transcriptional regulator, MatR, for malonate metabolism in Rhizobium leguminosarum bv. trifolii. European journal of biochemistry / FEBS **267:**7224-7230.
305. **Van Schaftingen E, Rzem R, Marbaix A, Collard F, Veiga-da-Cunha M, Linster CL.** 2013. Metabolite proofreading, a neglected aspect of intermediary metabolism. J Inherit Metab Dis **36:**427-434.
306. **de Vellis J, Shannon LM, Lew JY.** 1963. Malonic Acid Biosynthesis in Bush Bean Roots. I. Evidence for Oxaloacetate as Immediate Precursor. Plant Physiol **38:**686-690.
307. **Vennesland B, Evans EA.** 1944. The formation of malonic acid from oxalacetic acid by pig heart preparations. J Biol Chem **156:**783-784.
308. **Hayaishi O, Kornberg A.** 1952. Metabolism of cytosine, thymine, uracil, and barbituric acid by bacterial enzymes. J Biol Chem **197:**717-732.
309. **Kim JW, Yu BP.** 1989. Characterization of age-related malondialdehyde oxidation: the effect of modulation by food restriction. Mech Ageing Dev **50:**277-287.
310. **Hegre CS, Halenz DR, Lane MD.** 1959. The Enzymatic Carboxylation of Butyryl Coenzyme-A. J Am Chem Soc **81:**6526-6527.
311. **Kim YS, Kolattukudy PE.** 1978. Purification and properties of malonyl-CoA decarboxylase from rat liver mitochondria and its immunological comparison with the enzymes from rat brain, heart, and mammary gland. Arch Biochem Biophys **190:**234-246.

312. **Asadollahi R, Oneda B, Joset P, Azzarello-Burri S, Bartholdi D, Steindl K, Vincent M, Cobilanschi J, Sticht H, Baldinger R, Reissmann R, Sudholt I, Thiel CT, Ekici AB, Reis A, Bijlsma EK, Andrieux J, Dieux A, FitzPatrick D, Ritter S, Baumer A, Latal B, Plecko B, Jenni OG, Rauch A.** 2014. The clinical significance of small copy number variants in neurodevelopmental disorders. J Med Genet **51:**677-688.
313. **Ellis JM, Wolfgang MJ.** 2012. A genetically encoded metabolite sensor for malonyl-CoA. Chem Biol **19:**1333-1339.
314. **Zeevalk GD, Derr-Yellin E, Nicklas WJ.** 1995. Relative vulnerability of dopamine and GABA neurons in mesencephalic culture to inhibition of succinate dehydrogenase by malonate and 3-nitropropionic acid and protection by NMDA receptor blockade. J Pharmacol Exp Ther **275:**1124-1130.
315. **Sadhukhan S, Liu X, Ryu D, Nelson OD, Stupinski JA, Li Z, Chen W, Zhang S, Weiss RS, Locasale JW, Auwerx J, Lin H.** 2016. Metabolomics-assisted proteomics identifies succinylation and SIRT5 as important regulators of cardiac function. Proc Natl Acad Sci U S A **113:**4320-4325.
316. **Frezza C, Cipolat S, Scorrano L.** 2007. Organelle isolation: functional mitochondria from mouse liver, muscle and cultured fibroblasts. Nat Protoc **2:**287-295.
317. **Xia J, Sinelnikov IV, Wishart DS.** 2011. MetATT: a web-based metabolomics tool for analyzing time-series and two-factor datasets. Bioinformatics **27:**2455-2456.

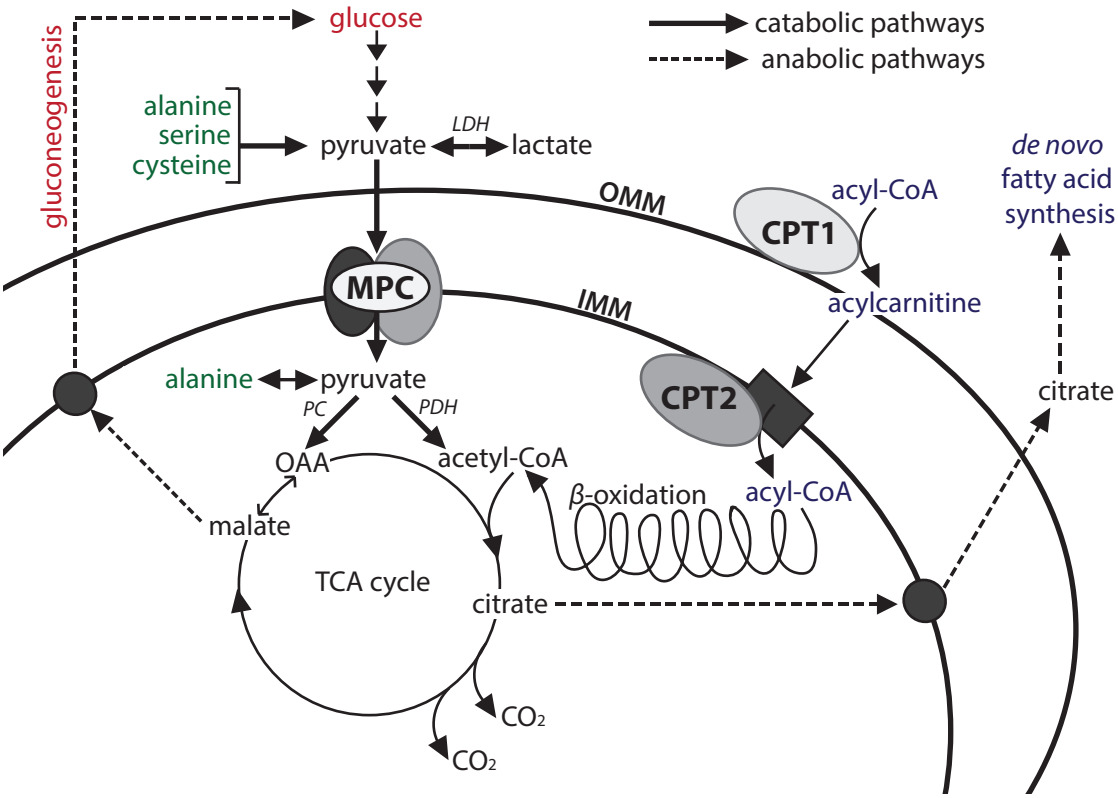

Fig. 1. Overview of pyruvate and fatty acid metabolism.
MPC, mitochondrial pyruvate carrier; CPT, carnitine-palmitoyltransferase; OMM, outer mitochondrial membrane; IMM, inner mitochondrial membrane; TCA, tricarboxylic acid; OAA, oxalacetate; LDH, lactate dehydrogenase; PDH, pyruvate dehydrogenase; PC, pyruvate carboxylase

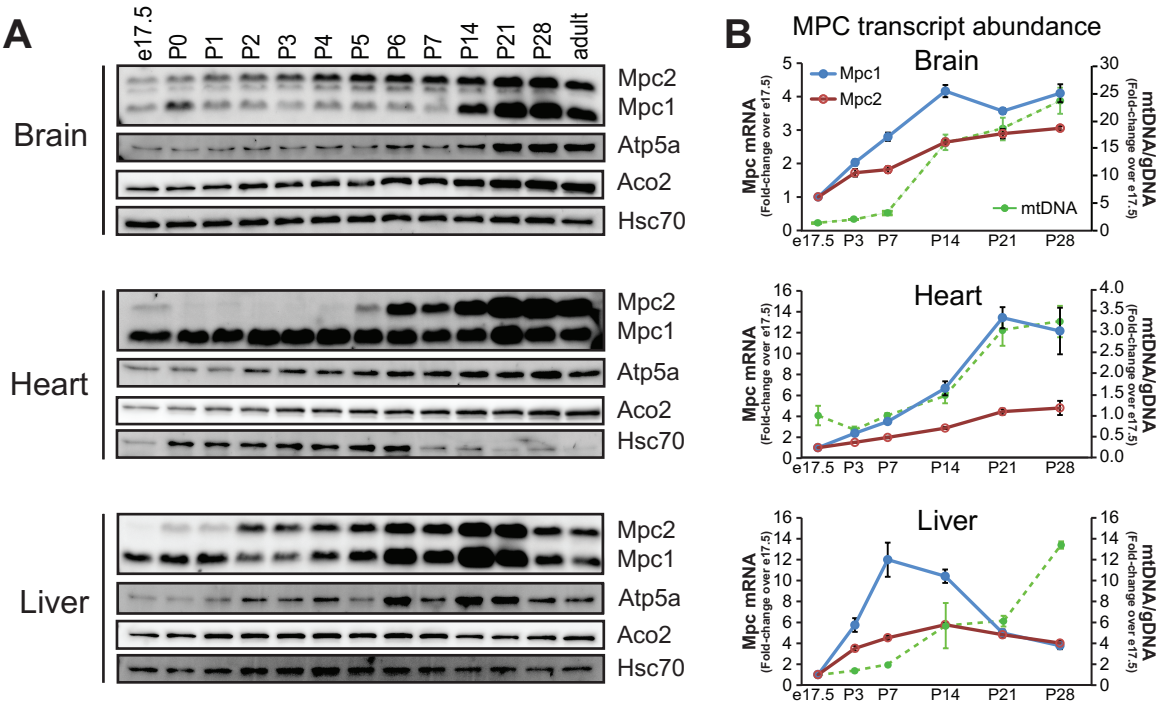

Fig 2.1. The mitochondrial pyruvate carrier is developmentally regulated in a tissue-specific manner.

(A) Western blot for Mpc1 and Mpc2 in mouse brain, heart, and liver across early postnatal development with Atp5a (mitochondrial inner membrane), aconitase 2 (Aco2, mitochondrial matrix), and Hsc70 (cytosol), demonstrating that tissue-specific differences in MPC expression are specific to the MPC. Mpc2 is present in embryonic tissues, although not readily visualized on the same exposure as adult tissues (see Fig. 2.4). (B) Relative mRNA abundance of Mpc1 and Mpc2 in brain, heart, and liver across mouse development by qRT-PCR and mitochondrial DNA content as determined by qRT-PCR of the mitochondrially-encoded Nd1 gene relative to nuclear loci and displayed as fold-change over e17.5 (mean ± SEM, n=3-4 per age).

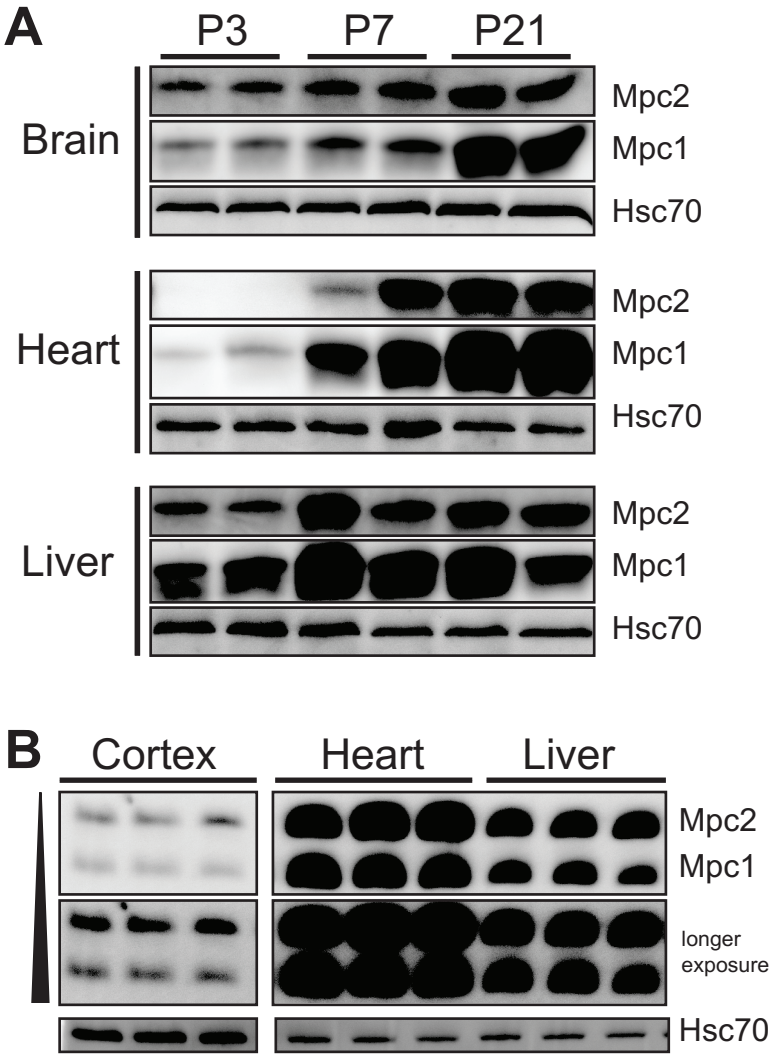

Fig 2.2. Tissue-specific developmental regulation of MPC components, Mpc1 and Mpc2.

(A) Western blots of MPC expression in mouse brain, heart, and liver at three developmental time points (postnatal day 3, 7, and 21). (B) Mpc1 and Mpc2 are expressed in equal ratios in adult mouse cerebral cortex, heart, and liver as determined by immunoblotting. Adult cortex image from same blot and same exposure. Hsc70 is shown as loading control. No significant differences in the ratio of Mpc1: Mpc2 were detected across adult tissues (n=5).

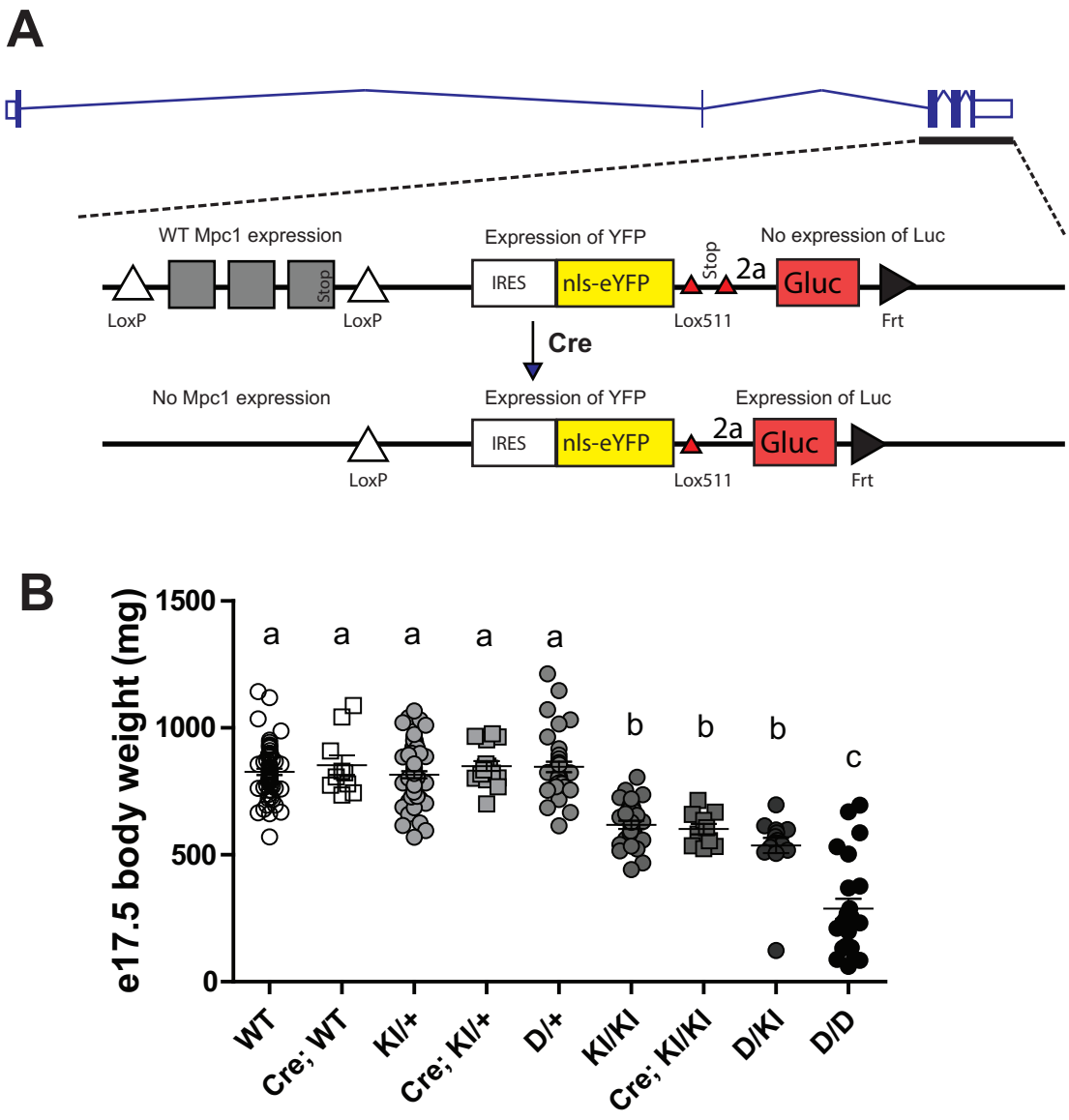

Fig 2.S1. Gene targeting strategy for Mpc1 hypomorphic allele in mouse. Related to Fig 2.3 and Fig 2.4. (A) Exon diagram of Mpc1 locus and schematic of Mpc1 knock-in allele. Mpc1 is encoded by a five exon gene, and the knock-in reporter construct was targeted to the last three exons of the Mpc1 locus. The Mpc1 deletion allele was generated by germline expression of a Cre recombinase transgene and subsequent inheritance of the deletion allele without Cre. (B) Body weights (mean ± SD, in mg) of e17.5 embryos from all crosses (n=10-64).

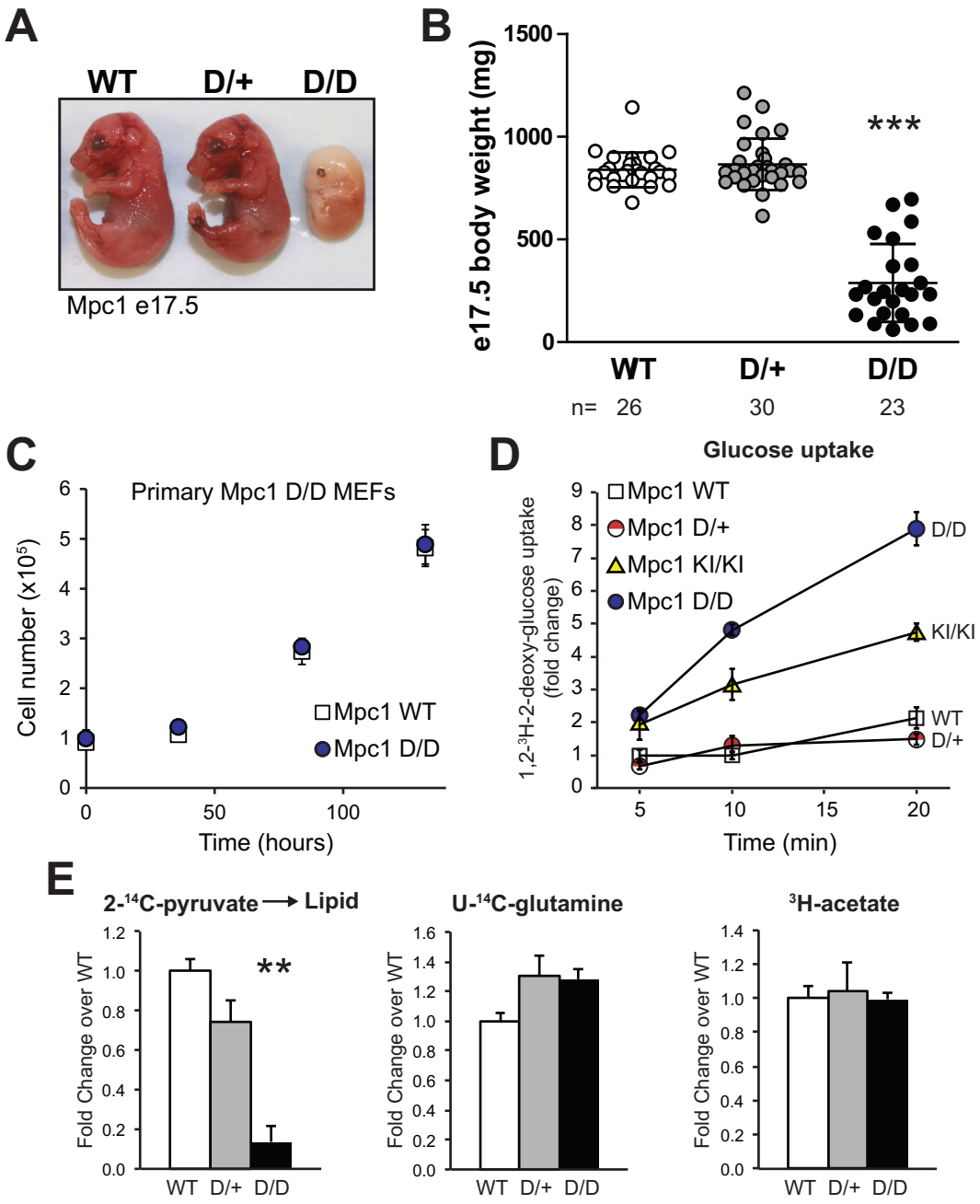

Fig 2.3. Developmental and metabolic requirement for mitochondrial pyruvate metabolism. (A) Photograph of WT, heterozygous, and homozygous Mpc1 deletion late-gestation (e17.5) embryos. (B) Timed matings between Mpc1 D/+ mice reveal expected Mendelian ratios. Body weight distribution of Mpc1 D/D e17.5 embryos and D/+ and wild-type (WT) littermate controls (mean ± SD, n=23-30). (C) Cell proliferation assay in primary Mpc1 WT and D/D mouse embryonic fibroblasts (MEFs), mean ± SD, n=3, representative of two independent experiments with cells derived from two embryos of each genotype. (D) Glucose uptake in primary Mpc1-deficient MEFs labeled with 0.5µCi [1,2-3H]2-deoxy-glucose at a final concentration of 6.5mM 2-deoxy-glucose for 5, 10, and 20 minutes (mean ± SEM, n=6). (E) Incorporation of radiolabeled substrates into the total lipid fraction in Mpc1 D/D primary MEFs (black bars) with wild-type (WT, white bars) and heterozygous (D/+, gray) controls. Counts were normalized to protein and are displayed as mean ± SEM (n=3). Significant differences among group means determined by Tukey multiple comparison test after one-way ANOVA and indicated by asterisks relative to WT and D/+ controls (***p<0.001, **0.001<p<0.01). D/D = Mpc1 deletion; KI/KI = Mpc1 knock-in (KI) hypomorph

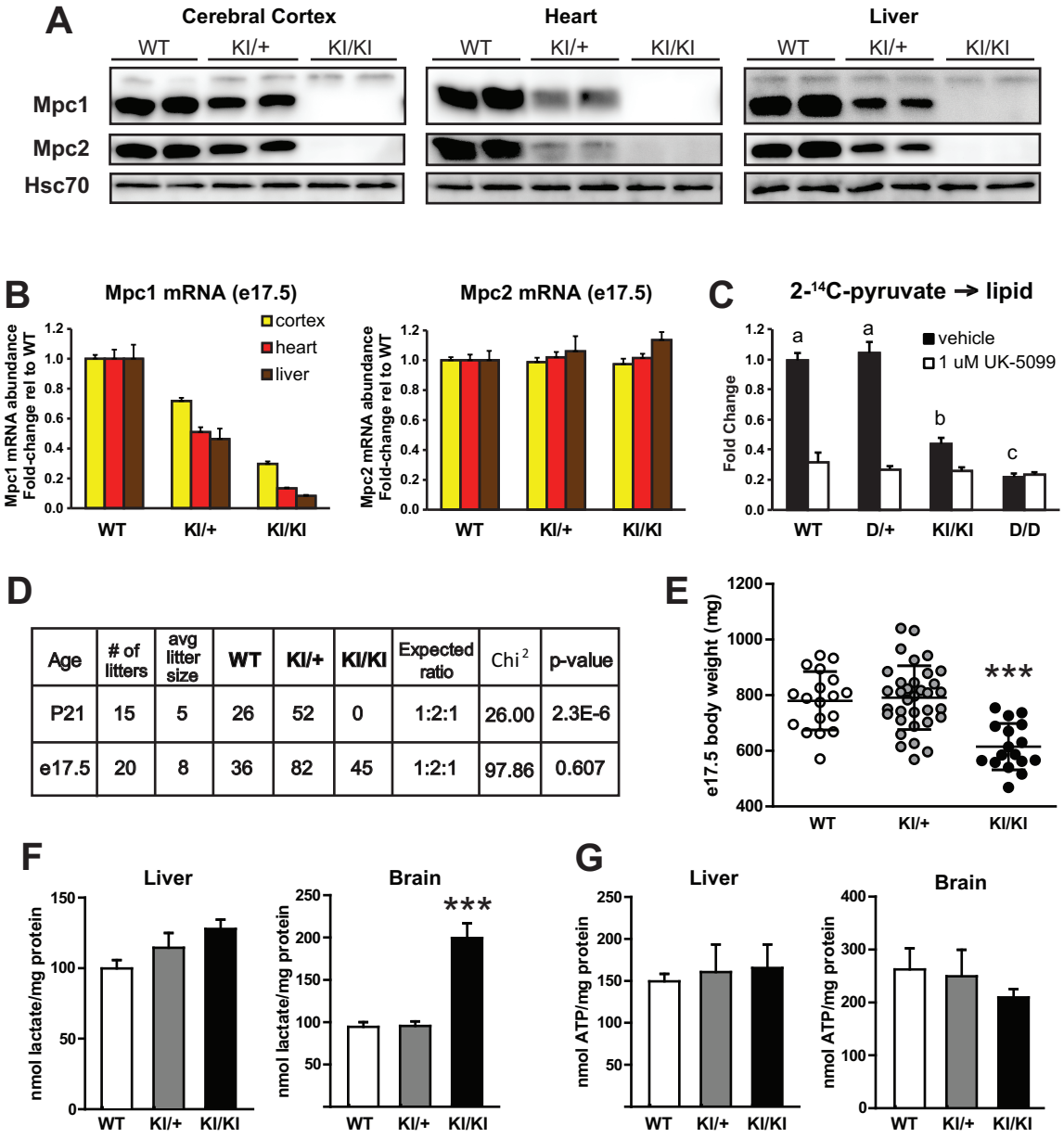

Age	# of litters	avg litter size	WT	KI/+	KI/KI	Expected ratio	Chi^2	p-value
P21	15	5	26	52	0	1:2:1	26.00	2.3E-6
e17.5	20	8	36	82	45	1:2:1	97.86	0.607

Fig 2.4. Mpc1 hypomorphic allele reveals requirement for mitochondrial pyruvate metabolism in mammalian embryonic development. (A) Western blotting and qRT-PCR (B) for Mpc1 and Mpc2 in tissues from e17.5 embryos carrying 0, 1, or 2 copies of the Mpc1 hypomorphic knock-in (KI) allele. Hsc70 is shown as a loading control. RT-PCR data was normalized to the average of four reference genes as described in Methods and is presented as mean ± SEM relative to WT (n=7-8 per genotype). (C) [2-14C]pyruvate incorporation into the total lipid fraction in Mpc1-deficient primary MEFs in the presence of MPC inhibitor UK-5099 or vehicle (DMSO) (mean ± SEM, n=5). (D) Matings between mice heterozygous for the Mpc1 knock-in (KI) allele do not yield expected Mendelian ratios of offspring at weaning at postnatal day 21 (P21); however, expected Mendelian ratios are observed in late-gestation litters (embryonic day 17.5). (E) Body weights (mean ± SD, in mg) of e17.5 embryos from KI/+ intercrosses (n=17-34 from 8 litters). (F) Steady-state lactate concentrations in Mpc1 KI/KI e17.5 liver and brain as determined by enzymatic assay (mean ± SEM, n=6) (G) Steady-state ATP concentrations in liver and brain of Mpc1 KI/KI e17.5 embryos and littermate controls (mean ± SEM, n=5). Significant differences among group means determined by Tukey multiple comparison test after one-way ANOVA and indicated by asterisks relative to WT and D/+ controls (***p<0.001).

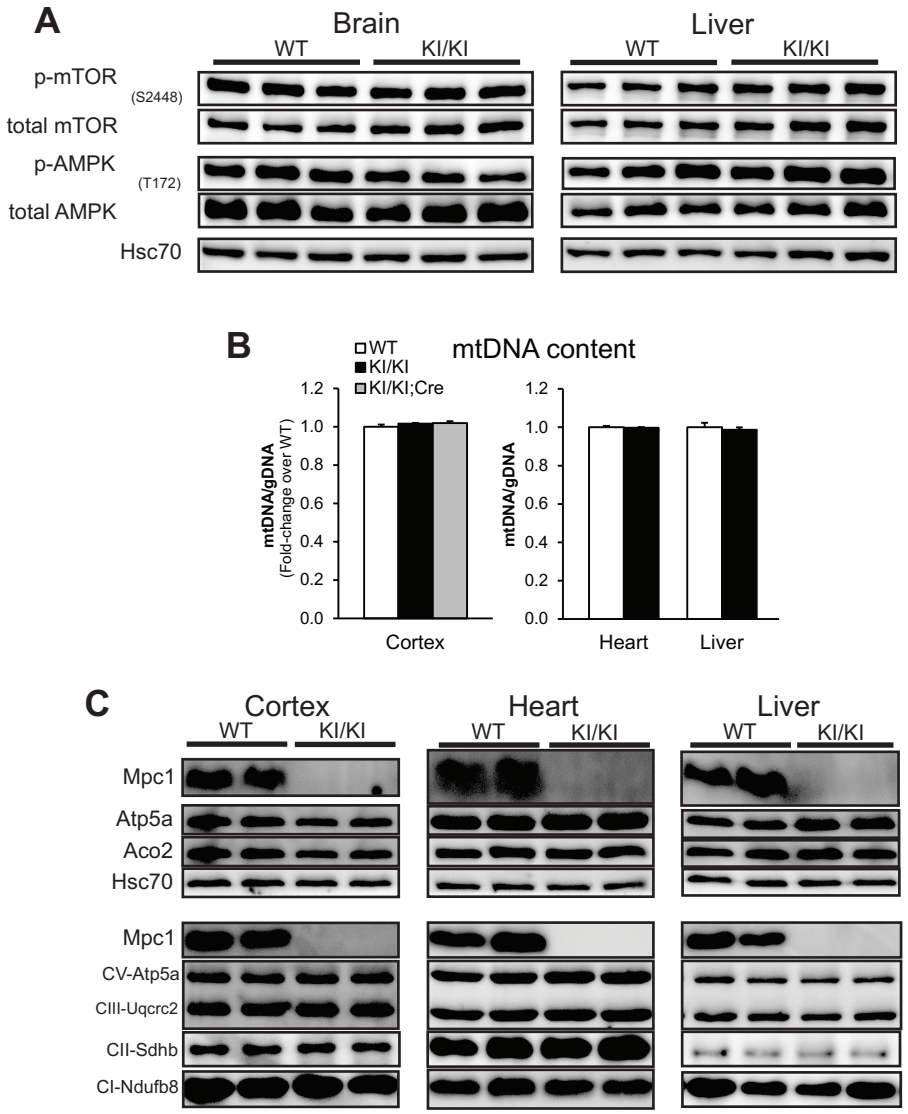

Fig 2.5. Normal mitochondrial abundance and energy-sensing signaling in tissues from Mpc1 KI hypomorph embryos. (A) Representative immunoblot for phosphorylation of canonical energy-sensing components of AMPK and mTOR signaling pathways. (B) No difference in mitochondrial DNA content as determined by qRT-PCR with primers specific to the mitochondrially-encoded Nd1 gene relative to nuclear loci on Chr7 and Chr12 (mean ± SEM, n=7-8). (C) Representative immunoblot for mitochondrial proteins in WT and Mpc1 KI/KI cerebral cortex, heart, and liver, with Hsc70 as a loading control. (Aco2=aconitase 2; CV=Complex V; CIII=Complex III; CII=Complex II; CI=Complex I)

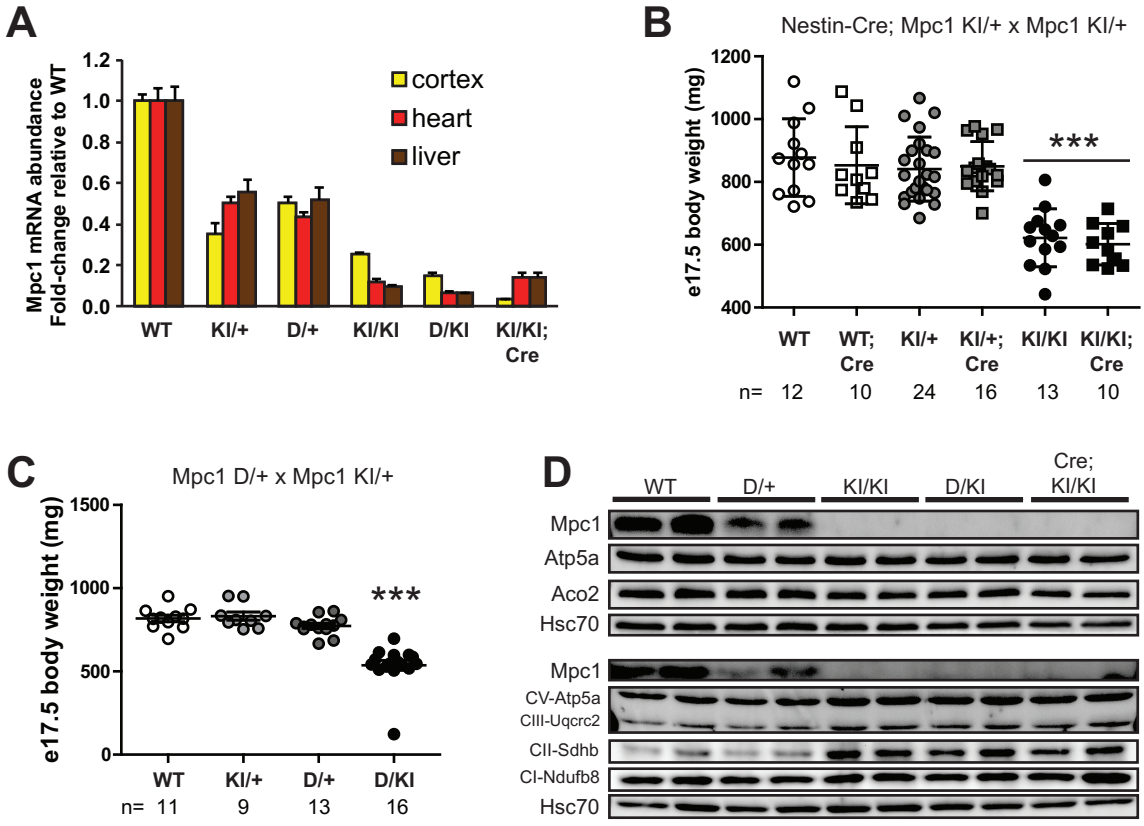

Fig 2.6. Mpc1 hypomorphic allelic series reveals threshold requirement for mitochondrial pyruvate metabolism during development.

(A) Mpc1 transcript abundance in cerebral cortex, heart, and liver of e17.5 embryos across an allelic series of Mpc1-deficient genetic models (mean ± SEM, n=8). (B) Nestin-Cre-mediated deletion of Mpc1 in embryonic nervous system does not affect e17.5 body weight (mean ± SD, n=10-24 from 11 litters) and conforms to expected Mendelian ratios ($\chi 2=2.44$, $p=0.786$). (C) Matings between Mpc1 D/+ females and Mpc1 KI/+ males yield expected Mendelian ratios in e17.5 litters ($\chi 2=2.18$, $p=0.535$), and D/KI offspring are viable, although significantly smaller than littermate controls (***$p<0.001$ by Tukey multiple comparison test after one-way ANOVA). See also Figure S1B. (D) Immunoblotting for inner mitochondrial membrane proteins in e17.5 cerebral cortex across Mpc1 hypomorphic allelic series, with Aco2 of the mitochondrial matrix for comparison and cytosolic Hsc70 as a loading control.

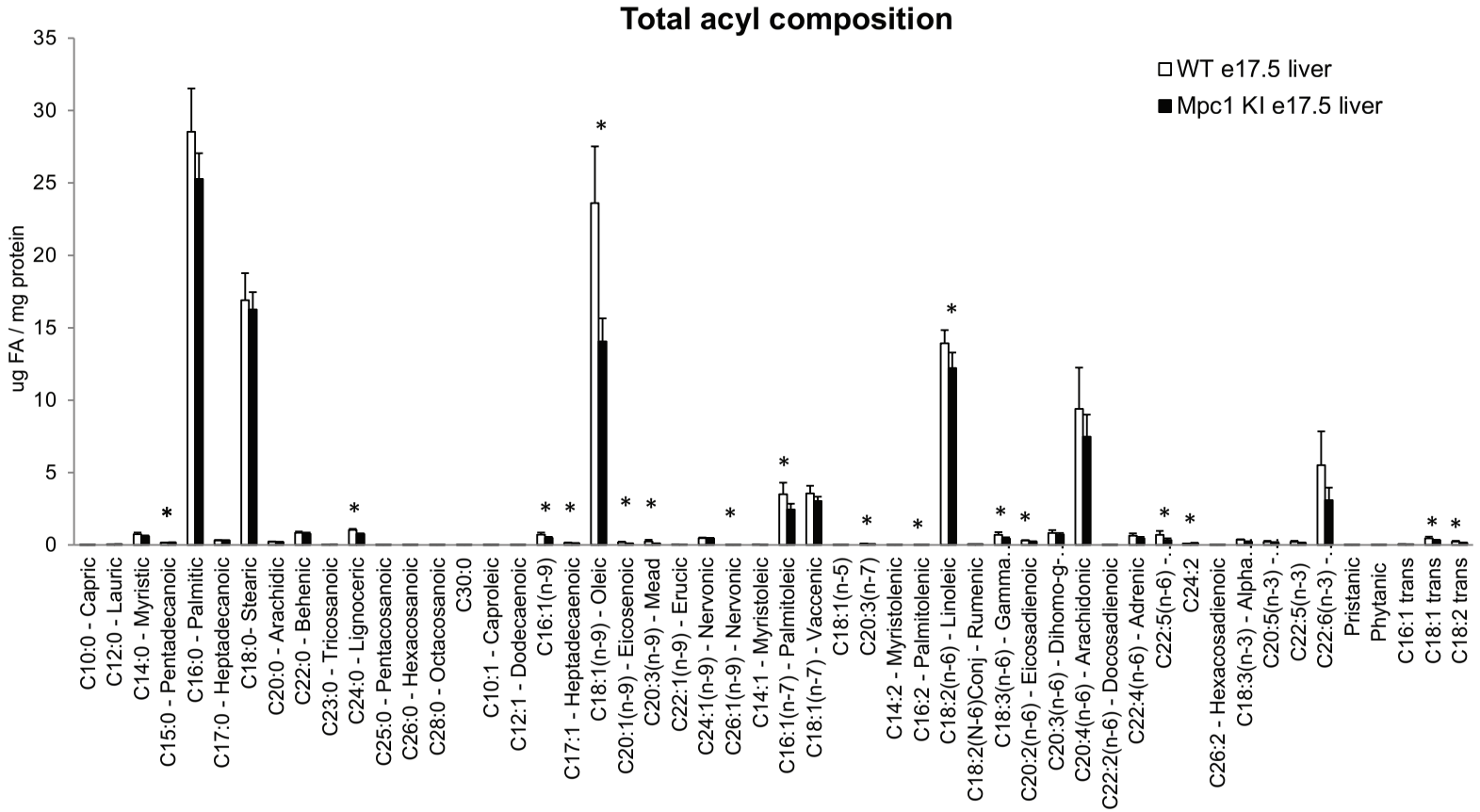

Fig 2.S2. Changes in lipid abundance and acyl composition reflect tissue-specific alterations in Mpc1-deficient liver. Related to Fig 2.7. Total acyl content is decreased in Mpc1 KI e17.5 liver. Acyl composition from total lipid extract was measured by GC-MS as pentafluorobenzyl bromide esters and is shown as μg FA/mg protein (mean ± SD, n=5). (*$p<0.05$ by Student's t-test)

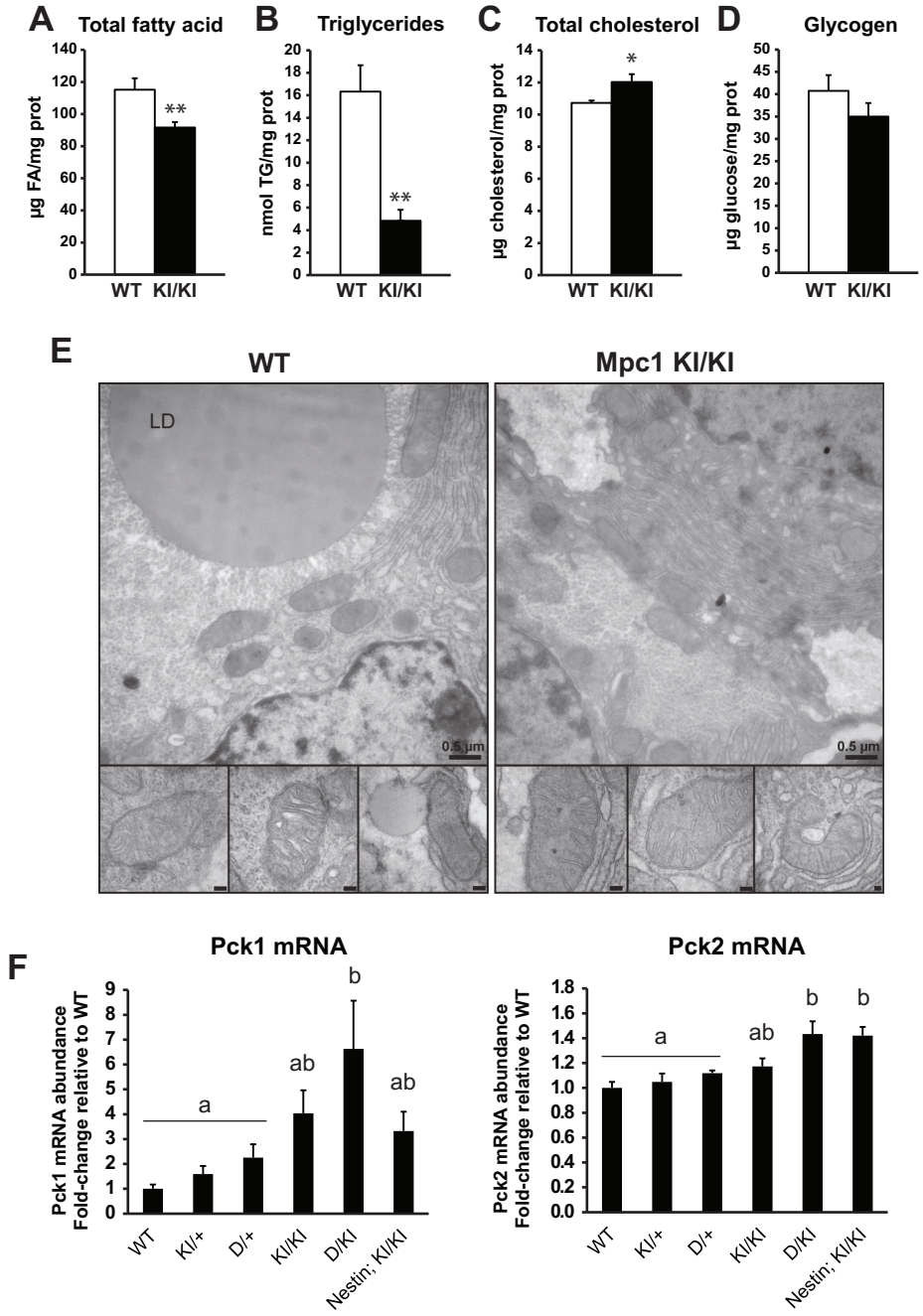

Fig 2.7. Alterations in energy balance and lipid metabolism in Mpc1-deficient fetal liver. (A) Liver total fatty acid content determined by GC-MS (mean ± SEM, n=5). (B) Triglyceride levels in e17.5 liver determined enzymatically (mean ± SEM, n=6). (C) Liver total cholesterol levels (mean ± SEM, n=4). (D) e17.5 liver glycogen content determined enzymatically after acid hydrolysis (mean ± SEM, n=5). (*p<0.05, **p<0.02) (E) Transmission electron micrographs of WT (left) and Mpc1 KI (right) e17.5 liver. Inset images showing normal mitochondrial morphology, inset scale bar = 100nm, LD=lipid droplet. (F) Pck1 and Pck2 mRNA abundance in e17.5 liver across Mpc1 hypomorphic allelic series (mean ± SEM, n=8) Significant differences as determined by Tukey post-hoc test (p<0.05) after one-way ANOVA are indicated by different letters.

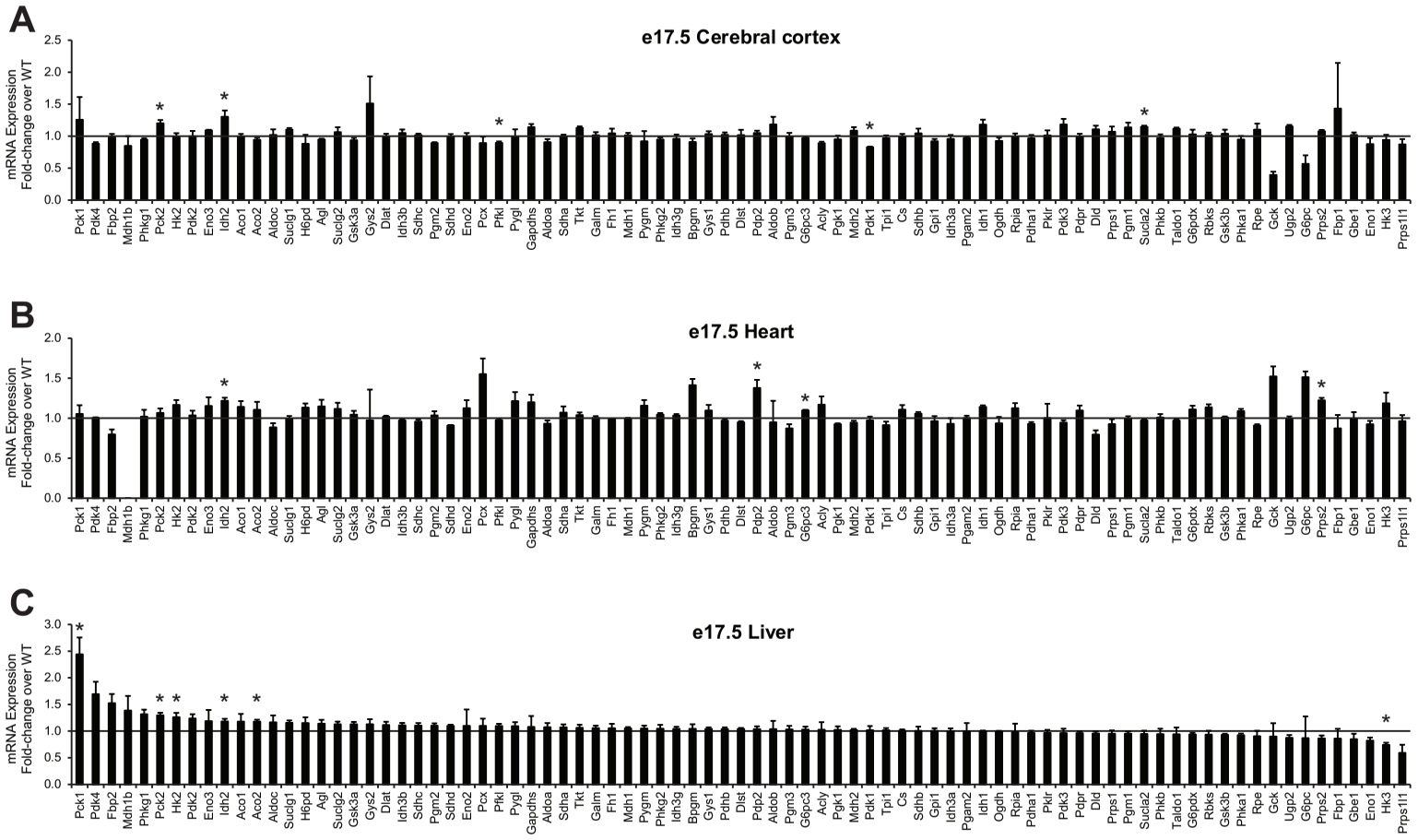

Fig 2.S3. Transcriptional regulation of glucose metabolism-related genes in Mpc1-deficient embryonic tissues. Related to Fig 2.7. (A) mRNA expression of genes involved in glucose metabolism in e17.5 Mpc1 KI/KI cerebral cortex, heart (B), and liver (C) by qRT-PCR array. Data is presented as fold-change relative to WT (mean ± SEM, n=3). Asterisks indicate significant differences by Student's t-test ($p<0.05$).

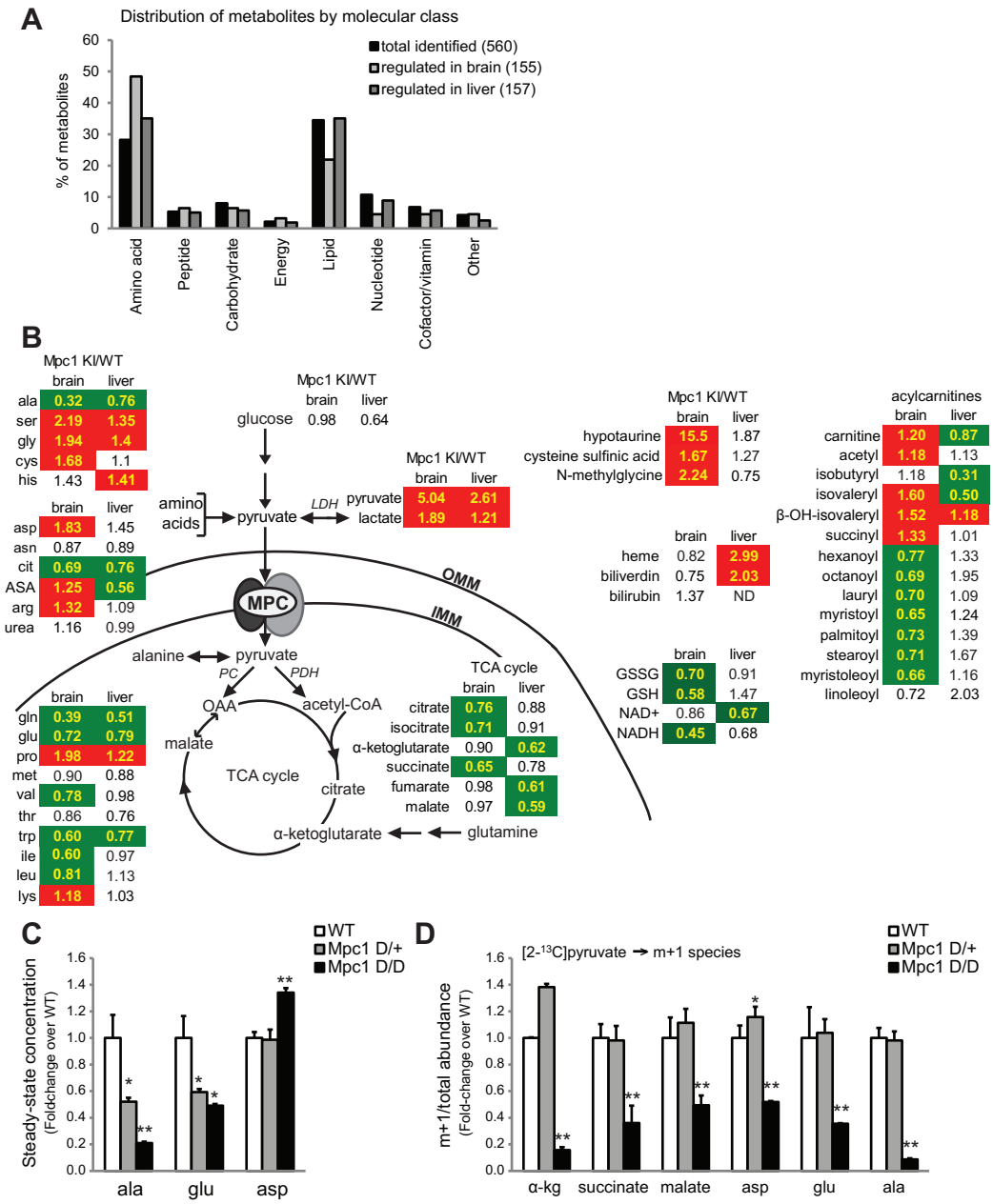

Fig 2.8. Steady-state metabolite concentrations reveal effects of MPC deficiency and compensatory metabolic adaptations. (A) Distribution of total metabolites identified by unbiased metabolomics across molecular classes compared to the distribution of significantly regulated metabolites in brain and liver. (B) Metabolites detected in both brain and liver that were significantly regulated by Mpc1 deficiency. Values shown are fold-change relative to WT, and red and green indicate significant up- and down-regulation, respectively ($p<0.05$ by Welch's two-sample t-test, n=8). Shown here are select metabolites directly related to pyruvate metabolism, TCA cycle intermediates, select amino acids, and select lipid metabolites. Additional list of significantly regulated metabolites in Table S1. (C) Steady-state concentrations of alanine (ala), glutamate (glu), and aspartate (asp) in Mpc1 D/D primary MEFs relative to WT MEFs. (D) [2-^{13}C]pyruvate flux. m+1 labeled metabolites over total metabolite abundance, determined by LC-MS, shown relative to WT (mean±SEM, n=4). (*$0.01<p<0.05$, **$p<0.01$ by pairwise comparison to WT after one-way ANOVA; cit=citrulline; ASA=argininosuccinic acid; α-kg=α-ketoglutarate)

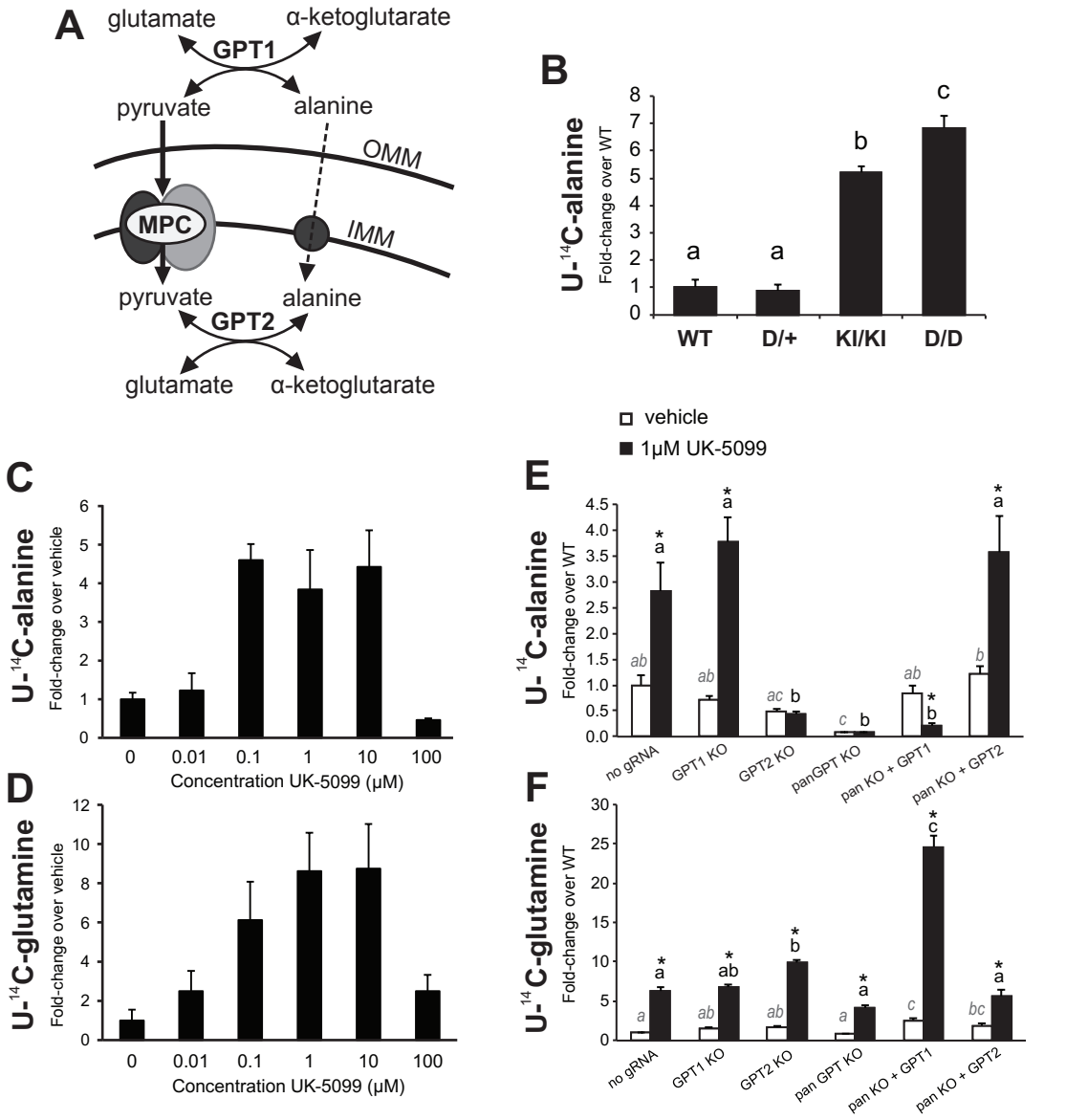

Fig 2.9. Mitochondrial amino acid utilization increases upon impaired mitochondrial pyruvate transport. (A) Alanine and pyruvate can be interconverted in either the cytosol or the mitochondrial matrix by the transaminase activity of glutamic-pyruvate transaminase 1 (GPT1, cytosolic) or glutamic-pyruvate transaminase 2 (GPT2, mitochondrial). Both transaminases utilize glutamate or α-ketoglutarate as co-substrates for the interconversion of pyruvate and alanine. While pyruvate enters the mitochondrial matrix via the MPC, alanine likely traverses the inner mitochondrial membrane (IMM) via a member of the solute carrier family 25 of inner membrane transporters. (B) [U-14C]alanine incorporation into the total lipid fraction is dramatically upregulated in Mpc1 D/D MEFs (mean ± SEM, n=3). In HEK293T cells, pharmacological inhibition of the MPC with UK-5099 robustly impairs mitochondrial pyruvate metabolism (Fig. 2.S4) while simultaneously stimulating mitochondrial flux of alanine (C) and glutamine (D) in a dose-dependent manner as determined by incorporation of radiolabeled substrates into the total lipid fraction. (E) To determine the relative contributions of GPT1 and GPT2 to this phenomenon, HEK293T cells lacking GPT1, GPT2, or both (pan GPT) were derived by CRISPR/Cas9 genome editing. The increase in mitochondrial flux of alanine is independent of cytosolic GPT1, and mitochondrial GPT2 alone is necessary and sufficient for the increase in alanine flux that accompanies impaired mitochondrial pyruvate transport (mean ± SEM, n=6). (F) Glutamine incorporation into lipid in GPT-deficient HEK293T cells in the presence or absence of UK-5099. Significant differences among group means are represented by letters and were determined by Tukey multiple comparison test ($p<0.05$) after one-way ANOVA. In E and F, italicized letters are used for comparison of vehicle-treated cells, bold letters are used for UK-5099-treated cells, and asterisks indicate significant up- or down-regulation of flux in response to UK-5099 treatment.

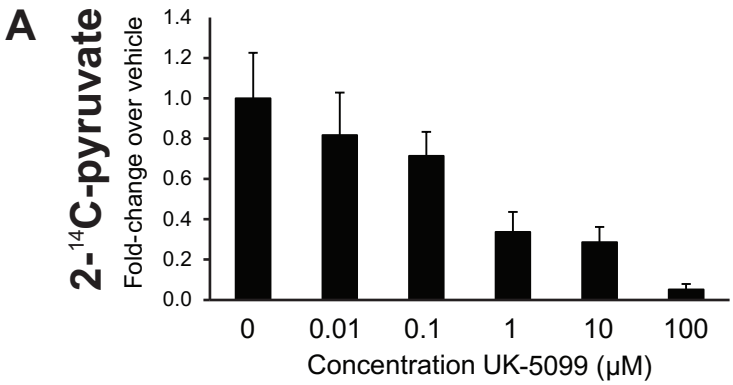

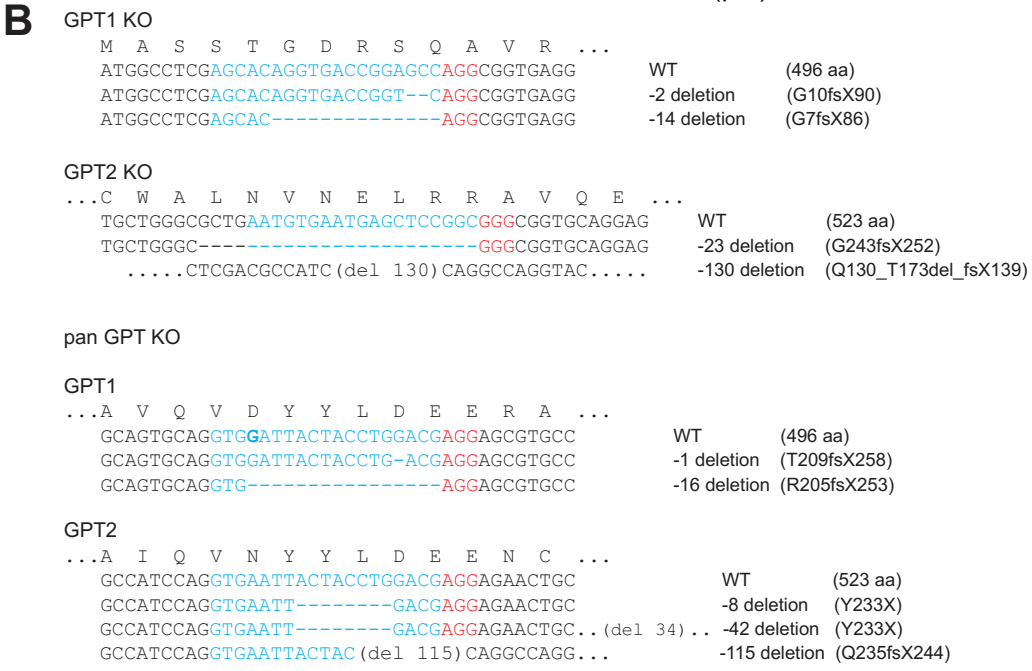

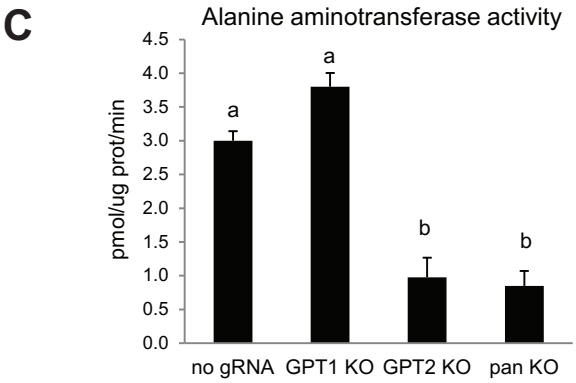

Fig 2.S4. Generation of GPT KO HEK293T cells. Related to Fig 2.9. (A) Dose-dependent impairment of [2-14C]pyruvate incorporation into the total lipid fraction in HEK293T cells treated with UK-5099, an inhibitor of the MPC (mean ± SEM, n=3). (B) Genomic mutations identified in GPT1, GPT2, and pan GPT knockout (KO) HEK293T clones used for flux experiments in Fig 9. The guide RNA (gRNA) target site is shown in blue with the protospacer-adjacent motif in red. Predicted mutations at the protein level are listed at right. (C) Alanine aminotransferase activity assay in select GPT KO HEK293T clones (mean ± SEM, n=4). Significant differences as determined by Tukey post-hoc test ($p<0.05$) after one-way ANOVA are indicated by different letters.

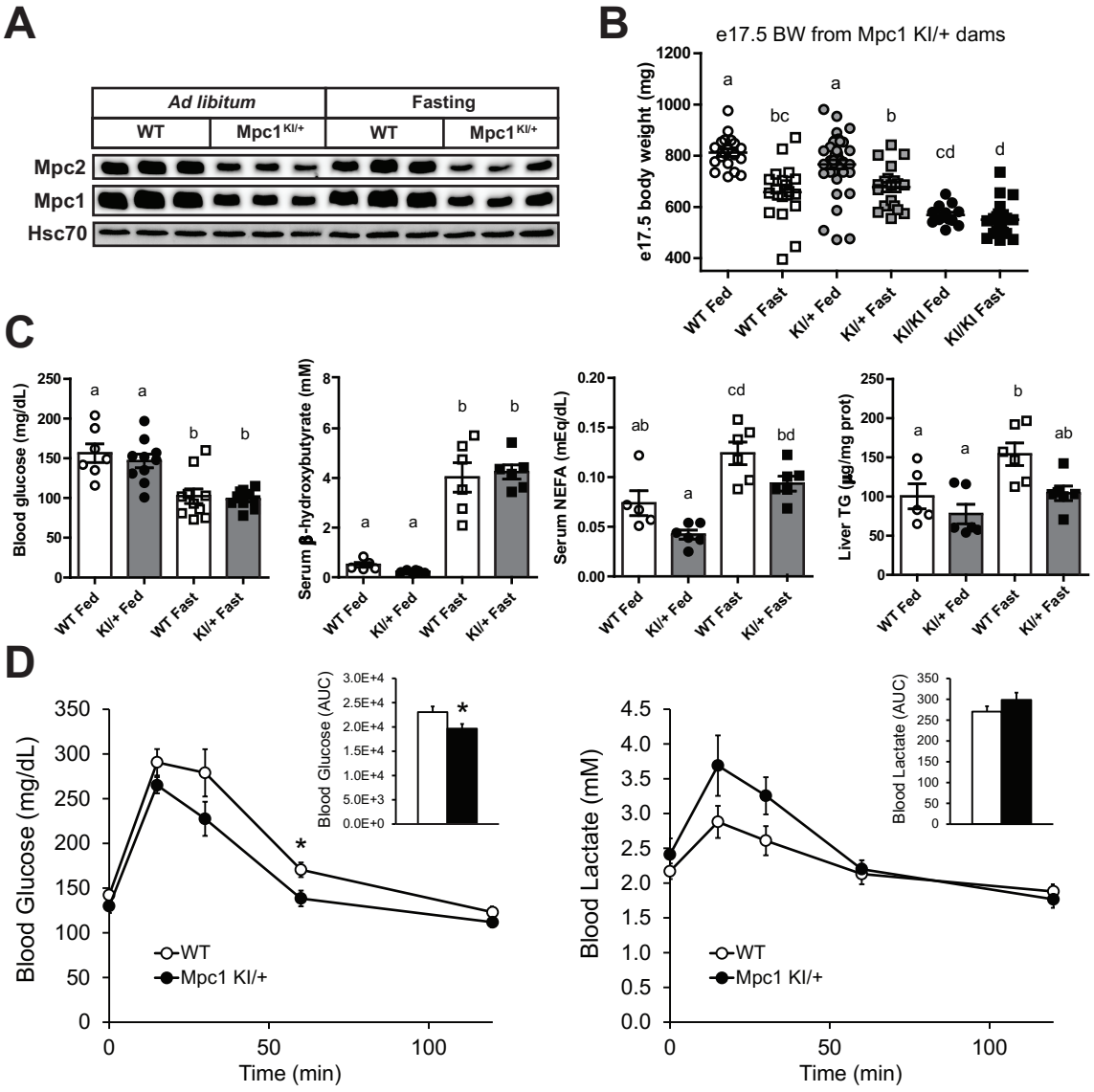

Fig. 4.1. Maternal response to late-gestation nutrient deprivation with impaired mitochondrial pyruvate transport.

(A) Immunoblot for Mpc1 and Mpc2 in maternal liver, 17.5 dpc, fed or 24h fasted. (B) Late-gestation (e17.5) fetal body weights from fed or fasted Mpc1 KI/+ dams. (C) Maternal blood glucose and serum β-hydroxybutyrate, non-esterified fatty acids (NEFA), and triglyceride (TG) concentrations (mean ± SEM, n=5-6). Maternal liver triglyceride content normalized to protein content (mean ± SEM, n=5-6). (D) Blood glucose and lactate concentrations during oral glucose tolerance test in pregnant dams at 17.5 dpc (mean ± SEM, n=10,9). Glucose (2g/kg) administered by oral gavage after 6h fast. Statistically significant differences ($p<0.05$) for pairwise comparisons after ANOVA indicated by letters. *$p<0.05$ by t-test or repeated measures ANOVA.

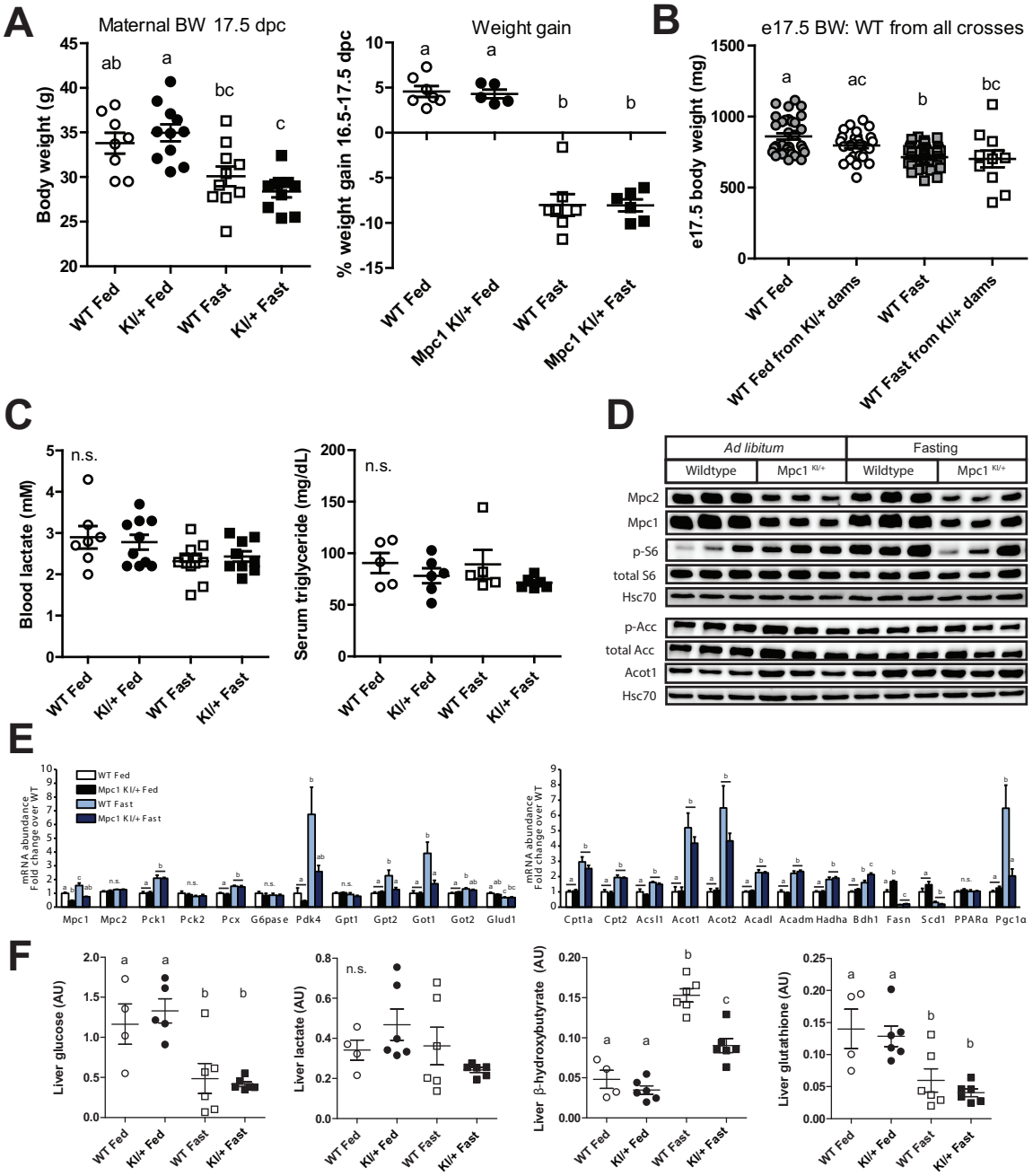

Fig. 4.S1. Maternal response to late-gestation nutrient deprivation.
(A) Maternal body weights at 17.5 dpc (mean ± SEM, n=8-11) and body weight differences from 16.5-17.5 dpc (8.01±1.20 % in WT dams and 8.05±0.67% in Mpc1 KI/+ dams, mean ± SEM, n=7,6) (B) WT fetal body weights at e17.5 from fed or 24h fasted WT or Mpc1 KI/+ dams. (C) Maternal blood lactate and serum triglyceride levels at 17.5 dpc (mean ± SEM, n=5-6). (D) Immunoblot of proteins regulated by fasting and nutritional status in maternal liver at 17.5 dpc, fed or 24h fasted. Mpc1 and Mpc2 blots also shown in Figure 4.1A. (E) Transcriptional regulation in WT and Mpc1-deficient maternal liver determined by qRT-PCR (mean ± SEM, n=5-6). (F) Steady-state metabolite abundances in maternal liver determined by 1H-NMR, normalized to protein content (mean ± SEM, n=4-6). Statistically significant differences ($p<0.05$) for pairwise comparisons after ANOVA indicated by letters.

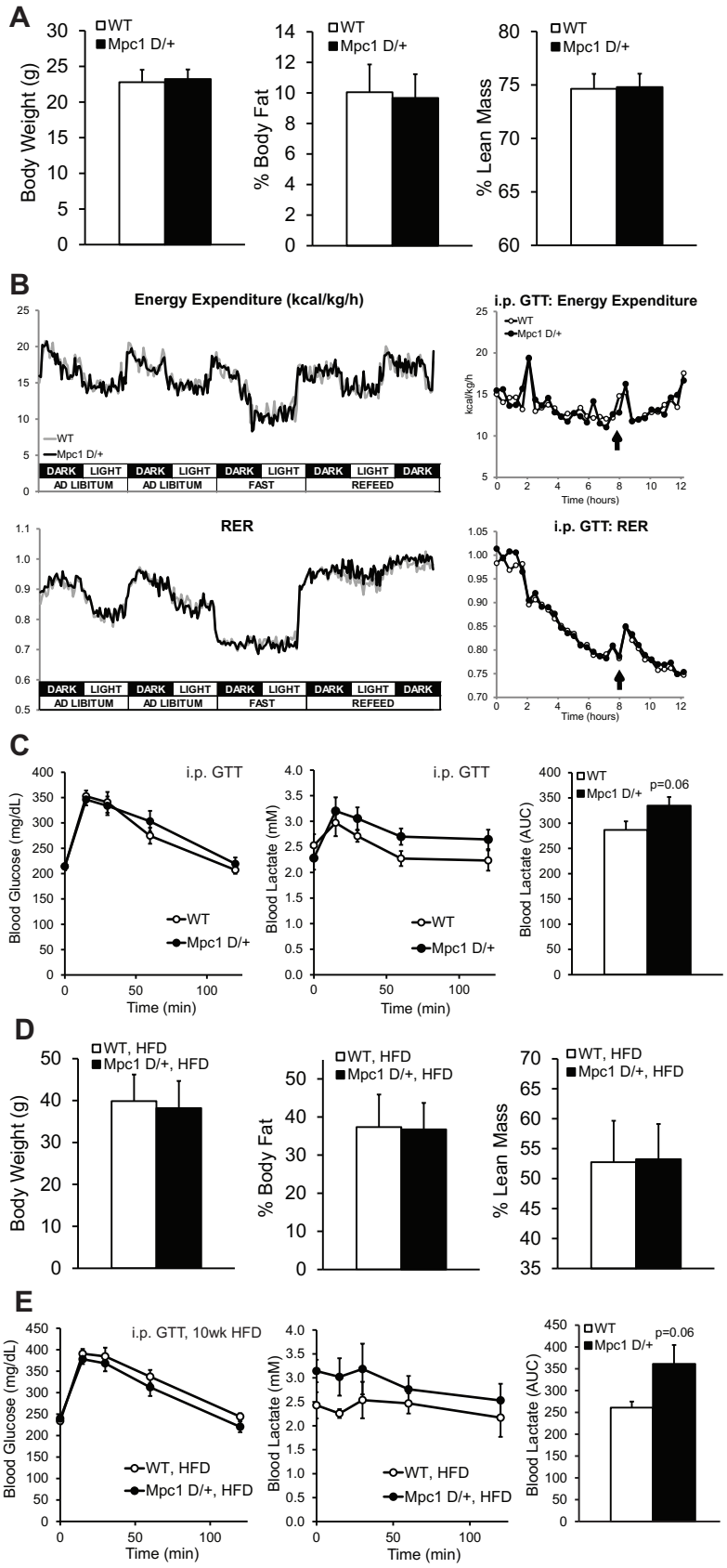

Fig. 4.S2. Mice heterozygous for Mpc1 deletion exhibit no changes in baseline body composition, energy expenditure, or glucose tolerance. (A) Body weights of 12-week old male Mpc1 D/+ mice (mean ± SD, n=13-14). Body composition (% body fat and % lean mass) of Mpc1 D/+ mice as determined by Echo-MRI. (B) No changes in energy expenditure or respiratory exchange ratio (RER) in Mpc1 D/+ males housed in metabolic cages during ad libitum feeding, a 24-hour fast, and re-feeding. There were no differences in food consumption, water intake, or ambulation at any point during the study (data not shown). (B, right panels) Mice housed in metabolic cages were subjected to an intraperitoneal (i.p.) glucose tolerance test (2g/kg body weight) after a 6-hour fast (initiated 2h into the light cycle). The arrow indicates time of glucose injection. Both Mpc1 D/+ mice and WT littermates responded similarly to glucose administration with an increase in energy expenditure and RER of similar magnitude and duration (n=11-12). (C) Blood glucose and lactate were measured during an i.p. glucose tolerance test administered exactly as the one performed in the metabolic cages. Mpc1 D/+ mice demonstrate a slight but not significant elevation of blood lactate in response to the glucose tolerance test (n=13). (D) Mpc1 D/+ mice were subjected to a 12 week high-fat diet starting from 6 weeks of age. Body weight and body composition determined by Echo-MRI (mean ± SD, n=15-17). (E) At 10 weeks on the high-fat diet, mice were subjected to an i.p. glucose tolerance test (0.75g/kg body weight). Mpc1 D/+ mice on a high-fat diet were more prone to elevated blood lactate during a glucose challenge than littermate controls.

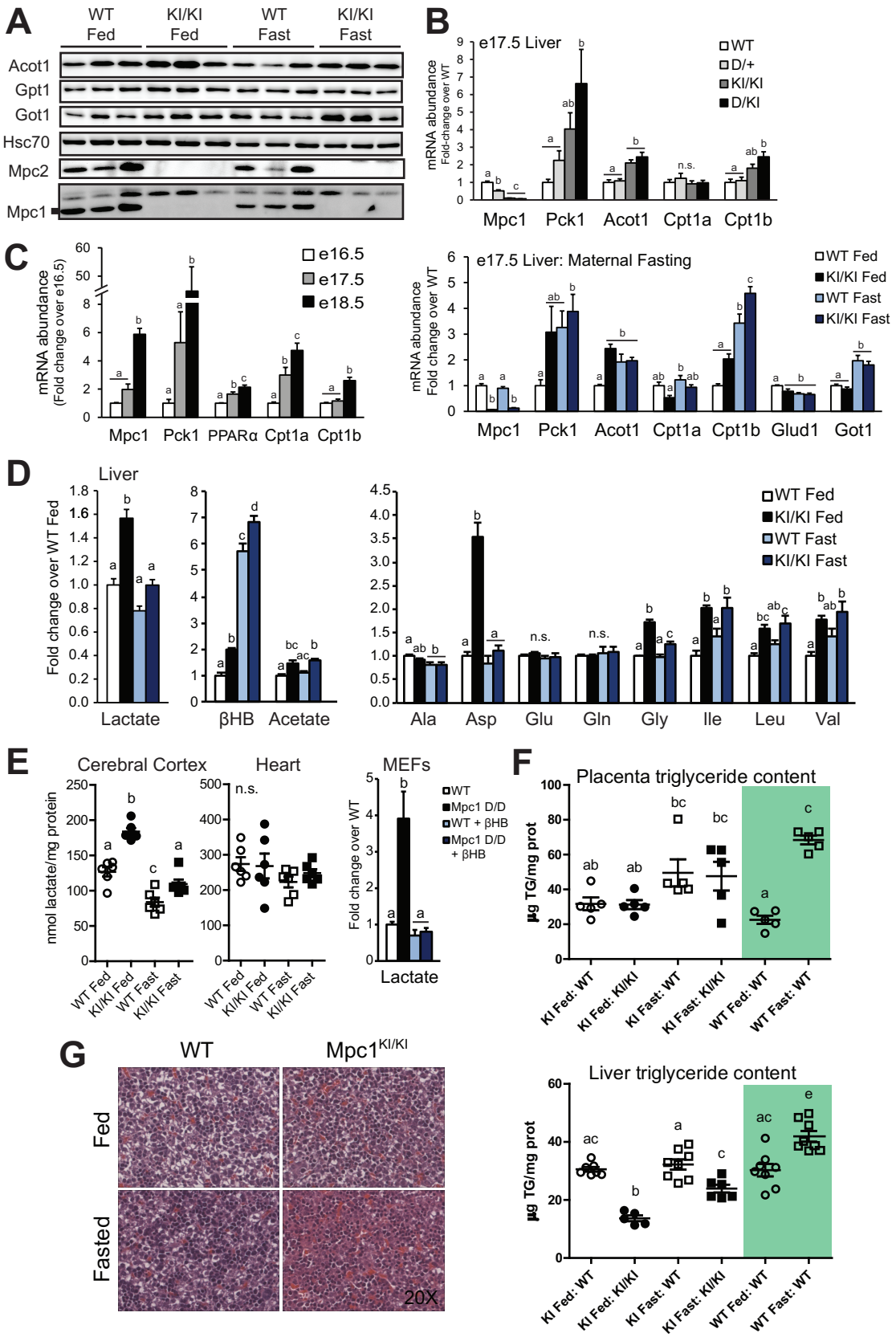

Fig. 4.2. Maternal fasting ameliorates fetal metabolic derangements in Mpc1 mutants.

Fig. 4.2. Maternal fasting ameliorates fetal metabolic derangements in Mpc1 mutants.

(A) Immunoblotting for MPC components in e17.5 fetal liver from fed or fasted MpcKI/+ dams. (B) Transcriptional regulation in e17.5 fetal liver across an allelic series of Mpc1-deficiency and in WT or KI/KI fetal liver in response to 24h fasting of Mpc1KI/+ dams, determined by qRT-PCR (mean ± SEM, n=5-8). (C) mRNA abundance of fasting-regulated genes in fetal liver during late gestation from e16.5-e18.5 (mean ± SEM, n=6).
(D) Steady-state metabolite abundances from e17.5 fetal liver, determined by 1H-NMR. Normalized to protein content and shown relative to WT fed (mean ± SEM, n=6).
(E) Lactate concentrations from fetal brain and heart measured enzymatically (mean ± SEM, n=6) and intracellular lactate concentrations from Mpc1 deletion (D/D) mouse embryonic fibroblasts (MEFs) under standard culture conditions ± 1mM β-hydroxybutyrate (βHB) for 24h, determined by 1H-NMR (mean ± SEM, n=3). (F) Triglyceride content of placenta and liver at e17.5, determined enzymatically (mean ± SEM, n=5-8). Data from WT fetuses of WT dams are shaded green. (G) Hematoxylin & eosin staining of e17.5 fetal liver of WT and KI/KI littermates from fed or 24h fasted Mpc1 KI/+ dams. Statistically significant differences ($p<0.05$) for pairwise comparisons after ANOVA indicated by letters.

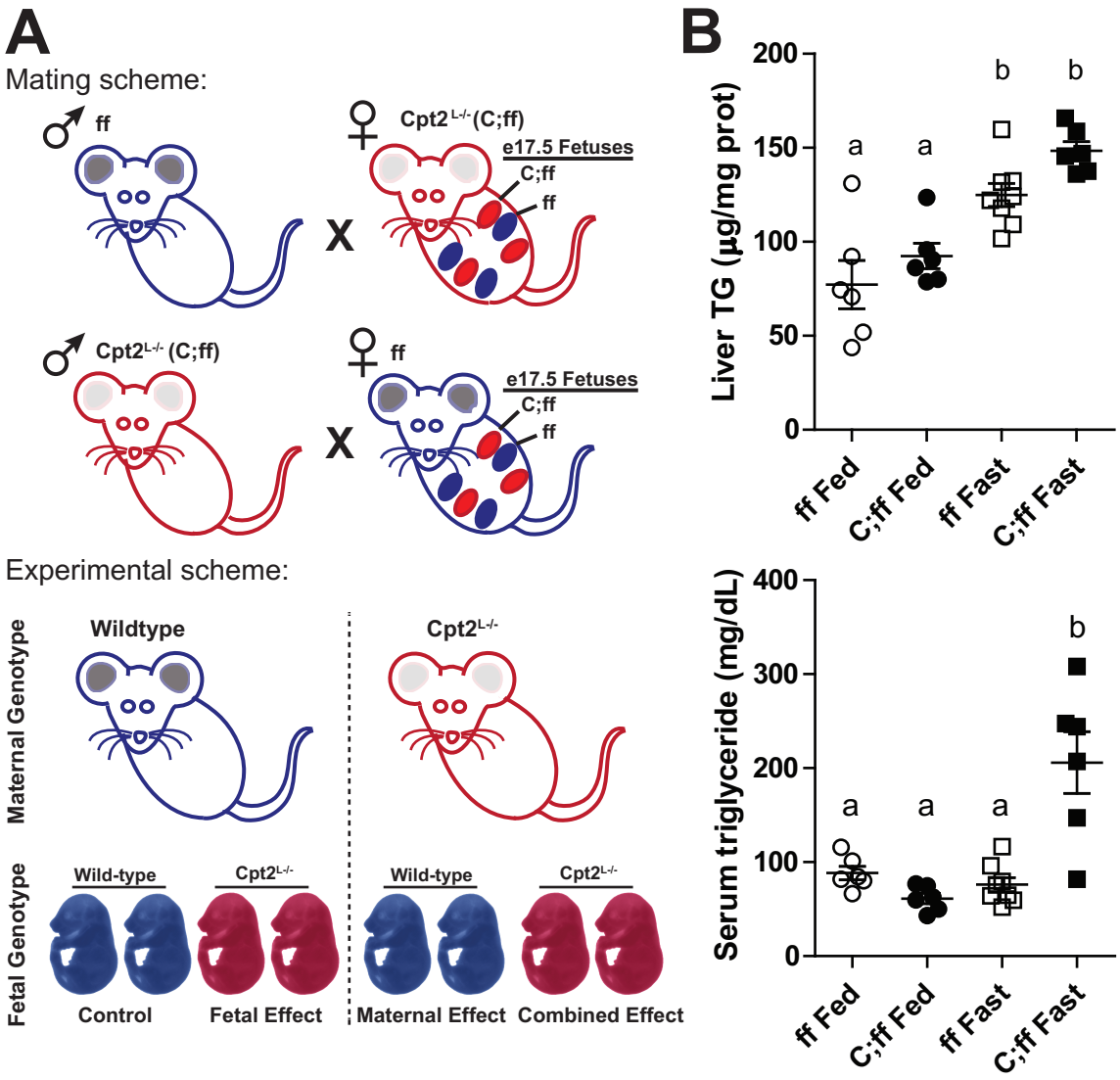

Fig. 4.S3. Liver-specific defect in fatty acid oxidation as a model of impaired maternal fasting metabolism.

(A) Schematic of breeding scheme for generation of fetuses with liver-specific deletion of carnitine palmitoyltransferase 2 (Cpt2) [Albumin-Cre; Cpt2 ff (C;ff)] with ff controls in late-gestation litters from both ff and C;ff dams. C;ff dams were chosen as a model of impaired fasting metabolism since the inability to perform mitochondrial β-oxidation of long-chain fatty acids prevents ketogenesis during fasting. (B) Maternal liver triglyceride content and serum triglyceride levels at 17.5 dpc, fed or 24h fasted (mean ± SEM, n=6-8).

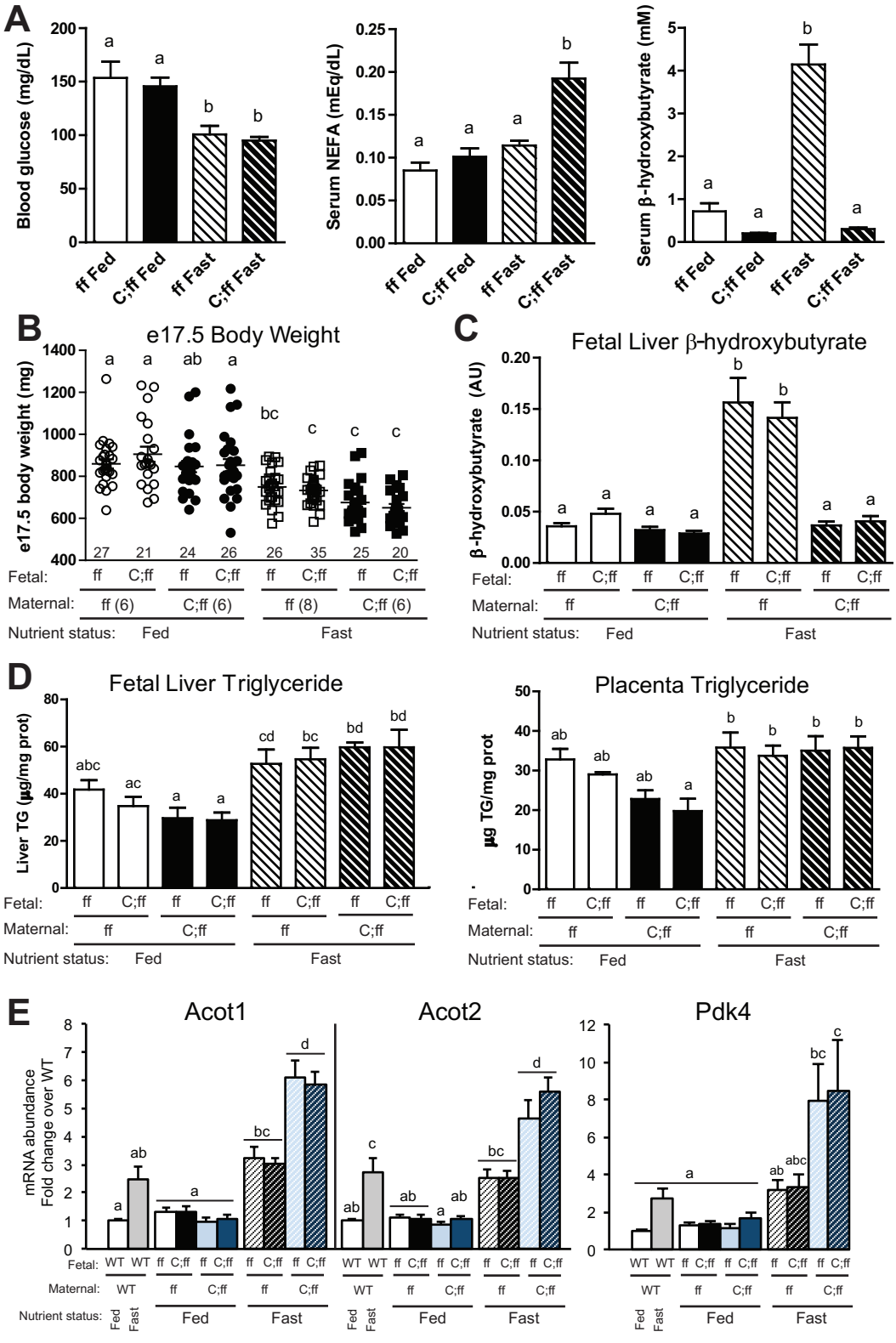

Fig. 4.3. The maternal response to fasting drives the fetal transcriptional program.

Fig. 4.3. The maternal response to fasting drives the fetal transcriptional program.

(A) Blood glucose and serum NEFA and β-hydroxybutyrate levels from fed and 24h fasted liver-specific Cpt2 knockout pregnant dams (C;ff) and ff controls at 17.5 dpc (mean ± SEM, n=6-8). (B) Fetal body weights of ff and C;ff progeny from ff and C;ff pregnancies (mean ± SEM, sample size indicated). (C) Fetal liver β-hydroxybutyrate concentrations determined by 1H-NMR (mean ± SEM, n=6). (D) Triglyceride content of placenta and liver at e17.5, determined enzymatically (mean ± SEM, n=5-6). (E) mRNA abundance of select fasting-regulated genes in e17.5 liver (mean ± SEM, n=6). Statistically significant differences ($p<0.05$) for pairwise comparisons after ANOVA indicated by letters.

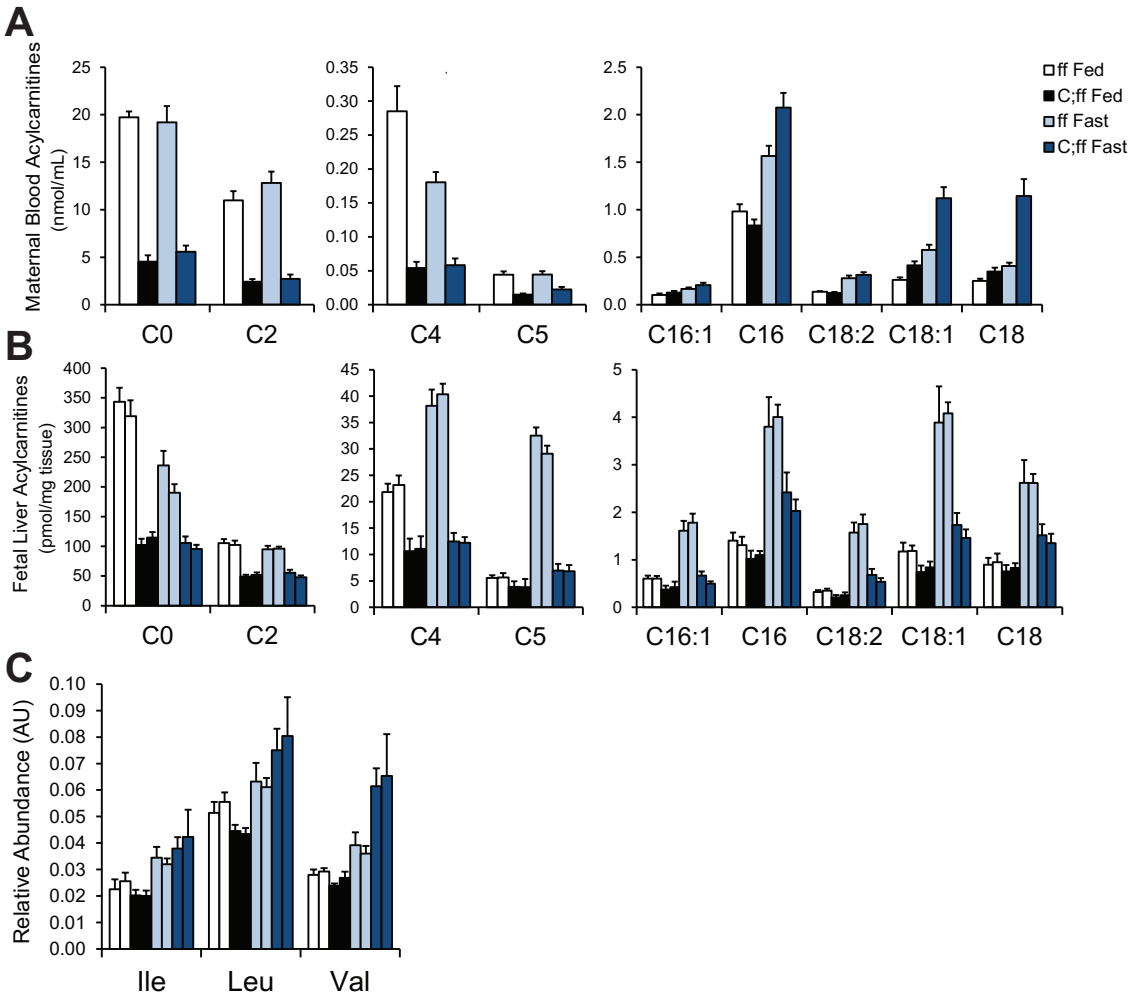

Fig. 4.4. The maternal response to fasting drives the fetal metabolic program. (A) Maternal blood acylcarnitine abundances at 17.5 dpc determined from dried blood spots after extraction, butylation, and tandem mass spectrometry (mean ± SEM, n=5-8). (B) Fetal liver acylcarnitine abundances at e17.5 (mean ± SEM, n=5). For each pair of colored bars, the left bar represents ff fetuses and the right bar represents C;ff fetuses from the maternal genotype-nutritional combinations represented in A. (C) Fetal liver branched-chain amino acid relative concentrations determined by ^{1}H-NMR (mean ± SEM, n=6).

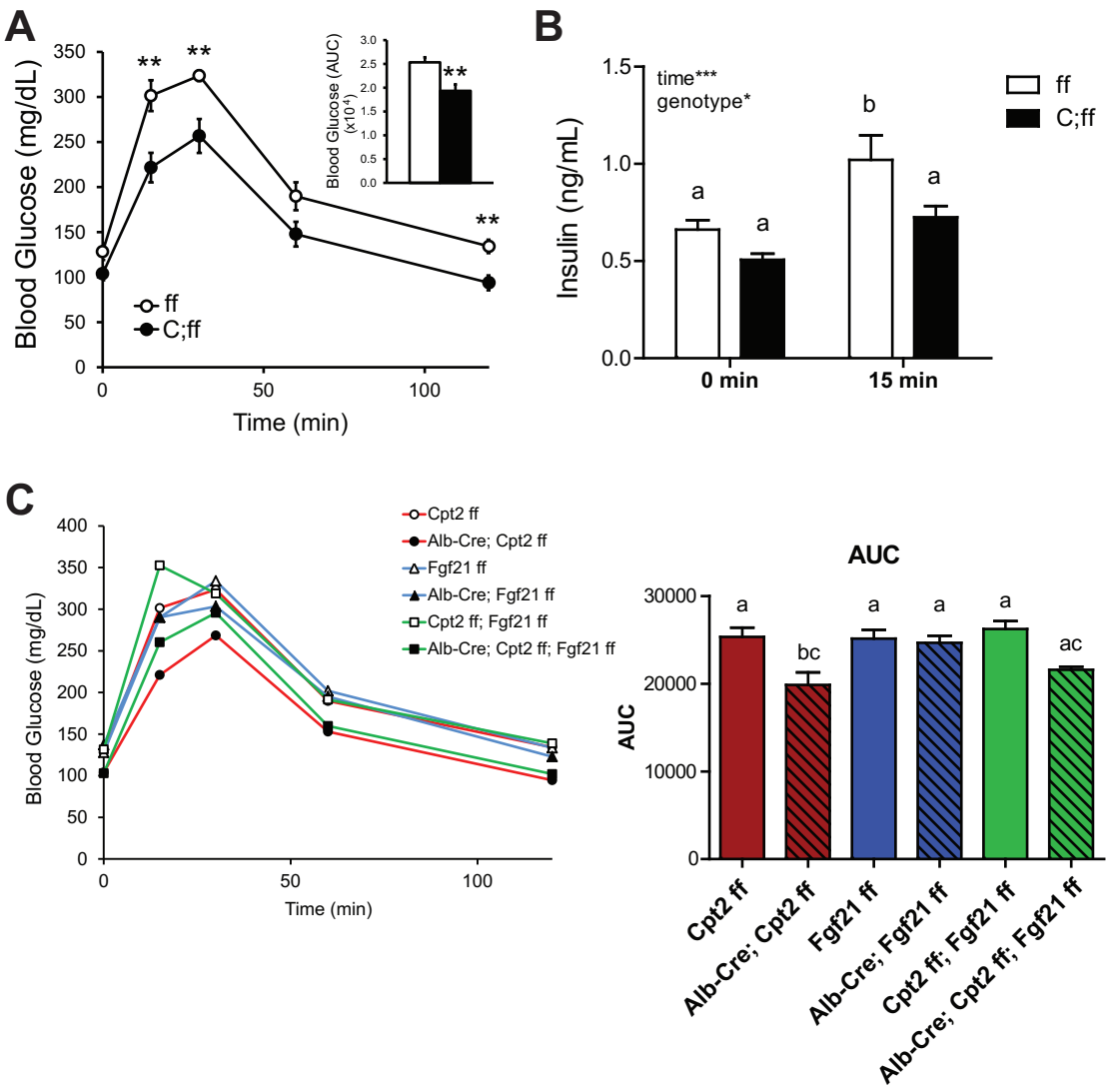

Fig. 4.5. Loss of hepatic fatty acid oxidation improves maternal glucose tolerance.

(A) Cpt2L-/- (C;ff) dams and ff controls were subjected to an oral glucose tolerance test (2g/kg) at 17.5 dpc after a 6h fast (mean ± SEM, n=7,9).

(B) Serum insulin concentrations at baseline and 15 minutes after glucose gavage, determined by ELISA (mean ± SEM, n=7,8).

(C) Oral glucose tolerance test on liver-specific Cpt2 KO, liver-specific Fgf21 KO, and Cpt2;Fgf21 double-knockout pregnant dams at 17.5 dpc. Area under the curve (AUC) shown at right (mean ± SEM, n=6-9).

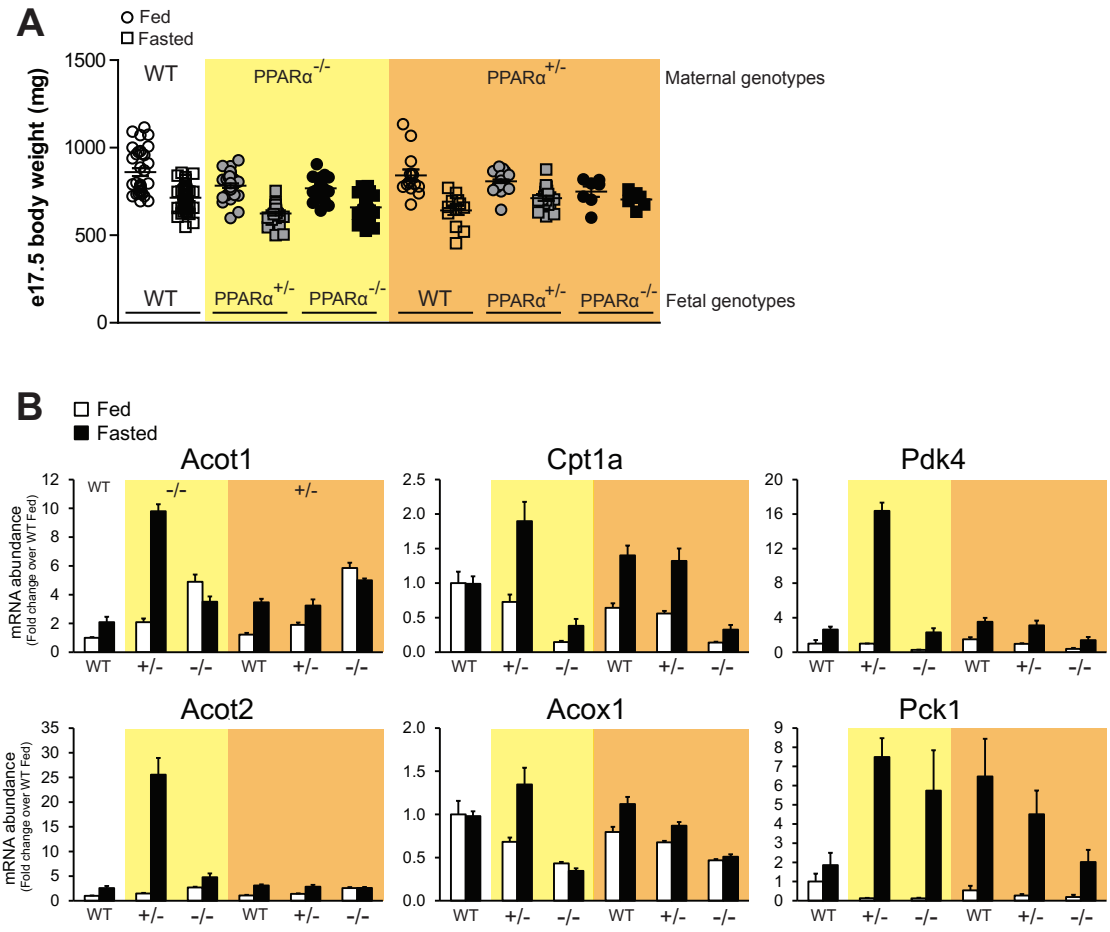

Fig. 4.6. PPARα-dependent fetal response to maternal fasting is potentiated by impaired maternal lipid metabolism.

(A) e17.5 body weights from WT dams, PPARα-/- dams carrying heterozygous or homozygous PPARα deletion litters (shaded in yellow), or all three fetal genotypes (WT, +/-, and -/-) from PPARα+/- intercrosses (shaded in orange). Circles are from fed litters and squares are from fasted litters. (B) mRNA abundance of several fasting-regulated genes in fetal liver, same genotypes as described in A. Open bars for fed samples; filled bars for fasted samples (mean ± SEM, n=6).

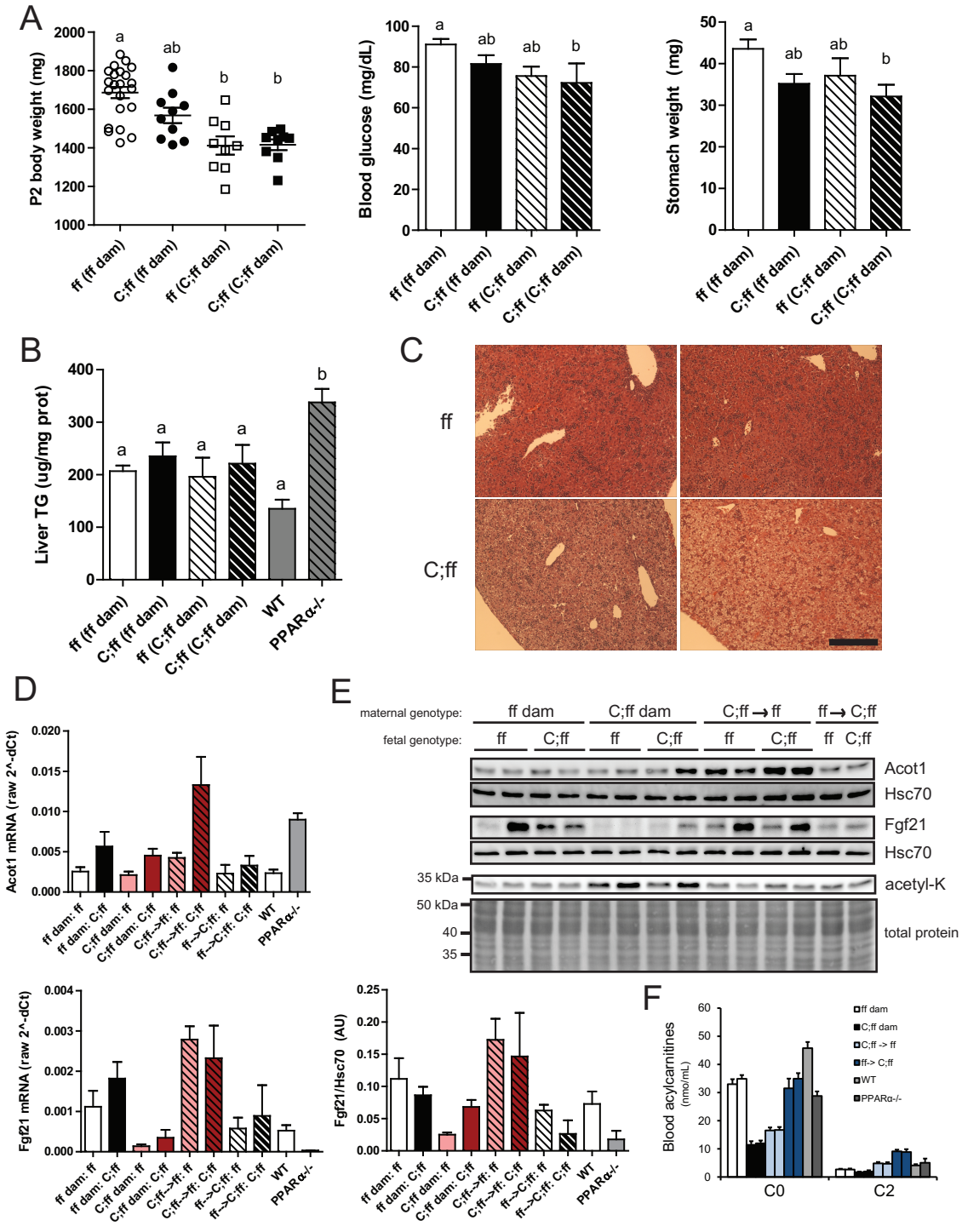

Fig. 5.1. Maternally-mediated effects of impaired liver fatty acid oxidation persist into the early postnatal period.

Fig. 5.1. Maternally-mediated effects of impaired liver fatty acid oxidation persist into the early postnatal period.

(A) Body weight, blood glucose, and stomach weight at postnatal day 2 (P2) (mean ± SEM, n=9-22).

(B) Triglyceride content of P2 liver of ff and C;ff pups from ff and C;ff dams as well as PPARα-/- pups from PPARα-/- dams (mean ± SEM, n=6).

(C) Hematoxylin & eosin staining of P2 livers from C;ff dam (scale bar is 0.2μm).

(D) Transcriptional regulation of Acot1 and Fgf21 in P2 livers from pups reared by birth mother or cross-fostered to dam of opposite genotype from P0-P2 (mean ± SEM, n=3-6).

(E) Immunoblot for Acot1, Fgf21, and acetyl-lysine (acetyl-K) in P2 livers from pups reared by birth mother or cross-fostered to dam of opposite genotype, and quantification of Fgf21 protein abundance relative to Hsc70 (mean ± SEM, n=3-4).

(F) Blood acylcarnitine concentrations from P2 pups (mean ± SEM, n=3-14). For each pair of colored bars, the left bar represents ff and the right bar represents C;ff (C0=free carnitine, C2=acetylcarnitine).

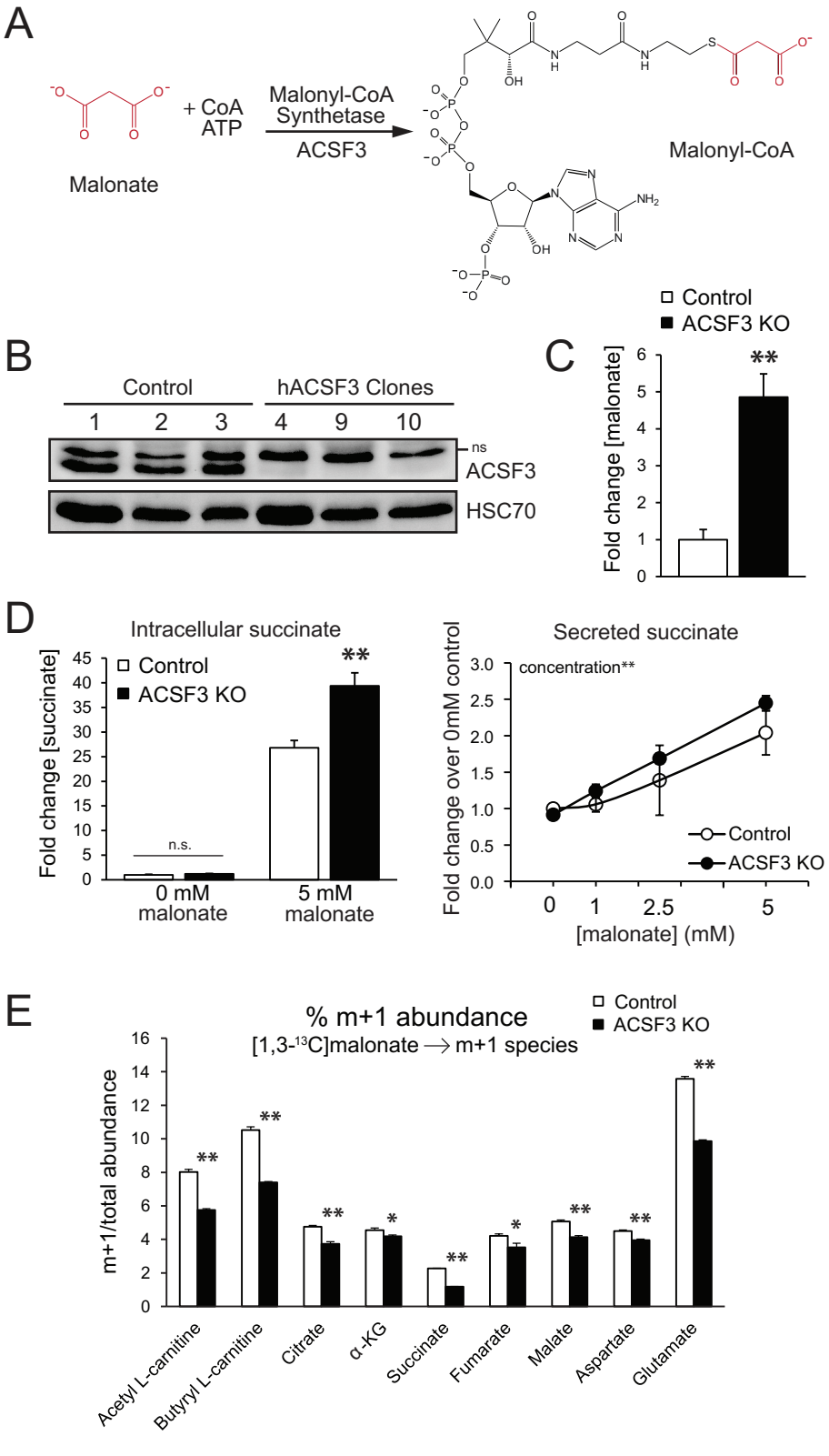

Fig. A.1. ACSF3 is a mitochondrial malonyl-CoA synthetase.

Fig. A.1. ACSF3 is a mitochondrial malonyl-CoA synthetase.
(A) The reaction catalyzed by acyl-CoA synthetase family member 3 (ACSF3), a mammalian mitochondrial malonyl-CoA synthetase.
(B) Immunoblot for ACSF3 in three control clones that were transfected with Cas9 only and three ACSF3 knockout (KO) clones. HSC70 is shown as a loading control. See Figure S1 for characterization of genomic mutations. (ns = non-specific band)
(C) Steady-state intracellular malonate and succinate (D) concentrations, in the presence or absence of 5 mM malonate for 24 hours (mean ± SEM, n=10).
(D) Succinate secretion into the culture medium upon increasing dose of malonate for 24h (mean ± SEM, n=4). Effect of concentration significant by 2-way ANOVA.
(E) [1,3-13C]malonate flux. % abundance of m+1-labeled metabolites determined by LC-MS/MS that are significantly down-regulated in ACSF3 KO cells labeled with 2.5 mM 1,3-13C-malonate for 4 hours (mean ± SEM, n=6, α-KG = α-ketoglutarate). *$p<0.05$, **$p<0.001$

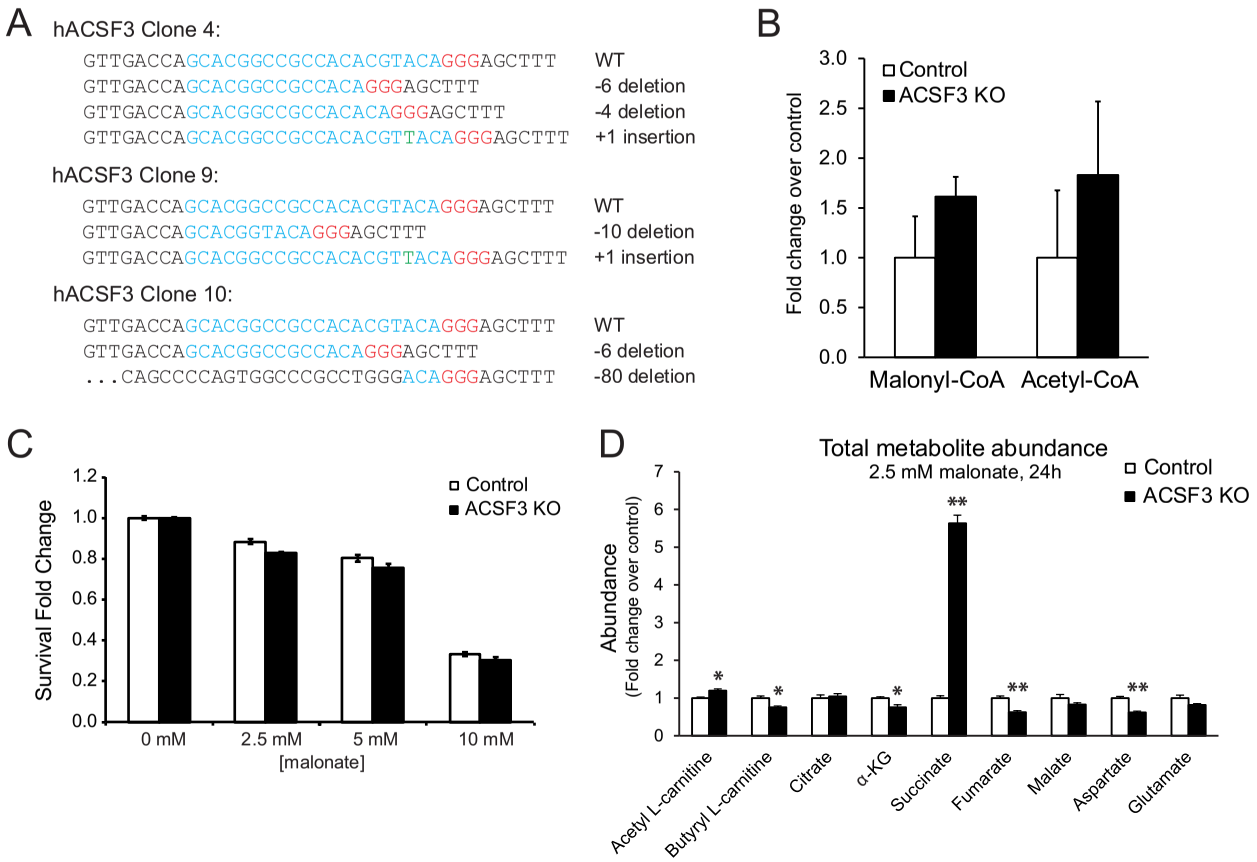

Fig. A.S1. Generation of ACSF3-deficient cells by CRISPR/Cas9 genome editing.

(A) Genomic mutations identified in ACSF3 in three knockout (KO) HEK293T clones. The guide RNA target site is shown in blue, with the protospacer-adjacent motif highlighted in red. Error-prone non-homologous end-joining repair has generated two to three different mutations per clone that result in loss of ACSF3 protein as shown in Figure 1B. Clone 4 was used in all experiments, and clones 9 and 10 were included in experiments conducted on three different clones. (B) Steady-state malonyl-CoA and acetyl-CoA concentrations determined by CE-MS after 24h 5mM malonate exposure followed by 6h washout with malonate-free medium to relieve SDH inhibition (mean ± SEM, n=3). (C) Cell survival of ACSF3 KO and control cells treated with 0, 2.5, 5, or 10 mM malonate for 72 hours (n=6). (D) Total metabolite abundance determined by LC-MS/MS from [1,3-13C]malonate labeling experiment in Figure 1E (mean ± SEM, n=6, *$p<0.05$, **$p<0.001$, α-KG = α-ketoglutarate).

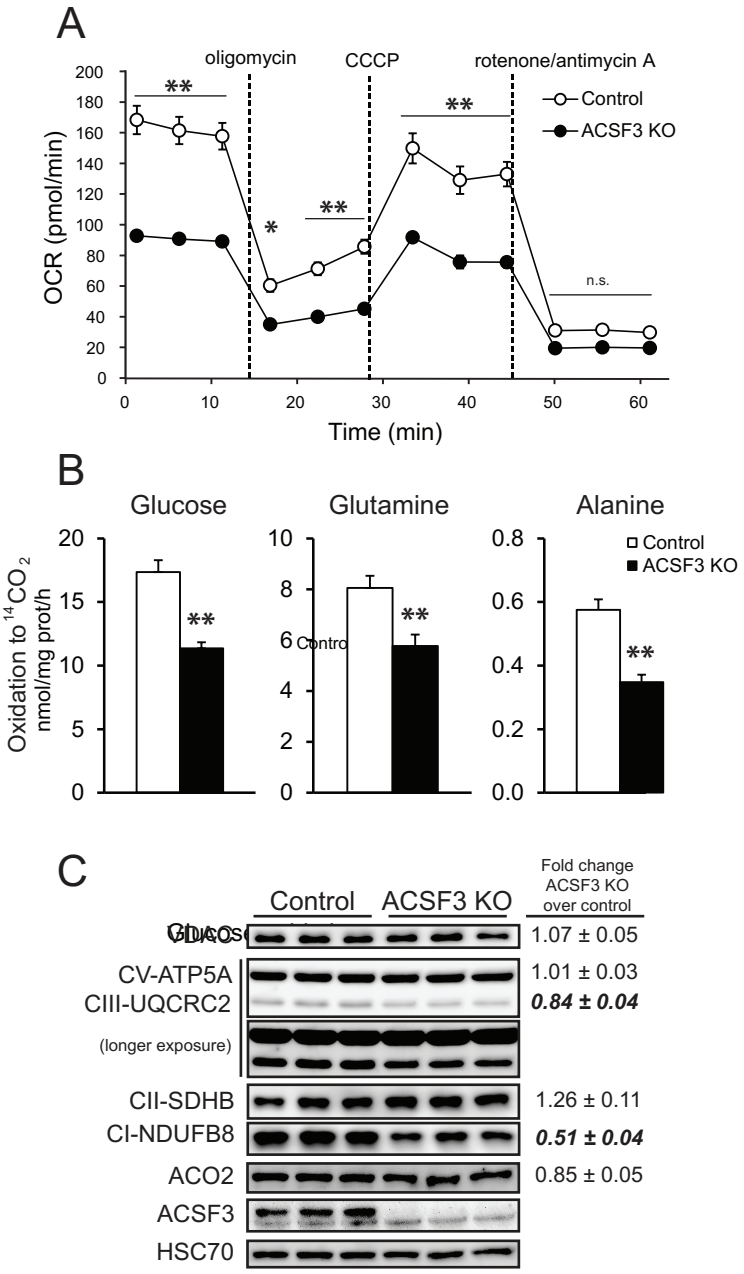

Fig. A.2. ACSF3 regulates mitochondrial metabolic efficiency.

(A) Oxygen consumption rate of ACSF3 KO cells in the presence of 10 mM glucose, 2 mM glutamine, and 1 mM pyruvate upon sequential administration of the specified mitochondrial inhibitors, normalized to cell number (mean ± SEM, n=5, representative of three independent experiments).

(B) Oxidation of [U-^{14}C]D-glucose, [U-^{14}C]L-glutamine, and [U-^{14}C]L-alanine to $^{14}CO_2$ in ACSF3 KO cells (mean ± SEM, n=6).

(C) Immunoblot of several mitochondrial proteins. VDAC (voltage-dependent anion channel 1) as outer mitochondrial membrane marker; ATP5A component of ATP synthase, Complex III subunit 2 (UQCRC2), SDHB subunit of Complex II, and NDUFB8 subunit of Complex I of the inner mitochondrial membrane; aconitase (ACO2) and ACSF3 of the mitochondrial matrix; and HSC70 as cytoplasmic loading control. Protein abundance was normalized to HSC70, and values shown are fold change protein abundance in ACSF3 KO cells over control cells (mean ± SEM, n=5, p<0.05 are in bold). *p<0.05, **p<0.001

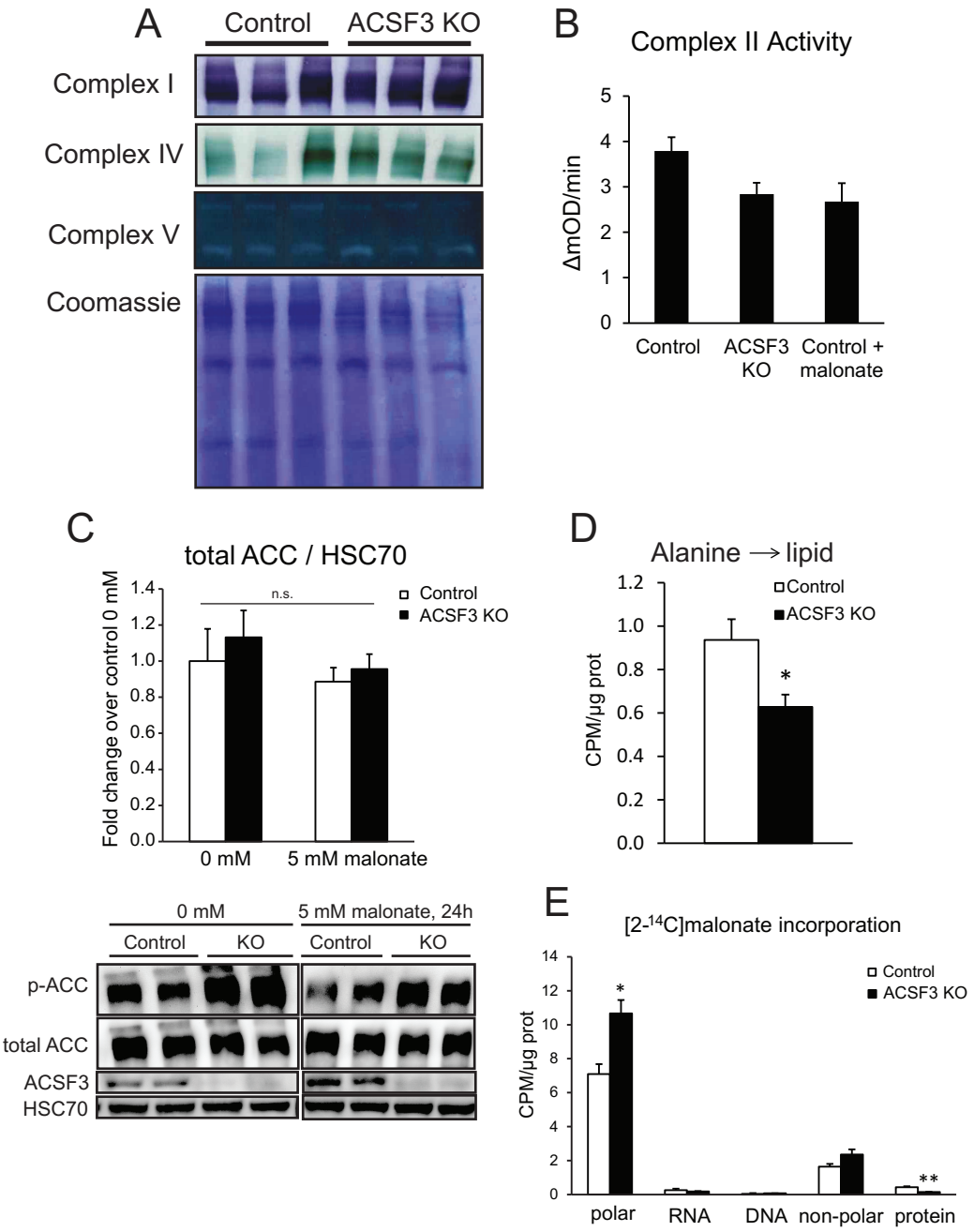

Fig. A.S2. ACSF3 promotes mitochondrial metabolic efficiency.
(A) Native gel electrophoresis and in-gel assays of respiratory complex function for Complex I, IV, and V. Coomassie shown as loading control (n=3 clones of each genotype, representative of three independent experiments) (B) Complex II activity by immunocapture and colorimetric assay (mean ± SEM, n=11-14 from three independent experiments). (C) Total ACC protein abundance is unchanged in ACSF3 KO cells (mean +/- SEM, n=6). Shown also is ACC phosphorylation and total ACC in ACSF3 KO and control cells as in Figure 3 with another n=2. Images were cropped from the same blot and exposure. (D) [U-^{14}C]alanine incorporation into the total lipid fraction (mean ± SEM, n=6, *p<0.05). (E) [2-^{14}C]malonate incorporation into different classes of biomolecules by biphasic extraction after 4h incubation with 0.2 µCi at 0.1 mM malonate (mean ± SEM, n=3, representative of two independent experiments, *p<0.05, **p<0.01).

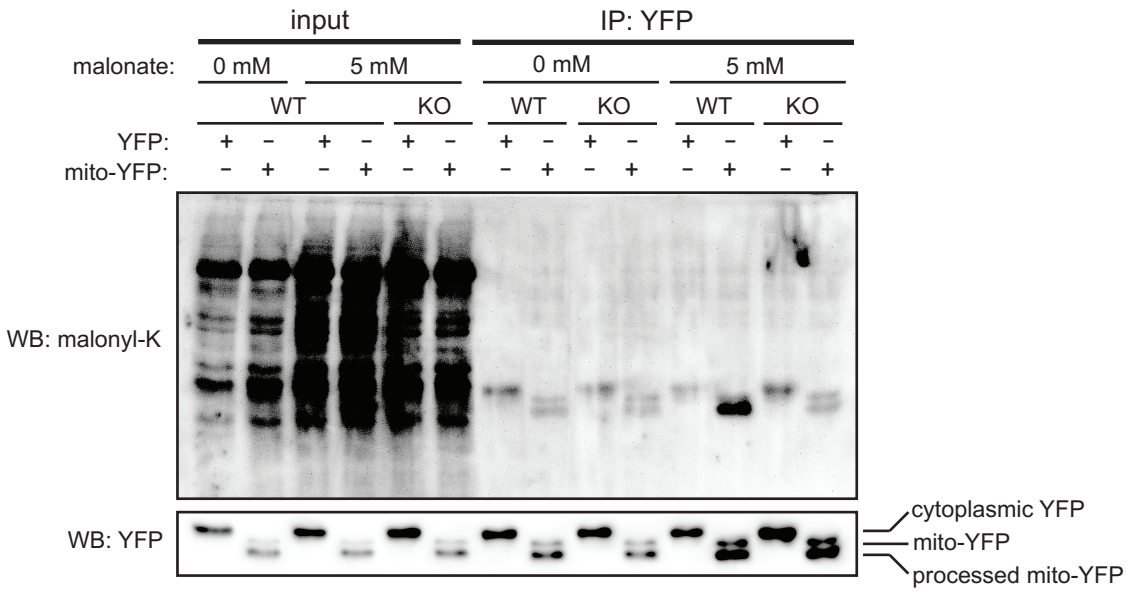

Fig. A.S3. ACSF3 is required for malonylation of a heterologous protein.
Immunoprecipitation of YFP and immunoblotting for malonylated lysine residues in ACSF3 KO and control cells transiently transfected with YFP or a mitochondrially-targeted YFP (mito-YFP) in the presence or absence of 5 mM malonate for 24h. The higher molecular weight band in the mito-YFP lanes is YFP with the mitochondrial targeting sequence intact before mitochondrial import and serves as an additional control.

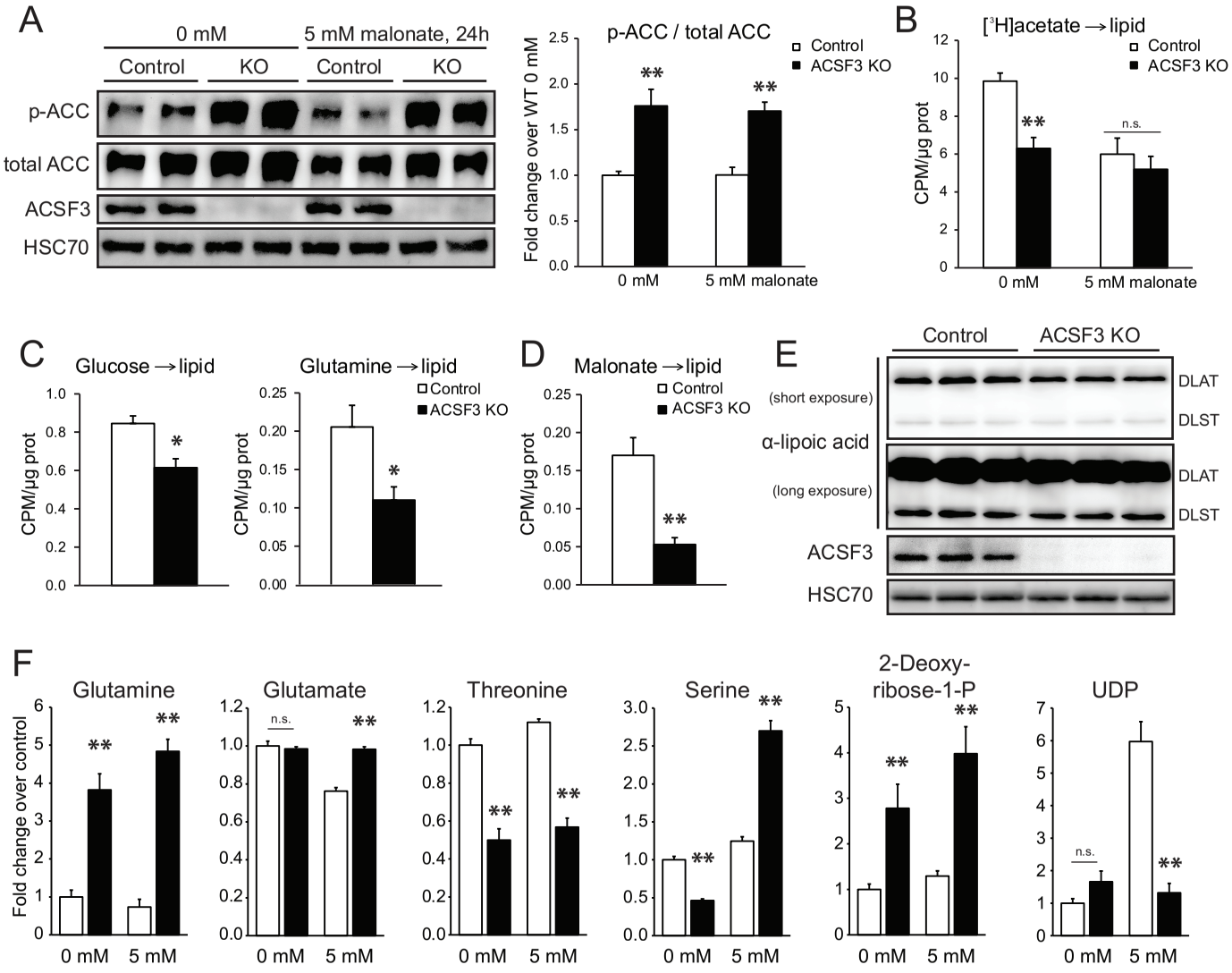

Fig. A.3. Metabolic alterations in ACSF3-deficient cells.

Fig. A.3. Metabolic alterations in ACSF3-deficient cells.
(A) Acetyl-CoA carboxylase (ACC) phosphorylation (Ser79) in ACSF3 KO and control cells in the presence or absence of 5 mM malonate for 24 hours (mean ± SEM, n=6 from two independent experiments, **p<0.01 for genotypic effect, with no effect of malonate treatment, determined by posttest after two-way ANOVA). See also Fig. A.S2.
(B) [^{3}H]acetate incorporation into total cellular lipids in the presence or absence of malonate (5mM) (mean ± SEM, n=6, representative of two independent experiments, **p<0.01 for genotypic effect, malonate treatment effect p=0.001 with significant interaction (p<0.05), determined by two-way ANOVA). (CPM = counts per minute)
(C) [U-^{14}C]glucose and [U-^{14}C]glutamine incorporation into the total lipid fraction (mean ± SEM, n=6, *p<0.05).
(D) [2-^{14}C]malonate into total cellular lipids (n=12, pooled from two independent experiments).
(E) Immunoblotting for lipoic acid-modified proteins, DLAT (E2 of pyruvate dehydrogenase) and DLST (E2 of α-ketoglutarate dehydrogenase), with HSC70 as loading control.
(F) Select metabolite levels in the presence or absence of 5 mM malonate for 24 hours (mean ± SEM, n=10, **p<0.01 by posttest after two-way ANOVA). More metabolites and two-way ANOVA results in Table A.S1.

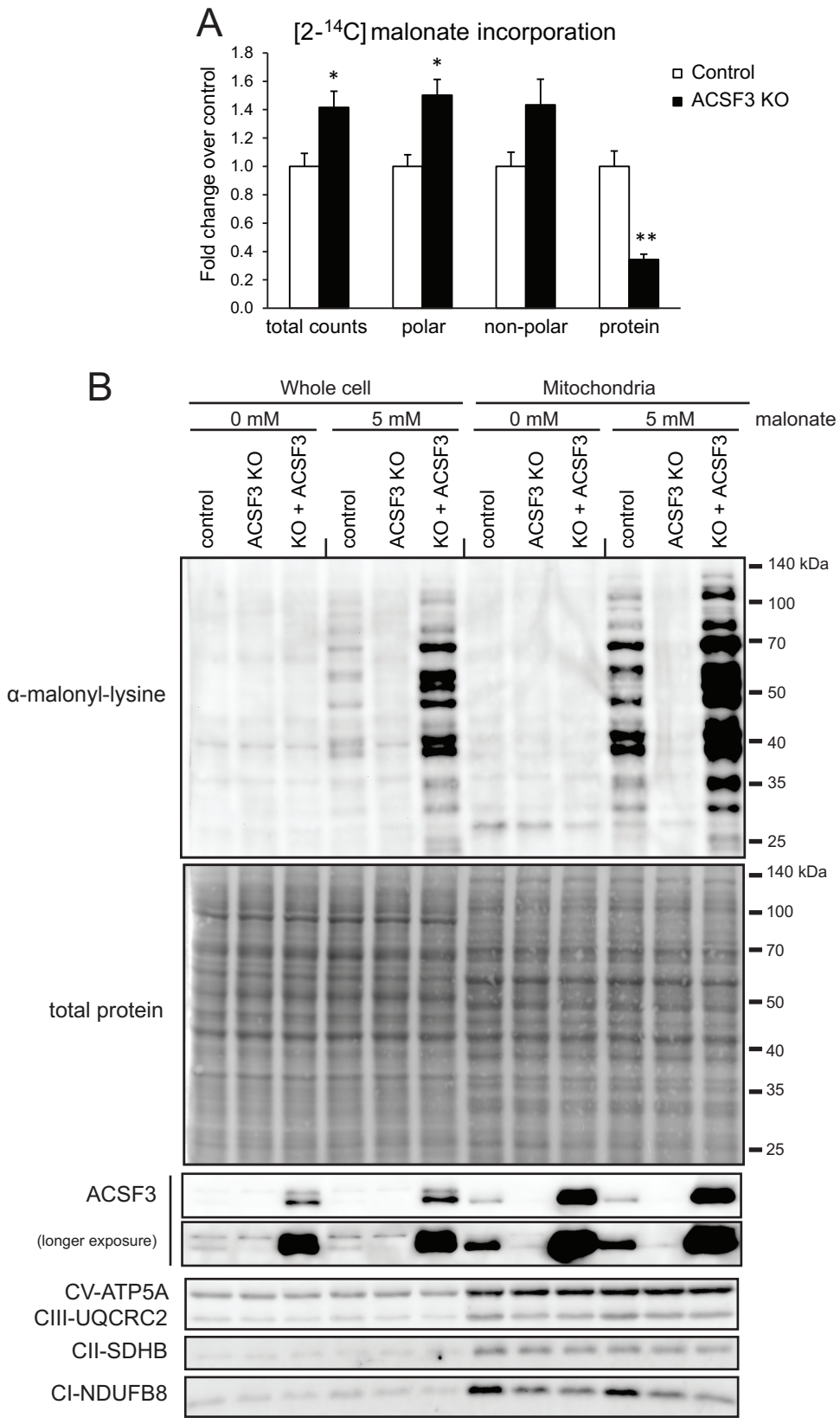

Fig. A.4. ACSF3 is required for mitochondrial protein malonylation.

Fig. A.4. ACSF3 is required for mitochondrial protein malonylation.
(A) [2-^{14}C]malonate incorporation into different classes of biomolecules by biphasic extraction after 4h incubation with 0.2 μCi at 0.1 mM malonate (mean ± SEM, n=3, representative of two independent experiments, *p<0.05, **p<0.01).
See also Fig. A.S2C.
(B) Immunoblotting for malonylated lysine residues in whole cell and mitochondrial extracts of cells in the presence or absence of 5 mM malonate for 24h. ACSF3 KO cells were transiently transfected with a human ACSF3 expression vector, and control cells were transfected with a mitochondrially-targeted YFP. Total protein staining by amido black shown as loading control. See also Fig. A.S3.

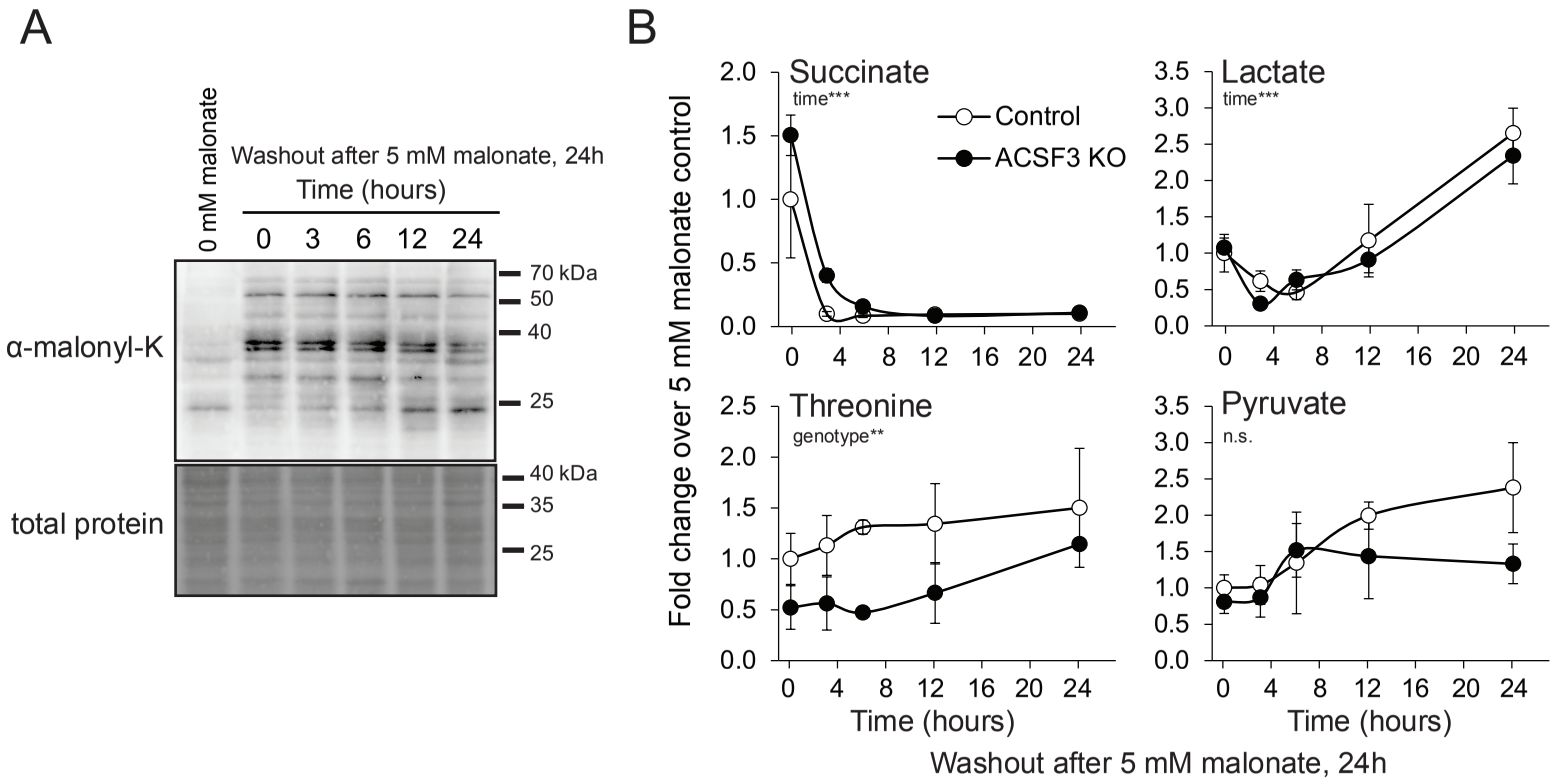

Fig. A.5. Mitochondrial protein malonylation persists following malonate washout.
(A) Immunoblotting for malonylated lysine residues in mitochondrial extracts of cells treated with 5 mM malonate for 24h before switching to malonate-free media for the times indicated (0-24h after malonate washout). See also Fig. A.S4.
(B) Steady-state concentrations of cellular succinate, lactate, pyruvate, and threonine determined by 1H-NMR (mean ± SEM, n=3) after 24h 5 mM malonate followed by incubation in malonate-free media for the times indicated. Statistical significance for time and genotype effects determined by two-way ANOVA, **p<0.01, ***p<0.001.

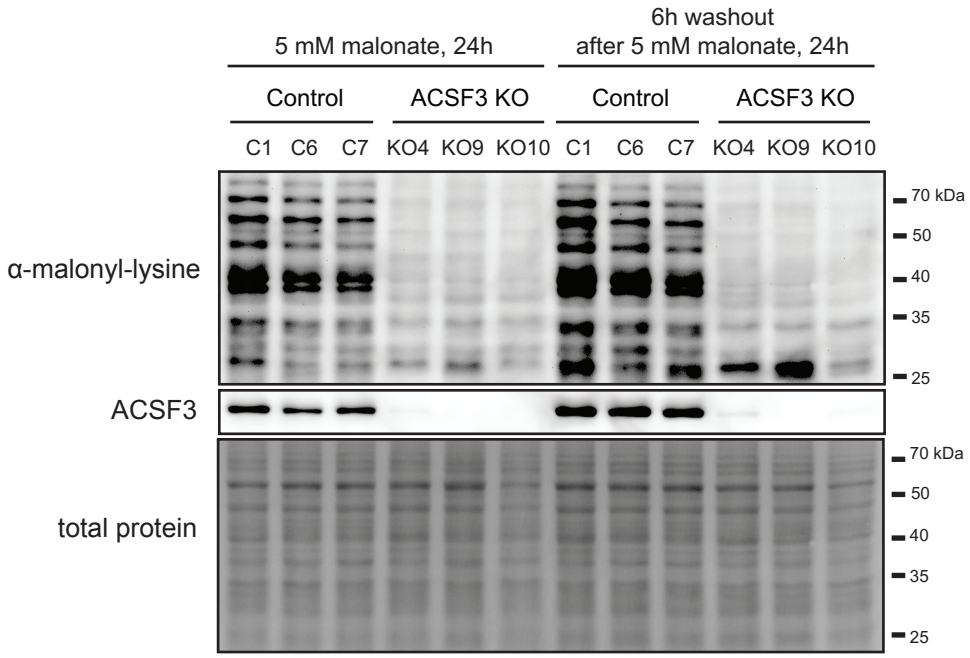

Fig. A.S4. Mitochondrial protein malonylation persists in the absence of malonate.

Mitochondrial protein malonylation in three independent ACSF3 KO and control clones after 6h washout in malonate-free culture medium, following 24h incubation with 5 mM malonate.

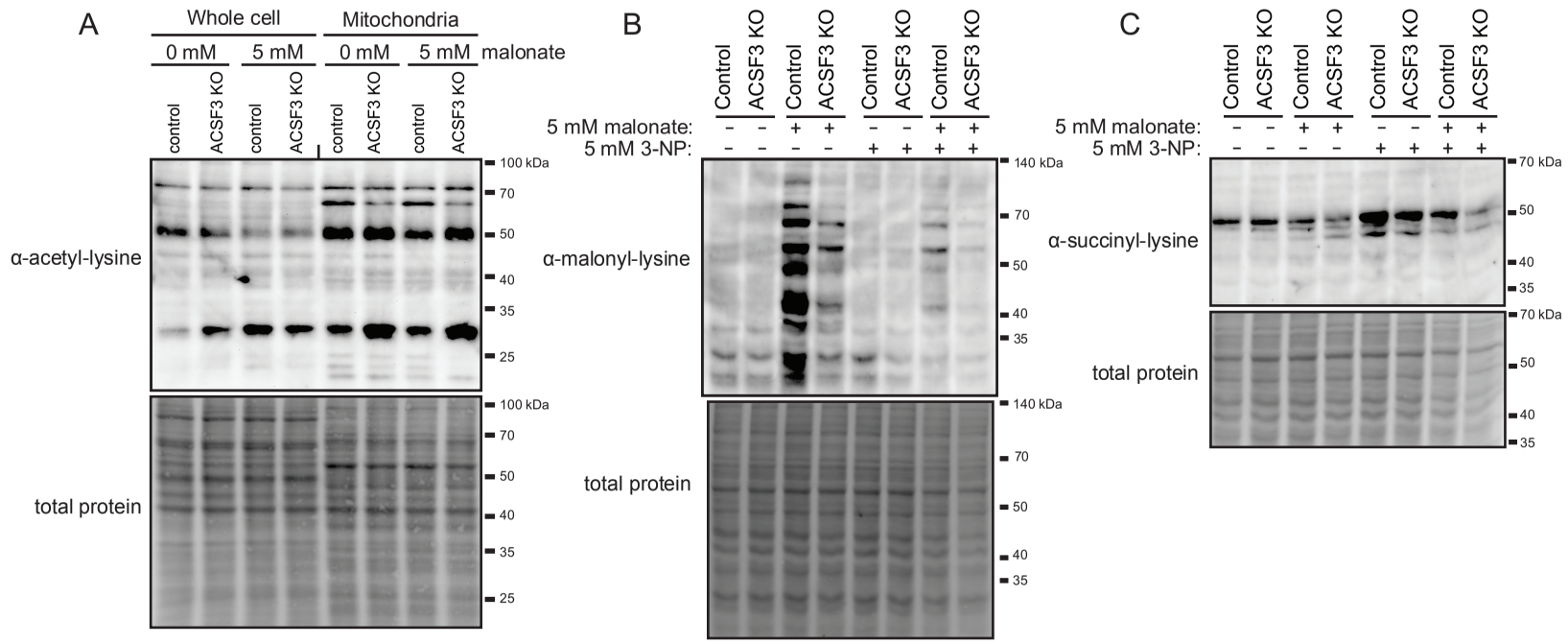

Fig. A.6. ACSF3 does not affect mitochondrial protein acetylation or succinylation.
(A) Immunoblotting for acetylated lysine residues in whole cell and mitochondrial extracts of cells in the presence or absence of 5 mM malonate for 24h. Total protein staining by amido black shown as loading control.
(B-C) Immunoblotting for malonylated (B) and succinylated (C) lysine residues in mitochondrial extracts of ACSF3 KO and control cells treated with 5 mM malonate, 5 mM 3-nitropropanoate (3-NP, SDH suicide inhibitor), or both for 24h. See also Fig. A.S5.

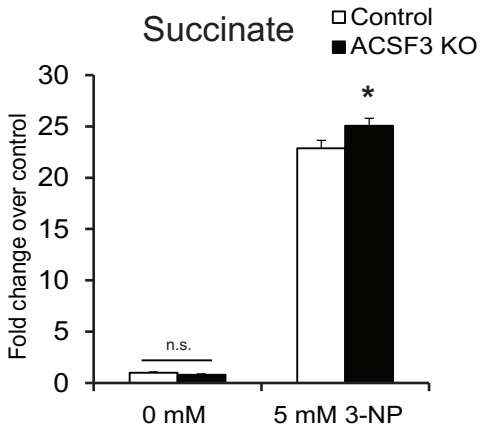

Fig. A.S5. SDH-inhibition by 3-nitropropanoate increases cellular succinate levels.

Steady-state succinate concentrations in cells treated with 5 mM 3-nitropropanoate (3-NP, a suicide inhibitor of SDH) for 24h, determined by ^{1}H-NMR (mean ± SEM, n=3, *p<0.05).

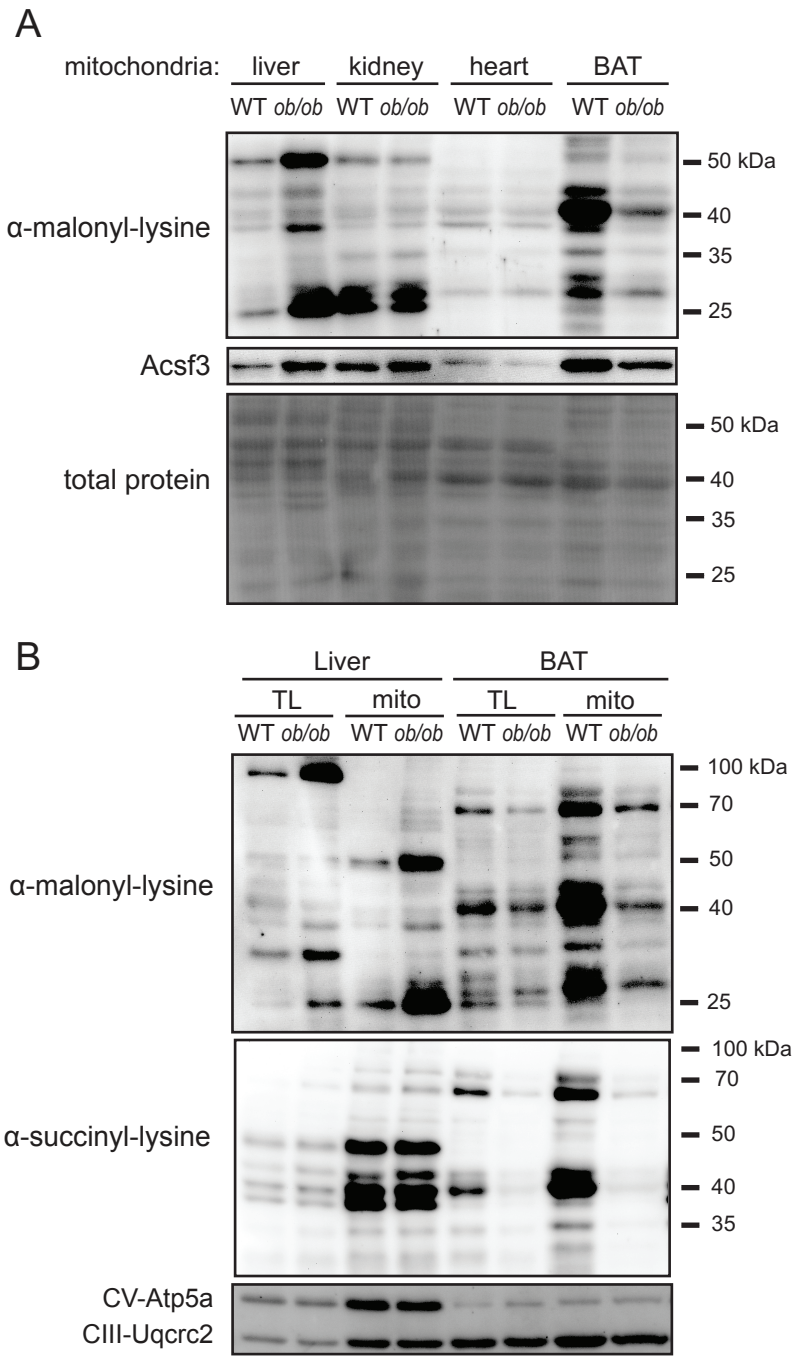

Fig. A.7. Tissue-specific differences in mitochondrial protein malonylation reflect Acsf3 abundance.

(A) Immunoblot of malonylated lysine residues in mitochondrial extracts from liver, kidney, heart, and brown adipose tissue (BAT) of wild-type (WT) and ob/ob mice. Total protein staining by amido black shown as loading control.

(B) Immunoblot of malonylated and succinylated lysine residues in mitochondrial extracts (mito) and total lysates (TL) of liver and BAT in WT and ob/ob mice. Complex V Atp5a subunit and Complex III component Uqcrc2 shown as loading control. Representative of n=3.

Caitlyn E. Bowman, B.S.

Curriculum Vitae

Personal Data

Department of Biological Chemistry
Rangos 480.15
855 N. Wolfe Street
Baltimore, MD 21205
cbowma14@jhmi.edu

Education and Training

Doctoral	
Ph.D. candidate	Johns Hopkins University School of Medicine Biochemistry, Cellular, and Molecular Biology Graduate Program Laboratory of Michael J. Wolfgang, Ph.D. Dept. of Biological Chemistry
Undergraduate	
2012	B.S., Biology with secondary emphasis in Psychology *Summa cum laude* Juniata College (Huntingdon, PA)

Publications

Original Research

1. Ellis JM, **Bowman CE**, and Wolfgang MJ. Metabolic and tissue-specific regulation of acyl-CoA metabolism. ***PLoS One*** (2015) *10*, e0116587.

2. Lee CF, Lo YC, Cheng CH, Furtmuller GJ, Oh B, Andrade-Oliveira V, Thomas AG, **Bowman CE**, Slusher BS, Wolfgang MJ, Brandacher G, and Powell JD. Preventing allograft rejection by targeting immune metabolism. ***Cell Reports*** (2015) *13*, 760-770.

3. Mitchell CJ, Getnet D, Kim MS, Manda SS, Kumar P, Huang TC, Pinto SM, Nirujogi RS, Iwasaki M, Shaw PG, Wu X, Zhong J, Chaerkady R, Marimuthu A, Muthusamy B, Sahasrabuddhe NA, Raju R, **Bowman C**, Danilova L, Cutler J, Kelkar DS, Drake CG, Prasad TS, Marchionni L, Murakami PN, Scott AF, Shi L, Thierry-Mieg J, Thierry-Mieg D, Irizarry R, Cope L, Ishihama Y, Wang C, Gowda H, and Pandey A. A multi-omic analysis of human naive CD4+ T cells. ***BMC Syst Biol*** (2015) *9*, 75.

4. Lei X, Rodriguez S, Petersen PS, Seldin MM, **Bowman CE**, Wolfgang MJ, and Wong GW. Loss of CTRP5 improves insulin action and hepatic steatosis. ***Am J Physiol Endocrinol Metab*** (2016) *310*, E1036-1052.

5. **Bowman CE**, Zhao L, Hartung T, and Wolfgang MJ. Requirement for the mitochondrial pyruvate carrier in mammalian development revealed by a hypomorphic allelic series. ***Mol Cell Biol*** (2016) *36*, 2089-2104.

6. Jernberg JN, **Bowman CE**, Wolfgang MJ, and Scafidi S. Developmental regulation and localization of carnitine palmitoyltransferases (CPTs) in rat brain. ***J Neurochem*** (2017) *142*, 407-419.

7. **Bowman CE**, Rodriguez S, Selen Alpergin ES, Acoba MG, Zhao L, Hartung T, Claypool SM, Watkins PA, and Wolfgang MJ. The mammalian malonyl-CoA synthetase ACSF3 is required for mitochondrial protein malonylation and metabolic efficiency. ***Cell Chem Biol*** (2017) *24*, 673-684 e674.

8. Kim SP, Li Z, Zoch ML, Frey JL, **Bowman CE**, Kushwaha P, Ryan KA, Goh BC, Scafidi S, Pickett JE, Faugere MC, Kershaw EE, Thorek DLJ, Clemens TL, Wolfgang MJ, and Riddle RC. Fatty acid oxidation by the osteoblast is required for normal bone acquisition in a sex- and diet-dependent manner. ***JCI Insight*** (2017) *2*, e92704.

9. **Bowman CE**, Selen Alpergin ES, Scafidi S, and Wolfgang MJ. Mitochondrial oxidative metabolism regulates late-gestation maternal-fetal metabolic communication. *In Preparation*.

Awards

Fellowships

American Heart Association Pre-doctoral Fellowship, Mid-Atlantic Affiliate,
July 2015-July 2017
"Regulation of cardiac energy metabolism by substrate availability"

NIH Training Grant Recipient
Biochemistry, Cellular & Molecular Biology Graduate Program
Johns Hopkins University School of Medicine, August 2012-July 2015

Awards

Travel Award, NICHD, Keystone Symposia: Maternal-Fetal Crosstalk
Washington, DC, October 2017

Caitlyn E. Bowman, B.S.

Editor's Choice Spotlight Article and Cover Art
Molecular and Cellular Biology, August 2016, Vol. 36, Issue 15
"Requirement for the Mitochondrial Pyruvate Carrier in Mammalian Development Revealed by a Hypomorphic Allelic Series"

Poster Award, "Metabolic role of the mitochondrial malonyl-CoA synthetase"; Molecular & Cellular Biology of Lipids, Gordon Research Conference, July 2015

Poster Award, "Role of type I acyl-CoA thioesterases in cellular fatty acid metabolism"; Navigating Lipid Research in Baltimore: From Cell to System, sponsored by American Society for Cell Biology, April 2014

Additional Honors

2017	Paul Talalay Young Investigators' Research Award
2008-2012	Quinter Scholarship, Juniata College
2010-2012	Juniata College Honor Society
2010-2012	Tri-Beta Biological Honor Society
2011-2012	Capital One/CoSIDA Academic All-District Team 2011, All-America Team 2012
2011	Charles C. Ellis Memorial Scholarship, Juniata College
2011	Dr. Homer C. and Ethel F. Will Endowed Scholarship in Biology, Juniata College
2010	NOAA Ernest F. Hollings Scholarship
2009	von Liebig Summer Research Fellowship, Juniata College

Teaching

Summer 2015, 2016	**Math Tutor** for high school students, Johns Hopkins Univ. SOM
2013-2014	"Day of Science" **Outreach Coordinator**, Johns Hopkins Univ. SOM Co-organized two student-run science outreach events for high school students
2011-2012	**Teaching Assistant**, Juniata College (Intro. Biology Discussion Leader)
2009-2012	Laboratory Assistant, **Science in Motion**, Juniata College, Huntingdon, PA

Organizational Activities

2016 Co-organized local meeting sponsored by the American Society for Cell Biology "Navigating Lipid Research in Baltimore" (Carnegie Institution, Baltimore, MD)